PROGRESS IN RESEARCH

APRIL 1, 2005 - MARCH 31, 2006

Prepared By

The Cyclotron Institute Staff

Texas A&M University

College Station, TX 77843-3366

Phone: (979) 845-1411
Fax: (979) 845-1899

Web: http://cyclotron.tamu.edu

July 2006

TABLE OF CONTENTS

SECTION II: HEAVY ION REACTIONS

SECTION III: NUCLEAR THEORY

SECTION IV: ATOMIC AND MOLECULAR SCIENCE

SECTION VI: PUBLICATIONS

SECTION VII: APPENDIX

Introduction
April 1, 2005 – March 31, 2006

Summarized here is the progress in research and operations at the Texas A&M Cyclotron Institute for the period April, 1, 2005 through March 31, 2006. Sections I through IV contain reports from individual research projects. Operation and technical developments are given in Section V. Section VI lists the publications with Cyclotron Institute authors and the Appendix gives additional information including talks presented by members of the Institute during the past year. The full volume of this year's Progress in Research is available solely on our web site (http://cyclotron.tamu.edu). *Since most of the contributions presented here are truly reports on progress in research, results and conclusions should not be quoted from the report without the consent of the authors.*

This has been a good year for Institute faculty. In the fall of 2004, Dr. Saskia Mioduszewski joined the Physics Department and Cyclotron Institute as an Assistant Professor. She was notified in late January that she had been named an A.P Sloan Foundation Fellow. Dr. John Hardy and Dr. Ian Towner shared the 2006 Bonner Prize for their work on $0^+ \rightarrow 0^+$ β decay. John also won a Texas A&M University Association of Former Students Award for Research this year. Dr. Ralf Rapp was promoted to Associate Professor of Physics with tenure effective September, 2006. Dr. Sherry Yennello was named a Fellow of the American Physical Society at the spring APS meeting. And Dr. Carl Gagliardi was named Deputy Spokesperson for the STAR collaboration.

We are now well into the Upgrade Project at the Institute which will ultimately lead to accelerated radioactive beams at intermediate energy. The progress on the project has been very good—we remain on schedule as of the second quarter of FY06. During the year the K500 cyclotron has continued to perform well and we have had significant pressure on beam time both for testing electronics components and for experiments. The experimental program continues to go very well. Some highlights of work over the past year are given below.

Research highlights:

(1) New on-line Penning-trap measurements of transition Q-values relevant to super-allowed beta decay are leading to better precision for several *ft* values. The first measurement, on ^{46}V, disagreed with a previous reaction-based result and led to concern that all reaction-based measurements might have suffered from previously undiscovered systematic errors. However, subsequent measurements, on ^{26}Al^{m} and ^{42}Sc, have confirmed previous reaction-based results on those transitions.

(2) Measurements of ^{7}Be and ^{8}B elastic scattering have led to an upward revision of the value of the ANC for $^{7}\text{Be} + \text{p} \rightarrow {}^{8}\text{B}$ and increase S_{17} from our ANC measurements by about 5%.

(3) Near Fermi-energy heavy ion collisions have been used to determine the nuclear symmetry energy in a clustered nuclear gas at temperatures and densities comparable to those of the neutrinosphere observed in a supernovae explosion.

(4) New measurements of ^{6}Li inelastic scattering demonstrate that they can be used effectively to study the giant monopole resonance (GMR), thus a ^{6}Li target bombarded by rare ion beams can be used to study the GMR in nuclei far from stability.

(5) Significant insights on the flavor, rapidity and system size dependence of anisotropic flows in relativistic heavy ion collisions have been obtained from a multi-phase transport model.

(6) TWIST completed its first measurement of the muon decay parameter $P_{\mu}\xi$ with a precision a factor of two better than any previous direct measurement.

(7) The ANC method has been used to determine the astrophysical factor for the neutron generating reaction, $^{13}C(\alpha,n)^{16}O$, in AGB stars. The result for the *S* factor is significantly smaller than previous measurements suggest.

(8) Based on the assumption of resonance interactions in the QGP, relativistic Langevin simulations of charm and bottom quarks have been performed for 200 GeV/A Au-Au collisions at RHIC. Including coalescence contributions to the hadronization into D and B mesons, the experimentally observed suppression and elliptic flow in (nonphotonic) single-electron decay spectra can be reasonably well described up to a p_t of about 5 GeV.

(9) Using the isoscaling technique and comparisons between experimental data and statistical multi-fragmentation model calculations, there is evidence that the symmetry energy for excited nuclear material is lower than that for ground states of nuclei.

(10) Fully self-consistent calculations of nuclear response functions for various isoscalar and isovector multipolarities have been completed for a wide range of nuclei. The results lead to a consistent value of the nuclear matter incompressibility coefficient for both relativistic and non-relativistic models, contrary to long standing claims of discrepancies.

As in the past, Institute scientists remain active in a number of collaborative research efforts around the world. Major programs include: experiments at TRIUMF laboratory to measure heavy ($A > 60$) superallowed β decays and a measurement of Michel parameters in normal μ^{+} decay; mass measurements using the Canadian Penning Trap (CPT) at Argonne National Laboratory; and continued work with both the BRAHMS and STAR collaborations at RHIC.

As in the past, I am pleased to acknowledge the effort made by Y.-W. Lui in assembling this report. Once again, he has managed it in a very prompt and efficient manner.

R.E. Tribble
July 19, 2006

SECTION I

NUCLEAR STRUCTURE, FUNDAMENTAL INTERACTIONS, AND ASTROPHYSICS

Double Folding Analysis of ^{6}Li Elastic and Inelastic Scattering on ^{116}Sn

X. Chen, Y.-W. Lui, H.L. Clark, Y. Tokimoto, and D.H. Youngblood

Giant resonances (GR) in ^{116}Sn excited by ^{6}Li inelastic scattering were studied by the deformed potential model and reported last year [1]. Multipole decomposition analysis [2] showed that the isoscalar giant dipole resonance (ISGDR) strength obtained in this analysis considerably exceeded the energy weighted sum rule(EWSR), indicating that the deformed potential model may not be adequate to study giant resonances excited by ^{6}Li scattering.

The folding model [3] has been widely used to generate the real part of the optical potential (OP) for alpha and heavy ion scattering. The folded potential is obtained by folding the nucleon-nucleon (N-N) effective interaction over target and projectile densities. One of the most widely used N-N effective interactions is the M3Y N-N interaction. In this report, a CD type density dependent N-N interaction, Paris version CDM3Y [4], was used to obtain the real part of optical potential for elastic scattering and real part of transition potential for inelastic scattering. The CD type density dependence function, which is a flexible hybrid of the original DDM3Y and BDM3Y form and which parameters are adjusted to get the correct saturation density and bind energy value, can be expressed as [4]

$$F(\rho) = C\left[1 + \alpha \exp(-\beta\rho) - \gamma\rho\right], \qquad (1)$$

where C=0.2658, α=3.8033, β=1.4099fm^3, and γ=4.0fm^3. The folding model calculations for optical potential and transition potential were carried out with code DFPD4 [5]. Phenomenological Woods-Saxon (W-S) potential was used to construct the imaginary part of OP and transition potential.

The elastic scattering data were fitted with the code ECIS [6]. The parameters obtained are shown in the Table I and the calculated angular distribution of the cross-section is plotted with data in Fig.1. A substantial renormalization factor N_R for real part of potential is needed here to fit ^{6}Li elastic scattering (Please see the Ref.[7] for more detail about the renormalization factor N_R.). Using the folded potential with W-S imaginary term, the cross section for inelastic scattering to low-lying 2^+ and 3^- states were calculated and shown with data in Fig.2 and Fig.3. The parameters used for double folding calculation are listed in Table II. Deformation parameters were obtained from electromagnetic B(EL) values by assuming the mass and coulomb deformation lengths are the same.

Table I. Optical model parameters obtained from the fits of the ^{6}Li+^{116}Sn elastic scattering. The M3Y(R) calculation used a W-S shape for the imaginary potential. N_R is the real renormalization factor for the folded potential.

E_{Li} (MeV)	Potential type	N_R	V (MeV)	r_0 (fm)	A (fm)	W (fm)	r_{I0} (fm)	a_I (fm)
240	Woods-Saxon		188.0	0.837	0.905	28.4	1.17	0.816
240	M3Y(R)	0.5631				23.935	1.19	0.9686

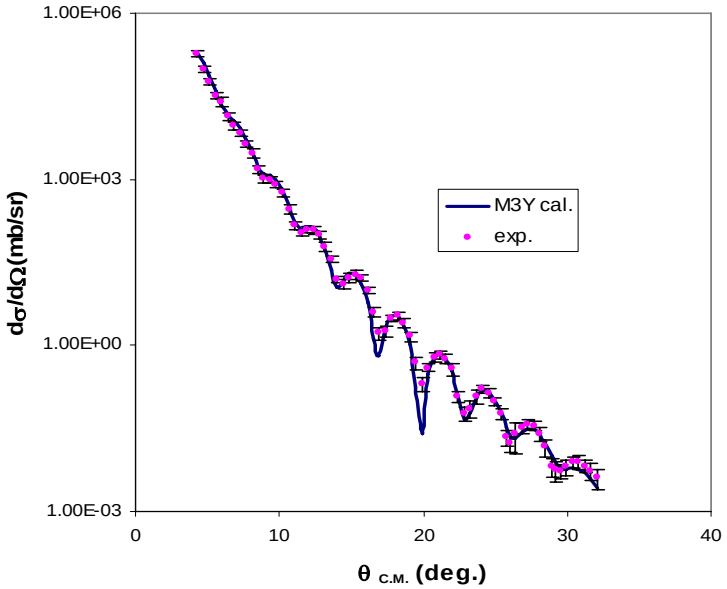

Figure 1. Angular distribution for ^{6}Li+^{116}Sn elastic scattering cross-section. The line shows the calculation using the M3Y(R) folded potential with a W-S imaginary term.

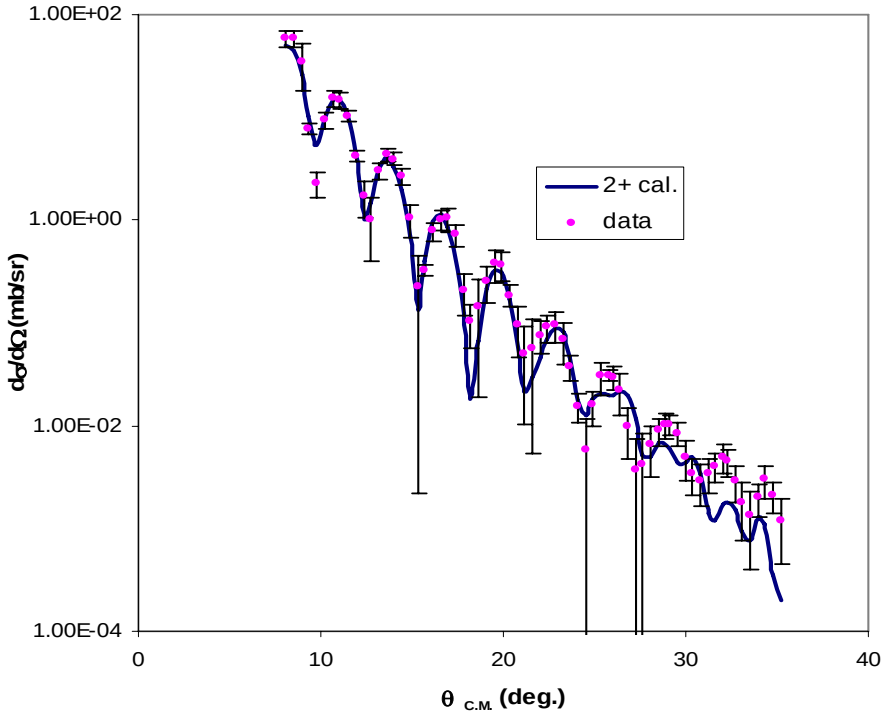

Figure 2. The line shows the calculated differential cross-section calculated using the M3Y(R) potential given in Table 1 for inelastic scattering to the 1.29 MeV 2^{+} state in ^{116}Sn plotted versus average center-of-mass angle. The electromagnetic B(EL) value was used. The data are shown by the circles. The error bars include statistical and systematic errors.

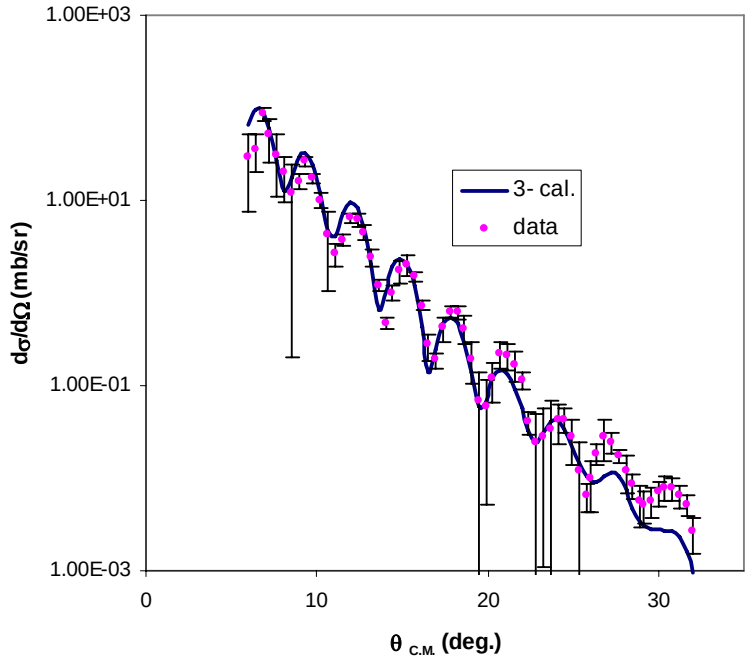

Figure 3. The line shows the differential cross-section calculated using the M3Y(R) potential given in Table 1 for inelastic scattering to the 2.27 MeV 3^- state in ^{116}Sn plotted versus average center-of-mass angle. The electromagnetic B(EL) value was used. The data are shown by the circles. The error bars include statistical and systematic errors.

Table II. Parameters used in double folding calculations for inelastic scattering to low lying 2^+ and 3^- states of ^{116}Sn

E_x(MeV); J^π	δ_m	N_R	W (MeV)	r_{i0} (fm)	a_i (fm)
1.29; 2^+	0.6441	0.5631	23.935	1.19	0.9686
2.27; 3^-	0.8397	0.5631	23.935	1.19	0.9686

Calculations for L=0-4 isoscalar excitations at E_x=16 MeV exhausting 100% of the respective sum rules are shown in Fig. 4. While the cross sections for the other multipoles are similar to those with the deformed potential, the ISGDR cross section is approximately a factor of 6 higher. Preliminary multipole decomposition using the folding model calculations result in strengths for L=0, 1, and 2 in approximate agreement with those obtained from α scattering[8]. The ISGDR cross section was also found to be quite sensitive to the details of the calculation for α scattering [9].

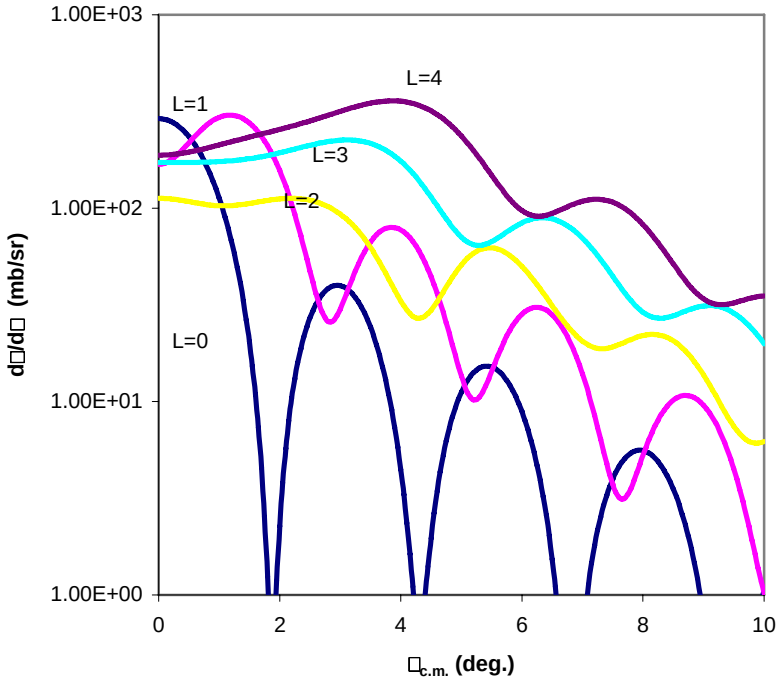

Figure 4. Angular distributions for L=0, 1, 2, 3, 4 excitations at E_x=16 MeV exhausting 100% of the respective EWSR's calculated with the M3Y(R) potential shown in Table 1.

We thank Dr. D. T. Khoa and Mr. Hoang Sy Than for their generous help and offer of the computer code to do the folding and the cross-section calculations.

[1] X. Chen, Y.-W. Lui, H.L. Clark, Y. Tokimoto, and D. H. Youngblood, *Progress in Research*, Cyclotron Institute, Texas A&M University (2004-2005), p.I-1.

[2] D. H. Youngblood, Y.-W. Lui, H. L. Clark, Phys. Rev. C **60**, 014304(1999).

[3] G.R. Satchler and W.G. Love, Phys. Rep. **55**, 183 (1979).

[4] D.T. Khoa, G.R. Satchler, Nucl. Phys. **A668,** 3 (2000).

[5] D.T. Khoa, unpublished.

[6] J. Raynal, Computing as a Language of Physics, ICTP International Seminar Course, (Trieste, Italy, 1971 (IAEA,1972)); M.A. Melkanoff, T. Sawada and J. Raynal, Methods in Computational Phys. **6**: Nuclear Physics (Academy Press, New York, 1966).

[7] M.E. Brandan, G.R. Satchler, Phys. Rep. **285**, 143(1997)

[8] D.H. Youngblood, Y.-W. Lui, H.L.Clark, B. John, Y. Tokimoto, and X. Chen, Phys. Rev. C **69**,034315 (2004).

[9] H.L. Clark, Y.-W. Lui, D.H. Youngblood, Nucl. Phys. **A687**. 80c (2001).

The Structure of ^{23}Al and the Consequences on the ^{22}Mg (p, γ) ^{23}Al Stellar Reaction Rate

Y. Zhai, V.E. Iacob, T. Al-Abdullah, C. Fu, J.C. Hardy, N. Nica, H.I. Park, G. Tabacaru, C.A. Gagliardi, L. Trache, and R.E. Tribble

There is interest in the structure of ^{23}Al due to its nuclear astrophysics significance [1,2]. The ground state spin and parity for ^{23}Al is uncertain, with assignments that include $1/2^+$, $3/2^+$ and $5/2^+$. Currently the NNDC data base gives $3/2^+$ for the ^{23}Al ground state. The mirror nucleus ^{23}Ne has $J^\pi = 5/2^+$ for its ground state. Recently it was claimed [3-5] that proton rich ^{23}Al is a halo nucleus. That can be explained only if the last proton in the $2s_{1/2}$ orbital, not $1d_{5/2}$ (level inversion), i.e. J^π = is $1/2^+$ for ^{23}Al. Using $1/2^+$ instead of $5/2^+$, we calculate the astrophysical S-factor and stellar reaction rate for ^{22}Mg $(p,\gamma)^{23}$Al and find an increase of 30-50 times over the current estimate for the temperature range T_9=0.1-0.3. This results in a significant depletion of ^{22}Mg before it β decays into ^{22}Na and, if confirmed, could explain the non-observation of the 1.275 MeV γ-ray from ^{22}Na which is the last step of the reaction chain which is named the hot NeNa cycle: ^{20}Ne(p,γ)^{21}Na(p, γ)^{22}Mg(β,ν)^{22}Na. Our ^{23}Al β-decay measurement [6] will be used to determine the J^π of the ground state of ^{23}Al.

In 2005, we had three experiments to produce and study ^{23}Al, beginning with production tests at two different ^{24}Mg beam energies, 45 and 48 MeV/u, respectively. At both energies ^{23}Al was produced and separated, but the latter was found more productive. Therefore, we produced ^{23}Al and studied its β-decay using a 48 MeV/nucleon ^{24}Mg beam from the K500 cyclotron via the ^{24}Mg(p, 2n)^{23}Al reaction on a hydrogen gas cryogenic target cell cooled by LN_2. The reaction products and projectiles entered the MARS recoil separator where the ^{24}Mg beam was filtered out and the fully stripped reaction products were spatially separated from one another, leaving a relatively pure ^{23}Al beam of about 4000 pps at the extraction slits in the MARS focal plane. Its β-decay was further studied using the fast tape transport system. This was the first time pure and intense ^{23}Al samples were produced and separated. This ^{23}Al beam came out of the vacuum system by passing through a 50 μm thick Kapton window, a 0.3 mm thick BC-104 scintillator, a dummy tape and a stack of aluminum degraders (30.5 mils). A 75-μm thick aluminized Mylar tape on the fast tape-transport system was used to collect ^{23}Al. Because the ranges of impurities in the beam are different from that of ^{23}Al, a pure ^{23}Al sample was collected on the tape. In our measurement, we collected ^{23}Al on the tape for 1 second. Then we shifted the RF phase to stop the ^{24}Mg beam. Following this we moved the ^{23}Al sample in 177 ms with the tape transport system to a counting station which consists of a HPGe γ detector and a β detector. β and β-γ coincidence data were recorded for a predetermined counting period of 3.2 seconds. This cycle was precisely clock controlled and was repeated continuously. The sample was positioned between the HPGe γ-ray detector and a 1-mm-thick BC404 plastic scintillator used to detect β particles. The BC404 was located 3 mm from the sample, while the HPGe was about 4.9 cm away. Time-tagged coincidence data were stored event by event in the computer. This experimental setup [7] is a typical one for measuring β-γ coincidences except that the HPGe detector was closer than usual. In two different parts of the experiment, we first measured the γ energy range 0-4 MeV with good statistics (Fig. 1a), then we measured γ energy range 0-9 MeV for about 20 hours (Fig. 1b). We also separated pure samples of ^{24}Al, by tuning MARS for this product, and

did a similar β-γ measurement. We use its known gamma-rays up to E_γ=7.8 MeV for energy and efficiency calibration in the range E_γ=4-9 MeV.

The ground and first three excited states of ^{23}Mg have $J^\pi=3/2^+$, $5/2^+$, $7/2^+$ and $1/2^+$, respectively. All of these states are easily accessible energetically to β-decay from ^{23}Al. Depending on which states are actually populated by allowed GT transitions – as determined by log*ft* values – the spin and parity of the parent ground state can be unambiguously determined. From the measured β singles and β-γ coincidence decay spectrum (Fig. 1) we can get the ^{23}Al β-decay scheme and the branching ratios. We find that it populates directly the $3/2^+$, $5/2^+$ and $7/2^+$ states, but not the $1/2^+$ state. Combined with GT transition rules, we clearly determine that ^{23}Al ground state spin and parity is $J^\pi=5/2^+$. We found preliminary β-branching ratios and log*ft* values for 14 states in total. It so appears that the larger capture rate implied by the lower spin value of ^{23}Al will not explain the missing cosmic 1275 keV cosmic γ-ray.

The future research plan is the following. An additional experiment at TAMU is going to add a BGO shield to the present HPGe γ-ray detector to reduce background in the β-γ decay spectrum of ^{23}Al and increase the ability to detect high energy γ rays. We also need better statistics for the γ energy range 4-9 MeV. So we can get more precise ^{23}Al β-γ decay energy level scheme, β & γ-branching ratio and a precise ^{23}Al half life.

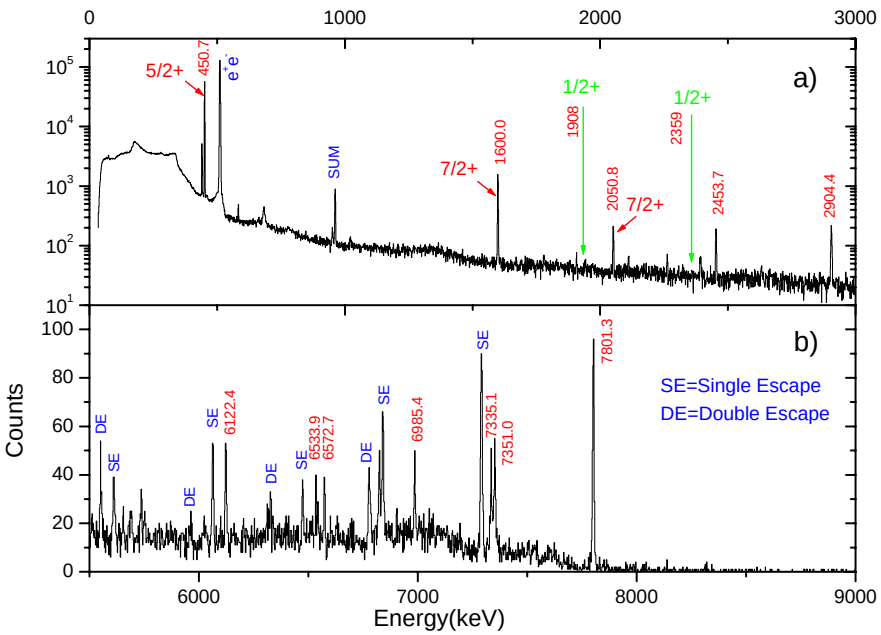

Figure 1. ^{23}Al β-γ coincidence spectrum.

[1] J. Jose, A.. Coc, M. Hernanz, Astroph. J. **520**, 347(1999).

[2] C. Rolfs and W.S. Rodney, *Cauldrons in the Cosmos*, (University of Chicago Press, 1988).
[3] X.Z. Cai *et al*., Phys. Rev. C **65**, 024610(2002).
[4] H.-Y. Zhang *et al.*, Chin. Phys. Lett. **19**, 1599(2002).
[5] D.Q. Fang *et al.*, Phys. Rev. C **61**, 064311(2000).
[6] Kai Siegbahn, Alpha, Beta and Gamma Ray Spectroscopy, vol. **2**, (American Elsevier publishing company Inc., New York 1974).
[7] V.E. Iacob *et al.*, *Progress in Research*, Cyclotron Institute, Texas A&M University (2005-2006), p.I-11.

Decay of ^{23}Al and Resonances in ^{22}Na(p,γ)^{23}Mg at Astrophysically Relevant Energies

L. Trache, V.E. Iacob, Y. Zhai, T. Al-Abdullah, C. Fu, J.C. Hardy, N. Nica,
H.I. Park, G. Tabacaru, and R.E. Tribble

Efforts were made for a long time to determine the reaction rate for the proton capture reaction ^{22}Na(p,γ)^{23}Mg, the most credible candidate for depleting ^{22}Na out of the NeNa cycle [1]. Data showed early on that resonant capture plays the overwhelming role. States in ^{23}Mg above the proton separation energy are resonances in this reaction and can play roles in the rate of this reaction at astrophysical energies. The problem received much attention related to the anomalous Ne isotopic ratio found in some meteorites (Ne-E anomaly) [2,3] and to the breakout of the NeNa cycle cited above. Confusion still exists about the precise position of resonances and their strength even after a few direct measurements [1,4] and many spectroscopic studies [5-10], leading to uncertainties for the reaction rate in stellar environments that may be yet of a few orders of magnitude [5,6]. The major problem arises from the large density of states at this excitation energy which could not be easily separated and identified. Some of these states are populated in the decay of ^{23}Al, including the isobaric analog state of its ground state which can be identified by its preferential population. In the present report we separate two important states, and identify the IAS.

Radioactive ^{23}Al was produced and separated using MARS and its β-decay was studied using the fast-tape transport system and beta and gamma-ray detectors. The details of the experiment and the results related to the determination of spin and parity of ^{23}Al ground state and of its lifetime are discussed in other contributions to this report [11,12]. In this experiment we determined for the first time the *ft*-value for the transition to a state at 7803 keV: *ft*=2042(120) s. This is in excellent agreement with the value expected for a pure Fermi transition from a T_z=-3/2 state: *ft*=2048(0.5) s, a fact which identifies it as the IAS of ^{23}Al ground state. This state was seen before [10] and assumed correctly to be the IAS, based on its preeminence in decay, but its *ft*-value could not be determined there, it was assumed to have log*ft*=3.4(2). The relevant part of the decay scheme of ^{23}Al is shown in Figure 1.

The states above the proton binding energy in ^{23}Mg (S_p=7580.3(14) keV) become resonances in the capture process and, therefore, their precise E_{exc}, J^π, and decay widths are needed to evaluate the resonant part of the reaction rate. Two beta-delayed proton decay studies [9,10] measured proton spectra resulting from the proton decay of ^{23}Mg excited states populated from the initial beta-decay of ^{23}Al. Proton peaks at energies from around 200 to 900 keV were seen. The relative populations are similar in the two experiments for all higher energy proton peaks, but differ sharply for the lowest state that both studies identify as the isobaric analog state. The experiment of Perajarvi *et al.* [10] is the only one that measures simultaneously proton and gamma-decay ratios. Tighe *et al.* [9], find a much stronger proton peak at E_p=223(20) keV, depopulating what they assume to be the $J^\pi=5/2^+$, T=3/2 IAS. Proton decay of that state could only occur through mixing of a T=1/2 component. The observed proton-decay is about 50 times larger than expected from calculations with commonly accepted isospin non-conserving interactions [13], and the authors conclude that they found "extremely strong isospin mixing", and, consequently, a very large resonance strength ωγ=45(25) meV. In the present experiment we identify the

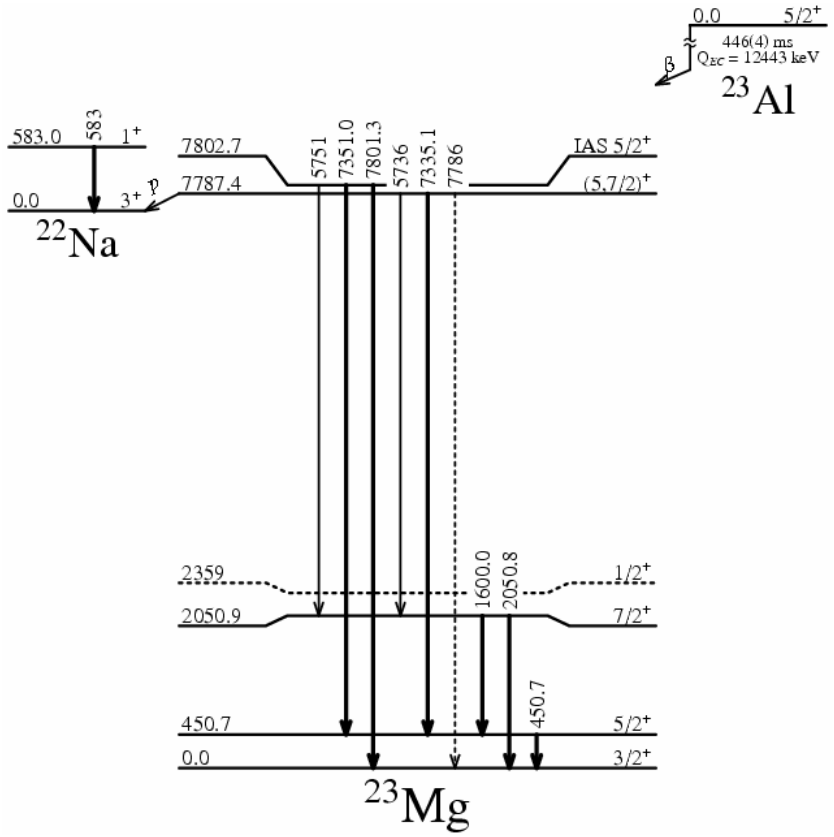

Figure 1. The decay scheme of ^{23}Al relevant for the above discussion.

IAS (log*ft*=3.33) at E_{exc}=7803(2) keV and find another state strongly populated (log*ft*=3.84) only 16 keV below at E_{exc}=7787(2) keV (see Fig. 1 of [11]). For these two states we find gamma-decay branches to the ground state/first excited state (451 keV)/second excited state (2051 keV) to be 100/45(5)/5.5(21) and 3.8(25)/100/20(5), respectively. Hints or assumptions about a doublet in this energy region exist in literature [1,10], but never before were the two states populated and separated in the same experiment. Both studies populated only the lower state and found that it decays to the first excited state at 451 keV, in agreement with what we find here as the dominant branch. We assume that the strong peak seen at low energy in the proton spectra measured with a resolution of 40 keV by Tighe *et al.* [9] is actually from the decay of the lowest state. This is a normal T=1/2 isospin state and therefore our assumption excludes the strong, anomalous, isospin mixing needed to explain their data. Its strong direct population in beta-decay determines its positive parity and restricts spin assignments to J=3/2, 5/2 and 7/2. Strong proton decay to the ^{22}Na $J^{\pi}=3^{+}$ ground state excludes 3/2. From the remaining two possibilities we could exclude 5/2 also based on two arguments: one related to the proximity to a state of same spin and parity (IAS) which would induce a strong "repulsion" even for small mixing matrix elements, and the second one based on the dissimilarity of their gamma-ray decay patterns (see branchings above). Therefore we propose $J^{\pi}=7/2^{+}$ for this state at E_{exc}=7787(2) keV, in agreement with the recent $J^{\pi}=(7/2^{+})$ assignment of Ref. [5].

Using the proton branching relative to higher energy peaks measured by [9] and the proton to gamma branchings determined in [10] for the same high energy peaks, we find for this state Γ_p/Γ_γ=0.080(17). From this and the lifetime of the state measured in a recent GAMMASPHERE experiment [5] $T_{1/2}$=10(3) fs, we determine the resonance strength $\omega\gamma$=2.6(9) meV for this state. This is in reasonable agreement with the value obtained from the direct measurement involving a difficult radioactive ^{22}Na target [1] and with the value adopted by the NACRE compilation [4]. The resonance strength for the IAS could not be determined or estimated without further assumptions.

In conclusion, we found a doublet in ^{23}Mg with small *ft*-values at 7803(2) keV and 7787(2) keV and identified the states as the isobaric analog state of ^{23}Al ground state and a $J^\pi = 7/2^+$ state with large proton decay branch. Both are resonances contributing to the depletion reaction ^{22}Na(p,γ)^{23}Mg. For the latter resonance at E_{res}=207(3) keV we find its resonance strength to be $\omega\gamma$=2.6(9) meV, making it the dominant contribution in the reaction rate at the temperatures of explosive H burning in ONe novae. To further improve our knowledge about this reaction rate a re-measurement of the beta-delayed proton and gamma decay of these ^{23}Mg states is desirable.

[1] F. Stegmuller *et al.*, Nucl. Phys. **A601**, 168 (1996) and references therein.

[2] D.C. Black, Geoch. Cosmoch. Acta **36**, 347 (1972).

[3] M. Arnould and W. Beelen, Astron. Astroph. **33**, 215 (1974); M. Arnould and H. Norgaard, Astron. Astroph. **64**, 195 (1978).

[4] S. Seuthe *et al.*, Nucl. Phys. **A514**, 471 (1990).

[5] D.G. Jenkins *et al.*, Phys. Rev. Lett. **92**, 031101 (2004).

[6] C. Angulo *et al.*, Nucl. Phys. **A656**, 3 (1999).

[7] S. Schmidt *et al.*, Nucl. Phys. **A591**, 227 (1995).

[8] S. Kubono, Nucl. Phys. **A588,** 305c (1995).

[9] R.J. Tighe *et al.*, Phys. Rev. C **52**, R2298 (1995).

[10] K. Perajarvi *et al.*, Phys. Lett. **B492**, 1 (2000).

[11] Y. Zhai *et al*., *Progress in Research*, Cyclotron Institute, Texas A&M University (2005-2006), p. I-5.

[12] V.E. Iacob *et al.*, *Progress in Research*, Cyclotron Institute, Texas A&M University (2005-2006), p. I-11.

[13] W.E. Ormand and B.A. Brown, Nucl. Phys. **A491**, 1 (1989).

Half-Life of ^{23}Al

V.E. Iacob, Y. Zhai, T. Al-Abdullah, C. Fu, J.C. Hardy, N. Nica, H.I. Park, G. Tabacaru, L. Trache, and R.E. Tribble

We report elsewhere on the decay scheme of ^{23}Al, and its application to nuclear astrophysics [1]. As with any β decay, the spin-parity of this nucleus and of the states in its β-decay daughter, ^{23}Mg, determine the properties of the observed β transitions between them. In fact, these spins and parities can be determined (or at least limited) by the *ft* values measured for the connecting β transitions. To extract accurate *ft*-values, however, we need not only precise branching-ratios but also an accurate half-life for the parent nucleus. The measurement reported here was prompted by the poor precision of the currently accepted [2] half-life of ^{23}Al, $t_{1/2}$=0.470(30) s.

Since ^{23}Al decays by β-delayed proton emission as well as by β-delayed γ rays, and both resulting daughter nuclei are themselves radioactive, a measurement of decay positrons with our standard proportional gas-counter [3] involves too many inseparable activities to yield a reliable result for ^{23}Al. Instead, we measured off-beam β-γ coincidences as a function of time using our fast tape-transport system – and analyzed the decay of those γ rays uniquely associated with ^{23}Al.

We used a ^{24}Mg primary beam at 48*A* MeV from the cyclotron impinging on a liquid-nitrogen cooled hydrogen target pressurized to 1.5 atm. The recoiling ^{23}Al ions were separated from the other ejectiles by the MARS spectrograph (see Ref. [1]), yielding a radioactive beam at the exit of MARS with a purity of about 99% and an intensity of about 4000 pps. The ^{23}Al nuclei at 39*A* MeV were then extracted into air, passed through a thin (0.3mm) plastic scintillator and a stack of aluminum degraders, and finally were implanted into the aluminized mylar tape of our fast tape transport system. We collected activity for 1s, then switched off the beam and moved the activity 90 cm in 180ms to the center of a detection system, located in a well shielded region. There, β singles and β-γ coincidences were obtained from a HPGe detector and a BC-404 plastic scintillator located on opposite sides of the collected sample; these data were taken for 3.2s and each recorded event was tagged with the time elapsed since the beginning of the detection period. The collect-move-detect cycles were then repeated until sufficient statistics had been accumulated.

In the off-line analysis, we selected only the most intense γ-ray peaks in the ^{23}Al decay (those at 451 and 1600 keV) and generated a net decay spectrum by subtracting from the time-spectrum associated with the peak of a given γ-ray, the corresponding background observed on either side of the peak. In Fig. 1 we present the net decay spectrum containing a total of about 1.3×10^5 events in the sum of the 451 and 1600-keV peaks. While the selection of the ^{23}Al decay events by their γ-ray energies simplifies the analysis significantly, the very different dead-time corrections in the β, γ and β-γ coincidence channels require a detailed analysis, especially since the total decay-rates in the β and γ detectors are not proportional to the decay rate of ^{23}Al. This can be easily observed in Fig. 1, where the scaled-down total γ-rate (solid line) obviously contains contributions from decays with longer half-lives than that of ^{23}Al.

Our preliminary result is $t_{1/2}$ (^{23}Al) = 447(4) s; this is consistent with the previously accepted value of 0.470(30) [2], but is significantly more accurate.

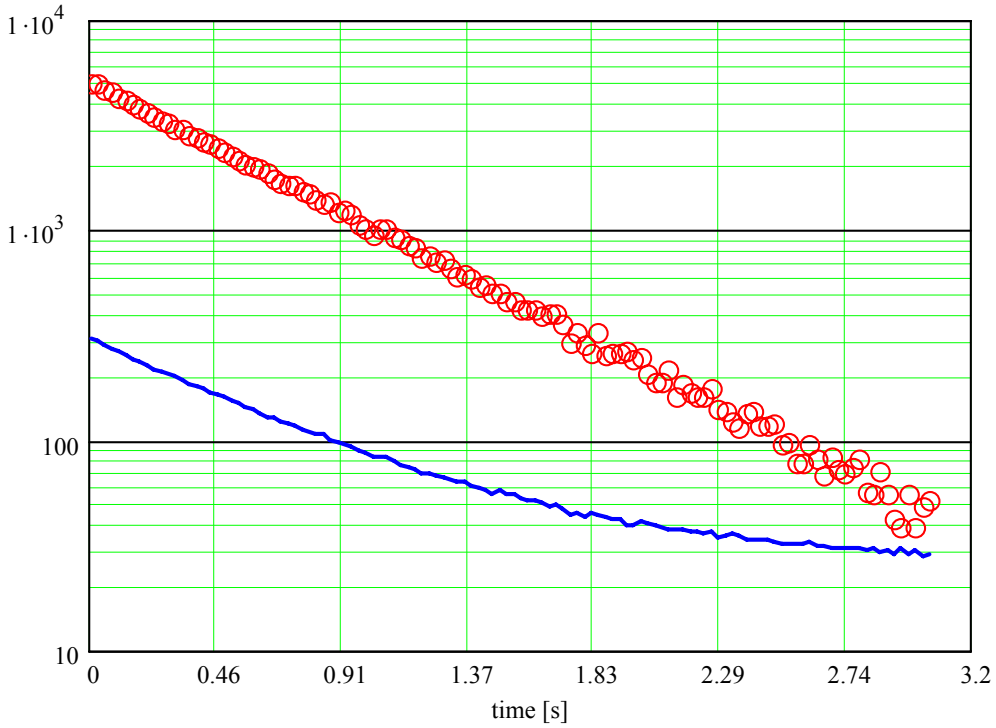

Figure 1. Net versus total γ-spectra observed in the decay of ^{23}Al. Open circles represent the net decay spectrum of ^{23}Al as observed in β–γ coincidences; only the two most intense γ-rays (451 and 1600 keV) were used in the selection; the spectrum contains about 1.3×10^5 events. The solid line represents a scaled-down total γ-spectrum containing contributions from ^{23}Al and its several descendents, all of which are radioactive and generate γ-rays.

[1] L. Trache *et al.*, *Progress in Research*, Cyclotron Institute, Texas A&M University (2005-2006), p.I-8.

[2] P.M. Endt**,** Nucl. Phys. **A521,** 1 (1990).

[3] V.E. Iacob *et al.*, *Progress in Research*, Cyclotron Institute, Texas A&M University (2005-2006), p.I-31.

Determination of the Proton Radiative Capture Rate for $^{17}F(p,\gamma)^{18}Ne$ Using the Neutron Transfer Reaction (^{17}O,^{18}O)

T. Al-Abdullah, F. Carstoiu, X. Chen, C.A. Gagliardi, Y.-W. Lui, G. Tabacaru, Y. Tokimoto, L. Trache, R.E. Tribble, and Y. Zhai

The electron-positron annihilation during the expansion of nova envelope leads to the emission of a γ-ray line at 511 keV and a continuum below it [1]. To observe these γ-rays, it is proposed [2] to study the nuclear reactions that create and destroy the long-lived isotope ^{18}F (τ=158 min). It is synthesized in the HCNO cycle and its abundance may be influenced by the reaction rate for $^{17}F(p,\gamma)^{18}Ne$. Since direct measurements have not been performed, the ANC method is applied to determine this rate at astrophysical energies. The ANCs for the 2^+ excited states at 1.98 MeV and 3.92 MeV in the nucleus ^{18}O will be sought through measuring the peripheral reaction $^{13}C(^{17}O,^{18}O)^{12}C$, and then transposed to the mirror states in ^{18}Ne with the same spectroscopic factors.

The experiment was performed using the MDM spectrometer and the Oxford detector to analyze the reaction products. The experiment was divided into three parts: measurement of the cross section values for the neutron transfer reaction $^{13}C(^{17}O,^{18}O)^{12}C$, and of the elastic scatterings for the entrance (^{17}O+^{13}C) and exit channels (^{18}O+^{12}C). To do these, ^{17}O and ^{18}O beams at 12 MeV/A were impinged on thin ^{13}C and ^{12}C targets, respectively. The cross section values were measured in the ranges $\theta_{C.M} = 6^o$-58^o and $\theta_{C.M} = 5^o$-32^o for elastic and transfer, respectively. The angular distributions for both the elastic scattering data sets were fit separately with volume Wood-Saxon forms to obtain the OMP, which are used as input files for the incoming and outgoing reaction channels in

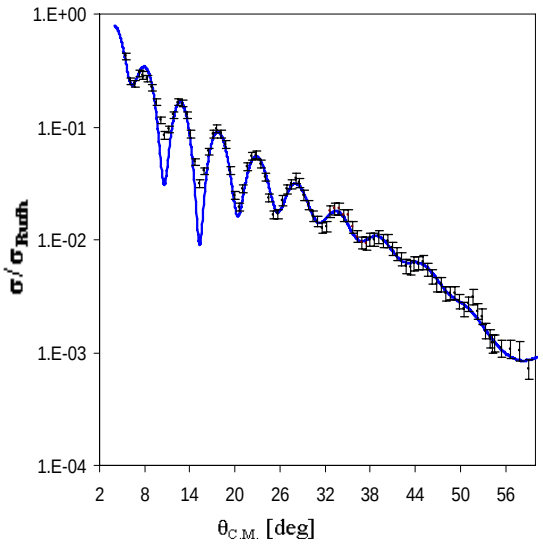

Figure 1. Fit of the elastic scattering cross section of 204 MeV ^{17}O on ^{13}C.

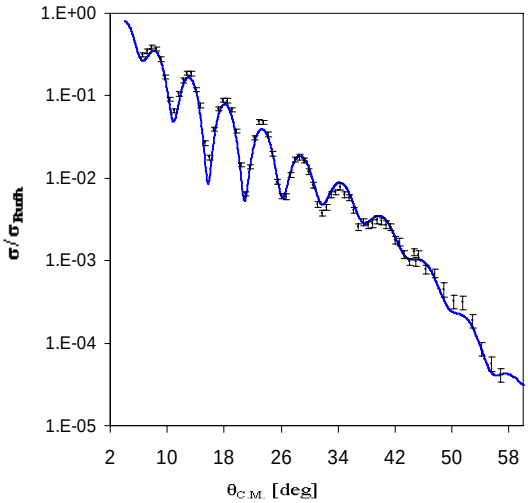

Figure 2. The angular distribution of the elastic scattering of 218 MeV ^{18}O on ^{12}C.

the DWBA calculations. The elastic scattering fits are shown in Figures 1 and 2.

The first excited states in ^{18}O, $J^{\pi} = 2^{+}$ at 1.98 MeV and $J^{\pi} = 4^{+}$ at 3.55 MeV, have been successfully populated and separated in the transfer measurements. Two components, $p_{1/2} \rightarrow d_{5/2}$ and $p_{1/2} \rightarrow d_{3/2}$, contribute to the $^{13}C(^{17}O,^{18}O^{*}(2^{+}))^{12}C$ reaction. Results of the DWBA calculations using the code Ptolemy are shown in figures 3 and 4 for the 2^{+} and 4^{+} states, respectively. The ANC in ^{13}C, which represents the other vertex in the reaction, was previously determined from the reaction $^{12}C(^{13}C,^{12}C)^{13}C$ [3]. Data analysis to extract the ANCs in ^{18}O is in progress. This is a particularly unique and interesting case because we were able to determine the optical potentials in both entrance and exit channels.

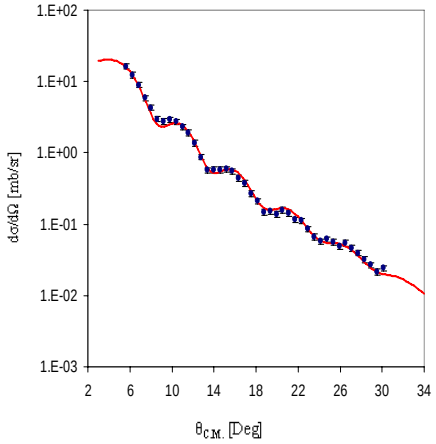

Figure 3. The angular distribution for $^{13}C(^{17}O,^{18}O^{*}(2^{+}))^{12}C$ reaction. The curve shows the DWBA fit for $d_{5/2} \rightarrow 2^{+}$ and $d_{3/2} \rightarrow 2^{+}$ components.

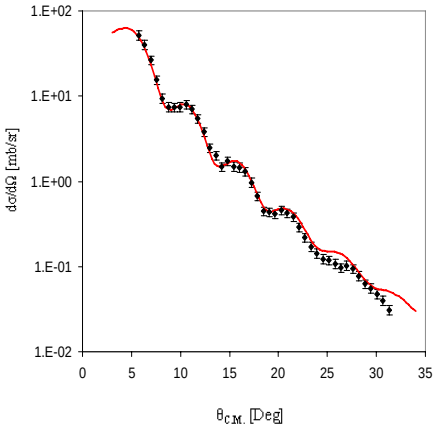

Figure 4. The angular distribution compared with DWBA calculations for the 4^{+} state.

[1] J. C. Blackmon, *et al*, Nuc. Phys. **A746**, 365 (2004).
[2] M. Hernanz, *et al*, Astrophys. J. Lett. **526**, 79 (1999).
[3] T. Al-Abdullah *et al*,(to be published).

Production of a New Radioactive Beam ^{12}N with MARS

A. Banu, T. Al-Abdullah, C. Fu, C.A. Gagliardi, L. Trache, R.E. Tribble, and Y.J. Zhai

The reaction rate for the radiative proton capture on the drip line nucleus ^{12}N is currently under investigation at the Cyclotron Institute using an indirect method. This reaction is important in the hot proton-proton chain of H burning in supermassive stars [1]. We intend to use the ^{14}N(^{12}N,^{13}O)^{13}C proton transfer reaction to extract the asymptotic normalization coefficient (ANC) for the virtual decay ^{13}O->^{12}N + p, and calculate from it the direct component of the astrophysical S-factor. A primary beam of ^{12}C from the K500 superconducting cyclotron is used to produce in-flight radioactive ^{12}N which is separated from other reaction products with the recoil spectrometer MARS. In early spring 2006, we studied the production and separation of ^{12}N, in preparation for the run in May of 2006.

Here we report on the production rate of the ^{12}N secondary beam, developed at the Cyclotron for the first time. A host of possible production reactions –^{12}C(p,n)^{12}N, ^{14}N(p,t)^{12}N, ^{12}C(^{3}He,t)^{12}N, ^{10}B(^{3}He,n)^{12}N– were considered to be studied in inverse kinematics. According to past measurements for these reactions [2], the ones more feasible for the energy regime of interest appeared to be ^{12}C(p,n)^{12}N and ^{10}B(^{3}He,n)^{12}N, with production cross sections of the order of a few mb. We chose to investigate the (p,n) reaction mechanism, used also successfully at MARS in the production of ^{7}Be, ^{11}C, ^{13}N, ^{14}O beams, and for which one benefits from a more forward focus that is propitious to the MARS acceptance [3].

We have used a primary beam of ^{12}C at 23 MeV/u impinging on a LN_2 cooled H_2 gas cell. The secondary ^{12}N nuclei have been produced in the H(^{12}C,^{12}N)n reaction. The entrance and exit windows of the gas cell were made of havar foil of 4 μm each and the pressure in the cell was p=1.5 atm. Due to the large negative Q-value of the reaction $Q_{(p,n)}$=-18.12 MeV, the energy of the primary beam has to be large. Therefore the energy of the recoiling products, which is larger than needed for the secondary proton transfer reaction (10-12 MeV/u), needs to be degrade it behind the production target. A 250-μm-thick Al foil was put behind the target cell as an energy degrader. Various production scenarios such as charge exchange around 0° (forward angle solution), around 180° (backward angle solution) or the fusion-evaporation mechanism were considered and the production was measured for each. To quantify the influence of the multiple scattering in the Al degrader foil, we have determined the production rate with and without it in place. We have found its influence to be marginal. MARS was tuned for each case and the ^{12}N production was determined by counting the ^{12}N yield in the target detector relative to the primary beam integrated in the Faraday cup in the coffin of MARS. The target detector used was a 300 μm 16 strip position sensitive Si detector. The secondary beam was tuned at very low intensities of the primary beam to restrict the bombarding rate to be below 100 Hz. The procedure has been described elsewhere [4]. The results are summarized in Table I. Obviously, the forward angle solution gives the largest production rate. With this productivity we expect to have secondary beams of around 10^5 pps. We will use this method for the main run in May 2006.

TableI. Summary of results for ^{12}N production.

Production mechanism	**degrader**	**E/A (^{12}N) [MeV/u]**	**N_{ev}(^{12}N) [events/nC]**
forward angle solution	250 μm Al	13.1	185
backward angle solution	250 μm Al	9.5	40
fusion-evaporation	250 μm Al	11.4	33
forward angle solution	none	19.6	173

[1] M. Wiescher *et al.*, Astrphys. J., **343**, 352 (1989).

[2] F.K. McGowan and W.T. Milner, Atomic and Nuclear Data Reprints, Vol.2, Charged-particle reaction list 1948-1971.

[3] R.E. Tribble *et al*., Nucl. Phys. **A701**, 278c (2002).

[4] A. Azhari *et al*., Phys. Rev. C **63**, 055803 (2001).

Doppler Shift as a Tool for Studies of Isobaric Analog States of Neutron-Rich Nuclei: Application to ^{7}He

V.Z. Goldberg, G. Chubarian , P. Boutachkov,[1] G.V. Rogachev,[1] A. Aprahamian,[1]
P.A. DeYoung,[1] J.J. Kolata,[1] L.O. Lamm,[1] G.F. Peaslee,[1] M. Quinn,[1] B.B. Skorodumov,[1]
F.D. Becchetti,[2] J.P. Bychowski,[2] and Y. Chen[2]
[1]*Institute of Structure and Nuclear Astrophysics, University of Notre Dame, Notre Dame, IN 46556*
[2]*Physics Department, University of Michigan, Ann Arbor, MI 48109*

The purpose of this work is to introduce a new experimental technique that allows the study of exotic neutron-rich nuclei in inverse kinematics using rare beams. The technique has two components: the population of isobaric analog states (IAS) of exotic nuclei through resonant reactions in a thick proton target (in line with ideas discussed in Ref.[1]), and subsequent measurement of the Doppler shift profile of the γ rays emitted after neutron decay of the IAS. This approach allows for the simultaneous measurement of the excitation function of the resonant (*p, n)* process, which leads to the population of IASs over a wide energy range from the initial RIB energy to zero, and provides some information on the double differential cross sections in one self-consistent measurement. The first application of this technique presented for the case of the IAS of ^{7}He in ^{7}Li.

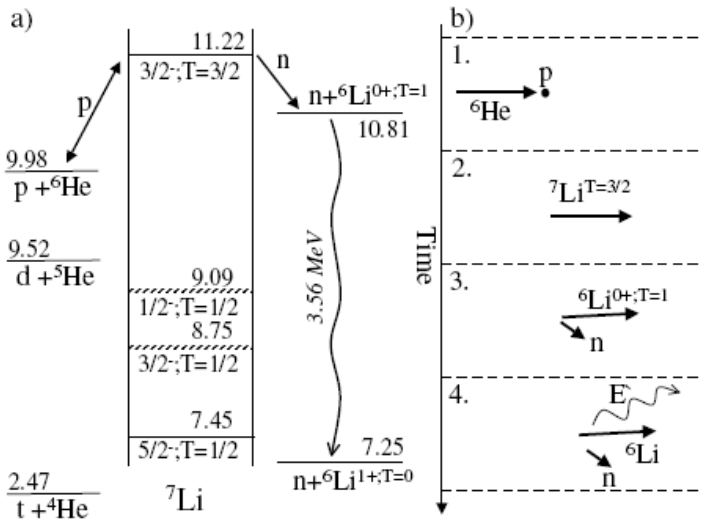

Figure 1. (a) Decay pathways for the T=3/2 resonance in ^{7}Li, and (b) the successive kinematics stages of the reaction.

Fig.1 gives the illustration of the successive transmutations following the proton capture into *T=3/2* resonance state in ^{7}Li. Because of isospin conservation, only two decay channels are allowed for the *T=3/2* state: proton decay to the initial channel and a neutron decay with the population of *T=1* states in the ^{6}Li nucleus. Usually the T> states in the daughter nuclei (3.56 MeV, T=1 in ^{6}Li in our case)

populated in the transmutation in question can undergo nuclear decay only through isospin-forbidden channels, and as a result the probability for γ decay is strongly enhanced. In case of ^{6}Li the γ decay dominates (100%).

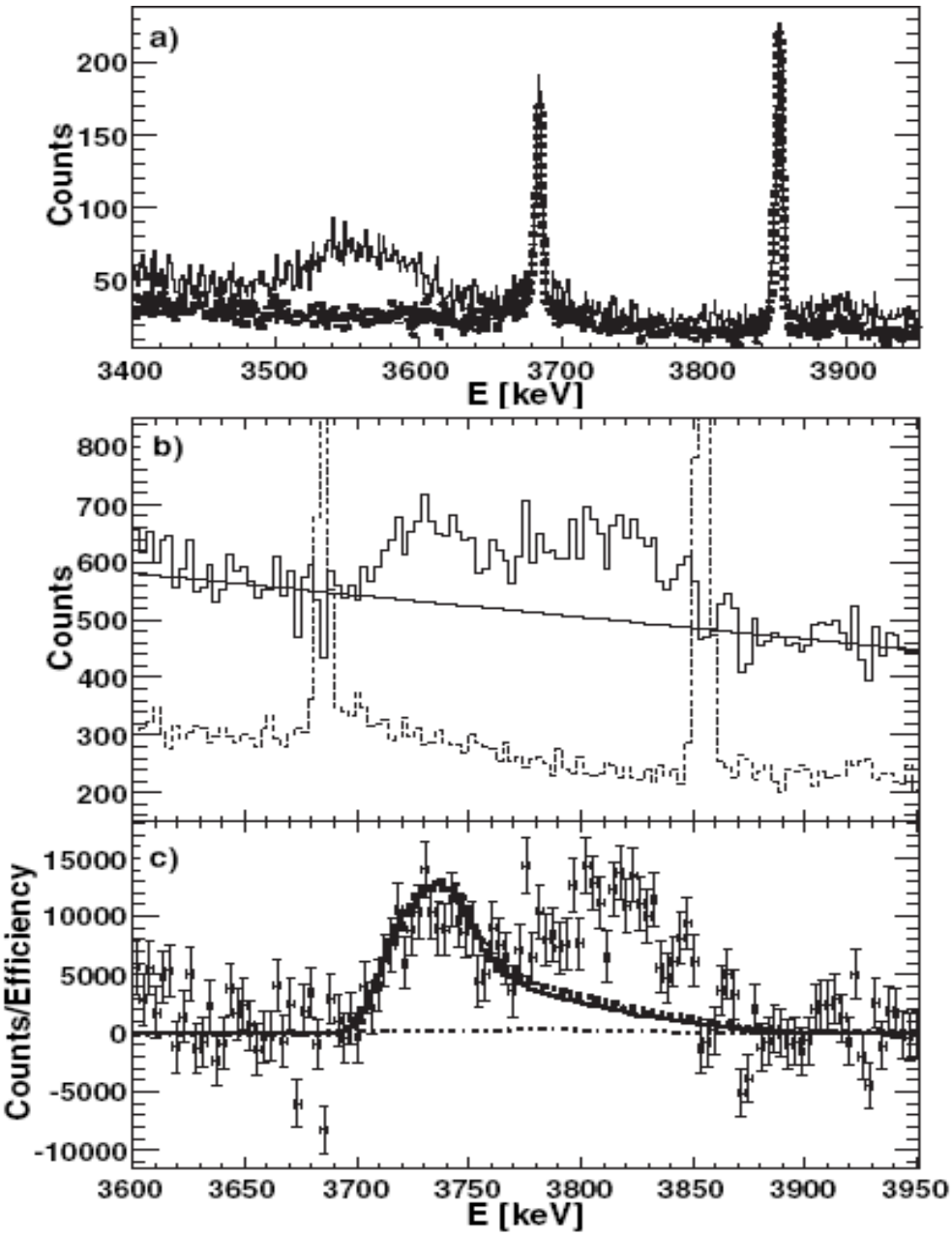

Figure 2. (a) Part of the γ-ray spectrum from the 90^0 Ge detector. The solid curve was obtained with a CH_2 target; the dotted curve was taken with a carbon target. (b) The spectrum in the 0^0 Clover detector obtained by subtraction of the carbon contribution; the dotted curve was taken with a carbon target. The Compton background is approximated by a straight line as shown. (c) The final spectrum of the Doppler-shifted 3.56 MeV γ rays. The solid line shows the contribution from the known *T = 3/2*, *J= 3/2*$^-$ state in ^{7}Li. The dotted line includes the effect of *T =1/2* resonances. The dash-dotted line close to the abscissa axis shows the contribution of the direct charge exchange process.

A ^{6}He beam with an intensity of $2 \cdot 10^{5}$ pps and an energy of 24 MeV stopped in a 57.4 mg/cm^{2} CH_2 target[2]. Two γ-ray detectors were placed around the target: a HPGe Clover at 0^0 and a single-crystal 55% efficiency HPGe detector at 90^0 relative to the beam direction. A portion of the 90^0 γ-ray spectrum is shown in Fig. 2(a). The main features of the spectrum are two narrow peaks at 3.68 and 3.85 MeV, and a broad bump with a centroid at 3.56 MeV. The two narrow peaks are from the decay of ^{13}C excited states populated in the ^{12}C(^{6}He, ^{5}He)^{13}C reaction. The bump at 3.56 MeV is the Doppler broadened 3.56 MeV γ-ray transition from the 0^+ state of ^{6}Li. A γ-ray spectrum obtained with a carbon target is shown by the thick dotted curve. The 3.56 MeV structure is not present in this case, providing clear evidence that it results from the interaction of ^{6}He with protons. The ^{7}He$_{g.s.}$isobaric analog state (IAS) population is shown as a continuous curve in Fig. 2(c). A possible contribution of T=1/2 states in ^{7}Li in the reaction in question is shown as the dotted curve in Fig. 2(c). The second curb at ~3.8 MeV in Fig.2(c) is a clear evidence for the IAS of an excited (unknown) state in ^{7}Li. As a summary, we demonstrated two important advantages of the proposed method: (1) its sensitivity to the single-particle strength of the isobaric analog resonances, coupled with (2) insensitivity to the energy resolution of the radioactive nuclear beam. We also showed that our data are incompatible with the results [3] on a low excited stated in ^{7}He, and brought evidence for the $\frac{1}{2}^-$ excited state in ^{7}He at higher excitation energy.

[1] V. Z. Goldberg, in *Proceedings of Exotic Nuclei and Atomic Masses (ENAM98) International Conference*, ed. B. M. Sherrill, D. J. Morrisey, and C. N. Davids (Springer, New York, 1998), p. 319.

[2] G.V. Rogachev *et al.*, Phys. Rev. Lett. **92**, 232502 (2004).

[3] M. Meister *et al.*, Phys. Rev. Lett. **88**, 102501 (2002).

The Structure of ^{12}N Using ^{11}C + p Resonance Scattering

C. Fu, G. Chubarian, V. Z. Goldberg, G. Tabacaru, X. D. Tang, R.E. Tribble, K. Peräjärvi,[1]
G. V. Rogachev,[2] F. Q. Guo,[1, 3] D. Lee,[1,4] D. M. Moltz,[3] J. Powell,[1]
B. B. Skorodumov,[5] B. A. Brown,[6] A. Volya,[2] and Joseph Cerny[1, 3]
[1]*Nuclear Science Division, Lawrence Berkeley National Laboratory, Berkley CA 94720*
[2]*Physics Department Florida State University, Tallahassee, FL 32306*
[3]*Department of Chemistry, University of California, Berkeley, CA 94720*
[4]*Department of Nuclear Engineering, University of California, Berkeley, CA 94720*
[5]*University of Notre Dame, Notre Dame, IN 46556*
[6]*Michigan State University, East Lansing, MI 48824*

Interest in the nuclear structure of ^{12}N (and ^{12}B) is primarily related to the idea that many low-lying levels in ^{12}N (and ^{12}B) should manifest one-particle-one-hole configurations, and therefore their features provide a test (and parameters) for Shell Model (SM) calculations. ^{12}N is more unstable to single particle decay than ^{12}B. Therefore, the nucleon widths of the levels in ^{12}N could provide direct information on their single particle structure.

In addition to the nuclear physics interest, studies involving ^{12}N around its ^{11}C + p threshold at 0.601 MeV are often also driven by nuclear astrophysics interests [4-8]. Namely, to be able to accurately determine the astrophysical rate of the ^{11}C(p,γ)^{12}N reaction, detailed knowledge of the low-lying level structure of ^{12}N is also required. The ^{11}C(p,γ)^{12}N reaction is associated with hot *pp* chains that might be able to bypass the triple alpha process in producing CNO material in low metallicity stars [1]. The ^{12}N excitation region in the vicinity of the ^{8}B + α threshold at 8.008 MeV is also important for astrophysics due to the formation of ^{11}C in the ^{8}B(α,p) reaction [1].

The level structure of ^{12}N has been investigated from 2.2 to 11.0 MeV in excitation energy using a ^{11}C + p resonance interaction with thick (gas and solid) targets and inverse kinematics [2]. The measurements were made at LBNL and TAMU facilities providing for radioactive beams of ^{11}C [3,4]. Excitation functions were fitted using an **R** -matrix approach. Fig.1 presents the R matrix fit to the low energy zero degree data. As a result sixteen levels in ^{12}N were identified, many of them are new. Spin-parity assignments, excitation energies and widths are proposed for these levels. A narrow state with a tentative low spin assignment was found about 200 keV below the ^{8}B + α threshold in ^{12}N.

Conventional **R** -matrix calculations generated cross sections at the highest energies which were too large. We related this effect to the increasing role of direct reactions and took their influence into account by adding imaginary parts (parameterized by a simple expression) to the phase shifts generated by the hard sphere scattering. Generally, the SM predictions were a good guide for the analysis of the lowest excited states. However, at higher excitation energies, the spread of the $d_{3/2}$ strength appeared to be underestimated and the predicted dominant $d_{3/2}$ levels appeared to be shifted to lower energies.

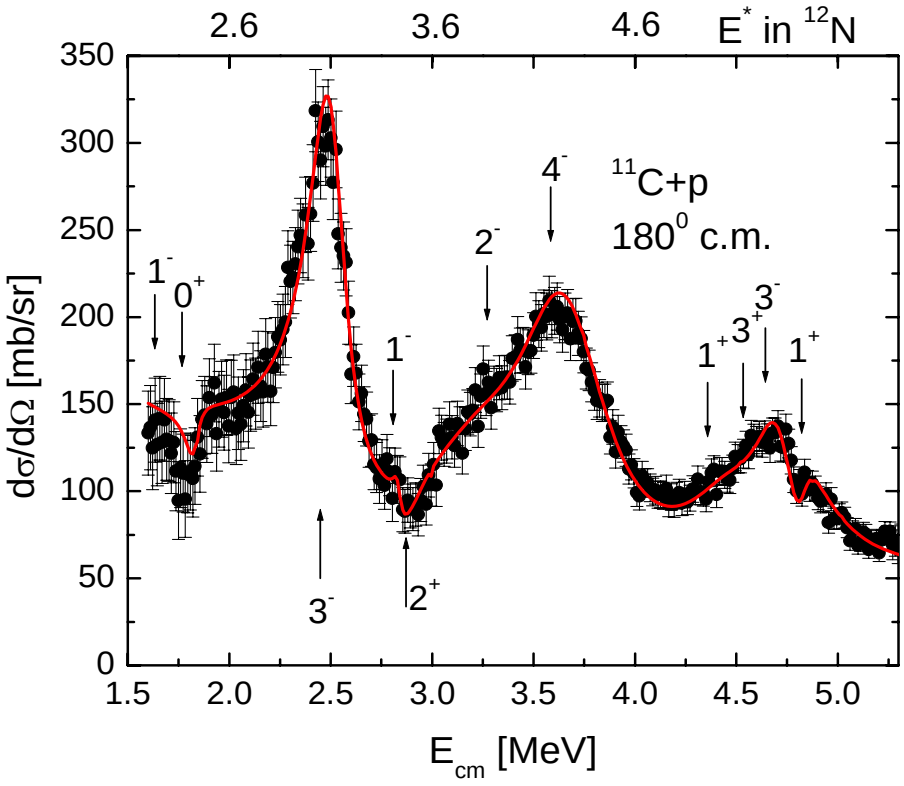

Figure 1. The zero degree (lab.sys.) excitation function and the corresponding *R* –matrix fit. Excitation energy *E** is $E_{c.m.}$ + 0.601 MeV.

[1] M. Wiescher, J. Görres, S. Graff, L. Buchmann, and F.-K. Thielemann, Astrophys. J. **343**, 352 (1989).

[2] V. Z. Goldberg, *Clustering Phenomena in Atoms and Nuclei,* ed. M. Brenner, T. Lönnroth, F. B. Malik, (Springer series In Nucl. and Part. Phys., 1992).

[3] Z. Q. Xie, Rev. Sci. Instrum. **69**, 625 (1998).

[4] R. E. Tribble, A. Azhari, C. A. Gagliardi, J. C. Hardy, A. Mukhamedzhanov, X. Tang, L. Trache, and S. J. Yennello, Nucl. Phys. **A701**, 278c (2002).

Study of ^{18}Ne Structure by ^{14}O+Alpha Elastic Resonance Reaction

C. Fu, V.Z. Goldberg, G.V. Rogachev[1], G.G. Chubaryan, Y. Zhai, T. Al-Abdullah,
L. Trache, G. Tabacaru, A. Banu, and R. E. Tribble
[1]*Department of Physics, Florida State University, Tallahassee, FL 32306*

It is well known that at high temperature the $^{14}O(\alpha,p)^{17}F(p,\gamma)^{18}Ne(\alpha,p)^{21}Na$ reaction sequence can provide a path into rp-process [1]. Therefore reactions involving ^{14}O are important to understand astrophysical processes. Simultaneously data on α cluster structure in N≠Z nuclei are very scarce, and the recent work [2] showed unusual features of α cluster states in these nuclei. To pursue these aims, we obtained a rather intensive beam of ^{14}O (up to 10^6 pps) in the energy range 40-80 MeV using resonances in the ^{14}N+p interaction [3] and MARS facilities [4]. The purity of the ^{14}O beam was better than 99%. The α-^{14}O resonance interaction was studied using Thick Target Inverse Kinematics (TTIK) method [5]. The time of flight method, providing for the possibility of detecting of low energy particles, was used to identify reaction products. However beam contaminations by ^{7}Be and ^{4}He at the level of 10^{-2}-10^{-4} contaminated small angle data. The light from a thin scintillation foil positioned before the entrance to the scattering chamber (Fig.1) was used as a start signal for the time of flight analysis and also its amplitude was analyzed to inhibit the contaminations.

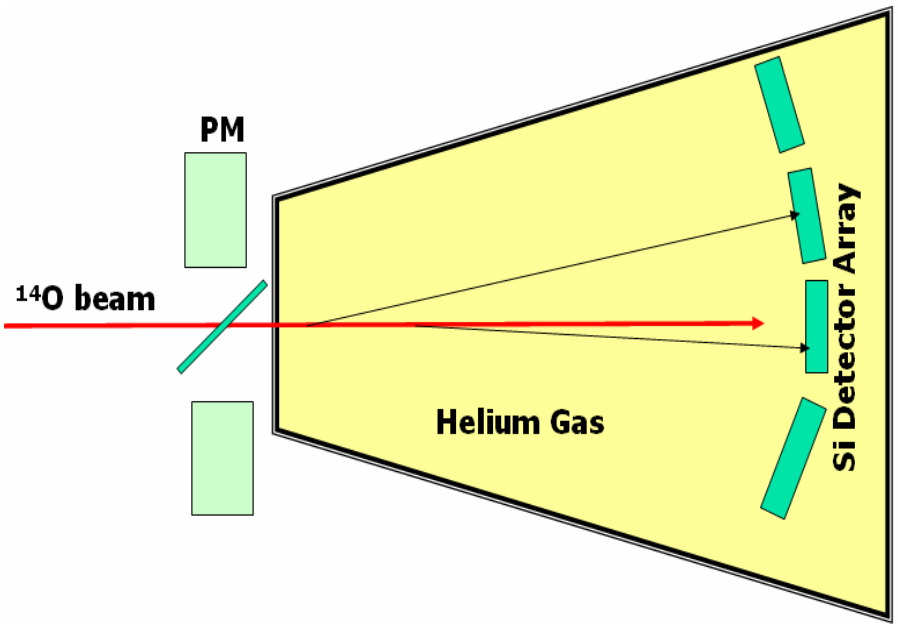

Figure 1. The setup of the experiment

Figures 2 and 3 present two dimensional E-t spectrum and a projection of the α particle banana onto energy axis for an one of 16 Si detectors. The analysis of the results is in progress.

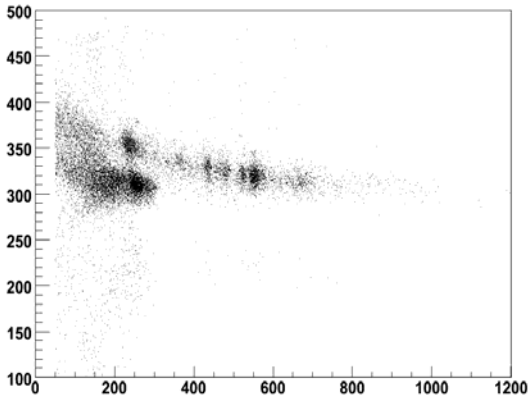

Figure 2. TOF-E spectrum.

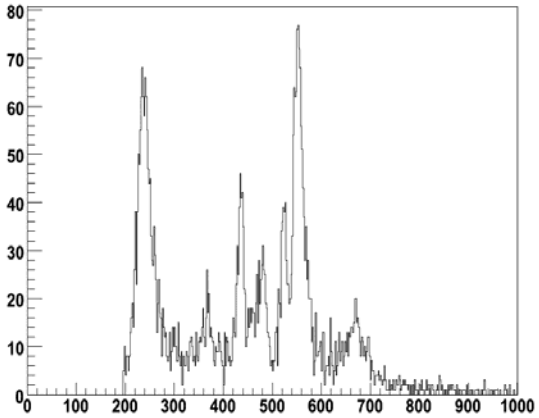

Figure 3. Energy spectrum of alpha particles.

[1] R.K. Wallace and S.E. Woosley, Astrophys. J., Suppl. **45**, 389 (1981).

[2] V.Z. Goldberg *et al.*, Phys. Rev. C **69**, 024602 (2004).

[3] Z. Kovacs *et al.*, Radiochim. Acta 91, 185(2003).

[4] R. E. Tribble *et al.*, Nucl. Phys. **A701**, 278c (2002).

[5] V. Z. Goldberg, *Clustering Phenomena in Atoms and Nuclei*, ed. M. Brenner, T. Lönnroth, F.B. Malik, (Springer Ser. In Nucl. and Part. Phys., 1992).

Superallowed Beta Decay

J.C. Hardy, V.E. Iacob, N. Nica, V.V. Golovko, H.I. Park, J Goodwin, C.A. Gagliardi,
L. Trache, and R.E. Tribble

Superallowed $0^+ \rightarrow 0^+$ beta decay between T=1 analogue states has been a subject of continuous and often intense study for five decades. The *ft* values of such transitions are nearly independent of nuclear-structure ambiguities and depend uniquely on the vector part of the weak interaction. Their measurement gives us access to clean tests of some of the fundamental precepts of weak-interaction theory, and, over the years, this strong motivation has led to very high precision being achieved in both the experiments and the theory used to interpret them. We have a major program at the Cyclotron Institute to study superallowed beta decay.

To obtain the *ft* value for any transition, three quantities must be measured: the half life of the parent, the Q_{EC} value for the transition of interest and the branching ratio for that transition. We produced a complete survey of existing data on these superallowed decays last year [1, 2]. There, all the experimental data for each transition were critically evaluated and final *ft* values obtained; then, small radiative and isospin-symmetry-breaking corrections [3] were applied and a final set of "corrected ft values", denoted $\mathcal{F}$t, were obtained. The results are shown in Figure 1.

Since these corrected $\mathcal{F}$t values are directly proportional to the vector coupling constant, G_V, the bottom panel of the figure demonstrates the constancy of G_V to better than three parts in 10^4, and also limits any possible induced scalar current to $f_S < 0.0013$ in electron rest-mass units. This confirms – to unprecedented precision – two out of three of the necessary consequences of the Conserved Vector Current (CVC) hypothesis. Since the nuclear-structure-dependent corrections, δ_{NS} and δ_C, were determined [3] completely independently of the superallowed decay data, the consistency of the $\mathcal{F}$t values is also a powerful validation of these calculated corrections: obviously they act very well to remove the considerable "scatter" that is apparent in the top panel and is effectively absent in the bottom one, where the corrections have been applied.

Once the consistency of the $\mathcal{F}$t values – and, with them, G_V – has been established, the average value obtained for G_V can be used to test a fundamental principle of the electroweak standard model, the unitarity of the Cabibbo-Kobayashi-Maskawa (CKM) matrix. The up-down element of that matrix, V_{ud}, is given by $V_{ud} = G_V / G_F$, where G_F is the weak interaction constant for the purely leptonic muon decay. The value of V_{ud} is a key component of the most demanding test available for the unitarity of the CKM matrix, the sum of squares of its top-row elements [1], and the possible failure of that test at the 0.35% level has focused considerable experimental attention on another element of the top row, V_{us}, which is determined from kaon decays.

In short, superallowed $0^+ \rightarrow 0^+$ beta decay provides a high-profile application of nuclear-physics measurements to the study of fundamental symmetries, a subject of vital interest to both nuclear and particle physicists.

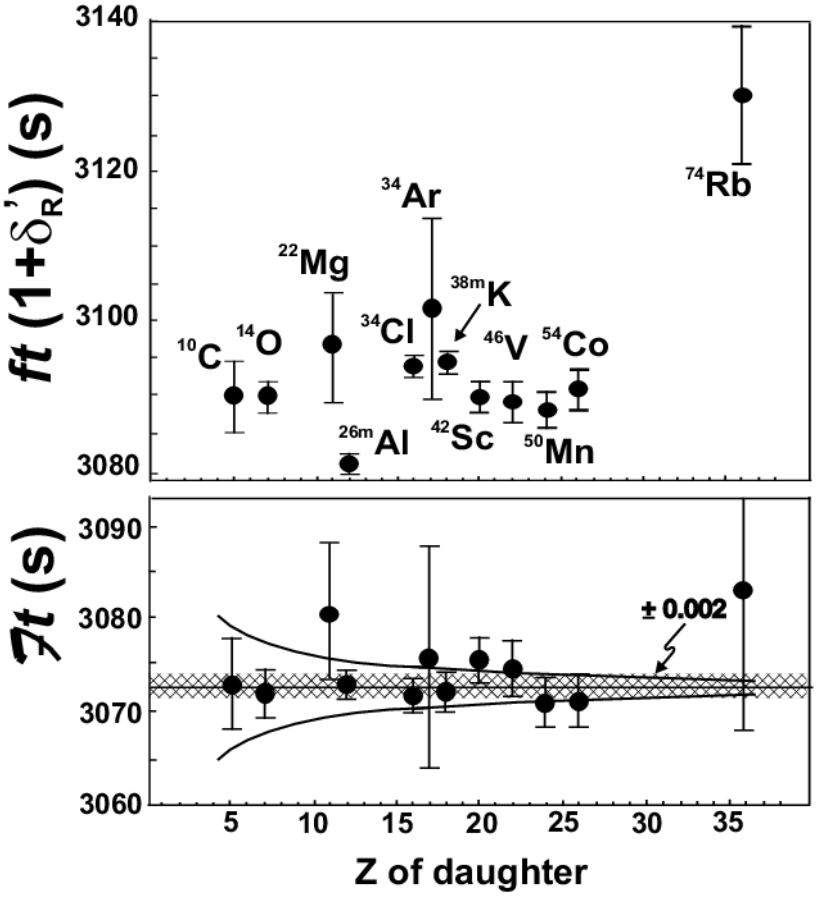

Figure 1. In the top panel are plotted the experimental *ft* values corrected only for δ_R', those radiative corrections that are independent of nuclear structure. In the bottom panel, the corresponding $\mathcal{F}t$ values are given; they differ from the top panel simply by the inclusion of the nuclear-structure-dependent corrections, δ_{NS} and δ_C. The horizontal crosshatched band indicates the average $\mathcal{F}t$ value with its uncertainty. The curved lines show the approximate loci the $\mathcal{F}t$ values would follow if the induced scalar coupling constant were $f_S = \pm 0.002$.

The 2005 survey [1, 2] presented a remarkably consistent picture for the nuclear results, one that naturally challenges us to improve our precision still further in order to better constrain critical weak-interaction parameters. Even though the body of world data already comprises the results of more than 125 individual measurements, it is still possible for well selected experiments to make real improvements. For example, the validation of the nuclear-structure-dependent correction terms can be improved by the addition of new transitions selected from amongst those with large calculated corrections. If the *ft* values measured for cases with large calculated corrections also turn into corrected $\mathcal{F}t$ values that are consistent with the others, then this must verify the calculations' reliability for the existing cases, which have smaller

corrections. Currently at TAMU we are studying the decays of ^{34}Ar [4] and ^{38}Ca for this reason; their precision can certainly be improved, and other new cases with large calculated corrections, such as ^{18}Ne and ^{30}S are planned.

Another area of potential improvement is in the limit set on scalar currents, which is particularly sensitive to the $\mathcal{F}t$ values for ^{10}C and ^{14}O. We are now re-measuring the half-life of ^{10}C [5] and have re-visited an old measurement of the ^{14}O branching ratio [6] with this goal in mind.

Considering the overall quality of world data on superallowed decays, no dramatic surprises were expected as new data appeared. However, last year came our measurement with the CPT Penning trap at Argonne National Lab of the Q_{EC} value of the ^{46}V superallowed beta-decay branch [7]. This was the first time a Penning trap had been used for any of the well-known superallowed transitions and the one chosen was the transition whose Q_{EC} value was least precisely known, with the expectation that it would simply improve the precision of the average. Instead, as can be appreciated from Figure 2, it indeed shrunk the error bars but it also changed the result considerably.

This raised a number of important questions:

- Could there be a systematic difference between on-line Penning-trap and reaction-based measurements? If so, which type of measurement is at fault? (See ref. [8] for a fuller discussion of this issue.)
- If the Penning-trap measurement for ^{46}V is correct, then the most precise previous determination of the Q_{EC} value, from a Munich (^{3}He, t) measurement [9], is seriously in error. Does that mean that the other six Q_{EC} measurements quoted in the same reference should be discarded too? (See Fig. 2.)
- If all the Q_{EC} values in ref. [9] were to be discarded and new Penning-trap results turn out to differ significantly from the remaining reaction results, then the excellent agreement among the $\mathcal{F}t$ values in the lower panel of Fig. [1] might well be destroyed. Will the calculated nuclear-structure-dependent corrections thus prove to be flawed?
- Will all this change the nuclear result for V_{ud}?

Our very recent measurements [10] with the Penning trap, JYFLTRAP, at the University of Jyväskylä appear to have settled the most important of these questions. We confirm the Savard *et al.* [7] result for ^{46}V but also find the Q_{EC} values for ^{42}Sc and ^{26}Al^m agree well with the survey results, which depend entirely on reaction-based measurements. Thus there is no indication of a systematic shift between Penning-trap and reaction measurements. Apparently ^{46}V was an anomalous case, for which only a single dominant measurement had previously been available [9], a measurement that appears simply to have been wrong.

We plan to continue these Q_{EC}-value measurements of superallowed decays with the Penning traps at both Argonne and Jyväskylä. Of particular interest are the cases of ^{50}Mn and ^{54}Co. The survey results for both these cases are strongly influenced by ref. [9] and they could change significantly if the results of that reference were to be eliminated.

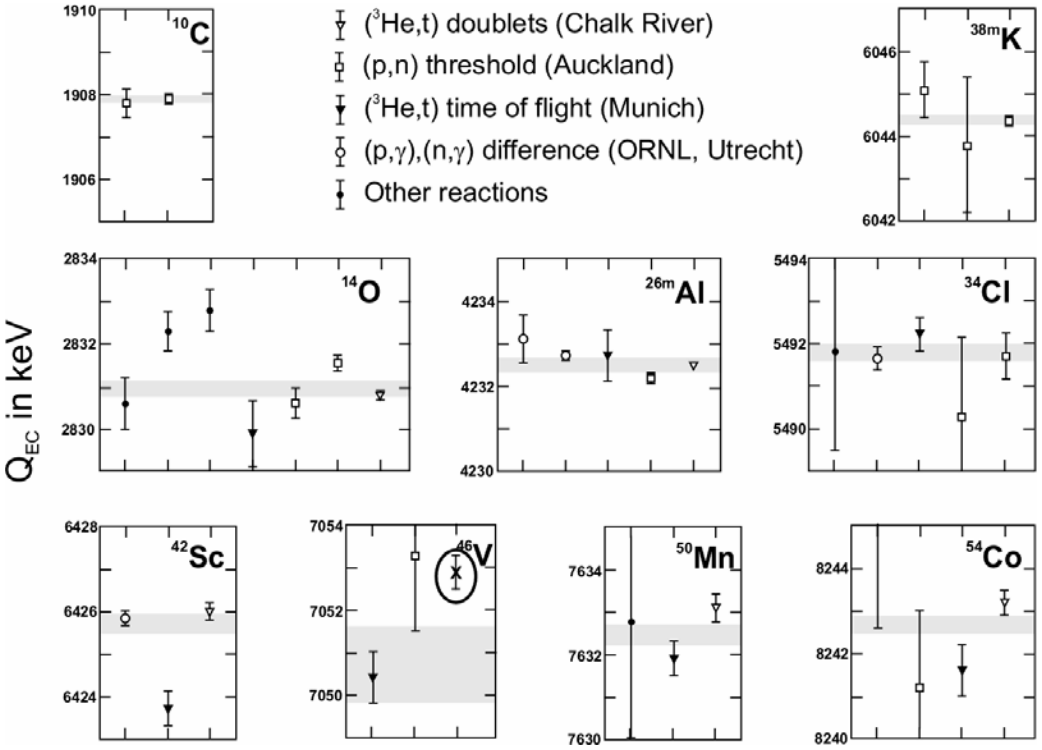

Figure 2. All Q_{EC}-value measurements that contribute to the 2005 survey of world data [1, 2] are plotted in chronological order, and identified by the type of reaction(s) employed. The shaded bands indicats the average values. The only Penning trap measurement is the recent ^{46}V result of Savard et al. [7]; it is indicated by an "X" and is circled.

[1] J.C. Hardy and I.S. Towner, Phys. Rev. C **71**, 055501 (2005).

[2] J.C. Hardy and I.S. Towner, Phys. Rev. Lett. **94**, 092502 (2005).

[3] I.S. Towner and J.C. Hardy, Phys. Rev. C **66**, 035501 (2002).

[4] V.E. Iacob *et al.*, *Progress in Research*, Cyclotron Institute, Texas A&M University (2005-2006), p.I-31.

[5] V.E. Iacob *et al.*, *Progress in Research*, Cyclotron Institute, Texas A&M University (2005-2006), p.I-28.

[6] I.S. Towner and J.C. Hardy, Phys. Rev. C **72**, 055501 (2005).

[7] G. Savard, F. Buchinger, J.A. Clark, J.E. Crawford, S. Gulick, J.C. Hardy, A.A. Hecht, J.K.P. Lee, A.F. Levand, N.D. Scielzo, H. Sharma, I Tanihata, A.C.C. Villari and Y. Wang, Phys. Rev. Lett. **95**, 102501 (2005).

[8] J.C. Hardy, I.S. Towner and G. Savard, Int. J. Mass Spectrometry, **251**, 95 (2006).

[9] H. Vonach *et al.*, Nucl. Phys. **A278**, 189 (1977).

[10] J.C. Hardy, *Progress in Research*, Cyclotron Institute, Texas A&M University (2005-2006), p. I-36; and T. Eronen, V. Elomaa, U. Hager, J. Hakala, A. Jokinen, A. Kankainen, I. Moore, H. Penttilä, S. Rahaman, A. Saastamoinen, T. Sonoda, J. Äystő, J.C. Hardy and V. Kolhinen, to be published.

Precise Half Life Measurements: the Case of ^{10}C

V.E. Iacob, V. Golovko, J. Goodwin, J.C. Hardy, N. Nica, H.I. Park, L. Trache, and R.E. Tribble

The half-life of ^{10}C was measured as part of our program to test the unitarity of the Cabibbo-Kobayashi-Maskawa (CKM) matrix via $0^+ \rightarrow 0^+$ superallowed β transitions; the case of ^{10}C is of particular interest because of its higher sensitivity to the presence of scalar currents [1]. The ^{10}C half-life has been measured twice before, with precisions of 0.10% [2] and 0.08% [3]. With our current techniques, we anticipate being able to improve that precision by more than a factor of two.

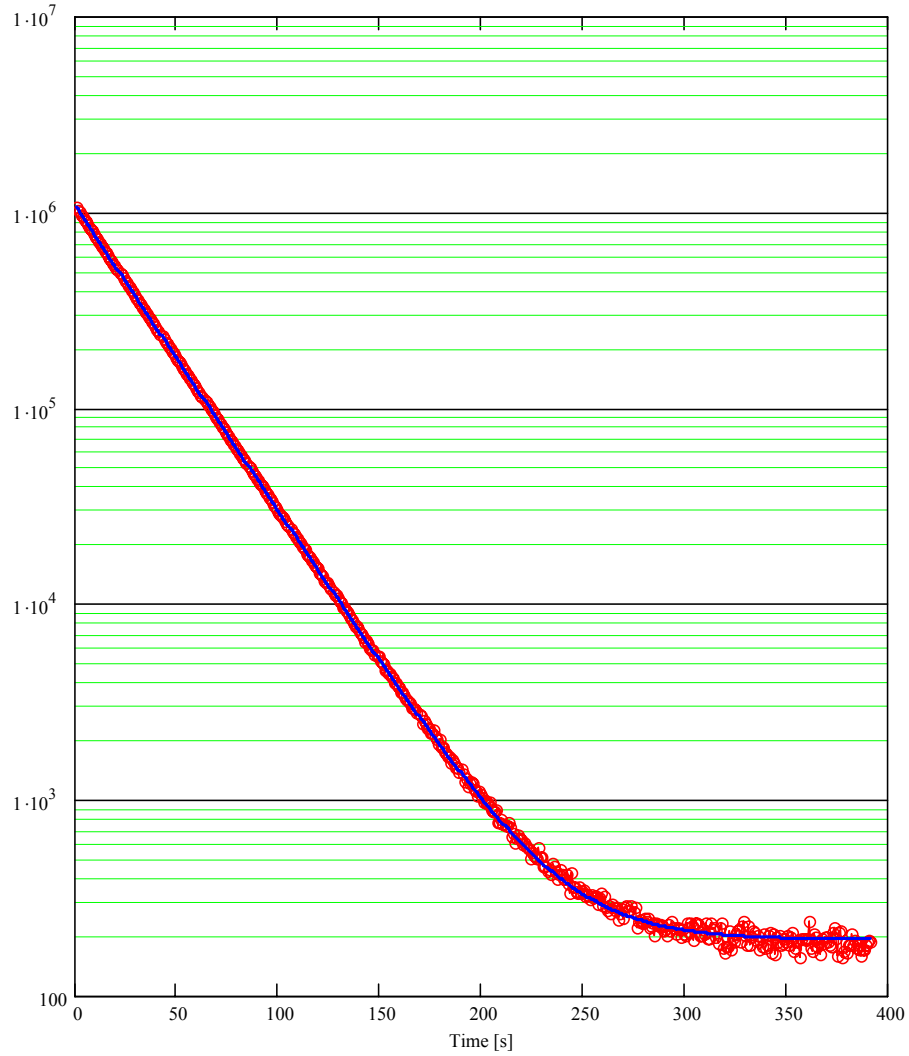

Figure 1. Total decay spectrum observed in the β-decay of ^{10}C.

To obtain ^{10}C, we used a ^{11}B beam primary beam at 23*A* MeV from the cyclotron to bombard a cryogenic hydrogen target pressurized to 1.5 atm. From the reaction products, a high purity ^{10}C

radioactive beam at 18.5*A* MeV was separated by the MARS spectrograph. This beam was then extracted into air, passed through a 0.3-mm-thick BC-404 plastic scintillator and a set of Al degraders optimized to stop the ^{10}C nuclei at the center of the 76-μm-thick aluminized mylar tape of our fast tape-transport system. We collected ^{10}C nuclei for 10, 15 or 20s; then the beam was switched off and the activity was moved 90cm in 180ms to the center of a 4π proportional gas counter located in a well shielded region. The observed decay positrons were then multiscaled over a 400s time span. Such collect-move-detect cycles were repeated until we had collected more than 4×10^7 decays. The total decay spectrum obtained in this experiment is presented in Fig. 1.

To ensure an unbiased result, we split the experiment into 20 different runs, each differing from the others in their discriminator threshold (150, 200 and 250mV), detector bias (2450, 2550 and 2650V) or dominant dead-time (3, 4 and 6μs) setting. As long-lived impurities could alter the deduced result for

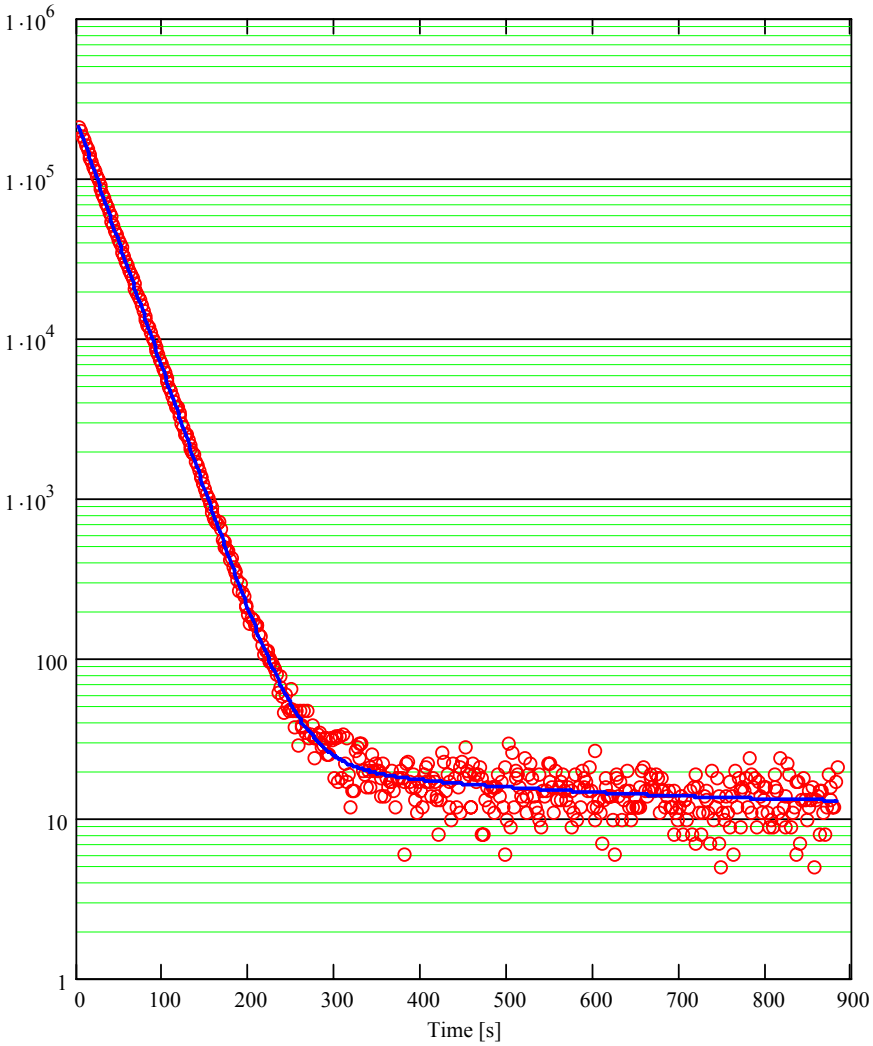

Figure 2. Evidence for the presence of ^{28}Al (caused by neutron activation of ^{27}Al) in the ^{10}C experiment: $t_{1/2}(^{28}\text{Al}) = 134.5$s

^{10}C, we also performed a run with 60s-0.180s-900s collect-move-detect time settings. The total decay spectrum obtained in this run is presented in Fig. 2. It became obvious from the slight slope between 300 and 900s that we do have a second, long-lived component in the spectrum. Analysis revealed that this came from 134.5-s ^{28}Al, which undoubtedly originated from neutron capture on ^{27}Al, a material present both in our support structures and as a coating on our mylar tape. Adjusting for the different collect-move-detect times in this run, we determined that, for the first channel of our usual decay spectrum, the ^{28}Al impurity was at the level of 2.5×10^{-4} as compared to the main ^{10}C component. We take account of this impurity in our analysis.

As a further test of the consistency of our results, we have re-done the fits over subsets of events: we removed the first few channels in the acquired spectra, thus eliminating (or at least diminishing) the contribution of any possible short-lived impurity and/or reducing possible rate-dependent counting losses. The results are presented in Fig. 3. As can be seen, the half-lives obtained for all different subsets are statistically consistent with one another, thus giving no indication of unidentified short-lived impurities or any rate-dependent counting losses. Our preliminary result for the half-life of ^{10}C is 19.313(10)s. When the analysis is complete, we expect a further reduction in the uncertainty. As it stands, our result agrees with, but is already more precise than, the previously accepted (average) value, 19.290(12)s.

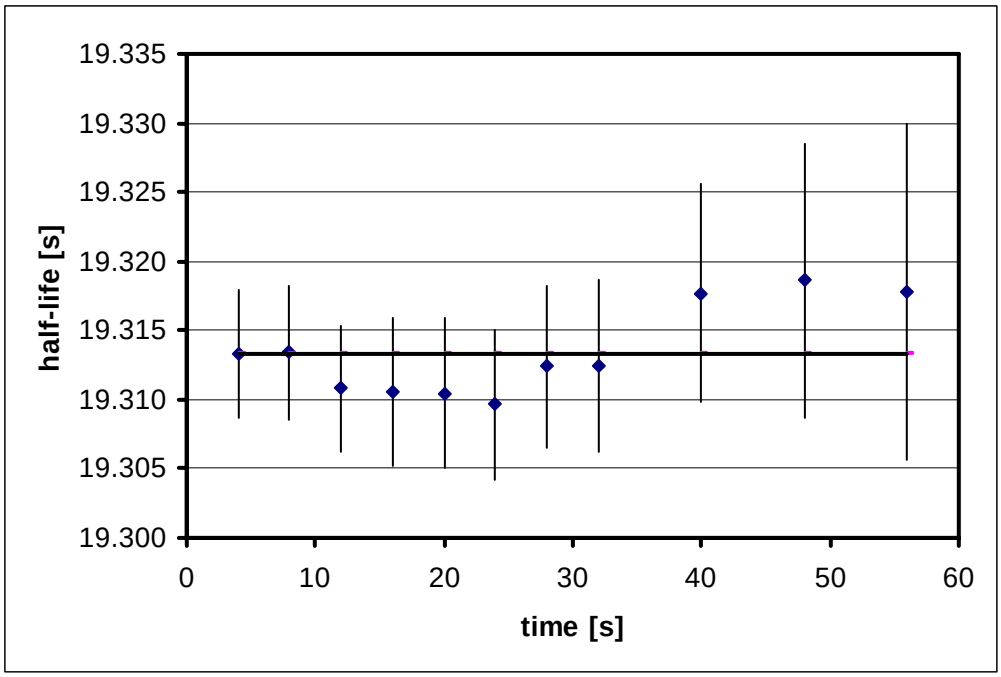

Figure 3. Test for possible systematic errors in the extracted half-life of ^{10}C caused by unidentified short-lived impurities or by rate-dependent counting losses. The abscissa represents the time interval at the beginning of the detecting-time for which the data were eliminated from the fit.

[1] J.C. Hardy and I.S. Towner, Phys. Rev. C **71**, 055501 (2005).

[2] G. Azuelos, J.E. Crawford and J.E. Kitching, Phys. Rev. C **9**, 1213 (1974).

[3] P.H. Barker and G.D. Leonard, Phys. Rev. C **41**, 246 (1990).

Precise Half-Life of the Superallowed β^+ Emitter ^{34}Ar

V.E. Iacob, J.C. Hardy, C.A. Gagliardi, V.E. Mayes, N. Nica, G. Tabacaru,
L. Trache and R.E. Tribble

As part of our program of precise measurements aimed at testing the Standard Model *via* the unitarity of the Cabibbo-Kobayashi-Maskawa(CKM) matrix, we have determined the half-life of the superallowed $0^+ \rightarrow 0^+$ β^+ emitter ^{34}Ar. This is a particularly difficult case since the daughter of this decay, ^{34}Cl, is itself radioactive with a half-life only about a factor of two longer than that of ^{34}Ar. Since we measure decay positrons, we are unable to distinguish between the parent and daughter activities, and the composite activity decays with what is very nearly a single component, a component that exhibits the half-life of the daughter! As a result, our first attempt to measure the ^{34}Ar half-life [1] yielded the value 847.0(37) ms, a result quoted with a precision of only 0.43%.

For a measurement to be meaningful in the context of a CKM unitarity test, it must achieve a precision of better than 0.1%. We therefore took considerable pains to refine our methods and last year we reported the development of a new technique that yields higher precision for such parent-daughter decays [2]. We report here a new measurement of the ^{34}Ar half-life, which preliminarily quotes a precision of ~0.1% and is expected to be improved still further in final analysis.

In the experiments analyzed with the novel technique, a high-purity (>99.3%) radioactive beam of ^{34}Ar was produced *via* the ^{1}H(^{35}Cl,2n)^{34}Ar reaction on an LN_2-cooled hydrogen gas target, and separated in the MARS spectrometer. The ^{34}Ar ions were collected in the 76μm-thick mylar tape of our fast tape-transport system, having passed first through a plastic scintillator (to measure the production rate) and a stack of aluminum degraders. The ^{34}Ar activity was collected for either 0.7s or 1s. At the end of this collection time the beam was switched off and the collected activity was moved 90 cm in 180 ms by the tape-transport system to a 4π proportional gas counter located in a low background region. The counter signals were then multiscaled for a period of 12s, yielding a 500-channel decay spectrum.

We collected about 400 million decay events, from both ^{34}Ar and its ^{34}Cl daughter. The experimental data were split into 64 separate runs, differing only in their detection parameters: dominant dead-time (ranging from 3 to 12 μs), detector bias (ranging from 2400 to 2700V) and discrimination threshold (150 or 200mV). The separate analysis of these individual runs allowed us to assess the uncertainty on the final result. Fig. 1 presents the half-life results run-by-run, with the various detector biases and discrimination thresholds identified for each. No systematic trend appears.

The constrained fitting method introduced and described in Ref. [2] takes account of the complete history of the decaying nuclei, including the initial production rate of the radioactive sample. In our case, the use of a cooled gas target with a pulsed accelerator beam led to a slight non-uniformity in the measured production rate at the beginning of each collection period (see Fig. 2). The characteristic shape of the production-profile requires a numerical integration for every collect-move-detect cycle in order to determine correctly the ratio of the ^{34}Ar to ^{34}Cl nuclei at the beginning of the detection time.

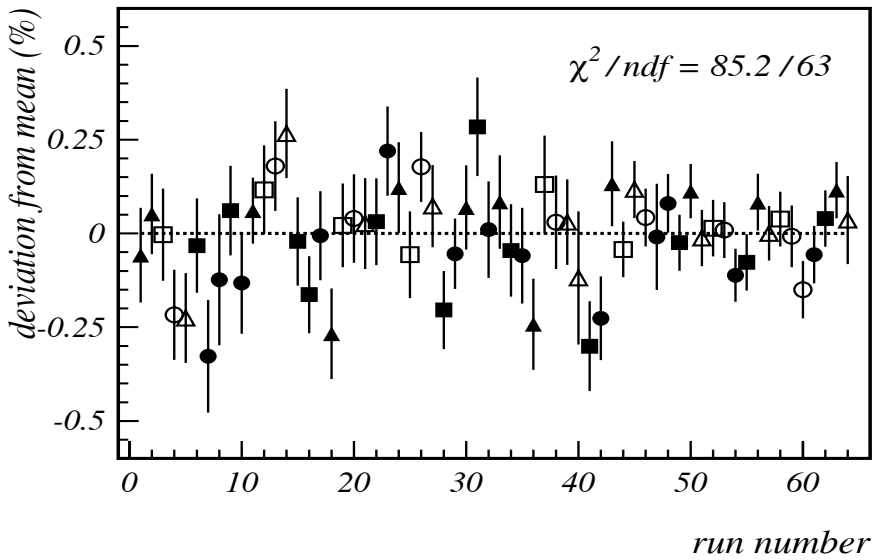

Figure 1. Values for the ^{34}Ar half-life obtained from each run, coded to indicate the specific acquisition parameters – discriminator threshold or detector bias – pertaining to each. Full/open symbols represent the two 150mV/200mV discriminator settings; circles/squares/triangles represent respectively the detection biases 2400V/2550V/2700V. The first 40 runs contain about 180 million events while the last 24 runs contain about 220 million events.

Our preliminary result for the ^{34}Ar half-life is 843.8(9) ms; we anticipate that the final analysis will drop the uncertainty significantly below 0.1%. The reported uncertainty contains the statistical error,

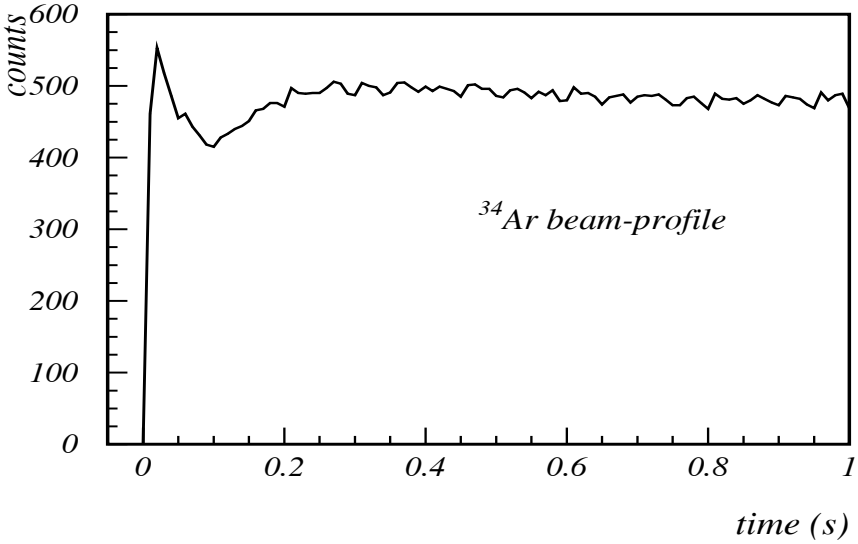

Figure 2. Typical radioactive-beam production-rate profile. The initial drop in production rate is generated by the lowering of the gas density along the beam path as the primary beam heats up the gas. A fan located inside the gas-target helps equalize the heat rapidly, leading to the plateau evident after 0.2 s.

the uncertainty in the half life of the daughter nucleus ^{34}Cl, the scatter associated with the dead-time corrections, the uncertainty in the impurity levels, the uncertainty due to the beam profile, the scatter associated with the discriminator thresholds, and the scatter in the results obtained from the various experiments. The result agrees with, but is four times more precise than, the currently accepted value [3], which was obtained more than 30 years ago.

[1] V.E. Mayes *et al.*, *Progress in Research*, Cyclotron Institute, Texas A&M University (2000-2001), p. I-28.

[2] V. E. Iacob, *et al.*, *Progress in Research*, Cyclotron Institute, Texas A&M University (2004-2005), p. I-21.

[3] J.C. Hardy, H. Schmeing, J.S. Geiger, and R.L. Graham, Nucl. Phys. **A223**, 157 (1974).

Mass Measurements and Superallowed Beta Decay

J.C. Hardy, I.S. Towner,[1] and G. Savard[2]
[1]*Queen's University, Kingston, Ontario, Canada and Cyclotron Institute, Texas A&M University, College Station, TX*
[2]*Physics Division, Argonne National Laboratory, Argonne, IL 60439 and Department of Physics, University of Chicago, Chicago, IL 60637*

The recent CPT Penning-trap measurement of the Q_{EC} value for the superallowed decay of ^{46}V [1] disagreed significantly with the previously accepted value [2], a survey result principally based on a 30-year-old (^{3}He,t) Q-value measurement by Vonach et al. [3]. Since this result reduced the consistency among the $\mathcal{F}t$ values for the nine most precisely characterized T=1 superallowed beta emitters, it raised the possibility of a systematic discrepancy between *on-line* Penning-trap measurements and the reaction-based measurements upon which Q_{EC} values depended in the past.

We have carefully re-analyzed (n,γ) and (p,γ) reaction measurements in the $24 \leq A \leq 28$ mass region, and compared the results to very precise *off-line* Penning-trap measurements of the stable nuclei ^{24}Mg, ^{26}Mg and ^{28}Si [4]. Since the Penning-trap results are quoted to 13, 32 and 1.9 eV, respectively, we consider them to be free of systematic problems at the ~100 eV level, which concerns us here. From our comparison, we conclude that if any systematic differences exist between *off-line* Penning-trap and individual (n,γ) measurements, they must be less than 100eV. For (p,γ) reactions the limit is not so small: in that case, we conclude that any systematic differences must be less than 200 eV.

Based on well-founded (n,γ) and (p,γ) reactions, we then established two values for the mass excess of ^{26}Al, -12210.27(11) keV and -12210.21(22) keV. The first value does not include any provision for possible systematic effects in the reaction measurements on which it is based; the second value includes such provisions. We proposed that these two values together provide a critical standard for reaction-based results, against which a future on-line Penning-trap mass measurement could be compared. If the Penning-trap result were to lie within the limits of our first value (the one uncorrected for possible systematic effects), then one could be reasonably confident that actual systematic effects are below the upper limits we set; in that case Penning-trap measurements, when they proliferate, could simply be averaged in with the earlier reaction-based results. If the Penning-trap result were to lie outside the limits of our first value but inside the limits of our second value (adjusted for systematics), then one must suspect that reaction measurements in general might suffer from undiagnosed systematic effects; wherever their quoted uncertainties are in the few-hundred-eV region, they would need to be increased accordingly.

Finally, if the Penning-trap result were to lie outside the range of even our systematics-adjusted result, then that could be a sign of serious systematic difficulties, which could call into question all reaction-based measurements of superallowed transition energies or, conversely, could cast doubt on the precision of on-line Penning-trap measurements of radioactive isotopes. This would require serious and urgent attention, particularly in the evaluation of superallowed beta decay and its associated weak-interaction tests.

Since this work was published [4], we have measured the mass of ^{26}Al with the JYFLTRAP Penning-trap facility at the University of Jyväskylä cyclotron facility [5]. This is the first time it has been measured with a Penning trap. Our result, -12209.95(16) keV, does not differ significantly from either of the values we offer as a test; however, it certainly agrees more nearly with the systematics-adjusted value. We cannot therefore exclude systematic differences of up to ~100 eV between reaction-based and *on-line* trap measurements but anything significantly greater is ruled out. This conclusion is further supported by our Penning-trap Q_{EC}-value measurement for ^{42}Sc [5], which agrees well with the most precise previous result obtained from (n,γ) and (p,γ) reaction Q values [2].

We conclude that new Penning-trap Q_{EC} -value measurements, when they appear, can safely be averaged on an equal footing with previous reaction-based results. To date, on-line Penning-trap results are being quoted with uncertainties comparable to the best of the earlier measurements, so no large changes should be expected in the resultant averages. Evidently the discrepancy found in the case of ^{46}V was due simply to a 30-year-old experimental mistake, not to some widespread systematic problem.

[1] G. Savard, F. Buchinger, J.A. Clark, J.E. Crawford, S. Gulick, J.C. Hardy, A.A. Hecht, J.K.P. Lee, A.F. Levand, N.D. Scielzo, H. Sharma, I Tanihata, A.C.C. Villari and Y. Wang, Phys. Rev. Lett. **95**, 102501 (2005).

[2] J.C. Hardy and I.S. Towner, Phys. Rev. C **71**, 055501 (2005).

[3] H. Vonach *et al.*, Nucl. Phys. **A278**, 189 (1977).

[4] J.C. Hardy, I.S. Towner and G. Savard, Int. J. Mass Spec. **251**, 95 (2006).

[5] T. Eronen, V. Elomaa, U. Hager, J. Hakala, A. Jokinen, A. Kankainen, I. Moore, H. Penttilä, S. Rahaman, A. Saastamoinen, T. Sonoda, J. Äystő, J.C. Hardy and V. Kolhinen, (to be published).

JYFLTRAP : Q-Values of the Superallowed Decays of $^{26}Al^{m}$, ^{42}Sc and ^{46}V

J.C. Hardy

A new collaboration has been formed based on the JYFLTRAP at the University of Jyväskylä cyclotron facility. As with our CPT collaboration, the goal of this group is to measure atomic masses related to superallowed β decay. Since a recent measurement by the Canadian Penning Trap (CPT) Mass Spectrometer [1] reported a result for the Q_{EC} value of the superallowed transition from ^{46}V that disagrees significantly with previous reaction-based measurements, concern has arisen that there might be undetected systematic errors either in the reaction measurements or in the on-line Penning-trap ones [2]. If this were the case, it could potentially lead to a significant shift in the value of V_{ud} extracted from the superallowed decays [3]. Although masses are ultimately measured at JYFLTRAP with a Penning trap, the production beams, delivery system and many other aspects of that system are quite different from those at the CPT facility. If measurements from both systems prove to be in agreement with one another, then at least some potential sources of systematic errors can be eliminated.

So far, we have completed measurements of the Q_{EC} values for $^{26}Al^{m}$, ^{42}Sc and ^{46}V and have prepared a manuscript for publication [4]. All ions of interest were produced at the IGISOL facility. We produced ^{46}V and $^{26}Al^{m}$ via (p, n)-reactions, with 20- and 15-MeV proton beams incident on enriched ^{46}Ti and ^{26}Mg targets respectively. For ^{42}Sc, we used a ^{3}He beam of 20 MeV on natural calcium. In these bombardments, not only were the superallowed emitters of interest produced in the primary reactions but ions from the target material itself – the beta-decay daughters of these emitters – were also released by elastic scattering of the cyclotron beam. All recoil ions were slowed down and thermalized in the gas cell of an ion guide filled with 150 mbar of helium. These ions were then transported by gas flow and electric fields through a differentially pumped electrode system into a high-vacuum region, accelerated to 30 keV and passed through a 55^{o} dipole magnet for a coarse mass selection with resolving power of 300-500.

The mass-separated ion beam was then transferred to the JYFLTRAP setup, which consists, first, of a radio-frequency quadrupole (RFQ) cooler used to improve the quality of the beam and bunch it for efficient injection into the Penning-trap system. The latter consists of two cylindrical traps housed inside the same superconducting 7-T magnet. The first trap is filled with helium buffer gas to allow for purification of the ion sample (mass resolving power up to a few times 10^{5}). The second Penning trap is where the actual mass measurement is made. A dipole excitation is used to establish a magnetron orbit with a fixed frequency and amplitude. Then, the ion cloud is exposed to a radiofrequency quadrupole electric field for a given time. The amplitude of the RF electric field is tuned so that, when the frequency corresponds to the cyclotron frequency of the ion of interest, the whole magnetron motion is converted to cyclotron motion. After the quadrupole excitation, the ions are extracted from the trap and their time-of-flight to a micro channel plate detector recorded. The frequency corresponding to the shortest time-of-flight is the true cyclotron frequency. To locate the precise resonance frequency, we scanned the frequency and recorded the time of flight over a range that spanned the resonance.

The Q_{EC} value of each ion of interest was obtained directly from the frequency ratio of the mother and the daughter nuclei. The cyclotron frequency measurements were interleaved: first we recorded a frequency scan for the daughter, then for the mother, then for the daughter and so on. This way, the slow

drift of the magnetic field, mostly due to drifts in the room temperature, could be treated properly by interpolation of the reference frequency to the time of measurement for the ion of interest. For each measurement, data were collected in several sets, each comprising ~10 pairs of parent-daughter frequency scans taken under the same conditions. Between sets, the excitation time was changed. Each of the resonance curves was fitted with a realistic function, which yielded values for the resonant frequency and its statistical uncertainty. Our results are given in Table I.

Table I. Q_{EC} values obtained from this measurement, compared with values from our 2005 survey of world data [3], and our subsequent CPT measurement [1].

Parent nucleus	Present result	2005 Survey value [3]	Savard *et al.* [1]
$^{26}Al^{m}$	4232.83(13)	4232.55(17)	--
^{42}Sc	6426.13(21)	6425.63(38)	--
^{46}V	7052.72(31)	7050.71(89)	7052.90(40)

There are three important conclusions we can draw from our results. First, we confirm our recent CPT measurement [1] of the ^{46}V Q_{EC} value, which disagrees with the previously accepted value [3]. The latter was a survey result principally based on a 30-year-old (^{3}He,t) Q-value measurement by Vonach et al. [5]. Second, since our results for $^{26}Al^{m}$ and ^{42}Sc agree well with the survey values, we can effectively rule out widespread systematic differences of more than ~100 eV between reaction-based Q-value measurements and those obtained with an on-line Penning trap (see ref. [2] for an elaboration of this point). Finally, we can conclude that no significant shift in the value of V_{ud} should be anticipated as more and more on-line Penning-trap measurements of the superallowed Q_{EC} values become available. Apparently ^{46}V was an anomalous case, for which only a single dominant measurement had previously been available [5], a measurement that appears simply to have been wrong.

We plan to continue these measurements to other superallowed decays.

[1] G. Savard, G. Savard, F. Buchinger, J.A. Clark, J.E. Crawford, S. Gulick, J.C. Hardy, A.A. Hecht, J.K.P. Lee, A.F. Levand, N.D. Scielzo, H. Sharma, I Tanihata, A.C.C. Villari and Y. Wang, Phys. Rev. Lett. **95**, 102501 (2005).

[2] J.C. Hardy, I.S. Towner and G. Savard, Int. J. Mass Spec. **251**, 95 (2006).

[3] J.C. Hardy and I.S. Towner, Phys. Rev. C **71**, 055501 (2005).

[4] T. Eronen, V. Elomaa, U. Hager, J. Hakala, A. Jokinen, A. Kankainen, I. Moore, H. Penttilä, S. Rahaman, A. Saastamoinen, T. Sonoda, J. Äystő, J.C. Hardy and V. Kolhinen, (to be published).

[5] H. Vonach *et al.*, Nucl. Phys. **A278**, 189 (1977).

Canadian Penning Trap: Q-Values of Superallowed Beta Transitions

J.C. Hardy

The collaboration based on the Canadian Penning Trap (CPT) Mass Spectrometer has continued to measure atomic masses related to superallowed β decay. Our result for the Q_{EC} value of ^{46}V, 7052.90(40) keV, which was reported in last year's Annual Report, has recently been published [1]. It was the first Penning-trap measurement of the Q_{EC} value of a "well known" superallowed transition and it disagrees significantly with the previously accepted value of 7050.71(89) keV, a survey result [2] principally based on a 30-year-old measurement [3] of the ^{46}Ti (^{3}He,t) ^{46}V reaction Q-value. Since the Q_{EC} values for all the best known superallowed transitions are currently based on reaction measurements, this raised concern [4] that there could be a previously undetected systematic error in all reaction measurements which, when corrected, might lead to a significant shift in V_{ud} from the value obtained in the survey.

In the past year, the collaboration has measured masses from which the Q_{EC} values for ^{10}C, ^{14}O, ^{26}Al^{m}, ^{34}Cl, ^{38}K^{m} and ^{42}Sc will be extracted. The data are still being analyzed.

[1] G. Savard, F. Buchinger, J.A. Clark, J.E. Crawford, S. Gulick, J.C. Hardy, A.A. Hecht, J.K.P. Lee, A.F. Levand, N.D. Scielzo, H. Sharma, I Tanihata, A.C.C. Villari and Y. Wang, Phys. Rev. Lett. **95**, 102501 (2005).

[2] J.C. Hardy and I.S. Towner, Phys. Rev. **C71**, 055501 (2005).

[3] H. Vonach *et al.*, Nucl. Phys. **A278**, 189 (1977).

[4] J.C. Hardy, I.S. Towner and G. Savard, Int. J. Mass Spec. **251**, 95 (2006).

Further Tests of Internal-Conversion Theory with Precise γ- and x-Ray Spectroscopy: the Decays of $^{134}Cs^{m}$, ^{137}Ba

N. Nica, J.C. Hardy, V.E. Iacob, H.I. Park, J. Goodwin, W.E. Rockwell, and M.B. Trzhaskovskaya[1]
[1]*Petersburg Nuclear Physics Institute,Gatchina 188300, Russia*

Internal conversion plays an important role in the assignment of spins, parities and radiation intensities, as well as in the building of level and decay schemes. After more than fifty years of theory and experiment the overall agreement between calculated internal-conversion coefficients (ICC's) and measured ones has now reached ~1%. This rather optimistic conclusion emerged from a comprehensive study published in 2002 by Raman *et al.* [1], in which various methods for calculating ICC's were reviewed and the results from each were compared with one hundred selected transitions whose experimentally determined ICC's were claimed to 5% precision or better. Of the various calculations examined, the best agreement with experiment was obtained by the "Relativistic Dirac-Fock" approach; surprisingly, though, the data showed a slight preference for a version of that calculation which completely ignored the presence of the atomic hole created by the conversion process. Since simple physical considerations show that the typical time for an electron to leave the atom is less than ~10^{-18} s, while the K-shell filling time is at least an order of magnitude longer (10^{-17} - 10^{-15} s depending on Z) [2], one should expect the presence of the hole to have a non-negligible impact on the wave function of the outgoing electron, at least in cases where the transition energy is just above the atomic-shell binding energy and thus the electron energy is low.

Even so, it was decided at the time to adopt the calculations that appeared to agree best with experiment even though they incorporated a "non-physical" assumption, and the most recent published ICC tables [3], as well as the Evaluated Nuclear Structure Data Files (ENSDF) maintained by the National Nuclear Data Center (NNDC) at Brookhaven, used the "no hole" approximation. Being readily available and pre-evaluated, ENSDF in particular is intensively used by scientists and technologists, usually without any further critical judgment. Consequently, it is clearly important that the validity of the ICC calculations used throughout ENSDF be firmly established since significant differences in calculated ICC coefficients can arise depending on whether the atomic hole is included or not. As was originally pointed out by Raman *et al.* [1], there are cases where differences of up to 10% can be expected.

Two years ago we reported a precise measurement of the K-shell conversion coefficient for the 80.2 keV, M4 transition in $^{193}Ir^{m}$ [4], a case originally suggested by Raman *et al.* [1] as providing the most sensitive test of the importance of the atomic hole. Our measurement, α_K=103.0(8), showed unequivocal agreement with the calculation that includes the "hole," α_K=103.5(1), and disagreement with the "no-hole" result, α_K=92.0(3). Based on our result, NNDC changed its policy and adopted the ICC values calculated with the atomic hole included; the consequent change in the ENSDF data files has had considerable impact on the nuclear-data users community.

At Texas A&M we have continued to make precise ICC measurements with the goal of further testing and possibly refining the ICC calculations. We have begun by re-examining those cases in the Raman *et al.* survey [1] that disagree significantly with both types of calculations. We seek to determine

whether these cases signal further problems with the theory or are simply experimental aberrations. We report here the re-measurement of two such transitions, in $^{134}Cs^{m}$ and ^{137}Ba.

Our method is to determine the K-shell conversion coefficient, α_K, for a single transition by measuring the peak areas of its K x-rays and γ ray (N_K, N_γ) as determined in a single well-calibrated HPGe detector. We obtain α_K from the formula $\alpha_K\omega_K = N_K/N_\gamma \times \varepsilon_\gamma/\varepsilon_K$, where ε_K and ε_γ are the detector efficiencies and ω_K is the fluorescence yield. We take ω_K from reference [5], which presents a global fit to experimental data and quotes a precision of better than 0.5% for the ω_K values tabulated for Cs and Ba. (We have previously verified experimentally the table's ω_K value for iridium [6].) Our biggest asset in these measurements is the very well known efficiency of our HPGe detector. It has been determined to a precision of 0.15% (relative) and 0.2% (absolute) for energies between 50 and 1400 keV [7,8].

The K x-ray energies for Cs and Ba lie in the 30-35 keV range, however, where our efficiency is not so precisely known since any photon groups available for calibration below 50 keV are themselves x-rays whose quoted intensities depend on ICC calculations. For this reason, in the present test we focus on the ratio of the α_K's for the two transitions studied. Since the K x-rays for Cs and Ba are within 1.3 keV in energy, the detector efficiencies, ε_K, for the two transitions virtually cancel out in the ratio, removing the effects of any imprecision in their individual values.

Our method is only applicable to level schemes in which a single transition converts in the K shell, a demand well satisfied in this study. The ^{137}Cs β^- decay is followed by a single 661.7-keV transition in the ^{137}Ba daughter, and the $^{134}Cs^{m}$ isomer decays predominantly (99%) by a 128-keV transition, which is followed by an 11-keV transition that is well below the K-shell binding energy.

In the case of 30-year ^{137}Cs we took advantage of a 100% pure and attenuation-free (virtually coverless) source purchased from Isotopes Products Laboratory. The $^{134}Cs^{m}$ case was more challenging since it is rather short lived (2.9 h) and we had to prepare our own source. We used 99.999% pure CsCl and $CsNO_3$ (other chemicals were also tested and rejected) and deposited 0.10-0.15-μm uniform layers on thin mylar. Calculations were done to determine the optimum thickness and to study the influence of thickness variations. Because the chemicals are hygroscopic, we used vacuum evaporation and manipulation in a dry nitrogen atmosphere. We then checked the layers with a microscope. The prepared sources were irradiated in the TRIGA reactor at the Texas A&M Nuclear Science Center by a thermal neutron flux of $\sim 7\times10^{12}$ n/cm^{2}s. The sources were sealed with thin kapton tape after activation.

Spectra were recorded from these $^{134}Cs^{m}$ sources, as well as from the long-lived ^{137}Cs source. The $^{134}Cs^{m}$ sources were also studied long after their original irradiation in order to look for impurities. In addition, spectra from ^{109}Cd, ^{133}Cs, ^{137}Ba, and ^{241}Am sources were taken to help us characterize backscattering and other effects. In all, about 80 spectra were acquired in a total of about 1000 h. The best three spectra of $^{134}Cs^{m}$, and two of ^{137}Cs were used to extract the ratio of K x-rays to γ-ray areas.

The effort and care invested in preparation of the $^{134}Cs^{m}$ source paid dividends. We identified only very weak impurities (0.3-0.9%) that affected the Cs K x-rays; these were easily corrected for. Only small corrections were needed as well for source attenuation (0.1%), K x-rays from the weak 139-keV cross-over transition (0.8%), and random summing (< 0.5%). The correction for the Voigt-shape of the x-ray peaks was done by simulation and found to be small (0.1%) and equal for both Cs and Ba x-rays, thus canceling out in ratio. Our biggest problem turned out to be x-ray backscattering, which led to "tails" on

the low-energy side of the x-ray peaks. After careful study, we applied a 1.1% correction for this effect to the ratio of Cs to Ba K x-rays.

Our result for the ratio $\alpha_K(^{134}Cs)/\ \alpha_K(^{137}Ba)$ is shown in the table. It agrees well with the Relativistic Dirac-Fock theory (with or without the inclusion of the atomic hole) and disagrees with the previous experimental result quoted by Raman *et al.*, which disagreed with all calculations. We can conclude that the apparent conflict between theory and experiment in these cases was not due to a failure of the theory but rather was caused by experimental inadequacies.

Table I. Our result for the ratio $\alpha_K(^{134}Cs)/\ \alpha_K(^{137}Ba)$ compared with several theoretical calculations and with previous experiments as surveyed in Ref. [1].

	α_K ratio	Uncertainty
This experiment	**30.02**	**0.27**
hole(frozen orbital)	29.96	
hole(SCF)	29.88	
no hole	29.52	
Experiment (*Raman et al.*[1])	**28.82**	**0.51**

[1] S. Raman, C.W. Nestor, Jr., A Ichihara, and M.B. Trzhaskovskaya, Phys. Rev. **C66**, 044312 (2002)

[2] J.C. Hardy, N. Nica, V.E. Iacob, M.B. Trzhaskovskaya and R.G. Helmer, Appl. Radiat. Isot. (To be published).

[3] I.M. Band, M.B. Trzhaskovskaya, C.W. Nestor, Jr., P. Tikkanen, and S. Raman, At. Data Nucl. Data Tables **81**, 1 (2002)

[4] N. Nica, J.C. Hardy, V.E. Iacob, S. Raman, C.W. Nestor Jr., and M.B. Trzhaskovskaya, Phys. Rev. C**70**, 054305 (2004)

[5] E. Schönfeld and H. Janssen, Nucl. Instrum. Methods Phys. Res. **A369**, 527 (1996)

[6] N. Nica, J.C. Hardy, V.E. Iacob, J.R. Montague, and M.B. Trzhaskovskaya, Phys. Rev. C **71**, 054320 (2005).

[7] J.C. Hardy, V.E. Iacob, M. Sanchez-Vega, R.T. Effinger, P. Lipnik, V.E. Mayes, D.K. Willis, and R.G. Helmer, Appl. Radiat. Isot. **56**, 65 (2002).

[8] R. G. Helmer, J. C. Hardy, V. E. Iacob, M. Sanchez-Vega, R.G. Neilson, and J. Nelson, Nucl. Instrum. Methods Phys. Res. **A511**, 360 (2003).

Measurement of Beta-Delayed Gamma Rays in the Decay of ^{32}Cl

C. Bordeanu,[1] A. Garcia,[2] J.C. Hardy, V. E. Iacob, D. Melconian,[2] N. Nica, H.I. Park,
G. Tabacaru, L. Trache, S. Triambak,[2] R.E. Tribble and Y. Zhai
[1]*Horia Hulubei – National Institute for Physics and Nuclear Engineering, Department of Physics (DFN 110) Str. Atomistilor nr. 407, Bucharest-Magurele, PO Box MG6, Rumania*
[2]*Center for Experimental Nuclear Physics and Astrophysics, Box 354290, University of Washington, Seattle, WA 98195*

As part of a larger project to determine the *ft*-value for the superallowed β transition from the 0^+, T=2 ground state of ^{32}Ar, the University of Washington authors require a reliable absolute γ-ray efficiency calibration standard for their HPGe detector. The β-delayed γ rays from the decay of ^{32}Cl cover the required range of energies, and since ^{32}Cl is also a daughter product of ^{32}Ar, its γ rays would provide a particularly convenient *in situ* calibration. To determine the ^{32}Cl properties to the required 1% precision, we performed a collaborative experiment on the decay of ^{32}Cl at Texas A&M using MARS, the fast tape-transport system and our well-calibrated HPGe detector [1].

We produced 298-ms ^{32}Cl via the ^{1}H(^{33}S,2n)^{32}Cl reaction at 30*A* MeV on an LN_2-cooled hydrogen gas target. The ejectiles entered the MARS spectrometer where the ^{33}S beam was stopped, and the fully stripped reaction products were spatially separated from one another, leaving a pure ^{32}Cl beam at the extraction slits. This beam then exited the vacuum system though a Kapton window, passed successively through a thin BC-404 scintillator and a stack of aluminum degraders, finally stopping in the aluminized mylar tape of our tape-transport system. Typically, we collected activity for 0.8 s, then moved the tape in 180 ms to a shielded counting location 90 cm away, where we recorded β-γ coincidences for 2 s. This cycle was clock-controlled and was repeated continuously.

The data set is very clean and is currently being analyzed at the Universoty of Washington.

[1] R.G. Helmer, J.C. Hardy, V.E. Iacob, M. Sanchez-Vega, R.G. Neilson and J. Nelson, Nucl. Instrum. Methods Phys. Res. **A511**, 360 (2003); R.G. Helmer, N. Nica, J.C. Hardy and V.E. Iacob, Int. J. Appl. Radiat. Isot., **60**, 173 (2004).

Plastic Scintillator Response Functions Simulated with the GEANT4 Code

V.V. Golovko, V.E. Iacob, and J.C. Hardy

Precise β^+-branching-ratio measurements are required to determine *ft*-values as part of our program to test the Standard Model via the unitarity of the Cabibbo-Kobayashi-Maskawa matrix. For the measurements to be useful in this test, their precision must be close to 0.1%. This is a particularly demanding requirement for β-decay branching-ratio measurements.

In a typical branching-ratio measurement, we collect the radioactive species in mylar tape, and then move the tape to a shielded counting station, where the sample is positioned between a thin plastic scintillator used to detect β particles, and a HPGe detector for γ rays. The signals from both detectors are recorded for all events in which there is a β-γ coincidence. Although we obtain the β branching ratio from the absolute intensity of the coincident γ rays, the relative efficiency of the β-detector as a function of β energy is critical to our achieving a precise result since different γ-ray peaks correspond to β transitions with different end-point energies.

We have previously simulated β-response functions using Monte Carlo calculations produced by the EGS package of codes [1] but, since there are always questions about the validity of any particular simulation code, we have now made similar Monte Carlo calculations with the GEANT4 code [2]. GEANT4 allows for the transportation of both β and γ particles through matter with software that is modular and flexible, and accounts for low-energy electromagnetic processes down to 250 eV (see Ref. [3]). In addition, it accommodates rather complicated three-dimensional geometrical models and a wide variety of materials. It also allows the user to output the simulated data at different stages in the process and at different levels of detail and refinement.

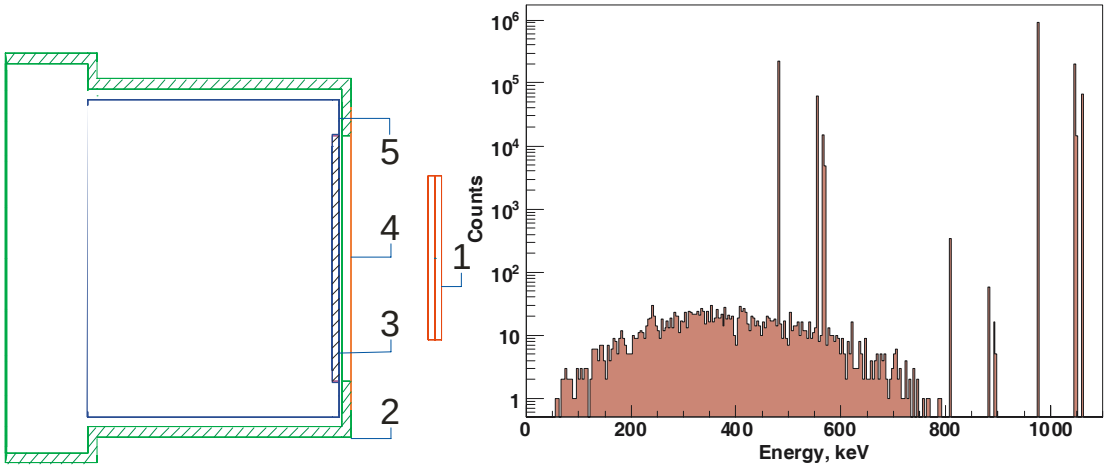

Figure 1. Left: Schematic drawing of the β-detector assembly (not exactly to scale). The radioactive source is contained in thin mylar foil (1), with emitted γ rays and electrons then passing through a havar foil (4) and into the plastic scintillator (3). The scintillator is optically coupled through the plastic light guide (5) to a photomultiplier tube. The scintillator and light guide are shielded from stray light by a cylindrical cover (2) made from PVC. Right: Decay spectrum of electrons for ^{207}Bi generated by GEANT4 as input to the Monte Carlo simulations.

The geometric model we used for GEANT4 incorporates the essential features of our experimental test arrangement. It appears on the left side of Fig. 1. The β-detector consists of a 1-mm thick BC404 plastic scintillator coupled via plastic light guide to a photomultiplier tube (not shown in the figure). The scintillator and light guide are enclosed in a cylindrical shell made from 1.5-mm-thick PVC with a 5-μm-thick havar-foil window located directly in front of the scintillator. The whole assembly is light tight but allows electrons to pass through the havar window with negligible energy loss. In our simulation calculations, the various materials in this assembly were defined either as pure elements or as the appropriate chemical mixtures.

We describe here the first results of simulations we have made for the decay of ^{207}Bi. In principle, it is possible to input each individual γ-ray and conversion-electron group in this decay into GEANT4, one by one. However the code includes a radioactive-decay module that derives for itself the full spectrum of particles emitted in the decay from the data available in the current ENSDF files. We followed the latter, much simpler approach. The primary spectrum of emitted electrons derived by the radioactive-decay module for the decay of ^{207}Bi is shown on the right side of Fig. 1. It, together with the equivalent spectrum of primary γ rays, was what we used as input for the GEANT4 Monte Carlo calculation.

In any Monte Carlo simulation the desired physical quantity is the energy deposited into the scintillator. However, in order to compare the calculated and experimental spectra it is necessary to simulate the statistical fluctuations in the process of charge carrier production and pulse electronic analysis. It is these fluctuations that lead to a finite peak width. For this purpose, we applied a Gaussian distribution with parameters (mean $\bar{x}$ and standard deviation σ) extracted from experimental data as a function of the deposited energy E_0. This is known in the energy region 0.8-3.8 MeV (see Ref. [4]) and we extrapolated these data to lower energies assuming that the Gaussian width, σ_{exp}, is linearly dependent on the energy of the incident electrons. First, we computed the experimental resolution (FWHM) at a particular deposited energy, E_0. Next, we generated a random energy, E_r, using a Gaussian distribution with $\bar{x} = E_0$ and $\sigma = \sigma_{exp}(E_0)$. Finally, the modeled spectrum obtained from GEANT4 was thus processed at all energies by a randomization algorithm written in C++ in the ROOT [5] analysis framework. In Fig. 2, the results are compared with data that we obtained experimentally with a ^{207}Bi conversion-electron source that we purchased from Isotope Products Laboratories.

The simulation is in good agreement with the measured spectrum. All features of the latter are present in the former. However, the experimental spectrum is not independently energy calibrated. Our next goal is to compare simulations with experimental data for several other conversion-electron sources, and from these comparisons derive a consistent energy calibration as well as the energy dependence of detector efficiency. We also plan to investigate the influence of peripheral objects located around the source and detector, and to examine systematically the differences between GEANT4 and EGS simulations.

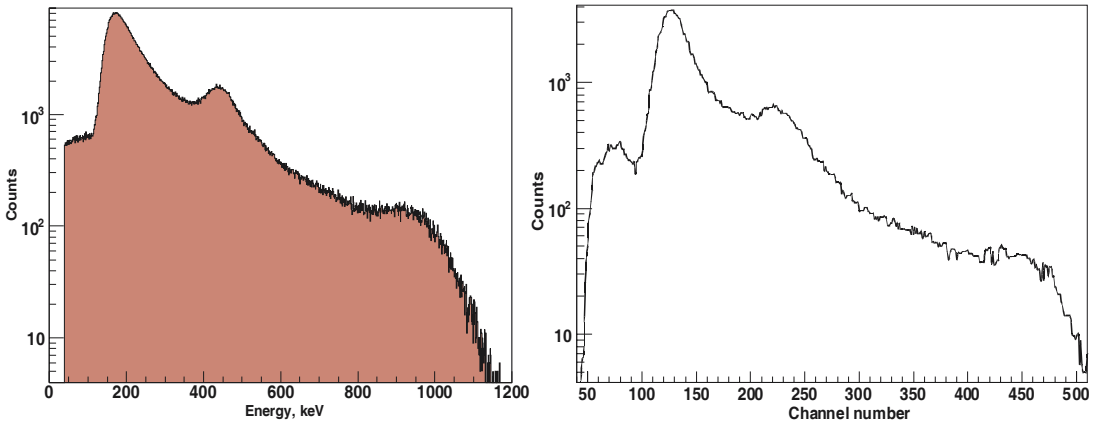

Figure 2. Deposited energy from β-particles that have been simulated by GEANT4 (left) and measured (right) for a ^{207}Bi source located 40 mm from the front face of the β-detector. The simulated spectrum incorporates the finite resolution of the detector.

[1] V.E Iacob and J.C. Hardy, *Progress in Research,* Cyclotron Institute, Texas A&M University (2004-2005), p. I-24.

[2] S. Agostinelliae, J. Allisonas, K. Amakoe, J. Apostolakisa, H. Araujoaj, P. Arcel, M. Asaig, D. Axeni, S. Banerjeebi, G. Barrandan, F. Behnerl, and L. Bellagambac, Nucl. Instrum. Methods Phys. Res. **A506,** 250 (2003).

[3] J. Apostolakis *et al.*, Technical report, CERN, 1999.

[4] E.T.H. Clifford, E. Hagberg, V.T. Koslowsy, J.C. Hardy, H. Schmeing, and R.E. Azuma, Nucl. Instrum. Methods **224,** 440 (1984).

[5] Rene Brun and Fons Rademakers, Nucl. Instrum. Methods Phys. Res. **A389**, 81 (1997).

Evaluated Nuclear Structure Data File (ENSDF) at Texas A&M

N. Nica,[1] and J.C. Hardy
[1]*under contract with Brookhaven National Laboratory*

In August 2005 we began, under contract, contributing to the *Evaluated Nuclear Structure Data File* (ENSDF) maintained by the National Nuclear Data Center at Brookhaven National Laboratory. This data file is sponsored by DOE and contains evaluated nuclear-structure and decay data in a standard format, updated regularly by an international network of evaluators. The evaluations are also published in *Nuclear Data Sheets*, a monthly journal published by Academic Press, a division of Elsevier Science. All experimental data known for each nuclide are collected and each type of experiment is presented as a separate data set. Finally a comprehensive data set containing the values determined by the evaluators is built as *Adopted Levels, Gammas*. By April 2006, the ENSDF database contained 15,700 data sets for 2982 nuclides.

The internet-accessible ENSDF has become more and more the central point of nuclear-data users and is extensively used by both basic and applied scientists. The data sets, especially the *Adopted Levels, Gammas,* are the most complete available image of each nuclide, which is built by comparison and integration of all known data. The evaluator is not a referee and does not give any verdict on the quality and impact of the data, but rather tries to achieve the best synthesis based on all published data. ENSDF is the most comprehensive nuclear structure data base, on which other evaluation products are based, and it is often the starting point for more refined evaluations.

So far, we have accepted two mass chains for evaluation, A=252, and A=140. The A=252 mass chain consisted of eight nuclei (Cm, Bk, Cf, Es, Fm, Md, No, Lr) and has already been published [1]. The A=140 mass chain is one of the largest, with sixteen nuclei (Te, I, Xe, Cs, Ba, La, Ce, Pr, Nd, Pm, Sm, Eu, Gd, Tb, Dy, Ho), and covers more than 1000 references, of which about 150 were published in the period since the last cut-off date. This evaluation is still in progress.

ENSDF can also be used as an effective research tool in our lab. Searches of particular parameters are possible in ENSDF, and the file is now readily accessible here for systematic studies of nuclear properties. When analyzing experiments or making theoretical studies, one can now easily access the most complete nuclear data set available anywhere.

[1] N. Nica, Nucl. Data Sheets **106**, 813 (2005).

Global Analysis of Muon Decay Measurements

C.A. Gagliardi, R.E. Tribble, and N.J. Williams

We have performed a new global analysis of muon decay measurements to establish model-independent limits on the space-time structure of the muon decay matrix element [1]. The most recent previous global analysis had been performed in 1988 [2]. Our analysis included new measurements of the Michel parameters ρ [3] and δ [4] by the TWIST Collaboration, as well as new measurements of the transverse polarization parameters η, η″, α′, and β′ [5]. We find new limits on the scalar, vector, and tensor couplings of right- and left-handed muons to right- and left-handed electrons. These couplings are given by $g^{\gamma}_{\varepsilon\mu}$, where ε and μ represent the chiralities of the electron and muon, respectively. In the standard model, $g^{V}_{LL} = 1$, and all the other coupling constants are zero.

Table I shows the results. The limits on those terms that involve the decay of right-handed muons to left-handed electrons are more restrictive than in previous analyses, primarily due to the inclusion of the new ρ and δ measurements. The limits on other possible non-standard model interactions are comparable to those in previous analyses. The value of the Michel parameter η found in the global analysis is -0.0036 ± 0.0069. This is slightly more precise than the value found in a more restrictive analysis of the transverse polarization parameters [5], and nearly a factor of two more precise than the previous accepted value [6]. All three of the recent measurements [3-5] play important roles in reducing the uncertainty in η. This reduces the contribution of η to the uncertainty in the Fermi coupling constant G_F to $\Delta G_F/G_F = 6.7 \times 10^{-5}$.

Table I. 90% confidence limits on the muon decay coupling constants.

	Ref. [2]	Present Work
$\lvert g^{S}_{RR}\rvert$	<0.066	<0.067
$\lvert g^{V}_{RR}\rvert$	<0.033	<0.034
$\lvert g^{S}_{LR}\rvert$	<0.125	<0.088
$\lvert g^{V}_{LR}\rvert$	<0.060	<0.036
$\lvert g^{T}_{LR}\rvert$	<0.036	<0.025
$\lvert g^{S}_{RL}\rvert$	<0.424	<0.417
$\lvert g^{V}_{RL}\rvert$	<0.110	<0.104
$\lvert g^{T}_{RL}\rvert$	<0.122	<0.104
$\lvert g^{S}_{LL}\rvert$	<0.550	<0.550
$\lvert g^{V}_{LL}\rvert$	>0.960	>0.960

[1] C.A. Gagliardi *et al*., Phys. Rev. D **72**, 073002 (2005)

[2] B. Balke *et al*., Phys. Rev. D **37**, 587 (1988); W. Fetscher and H.-J. Gerber, in S. Eidelman *et al*., Phys. Lett. B **592**, 1 (2004).

[3] J.R. Musser *et al*. (TWIST Collaboration), Phys. Rev. Lett. **94**, 101805 (2005).

[4] A. Gaponenko *et al*. (TWIST Collaboration), Phys. Rev. D **71**, 071101R (2005).

[5] N. Danneberg *et al*., Phys. Rev. Lett. **94**, 021802 (2005).

[6] S. Eidelman *et al*. (Particle Data Group), Phys. Lett. B **592**, 1 (2004).

TWIST: Measuring the Space-Time Structure of Muon Decay

C.A. Gagliardi, J.R. Musser, R.E. Tribble, and the TWIST Collaboration

This past year, TWIST completed its first measurement of $P_\mu\xi$, where P_μ is the polarization of the muon in pion decay and ξ is one of the four Michel parameters that characterize the energy and angular distributions of the positrons emitted in polarized muon decay. We find $P_\mu\xi = 1.0003 \pm 0.0006(\text{stat.}) \pm 0.0038(\text{syst.})$, consistent with the Standard Model expectation that $P_\mu\xi = 1$ and a factor of two more precise than the previous best direct measurement [1]. This analysis, which is based on data that were taken in Fall, 2004, was the Ph.D. research of Dr. Blair Jamieson of University of British Columbia. Our group did not play as direct a role in the $P_\mu\xi$ analysis as we have in previous and on-going TWIST measurements of the Michel parameters ρ and δ, but we nonetheless made important contributions during the estimation of the systematic uncertainties. A paper describing this measurement is being prepared.

The leading systematic uncertainties in the initial $P_\mu\xi$ measurement involve our understanding of the depolarization of the muons as they cross the fringe field of the solenoid magnet (± 0.0033) and when they interact with the Al stopping target after they have come to rest (± 0.0012). To evaluate and minimize these systematic uncertainties, it's valuable to have a reliable method to estimate relative changes in the muon polarization independent of our Michel parameter fits. For the initial $P_\mu\xi$ measurement, the integral forward-backward asymmetry within the Michel fit fiducial region was used for this purpose. Figure 1 illustrates its application to the 2004 data. After the black box had been opened and we were no longer blind to the value of $P_\mu\xi$, we proposed that an alternative calculation, performed by optimizing the fiducial and weighting each event with a power of the expected Standard

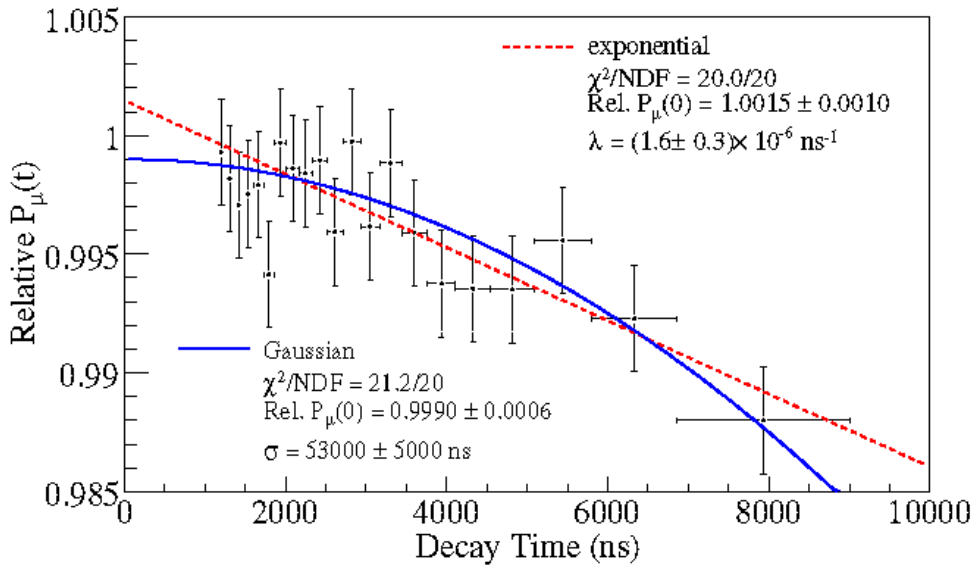

Figure 1. The relative muon polarization vs. decay time for the 2004 data, measured using the integral forward-backward asymmetry. The curves show two different extrapolations to t=0, assuming exponential and Gaussian forms for the depolarization.

Model asymmetry, would reduce the size of the statistical uncertainties by a factor of ~2. This new asymmetry calculation has now been adopted by the Collaboration for all future analyses.

During Fall, 2005, TWIST had an engineering run to see if more careful procedures for beam emittance measurements using the Time Expansion Chamber could reduce the uncertainties in the muon depolarization when crossing the fringe field. Two data sets were taken under "standard" conditions, and two additional data sets were taken with the field in the last beam line dipole magnet shifted by +6 Gauss. The results were very encouraging. The apparent polarization was consistent for each pair of data sets taken under similar conditions, as expected, and the change in the average polarization for the two data sets taken with the last dipole shifted agreed with the Monte Carlo prediction.

In parallel, Mr. Robert MacDonald of University of Alberta is reanalyzing the 2004 data to obtain improved measurements of ρ and δ. Several significant improvements have been implemented in our Monte Carlo simulation and helix fitting codes. Overall, these improvements are expected to reduce the systematic uncertainties in ρ and δ by a factor of ~2, compared to those in the analysis of the TWIST 2002 data [2,3]. The statistical uncertainties will be comparable to those in the previous analyses. One of us (CAG) has been working with Dick Mischke and Art Olin of TRIUMF to advise Mr. MacDonald during his analysis.

TWIST expects to take its final data during 2006-07. We anticipate the final precisions for the Michel parameters ρ and δ will be approximately ±0.0003. The final precision for $P_\mu\xi$ will be ±0.001 or better.

[1] I. Beltrami *et al*., Phys. Lett. B **194**, 326 (1987).
[2] J.R. Musser *et al*. (TWIST Collaboration), Phys. Rev. Lett. **94**, 101805 (2005).
[3] A. Gaponenko *et al*. (TWIST Collaboration), Phys. Rev. D **71**, 071101R (2005).

SECTION II

HEAVY ION REACTIONS

Experimental Determination of the Symmetry Energy of a Low Density Nuclear Gas

S. Kowalski, J.B. Natowitz, S. Shlomo, R. Wada, K. Hagel, J.S. Wang, T. Keutgen,[1] T. Materna, Z. Chen, Y. Ma,[2] L. Qin, A.S. Botvina,[3] M. Cinausero,[4] Y. El Masri,[1] D. Fabris,[5] M. Lunardon,[5] Z. Majka,[6] S. Moretto,[5] G. Nebbia,[5] S. Presente,[5] G. Prete,[5] V. Rizzi,[5] G. Viesti,[5] and A. Ono[7]

[1]*FNRS and IPN Université Catholique de Louvain, Louvain-la-Neuve, Belgium*,

[2]*Shanghai Institute of Nuclear Research, Chinese Academy of Sciences, Shanghai, China,*

[3]*Institute for Nuclear Research, Russian Academy of Science, Moscow, Russia,*

[4]*INFN, Laboratori Nazionali di Legnaro, Legnaro, Italy,*

[5]*INFN and Dipartimento di Fisica dell' Universitá di Padova, Padova, Italy,*

[6]*Jagiellonian University, M Smoluchowski Institute of Physics, Krakow, Poland,*

[7]*Department of Physics, Tohoku University, Sendai, Japan*

In a recent theoretical paper, Horowitz and Schwenk have reported the development of a Virial Equation of State (VEOS) for low density nuclear matter [1]. This equation of state, derived from experimental observables should be "model-independent" and therefore can be used to "set a benchmark for all nuclear equations of state at low densities." Its importance in both nuclear physics and in the physics of the neutrino sphere in supernovae is emphasized in the VEOS paper [1]. An important feature of the VEOS is the natural inclusion of clustering which leads to large symmetry energies at low baryon density.

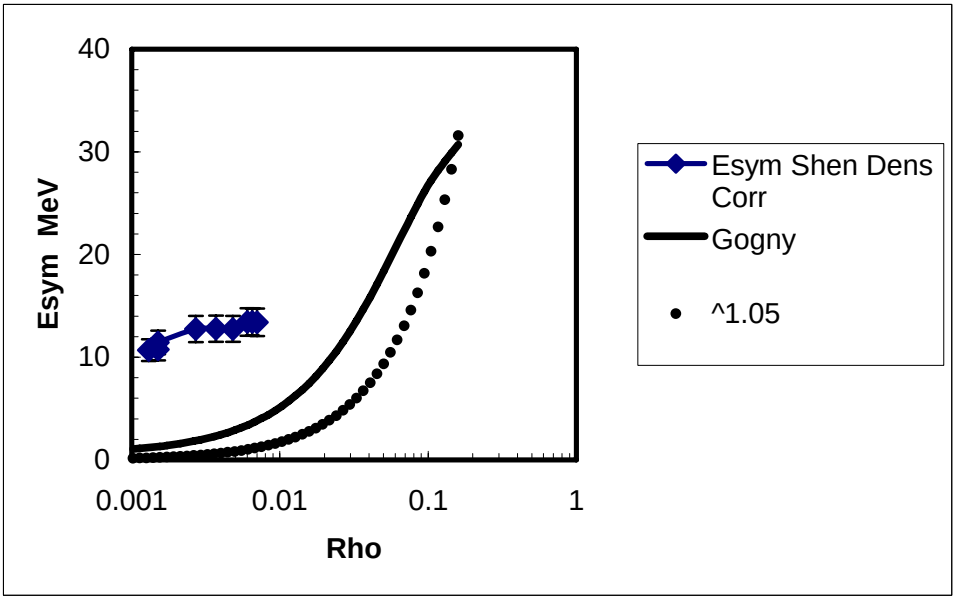

Figure 1. Derived symmetry energy coefficients as a function of baryon density. Solid diamonds indicate results using densities of column 4 in Table 1..Solid line indicates the variation predicted by the Gogny interaction. The dotted line represents the function 31.6 x $(\rho/\rho_0)^{1.05}$ [3].

The reactions of 35 MeV/nucleon ^{64}Zn projectiles with ^{92}Mo and ^{197}Au target nuclei were studied at the K-500 Super-conducting Cyclotron Facility at Texas A\&M University, using the 4π detector NIMROD. For nuclear gases with average proton fraction, Yp ~0.44, and densities at and below 0.05 times normal nuclear density, experimental symmetry energy coefficients of 10 – 14 MeV have been derived from experimentally determined symmetry free energies , F_{sym} , determined using the isoscaling method. A detailed description of this work may be found in reference 2. The symmetry energies are far above those obtained in common effective interaction calculations and reflect cluster formation, primarily of alpha particles, not included in such calculations. The symmetry energy coefficients are plotted against density in Figure1 where they are compared to those which are predicted by the Gogny effective interaction and to the 31.6 x $(\rho/\rho_0)^{1.05}$ dependence suggested by a recent analysis of isospin diffusion data [3].

[1] C.J. Horowitz and A. Schwenk, ArXiv preprint nucl-th/0507033 (2005).
[2] S. Kowalski et al, ArXiv Preprint nucl-ex/0602023, Phys. Rev. C (submitted).
[3] L.W. Chen, C.M. Ko nd B.A. Li, Phys. Rev. Lett. **94**, 032701 (2005).

Refining Reaction Dynamics in Fermi Energy Heavy Ion Reactions

R.Wada, Z. Chen, T. Keutgen, K. Hagel, J. Wang, L. May, M. Codrington, L. Qin,
J.B. Natowitz, T. Materna, S. Kowalski, and P.K. Sahu

In heavy ion reactions in the Fermi energy domain, many intermediate mass fragments (IMFs) are commonly produced. At a time of formation their characteristic properties, such as the excitation energy and isotope distributions, are governed by the physical nature of the source, such as temperature, density and N/Z ratio, from which they originate. These physical conditions of the sources are directly related to the reaction dynamics and the nature of nuclear matter. Therefore IMFs may provide a unique probe to study reaction mechanism and nuclear properties. However most of IMFs experimentally measured are not direct reaction products (primary IMFs) , but they are secondary products produced through sequential cooling processes. These secondary decay processes may significantly distort the characteristics of the primary IMFs and obscure the physical nature of the source. Therefore it is desirable to reconstruct the characteristics of the primary fragments in order to extract the physical natures of the sources and to refine the reaction dynamics.

Aiming at this goal, reaction systems with different N/Z ratios have been studied. In the experiment ^{64}Zn, ^{64}Ni and ^{70}Zn beams were incident on ^{58}Ni, ^{64}Ni, ^{112}Sn, ^{124}Sn, ^{197}Au and ^{232}Th targets at 40 A MeV. In order to reconstruct the primary IMFs, neutron and charged particles are detected in coincidence with IMFs. In this report we concentrate on the light particles. Another brief report for the analysis of the IMFs is given in a separate article in this annual report.

Neutrons were detected by sixteen detectors from the Belgian-French neutron detection array, DEMON. Light Charged particles (LCPs) were detected by 16 single crystal CsI(Tl) detectors. Both particles were recorded in coincidence with IMF observed at 20^o. Neutron-γ separation and charged particle identification were made by pulse shape discrimination methods. Neutron energy is obtained from the time of flight measurement and the neutron detection threshold was calibrated by a ^{22}Na source. The energy calibration of the CsI detector was performed using a Si detector in front of each CsI detector during the beam time.

In Figure 1, typical neutron velocity spectra associated with ^{6}Li of different velocity are shown. Neutrons in coincidence with ^{6}Li in three different velocity windows, $V_{6Li} \leq 4.5$cm/ns, 5.5cm/ns $\leq V_{6Li} \leq$ 6.5cm/ns and 6.5cm/ns $\leq V_{6Li} \leq$ 7.5cm/ns are presented from top to bottom, respectively. spectra at different neutron detection angles are shown from left to right. The angles indicated on the top of each row are the opening angle, θ_{IMF-N}, between the Si telescope (θ=20^o) and the demon detectors. In this plot neutrons are detected in perpendicular to the reaction plane determined by the Si telescope and the beam. Neutron spectra associated with ^{6}Li in the velocity window of 4.5cm/ns $\leq V_{6Li} \leq$ 5.5 cm/ns, which is tentatively used as a reference, are shown by dashed line histograms in each spectra . As seen in the figure, no significant differences from the reference spectra are observed in shape and amplitude at different angles and for different IMF velocity windows. This indicates that there are very few excess neutrons focused along the direction of IMF, indicating that a very small amount of neutrons are emitted directly from the parent nuclei of the detected ^{6}Li isotopes. A similar observation has been made in our

previous work in which the charged particle multiplicities associated with IMFs are extracted in the Xe+Sn reaction at 50 AMeV[1].

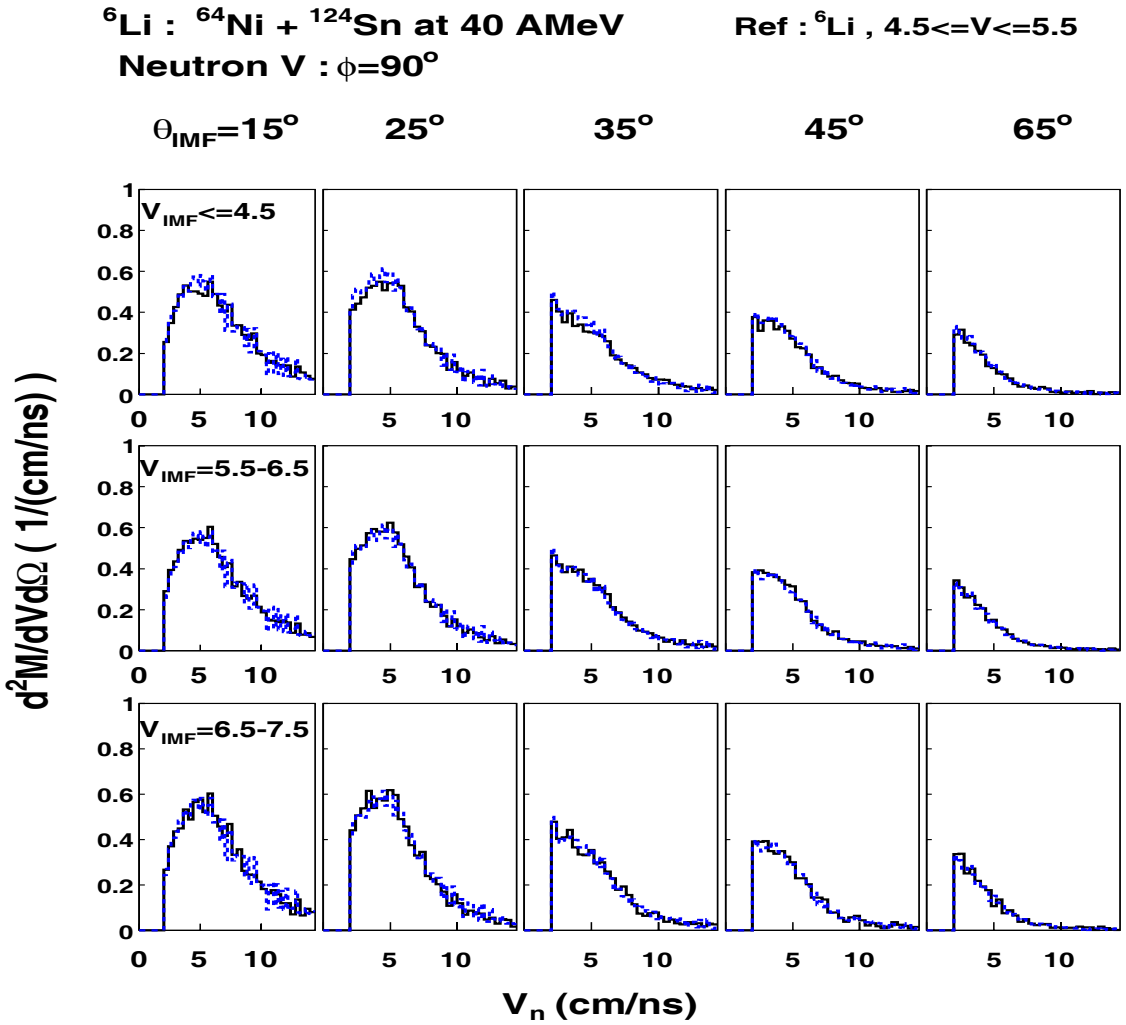

Figure 1. Neutron velocity spectra observed at different angles in coincidence with ^{6}Li in different vlocity windows for ^{64}Ni+^{124}Sn. See details in the text.

In Figure 2 a similar plot is shown for neutrons associated with ^{18}O. Comparing to the reference spectra, a notable excess of neutrons is observed, especially at small angles, $\theta_{IMF\text{-}N}$,. In the lowest velocity window of ^{18}O (top row), these excess neutrons are distributed in a wider range of $\theta_{IMF\text{-}N}$. The peak position of the excess neutrons at $\theta_{IMF\text{-}N}$ =15^{o} shifts toward the higher velocity side when the IMF velocity becomes higher. These observations strongly indicate that these excess neutrons originate from the parent nuclei of the detected ^{18}O, reflecting the kinematic focusing of neutrons along the direction of IMFs. For a higher velocity of ^{18}O (bottom row), the kinematical focussing becomes stronger and at the velocity window of 7.5cm/ns $\leq V^{18}_{O} \leq$ 8.5cm/ns the excess is only observed at $\theta_{IMF\text{-}N}$= 15^{o}. At larger angles a small depletion of neutrons is observed on the higher velocity side. A similar effect is also observed for the charged particle velocity spectra.

In order to reconstruct the characteristic properties of the primary IMFs, a further quantitative analysis is now underway.

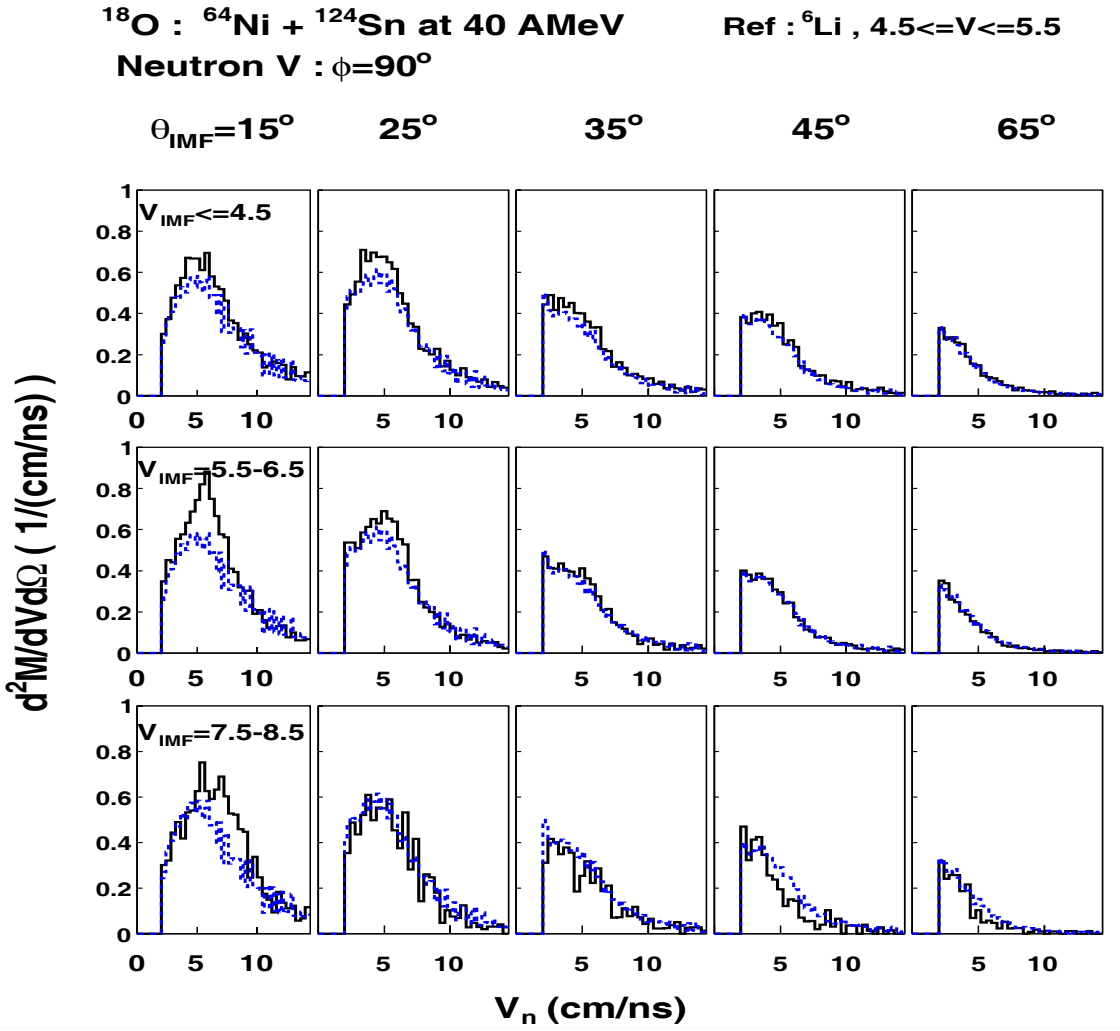

Figure 2. Similar neutron spectra to Fig.1, but in coincidence with ^{18}O.

[1] N. Marie *et al.*, Phys. Rev. C **58**,256 (1998).

Isoscaling in Central Heavy Ion Collisions at Intermediate Energy

Z. Chen, R. Wada, T. Keutgen, K. Hagel, J. Wang, L. May, M. Codrington,
L. Qin, J. B. Natowitz, T. Materna, S. Kowalski, and P.K. Sahu

The isoscaling of intermediate mass fragments (IMFs) has been studied in ^{64,70}Zn, ^{64}Ni + ^{232}Th, ^{197}Au, ^{112,124}Sn, ^{58,64}Ni reactions at 40MeV/nucleon. IMFs were measured by a Si quadrant telescope, backed by four CsI detectors at 20º. The Si telescope consisted of four 5cm x 5cm area detectors, having thicknesses of 129, 300, 1000, 1000 micro-meters. Isotopes of IMFs are clearly identified up to Z=12 with an energy threshold of about 4-8 MeV/nucleon, depending on Z of IMFs. In order to determine the isotope ratio between two different reactions, the ratio is plotted as a function of IMF energy.

In Fig. 1, the differential multiplicities of ^{10}B (left) and ^{24}Mg (right) isotopes (upper) and their yield ratios (bottom) are shown for the two reactions, ^{70}Zn + ^{124}Sn (solid line) and ^{64}Zn + ^{112}Sn (dashed line). The yield ratios depend slightly on the IMF energy. For all the cases the ratios show a rather flat distribution from 10 to 30 MeV/nucleon, in which the contribution from a nucleon-nucleon source component is dominant at this angle.

In Fig. 2, the isotopic yield ratios of IMFs for the two reactions ,^{70}Zn + ^{112}Sn and ^{64}Zn + ^{112}Sn (left) and for ^{64}Ni + ^{124}Sn and ^{64}Zn + ^{112}Sn (right) are shown by symbols as a function of atomic number Z (upper) or neutron number N (lower). The errors correspond to the maximum deviation from the average value in the given energy range (about 10 to 30MeV/nucleon). The ratios are fit by the function:

$$Y1/Y2 \sim \exp(\alpha N+\beta Z)$$

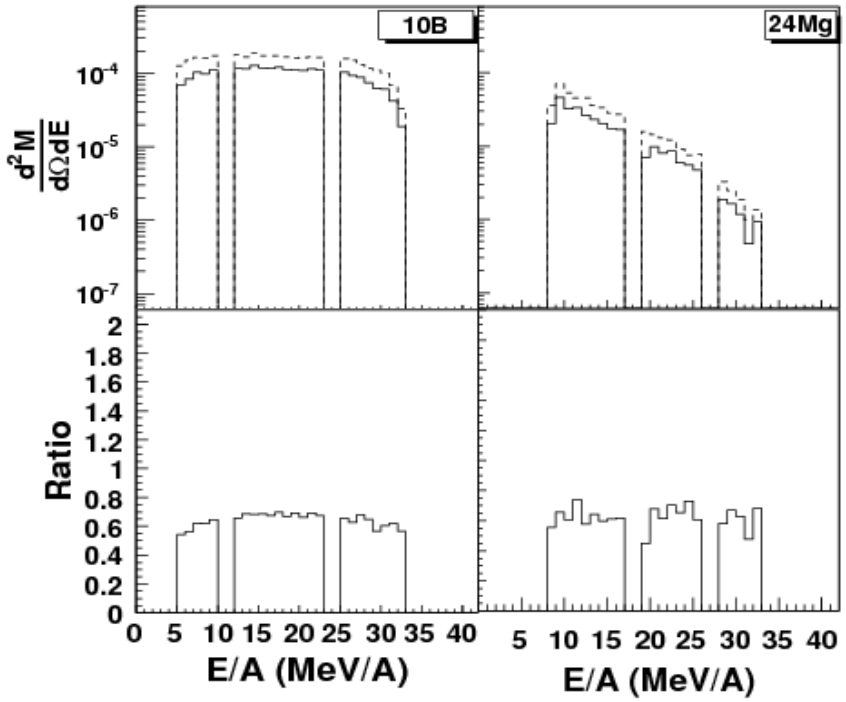

Figure 1. ^{10}B and ^{24}Mg multiplicity distributions (upper) and isotope yield ratios (bottom) for 40 Mev/nucleon ^{70}Zn + ^{124}Sn (solid line) and ^{64}Zn + ^{112}Sn (dashed line)

The solid lines indicate the results obtained for individual fits for a fixed Z or a fixed N. The dashed lines correspond to the results with parameters obtained by averaging over those of the individual fits. A good fit with a unique parameter set of α and β indicates that an isoscaling relationship holds for the entire range of IMFs observed for these reactions. This feature is also observed for all combinations of other reactions performed in this experiment.

More detailed analysis is now underway.

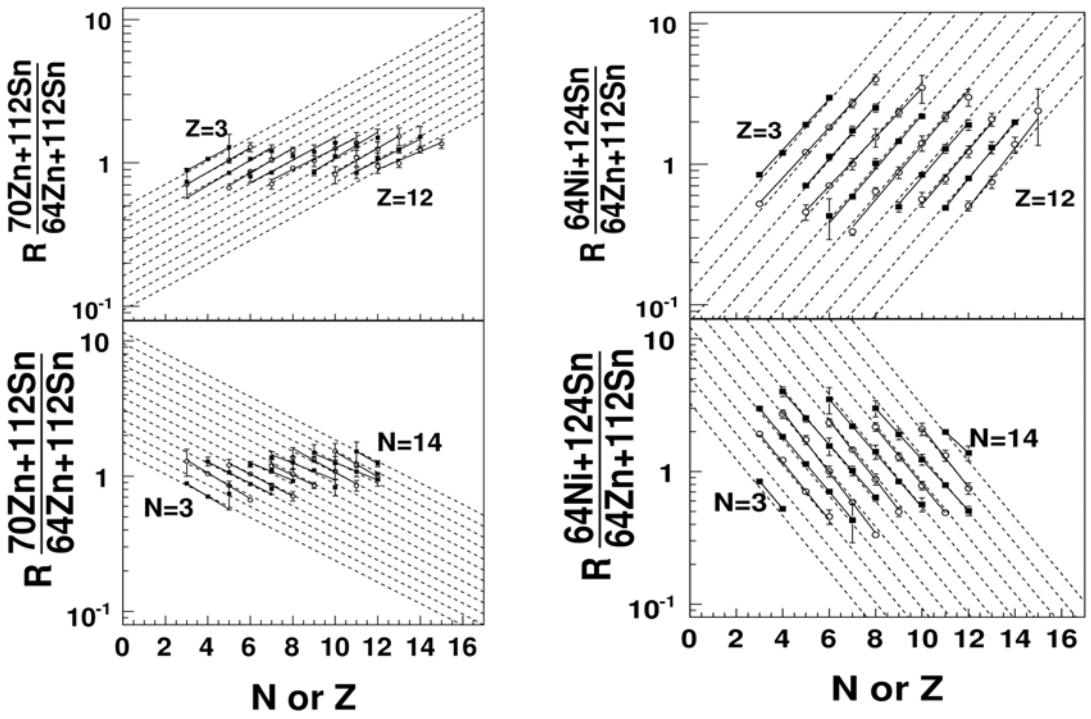

Figure 2. Isotopic yield ratios for 40MeV/nucleon $^{70}Zn+^{112}Sn/^{64}Zn+^{112}Sn$ (left) and $^{64}Ni+^{124}Sn/^{64}Zn+^{112}Sn$ (right)

Exploring New Ways to Produce Heavy and Superheavy Nuclei with Bigsol

T. Materna, Z. Chen, K. Hagel, J. Natowitz, L. Qin,
P.K. Sahu, R. Wada, D. Fabris,[1] M. Lunardon,[1] M. Morando,[1] S. Moretto,[1]
G. Nebbia,[1] S. Pesente,[1] V. Rizzi,[1] G. Viesti,[1] V. Bocci,[2] M. Barbui,[3]
A. Andrighetto,[3] M. Cinausero,[3] G. Prete,[3] Z. Majka,[4] A. Wieloch,[4] and S. Kowalski[5]
[1]*Dipartamento di Fisica dell'Universitá di Padova and INFN Sezione di Padova, Italy*
[2]*Dipartimento di Fisica dell'Università di Brescia and INFN, Italy*
[3]*INFN Laboratori Nazionali di Legnaro, Italy*
[4]*Smoluchowski Institute of Physics, Jagiellonian University, Krakow, Poland*
[5]*Institute of Physics, Silesia University, Katowice, Poland*

The synthesis of superheavy elements (SHE) has been an important field in both theoretical and experimental nuclear physics for many years. Fusion of the doubly-magic neutron-rich ^{48}Ca projectiles with transuranium target nuclei has led during the past 6 years to the synthesis of elements with Z = 113-116 and 118 [1]. The cross-sections involved are at the limit of the sensitivity achievable with the current technology. Our aim is to investigate possible alternative reactions to produce such elements. For example, one of the reactions might be one in which the fissile target nucleus (e.g. ^{238}U and ^{232}Th) would fission as the projectile approaches and where one of the fragments would fuse with the projectile nucleus. The fission fragments being neutron-rich and close to shell closure, they should enhance the fusion and survival probabilities of the formed superheavy nucleus [2].

Experiments have been performed in 2003 and 2004 in collaboration with the Instituto Nazionale di Fisica Nucleare (INFN, Italy). The superconducting solenoid BigSol was used to collect the reaction products and to focus them towards a Bragg chamber, with a back plane covered with scintillators, at about 4 meters from the magnet. Two position-sensitive PPACs were placed before the Bragg chamber, allowing time of flight measurement and trajectory reconstruction.

The reactions studied in 2004 were projectiles of ^{172}Yb (15, 10 and 7.5 A.MeV), ^{197}Au (7.5 A.MeV), ^{136}Xe (7.5 A.MeV) and ^{84}Kr (25, 15 and 7.5A.MeV) on a ^{232}Th target and with ^{238}U (7.5 A.MeV) projectiles on ^{nat}Ti, ^{64}Zn, ^{90}Zr and ^{232}Th targets. The analysis of the collected data is complete. A few tens of events are consistent with the expected signature of superheavy ions. These events have passed all the rejection tests we could implement with our current setup. The setup was optimized to make a survey and needs to be improved significantly before a possible synthesis of superheavy elements can be claimed. In particular, a better separation of the candidates from the high cross-section products (elastics, deep-inelastics,…) must be achieved to allow for the use of Silicon detectors capable of measuring alpha-decay chains to identify the produced elements

The SHE candidates appear mostly in systems at lower energy (7.5 A.MeV), in the reactions ^{197}Au + ^{232}Th and ^{238}U + ^{64}Zn. Our group plans to investigate in more details these reactions in August of this year with a further improved experimental setup. Our goal is to confirm the existence of these candidates and to characterize them better in order to build a more discriminating setup in the future.

[1] Yu. Ts. Oganessian *et al.*, Phys. Rev. C **69**, R021601 (2004); Yu. Ts. Oganessian *et al.*,Nature **400**, 242 (1999); Yu. Ts. Oganessian *et al.*, Scientific American **282**, 45 (2000); Yu. Ts. Oganessian *et al.*, Phys. Rev. C **63**, R011301 (2001); Yu. Ts. Oganessian, "JINR Preprint and Communications", D7-202-287, Dubna, 2002.

[2] Y. Aritomo, T. Wada, M. Ohta, and Y. Abe, Phys. Rev. C **59**, 796 (1999).

Kinematical Simulation of In-Flight Alpha and Fission Decay of Heavy Nuclei in Super-Heavy Mass Region

P.K. Sahu, J.B. Natowitz, R. Wada, K. Hagel, T. Materna, and Z. Chen

The production and detection of super-heavy nuclei has generated a lot of interest in recent years. Measurements of alpha decay and spontaneous fission decay has typically been used as tool to confirm the production of implanted super-heavy nuclei by the GSI and Dubna groups[1,2]. With the motivation of exploring detection systems for in-flight decay of super-heavy nuclei with Z about 120-125, we have carried out a preliminary simplified kinematical simulation of alpha and fission decay of heavy-nuclei, which are in motion with a velocities of 2-6 cm/ns. For the first simulation the half life of the heavy nucleus was assumed to be 1 ns. The half life gives information about the decay position relative to the target location. The alpha and fission half life have been assumed to be the same in the present simulation. However, any half life and exit channel can be kinematicaly simulated to have some preliminary ideas which will be helpful in deciding the experimental setup. A strip detector array is assumed to be symmetrically placed around the beam axis to detect alpha particles and fission fragments emitted by the in-flight heavy nuclei, the width of each silicon strip is 1 cm and its distance from the beam axis is 12.5 cm.

The energy and angular distributions of first chance alpha, first chance fission and fission of a daughter after alpha emission, have been simulated. The alpha energy chosen in the frame of the moving heavy nuclei is 20 MeV. The recoiling daughter produced by alpha emission decays via asymmetric fission. The first chance asymmetric fission decay of the in-flight heavy nuclei has also been simulated. The energies of the asymmetric fission fragments in their respective center-of-mass frames have been calculated by using the Viola's total kinetic energy systematic for asymmetric fission channels [3].

The mass and charge of the heavy nuclei was currently taken as 300 and 116 respectively, and the fission channels were assumed to be asymmetric with ^{132}Sn and ^{168}Dy in the first chance fission, and ^{132}Sn and ^{164}Gd in the fission of daughter. The characteristics of first chance fission and recoil fission of daughter are very similar since the heavy recoil velocity is almost negligible. The simulations have also been done in the presence of a blocker having an opening aperture which selects an initial angle of the heavy in-flight nuclei of 6-20 deg. In this case the yield distributions of alpha particles and fission products are shifted backward relative to the case where the in-flight nucleus was moving straight in the beam direction. The Fig. 1 shows the yield distributions in various strip detectors along the beam direction for the first chance alpha, first chance fission with both light and heavy fragments and recoil daughter fission with only light fragment. In the left side of the figure the in-flight heavy nucleus is moving in the beam direction, whereas in the right side of the figure the in-flight nucleus is moving at an opening angle of 6^0-20^0 with respect to the beam direction in the presence of a blocker.

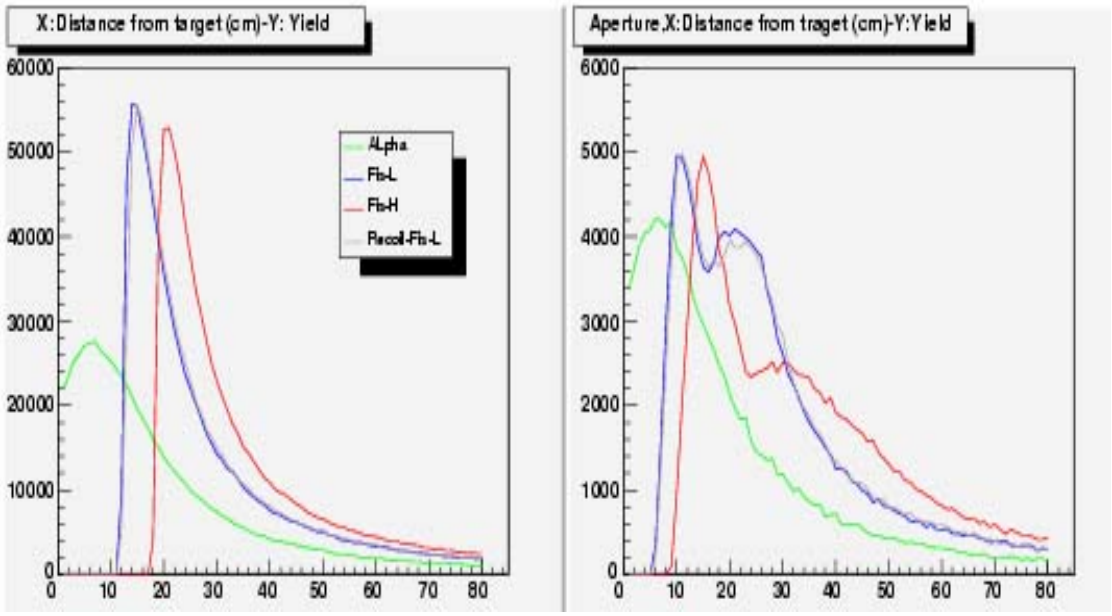

Figure 1. The yield distributions of alpha, fission (light and heavy marked by L and H) along the beam direction with and without blocker.

[1] S. Hofmann and G. Munzenberg, Rev. Mod. Phys. **72**, 733 (2000).

[2] Yu.Ts. Oganessian *et al.*, Phys. Rev. C **69**, 054607 (2004); Phys. Rev. C **62**, 041604 (2000).

[3] V.E. Viola, K. Kwiatkowski, and M. Walker, Phys. Rev. C **31**, 1550 (1985).

Reaction Tomography at 47A Mev

L.J. Qin, R. Wada , K. Hagel , J.B. Natowitz, J.S. Wang, Y. Ma, T. Materna,
T. Keutgen, Z. Chen, and P.K. Sahu

We are investigating the dynamics and thermodynamics in light ion and heavy ion collisions near the Fermi Energy by comparing the yields , spectra and angular distributions of observed products from different reaction systems at same incident energy.A large series of heavy ion reaction systems have been studied with NIMROD. They include

$^{1}H + {}^{112}Sn$	$^{1}H + {}^{124}Sn$
$^{2}H + {}^{112}Sn$	$^{2}H + {}^{124}Sn$
$^{3}He + {}^{112}Sn$	$^{3}He + {}^{124}Sn$
$^{4}He + {}^{112}Sn$	$^{4}He + {}^{124}Sn$
$^{10}B + {}^{112}Sn$	$^{10}B + {}^{124}Sn$
$^{20}Ne + {}^{112}Sn$	$^{20}Ne + {}^{124}Sn$
$^{40}Ar + {}^{112}Sn$	$^{40}Ar + {}^{124}Sn$
$^{64}Zn + {}^{112}Sn$	$^{64}Zn + {}^{124}Sn$

all with the same incident energy, 47 Mev/A .

In our data analysis, we expect to be able to separate emission resulting from nucleon-nucleon collisions from that resulting from the thermalized system and obtain a much cleaner picture of the dynamic evolution of the hotter systems. This series of experiments provides us an opportunity to probe temperature evolution , in-medium nucleon-nucleon cross sections ,isospin effects ,and symmetry energy by creating similar systems with different densities and different N/Z ratios in the interaction region [1-3, 5, 6].

A common technique i.e Three Source Fitting has been used to to fit the observed spectra assuming contributions from three sources, a projectile like fragment (PLF) source, an intermediate velocity (*NN*) source, and a target like fragment (TLF) source . This allows us to characterize light particle emission and provides us a schematic picture of the emission process and estimation of the multiplicities and energy emission at each stage of the reaction [4].

In our approach, we select the most violent events by taking into account only the events with the 30% largest light particle multiplicity. In Figure 1 below are the velocity plots of p ,d ,t, ^{3}He , ^{4}He from $^{10}B+^{124}Sn$, $^{64}Zn+^{112}Sn$, $^{64}Zn+^{124}Sn$ respectively .

From these velocity plots, we can see that emission in the different systems looks qualitatively similar but the intensities are quite different

$^{10}B+^{124}Sn$

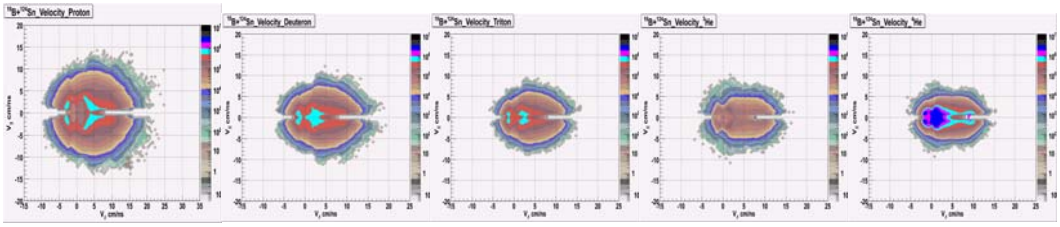

$^{64}Zn+^{112}Sn$

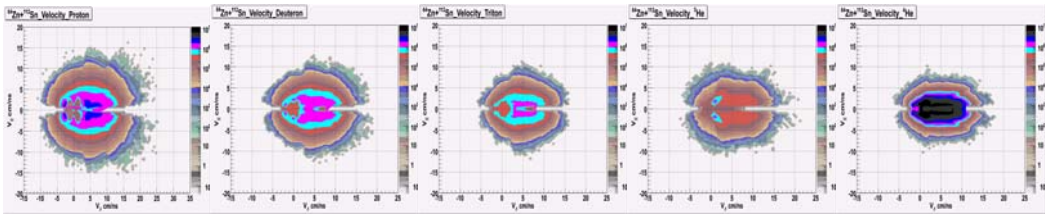

$^{64}Zn+^{124}Sn$

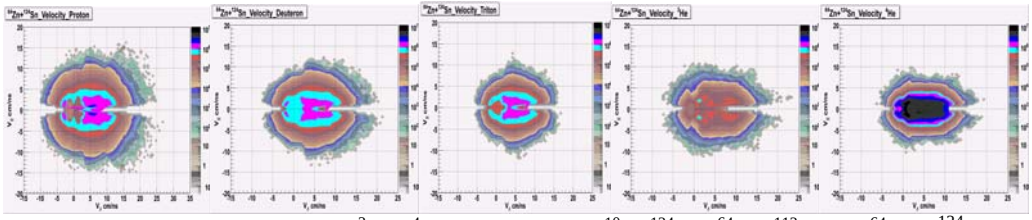

Figure 1. Velocity plots of p ,d ,t, ^{3}He , ^{4}He emission from $^{10}B+^{124}Sn$, $^{64}Zn+^{112}Sn$ and ^{64}Zn $+^{124}Sn$

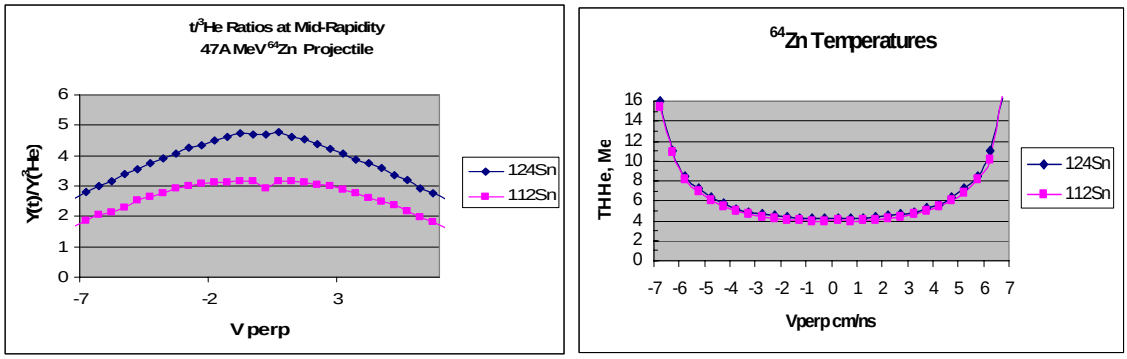

Figure 2. (Left) t/^{3}He ratios at mid-rapidity. (Right)^{64}Zn temperatures.

We also generated plots of t/ ^{3}He ratios and ^{64}Zn temperatures from source fitting parameters at mid-rapidity Vp 5-6 cm/ns. These are in Figure 2 and show that the t/ ^{3}He ratios are different, reflecting the different N/Z in the system. Double isotope ratio temperatures, T_{HHe}, are very similar. Further analyses are under way.

[1] Jian-Ye Liu *et al.*, Phys. Rev. Lett. **86**, 975 (2001).
[2] Lie-Wen Chen *et al.*, Phys. Rev. Lett. **90**, 162701 (2003).
[3] Ph. Chomaz *et al.*, Phys Lett B **447**, 221 (1999).
[4] K. Hagel *et al.*, Phys. Rev. C **62**, 034607 (2000).
[5] Y Zhang *et al.*, Phys. Rev. C **71**, 024606 (2005).
[6] http://cyclotron.tamu.edu/nimrod.htm.

Progress in BRAHMS

K. Hagel, R. Wada, T. Materna, S. Kowalski, J.B. Natowitz, and the BRAHMS Collaboration

BRAHMS measured Cu + Cu collisions at $\sqrt{s_{nn}} = 200\,\mathrm{GeV}$ and $\sqrt{s_{nn}} = 63\,\mathrm{GeV}$ as well as p + p collisions at $\sqrt{s_{nn}} = 200\,\mathrm{GeV}$ during RHIC Run-V. The Cu + Cu measurement provides for a mass and energy variation to compare to the Au + Au measurements at both energies. The measurement of p + p collisions provides a substantial improvement in statistics for the baseline measurement especially in the forward direction. The mass and energy variation is expected to help to disentangle the effects of jet quenching; where the energy loss ∝ multiplicity, or A, and gluon saturation, where the saturation scale Q_S varies as $A^{1/6}$. We made measurements concentrating on high p_t as well as a study of the soft physics by measuring rapidity distributions over the entire range from mid-rapidity to near y=4.

Preliminary results of the jet suppression from the low energy Cu + Cu data have been extracted. These preliminary results are shown in figure 1 where the R_{AA} of 62 GeV Cu + Cu is compared to R_{AA} of 62 GeV Au + Au. We note that the suppression of 62 GeV Cu + Cu for given centrality is less than that of 62 GeV Au + Au. It is also noted that where there is a region of rough overlap of the average number of binary collisions, that the suppression for the two energies is similar with the bins of lower average binary collisions of the Cu + Cu displaying the least suppression.

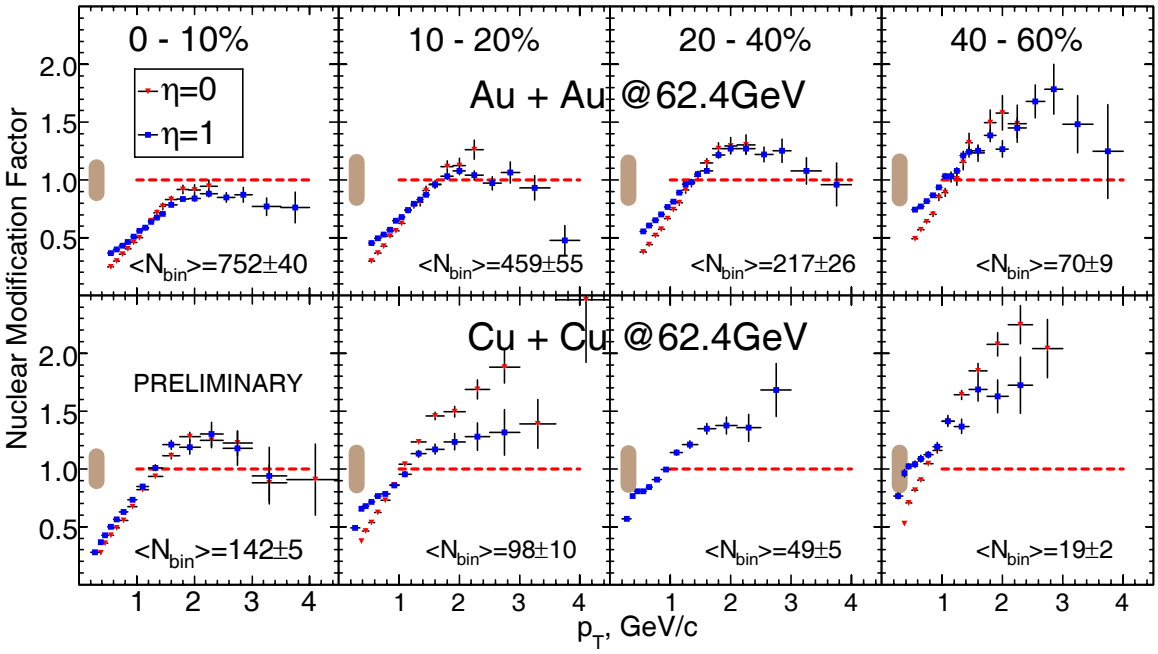

Figure 1. Comparison of R_{AuAu} and R_{CuCu} at 62.4 GeV for different centralities. The number of estimated binary collisions is shown in the bottom of each panel.

We have also continued the analysis of the earlier runs, particularly the Au + Au system at $\sqrt{s_{nn}} = 200\,\mathrm{GeV}$ and $\sqrt{s_{nn}} = 63\,\mathrm{GeV}$. In figure 2 we compare the R_{AA} for Au + Au at 200 and 62.4 GeV.

We observe that the degree of suppression at 62.4 GeV is much less than at 200 GeV for all centralities. The degree of suppression increases with increasing centrality for both energies. As in the comparison between Au + Au and Cu + Cu, little difference between η=0 and η=1 is observed.

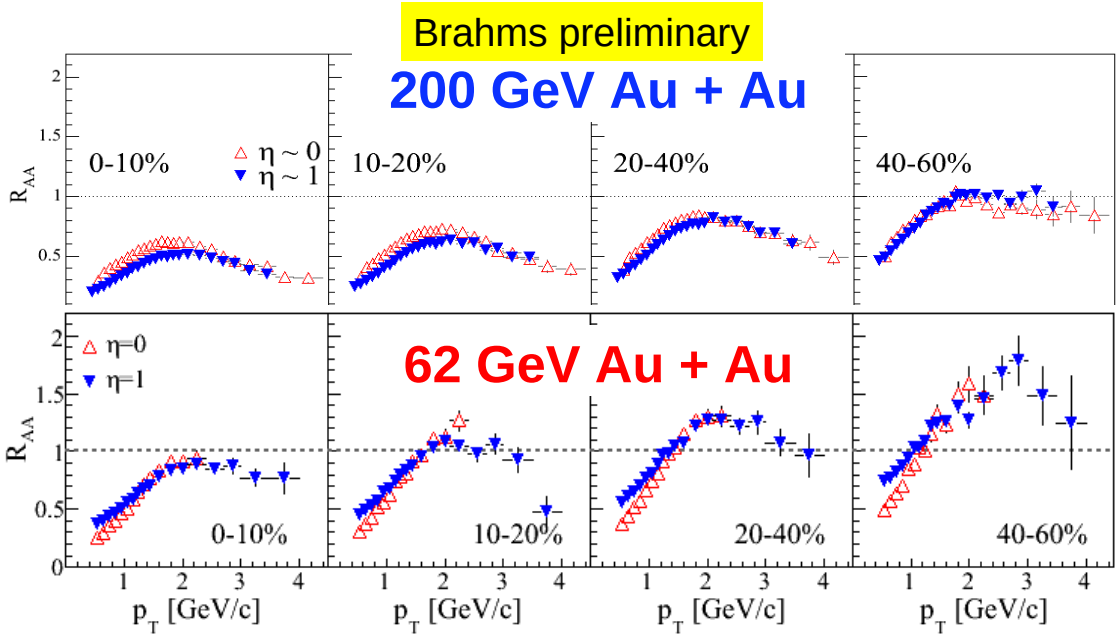

Figure 2. Comparison of R_{AuAu} at 200 and 62.4 GeV for different centralities.

We are spending significant effort to extract the spectra of all charged particles for all of the systems studied. This has required a reevaluation of all of the acceptances, efficiencies and corrections as the experiment has evolved especially in the forward direction during the later high statistics runs. These reevaluations are in progress and are well along. Once completed, they will aid in evaluating the suppression in the forward direction.

Our local group continues the analysis of the p + p data as well as providing a substantial contribution to the infrastructure of the experiment especially in software. We have taken charge of the calibration of the vertex counters as well as the time of flight hodoscopes for RHIC Run-V. We are currently working on a high statistics analysis of the p + p spectra of pions, kaons and protons. It is also necessary for this run to evaluate acceptances and corrections for the different counters which were inserted for the p + p running. These efforts are in progress and results should be available soon.

NIMROD Upgrade

S. Wuenschel, K. Hagel, R. Wada, L. May, F.P. Abbegglen, B. Olsen, G.J. Derrig, S.N. Soisson, B.C. Stein, J.B. Natowitz, and S.J. Yennello

From its beginning, NIMROD has been a nearly 4pi detector. In its initial configuration, it consisted of 8 forward rings, covering from ~3 to 45 degrees, coupled to the back portion of the former Texas A&M CsI ball [1]. Each forward ring was composed of 12 modules containing an ionization chamber (IC) and a CsI crystal. Two modules per ring included a 300μm thick silicon detector between the IC and the CsI. Another two modules per ring included 150μm and 500μm silicon detectors between the IC and CsI. The backward direction was composed of 46 CsI, ion chambers, and some silicon detectors.

For several years, it has been a priority to mate the forward rings of NIMROD with the forward hemisphere of the ISiS array [2, 3]. The ISiS array, will replace the CsI ball in the backward direction. This will greatly increase the backward angle granularity and detection by providing 72 IC-Si-CsI modules.

Since the last project update, a number of improvements have been made. To increase the NIMROD forward angle detection, 300μm silicon detectors have been acquired for the remaining IC– CsI modules. NIMROD-ISiS signals will be treated modularly with motherboards mounted directly on the outer chamber wall. These motherboards will fit around the CsI bias supply boards.

The NIMROD motherboard has undergone several iterations over the last year due to cross talk issues between the CsI and ion chamber within a module. The latest configuration eliminated this cross talk and provided clean IC signals. This configuration placed the IC preamplifier inside the reaction chamber a minimal distance from the detector.

Chambers for the ISiS modules as well as the NIMROD ring 10-11 have been designed and are being constructed. The ISiS chamber will have 18 Indiana motherboards plugged vertically into it.

Both the NIMROD and Indiana motherboards have been built to accommodate IUCF preamplifiers. These preamplifiers have been tested and shown to produce isotopic resolution through, conservatively, Z=8 when used with a NIMROD IC-Si-Si-CsI module (Figure 1). Increased statistics may result in isotopic resolution for higher Z elements.

Ribbon coaxial cables were obtained from AMP/TYCO for relaying signals modularly from the NIMROD and ISiS motherboards. These cables connect to a splitting panel. The panel allows the output signals to be distributed to the various next stage electronics. Ideally, this set up will reduce confusion when correlating signals between the computer and detector.

Further electronics have been obtained for analyzing the signals from the NIMROD/ISiS system. Three new constant fraction discriminators (CFD) will provide trigger signals from the ISiS detectors. Fast signals from the ISiS Si shapers will be multiplexed into small groups for each CFD channel. A trigger module will now be used to regulate the electronic triggering and downscaling mechanisms.

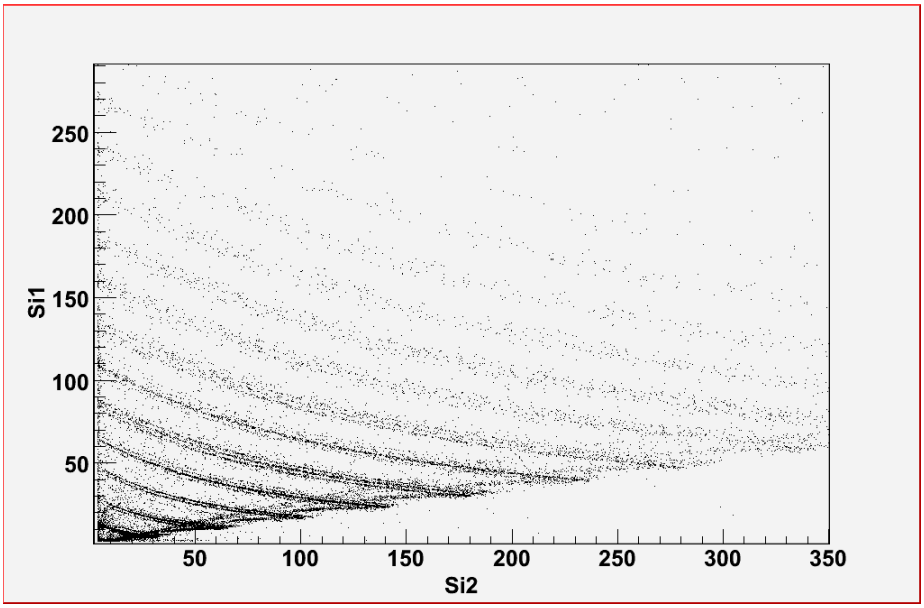

Figure 1. 150 μm Si vs 500 μm Si taken during a test run.

[1] B. Xiao *et al.*, *Progress in Research*, Cyclotron Institute, Texas A&M University (1991-1992), p. 126, *Progress in Research*, Cyclotron Institute, Texas A&M University (1992-1993), p. V-144

[2] J. Wang *et al.*, *Progress in Research*, Cyclotron Institute, Texas A&M University (2001-2002), p. V17-18

[3] K. Kwiatkowski *et al.*, Nucl. Instrum. Methods Phys. Res. **A360** , 571 (1995).

Current Status of the FAUST Array

B.C. Stein, S.N. Soisson, A.L. Keksis, S. Wuenschel, D.V. Shetty, G.A. Souliotis, and S.J. Yennello

Over the past ten years, the Forward Array Using Silicon Technology (FAUST) has been employed in several heavy ion reaction experiments [1-5]. During this time, manufacture has ceased on key components of both preamplifier designs used during the original construction of FAUST. This has left a situation where failing preamplifiers cannot be repaired or replaced. Manufacture of position sensitive silicon detectors (PSDs) have also improved over this time. PSDs are an economical way to increase the granularity of an array due to the reduced number of necessary electronics modules compared with silicon strip detectors of comparable position sensitivity. With this in mind, we have begun a two part upgrade to the FAUST array focusing on updating both the preamplifiers and improving the angular resolution of the array through the use of position sensitive silicon detectors.

During the summer of 2005, the Lecroy HQV810 silicon preamplifiers were replaced by the Indiana University (IU) preamplifier design. To accommodate the larger size of the IU preamps it was necessary to move the location of the preamps to the outside of the vacuum chamber. Previously the preamps had been located inside of the vacuum chamber to keep them physically close to the detectors thereby keeping the cable length between these two components small. Keeping the preamps close to the detector usually improves the resolution of a detector due to a reduction in electronic noise. Knowing that the IU preamps must be installed outside the FAUST vacuum chamber, tests were run to determine the effect of cable length on the resolution of the FAUST silicon detectors. It was determined that minimal signal degradation could be achieved with cable lengths of five feet or less. All of the preamplifiers installed during the upgrade are being mounted as to require a cable length no greater than 3.5 feet. Eight of the InterFet IFPA300 photodiode preamplifiers were also replaced with IU preamps to test the performance of these new preamplifiers when coupled with photodiodes. Preparations for the remainder of the upgrade were also completed at this time. This includes accommodating all 68 of the Si/CsI mounts for dual-lateral PSDs, as well as modifying the signal pass-through plate on the vacuum chamber. The new pass-through plate will allow for 464 signals and can be expanded to allow as many as 544 signals. The FAUST array that includes 68 dual-lateral PSDs will require 340 signals so there is adequate room for growth within the new design.

During the Fall 2005 and continuing into the Winter 2006, FAUST was run with the aforementioned partial upgrade. The Indiana Preamplifier design performed better than expected with the only concern being some micro-phonic sensitivity. It was observed that vibrations from the turbo-pumps caused standing waves in our preamplifier signals. This was easily solved through vibrational dampening and could be improved more through the use of better shielded cables. We observed isotopic resolution up to Oxygen during online analysis which is comparable with the best resolution previously achieved with the FAUST array. It is hoped that during full analysis, isotopic resolution will be seen up to Neon. The IU preamplifiers coupled with photodiodes also performed well and additional IU preamplifiers have been purchased to finish outfitting the array. Currently work is underway to develop dual-lateral design PSDs for installation during the second phase of the upgrade.

[1] F. Gimeno-Nogues *et al.,*. Nucl. Instrum. Methods Phys. Res. **A399**, 94 (1997).
[2] R. Laforest *et al.*, Phys. Rev. C **59** , 2567 (1999).
[3] D.J. Rowland *et al.*, Phys. Rev. C **67** , 064602 (2003).

Studying the Evolution of the Nuclear Symmetry Energy of Hot Fragments from the Compound Nucleus Regime towards Bulk Multifragmentation

G.A. Souliotis, A.S. Botvina,[1] D.V. Shetty, A.L. Keksis, M. Jandel,
M. Veselsky and S.J. Yennello
[1]*Institute for Nuclear Research, Russian Academy of Science, Moscow, Russia*

The evolution of the symmetry energy coefficient of the binding energy of hot fragments with increasing excitation was explored in multifragmentation processes following heavy-ion collisions below the Fermi energy. High-resolution mass spectrometric data on the isotopic distributions of projectile-like fragments from collisions of 25 MeV/nucleon ^{86}Kr and ^{64}Ni beams on heavy neutron-rich targets were systematically compared to calculations involving a two-stage Monte Carlo approach based on the Deep-Inelastic Transfer (DIT) code [1] for the primary interaction stage and the Statistical Multifragmentation Model (SMM) [2] for the de-excitation stage. The study indicated a likely decrease of the symmetry energy coefficient from the conventional value of ~25 MeV at the compound nucleus regime (E*/A < 2

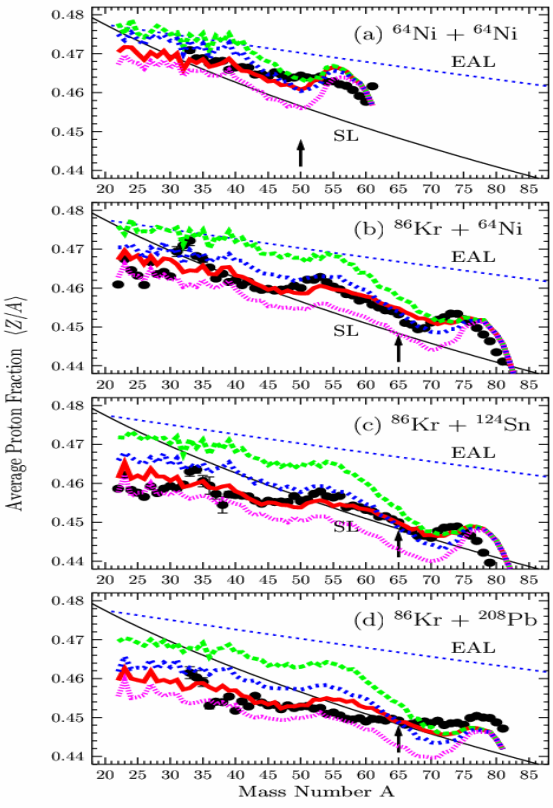

Figure 1. Average Z/A vs A. (a) ^{64}Ni (25 MeV/nucleon)+ ^{64}Ni (BigSol data). (b), (c), (d) ^{86}Kr (25 MeV/nucleon) + ^{64}Ni, ^{124}Sn, ^{208}Pb, respectively (MARS data). Solid points: experimental data. Thin solid line (SL): line of stability. Thin dotted line (EAL): evaporation attractor line. Thick lines: DIT/SMM calculations. Dotted lines, top to bottom: with C_{sym} = 25, 20, 15 MeV, respectively, in the SMM code. Thick solid line: with C_{sym}(E*/A) in SMM given by the thick line in Fig. 2 [3]. The arrow in the various panels indicates an approximate separation between the multifragmentation regime (to the left) and the compound nucleus regime (to the right of the arrow) based on velocity considerations [4] and on the DIT/SMM calculations.

MeV) towards ~15 MeV in the bulk multifragmentation regime (E*/A > 4 MeV). The isotopic distributions of the hot fragments were found to be very wide and extend towards the neutron drip-line for the most neutron-rich systems studied [3]. Apart from a nuclear physics standpoint, these findings may have important implications to the composition and evolution of hot astrophysical environments, such as core-collapse supernova and the ensuing nucleosynthesis processes, such as the r process.

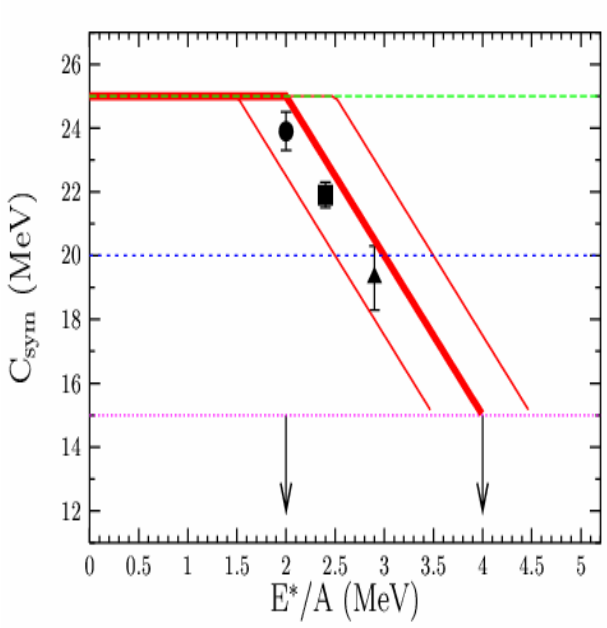

Figure 2. Thick solid line: form of $C_{sym}(E^*/A)$ dependence employed in the SMM calculations,expressing the evolution of the symmetry energy of hot fragments with respect to excitation [3] shown if Fig. 1. Thin solid lines: other forms of $C_{sym}(E^*/A)$ evolution tested. Thin horizontal lines (from top to bottom): C_{sym} = 25, 20, 15 MeV, respectively, used in the calculations of Fig. 1. Solid points: values of C_{sym} from the heavy-residue isoscaling analysis of the ^{86}Kr (circle, square) and ^{64}Ni (triangle) reactions of [4]. The arrows indicate the various de-excitation regimes (schematically): the compound nucleus regime (to the left of the left arrow), the bulk multifragmentation regime (to the right of the right arrow) and the transition region (in between arrows) where the evolution of the symmetry energy is observed.

[1] L. Tassan-Got and C. Stephan, Nucl. Phys. **A524**, 121 (1991).

[2] A.S. Botvina *et al.*, Phys. Rev. C **65**, 044610 (2002); Eur. Phys. J. A **25**, 57 (2005).

[3] G.A. Souliotis *et al.*, nucl-ex/0603006 (2006).

[4] G.A. Souliotis *et al.*, Phys. Rev. C **73**, 024606 (2006).

A Possible Dual-Lateral Upgrade to the FAUST Detector Array

S.N. Soisson, B.C. Stein, M. Jandel, G.A. Souliotis, D.V. Shetty, A.L Keksis,
S. Wuenschel, and S.J. Yennello

In the last several years advances in silicon strip technology and continuous position-sensitive detectors have allowed for more precise measurements of the emission angle of fragments from heavy-ion reactions. By achieving a greater understanding of the emission pattern of fragments from heavy-ion collisions, it is possible that the different modes of disassembly of excited nuclei can be differentiated [1]. Because of the success of FAUST due to its reconstruction capabilities it is a prime candidate for a move towards greater position sensitivity to allow for a greater understanding of multifragmentation reactions.

Micron Semiconductor, the manufacturer of the current FAUST silicon detectors, was contacted to discuss the possibility of creating a position-sensitive detector for FAUST. In looking at current technology and the design constraints of FAUST, a dual-axis lateral position-sensitive detector has been chosen to allow for the desired position sensitivity without sacrificing isotopic resolution [3, 4]. Micron Semiconductor has manufactured and delivered several prototypes that fit within the mechanical constraints of FAUST, however they have not met design specifications as of yet. These detectors have an area of 20mm x 20mm. There are two conductive strip contacts along opposite edges on each side of the detector. The contacts on the front side are perpendicular to those on the back side. The front of the first side prototype detector has a resistivity of 6.8 kΩ while the back side has 22 kΩ. Optimal resistivity on each side has yet to be determined. The active area is surrounded by guard rings on both the front and back side. When an incident particle hits the detector the charge is split between the contacts on each resistive layer. This allows for the total energy to be determined by the summation of either the contacts on the front side or the back side of the detector. The position of each axis can be easily determined using a conventional formula such as $X \propto (Q_1 - Q_2)/(Q_1 + Q_2)$, where Q is the charge collected from one contact.

In the past several months, the first proto-types have been tested. In Figure 1 we see the position reconstructed using the method above. The position resolution is quite clear giving the shape of the mask in front of the detector, however, there are problems concerning the edges of the detector near the conductive strips. Clearly shown on three sides of the detector there is concave bowing. This concave bowing should be corrected by applying voltage to the guard rings. Unfortunately, the guard rings on the first proto-type have been unable to accept voltage. Additionally, to achieve position resolution as in figure 1 the depletion voltage must be reached but a reduction in the energy resolution given by the peaks of a ^{228}Th alpha source occurs as you approach this value. Inconsistent position linearity has also occurred and the determination of position has been a function of bias applied, even if saturation of the semiconductor has been reached. This we believe has been due to the extremely high leakage currents which are on the order of 1.5μA per detector and can fluctuate independently of applied conditions.

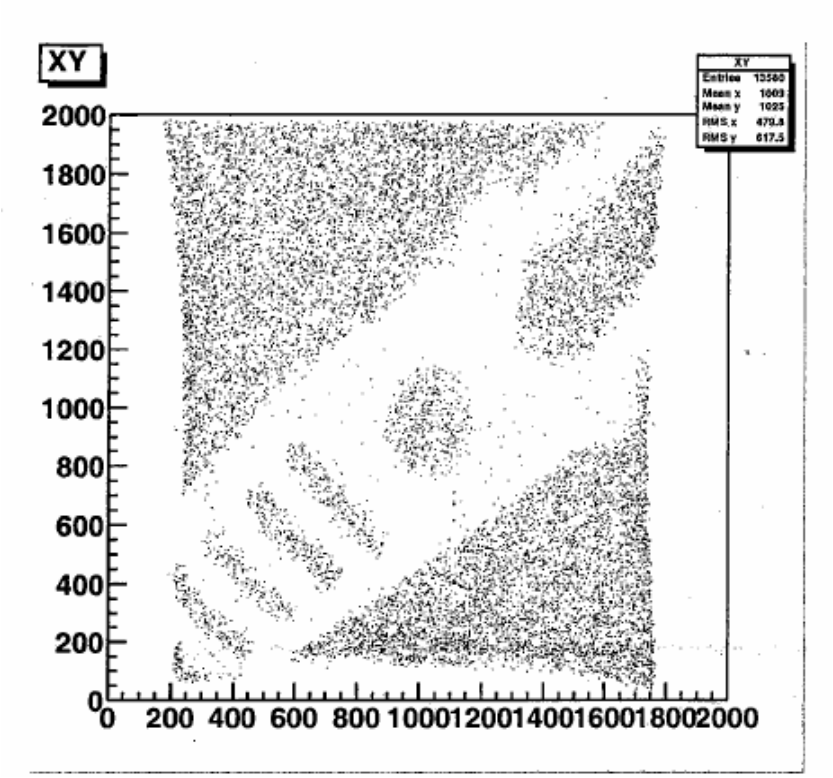

Figure 1. The x y position resolution of the first proto-type detector.

Micron semiconductor has pursued solutions to these problems and has delivered a second proto-type which has recently arrived. It is hopeful that this current proto-type meets our specifications and within the next year the series can be delivered in full.

[1] R. J. Charity *et al.*, Phys. Rev. C **46** 1951 (1992).
[2] F. Gimeno-Nogues, *et al.*, Nucl. Instrum. Methods Phys. Res. **A399**, 94 (1997).
[3] M. Liindroos and O. Skeppstedt, Nucl. Instrum. Methods Phys. Res. **A306**, 225 (1991).
[4] H. J. Woltring, IEEE Trans. Electron Devices **22**, 581 (1975).
[5] K. Kovačević, M. Zadro, Nucl. Instrum. Methods Phys. Res. **A423**, 103 (1999).

Excitation Energy Evolution of the Density in Nuclear Mmultifragmentation

D.V. Shetty, S.J. Yennello, G.A. Souliotis, A.L. Keksis, S.N. Soisson, B.C. Stein, and S. Wuenschel

In multifragmentation reactions, the thermal pressure due to sufficiently large excitation energy drives the nuclear system, to a low density region, beyond which it ceases to exist in a mono-nucleus state and disassembles into many fragments. This density is often referred to as the " break-up " or the "freeze-out" density. Theoretically, the freeze out density in all statistical models is defined as that density in the space-time evolution of the fragmenting system where the nuclear interaction among the generated fragments become frozen, and the fragments thereafter mediate with each other only through their Coulomb interactions. The freeze-out density is generally taken to be independent of the excitation energy and differs appreciably from model to model. Experimentally, two different methods have been adopted so far to study the evolution of density as a function of excitation energy. In one study [1], the density has been determined from Coulomb barriers required to fit the intermediate mass fragments kinetic energy spectra. In another [2], it has been determined from the analysis of apparent level density parameters required to fit the measured caloric curves. Both studies show that the density of the multifragmenting system decreases with increasing excitation energy. However, the two sets of results are not in agreement with each other at higher excitation energies ($E^* > 5$ MeV/nucleon). It is observed that densities derived from Coulomb barrier systematics are comparatively lower than those derived from the level density parameters at higher excitation energies.

In this work, we determine the density by requiring a fit to the excitation energy dependence of the isoscaling parameter and the excitation energy dependence of the temperature (i.e. the caloric curve) simultaneously. We make use of the expression for the isoscaling parameter α as a function of excitation

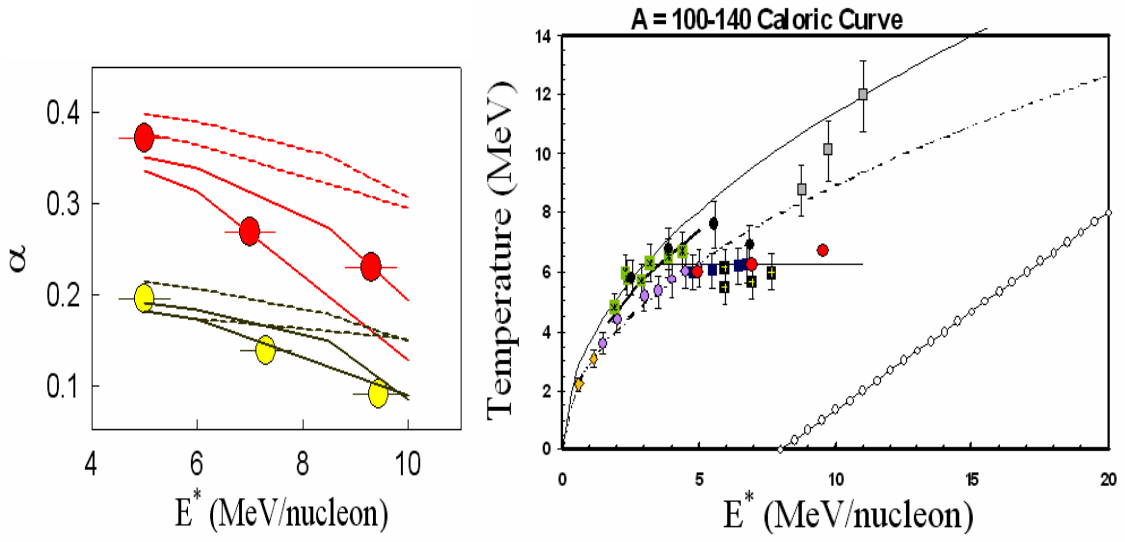

Figure 1. Experimental isoscaling parameter α and temperature as a function of excitation energy. The data points (other than the red symbols) in the right figure is taken from Ref. [2].

energy and the expanding Fermi gas relation, assuming that the temperatures in both relations are correlated. Fig. 1 (left) shows the isoscaling parameter α as a function of the excitation energy for the A ~ 100 nuclei. Fig. 1 (right) shows the temperature versus the excitation energy plot (solid red symbols) obtained from the present study that is consistent with the excitation energy dependence of the α parameter.

Fig. 2 shows the excitation energy dependence of the density from the present measurements (symbols with error bars). The results of Viola et al.[1], and Natowitz et al.[2], are also shown for comparison. The solid curve in the figure corresponds to the breakup density calculated from the statistical multifragmentation model by Bondorf et al., [3]. The present measurements show a decrease in the density with increasing excitation energy and are in good agreement with those determined from the apparent level density parameter by Natowitz et al. The closer agreement between the present measurements and the calculated density seem to indicate that the density obtained from the present measurements and those obtained from the apparent level density parameter might be characteristic of much earlier stage of the expanding system i.e., before the freeze-out, and when the fragment yield or charge distribution is determined and the density is still evolving with excitation energy. The density obtained from the Coulomb barrier systematic might be characteristic of a later stage i.e., the freeze-out stage, where the density has ceased to evolve and the fragment kinetic energy is determined. This indicates that two characteristics volume and density might be important in understanding the multifragmentation process.

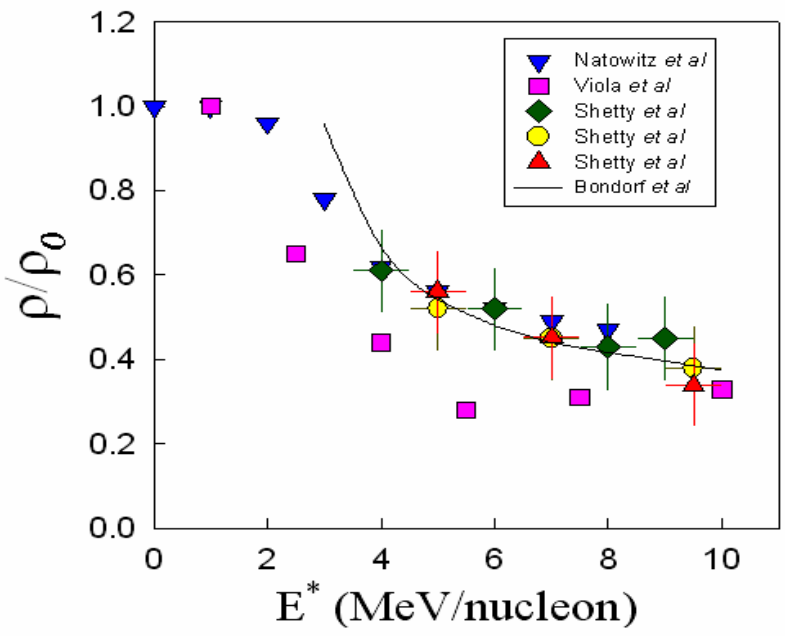

Figure 2. Comparison between various methods for extracting the density as a function of excitation energy.

[1] V. Viola *et al.*, Phys. Rev. Lett. **93**, 132701 (2004).

[2] J.B. Natowitz *et al.*, Phys. Rev. C **66**, 031601(R) (2002).

[3] J. Bondorf *et al.*, Nucl. Phys. **A444**, 460 (1985)

Nuclear Expansion and Symmetry Energy at Low Density

D.V. Shetty, S.J. Yennello, G.A. Souliotis, A.L. Keksis, S.N. Soisson, B.C. Stein, and S. Wuenschel

In this report we try to obtain information on the density dependence of the symmetry energy by comparing the experimental isoscaling data with the Statistical Multifragmentation Model (SMM) calculation and the expanding Fermi gas relation. Fig. 1 (left) shows the symmetry energy as a function of excitation energy obtained by comparing the experimental isoscaling parameter with those of the statistical multifragmentation model calculation in Fe + Fe and Ni + Ni, and Fe + Ni and Ni + Ni pair of reactions. The temperature as a function of the excitation energy (caloric curve) obtained from the statistical multifragmentation model agrees very well with the vast body of data that exist in the literature for the caloric curve. Fig. 1 (right) shows the density as a function of the excitation energy obtained using the expanding Fermi gas relation (or assuming the break-up density in SMM to be evolving) that reproduces the Caloric curve obtained in this mass region. The correlation between the symmetry energy and the density as a function of excitation energy obtained is then used to plot the density dependence of the symmetry energy. Fig 2 shows the symmetry energy as a function of the density (solid circles). The solid square corresponds to the experimental data obtained by fitting the experimental differential cross-section data in a charge exchange reaction using the isospin dependent optical potential by Khoa *et al.* [1]. The solid curve corresponds to $E_{sym}(\rho) = 31.6(\rho/\rho_0)^{0.69}$ MeV, which was obtained by comparing the present data with the AMD calculation as discussed in Ref. [2, 3]. This dependence was obtained by comparing the experimentally determined isoscaling parameter with those predicted by the Anti-symmetrized Molecular Dynamic (AMD) calculation. The close agreement between the two different approaches for determining the density dependence of the symmetry energy as shown in fig. 3 is

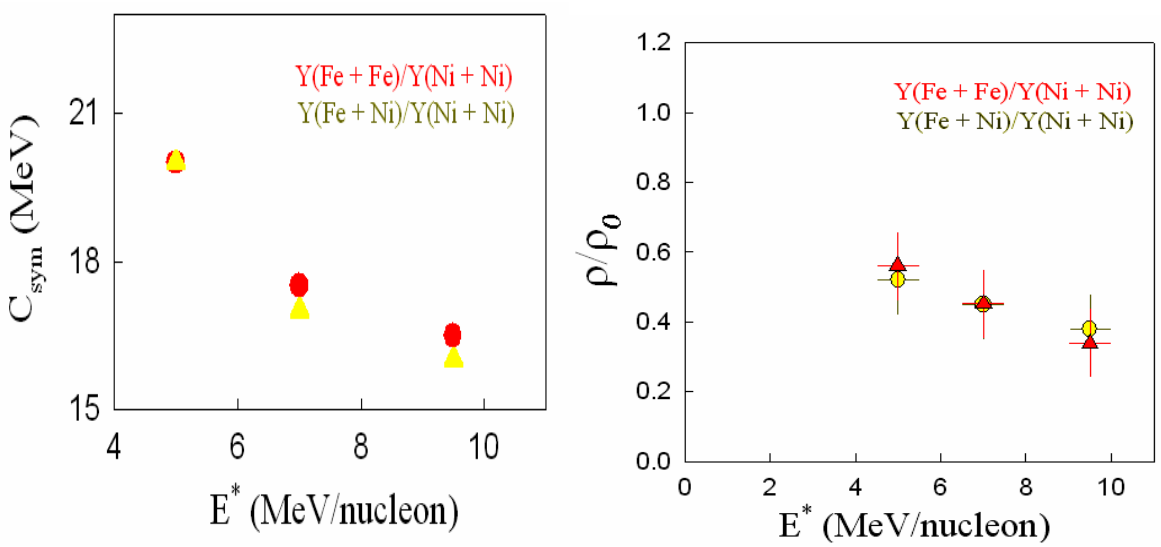

Figure 1. (left) Symmetry energy as a function of the excitation energy. (Right) Density as a function of excitation energy for the Fe + Fe and Ni + Ni, and Fe + Ni and Ni + Ni reaction pairs.

encouraging. The decrease in the symmetry energy therefore appears to be related to the decrease in density with increasing excitation.

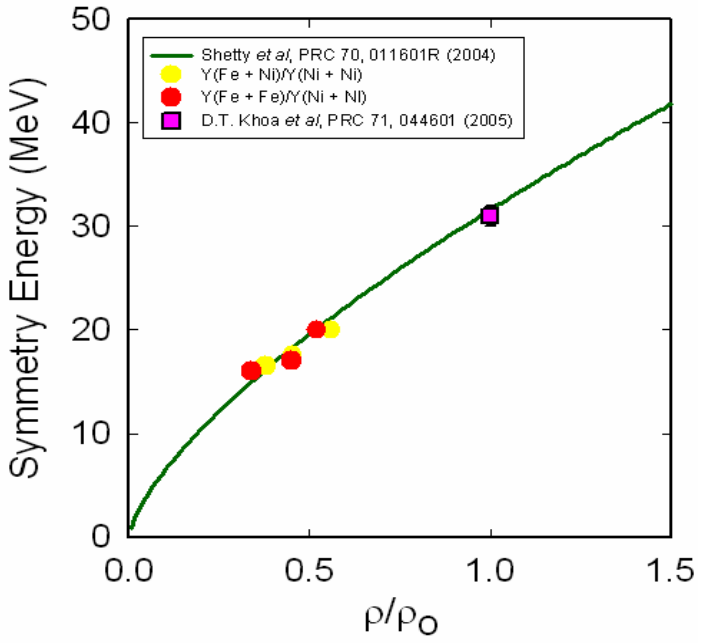

Figure 2. Comparison of the density dependence of the symmetry energy obtained from the dynamical model and the statistical model approach.

[1] D.T. Khoa *et al.*, Phys. Rev. C 71, 044601 (2005).

[2] D.V. Shetty *et al.*, Phys. Rev. C 70, 011601 (2004).

[3] D.V. Shetty *et al.*, nucl-ex/0512011 (2005).

Symmetry Energy and Multifragmentation of ^{40}Ar, ^{40}Ca + ^{58}Fe, ^{58}Ni Reactions at 25, 33, 45 and 53 MeV/nucleon

D.V. Shetty, J. Iglio, S.J. Yennello, G.A. Souliotis, M. Jandel, A.L. Keksis, S.N. Soisson, B.C. Stein, S. Wuenschel and A.S. Botvina[1]

[1]*Institute for Nuclear Research, Russian Academy of Science, Moscow, Russia*

Recently, the possibility of extracting information on the symmetry energy and the isospin of the fragments in a multifragmentation reaction has gained tremendous importance. Traditionally, the symmetry energy has been extracted by fitting the binding energy in their ground state with various versions of the liquid drop mass formula. The properties of the nuclear matter are then determined by theoretically extrapolating the nuclear models designed to study the structure of real nuclei. However, real nuclei are cold, nearly symmetric and found at equilibrium density. It is not known how the symmetry energy behaves at temperature and density away from the normal nuclear matter. In a multifragmentation reactions the fragments produced are highly excited and neutron-rich; their yields depend on the available free energy, which in turn depends on the symmetry energy and the extent to which the fragments expand. It has been shown that the isoscaling parameter α is proportional to the symmetry energy part of the fragment binding energy. Therefore, by studying the isoscaling parameters one can extract information about the symmetry energy and the properties of the fragments under non-normal nuclear conditions.

Fig. 1 (left) shows a comparison of the Statistical Multifragmentation Model (SMM) calculated α with the experimentally determined α as a function of excitation energy for different values of the symmetry energy γ. The dotted lines correspond to the primary fragments and the solid lines to the

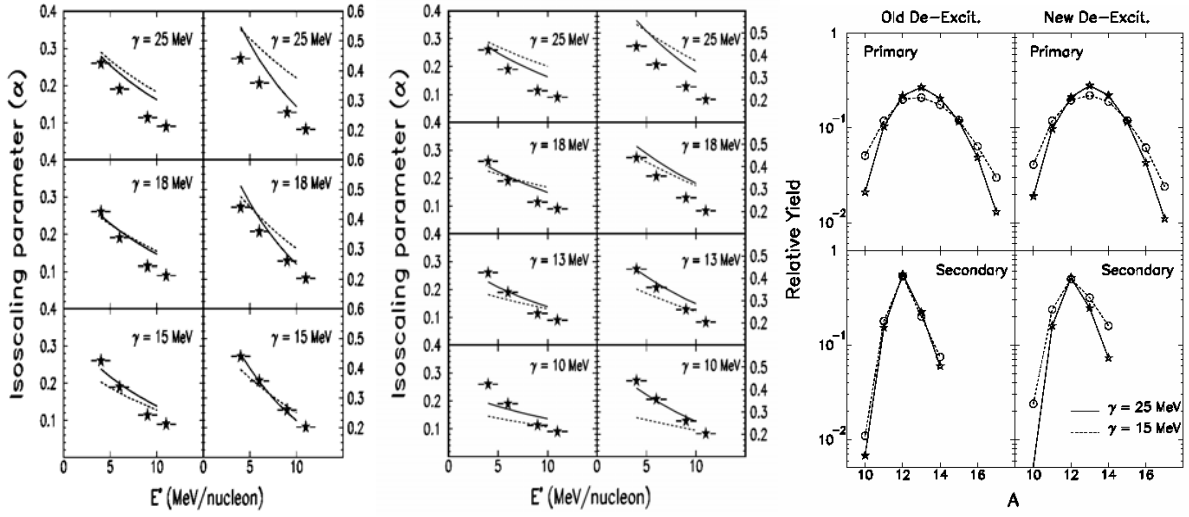

Figure 1. (Left) Comparison of the SMM calculated α with the experimentally determined α. The left panel in the figure corresponds to the Ar + Ni and Ca + Ni pair of reactions, and the right to Ar + Fe and Ca + Ni pair. (Center) same as the left, but with evolving symmetry energy during sequential decay of the hot primary fragments. (Right) Comparison between the calculated fragment isotopic distributions for the C element using two different assumptions.

secondary fragments. It is observed that the experimentally determined α can be reproduced simultaneously at all excitation energies by assuming a single value of the symmetry energy, γ = 15 MeV. This value of symmetry energy is significantly lower than the value of γ = 25 MeV used for ground state nuclei near saturation density.

Fig. 1 (center) shows the same calculation, which takes into account the mass evolution of the hot primary fragments due to lower symmetry energy during their sequential de-excitations. It is observed that in this case, the experimental α values can be explained by symmetry energy γ = 10 – 13 MeV. The difference in the two calculations can be understood by comparing the final fragment yield distributions as shown in fig. 1 (right). It is observed that the calculation with the standard de-excitation leads to a narrow final distribution and the isotopes are concentrated close to the β-stability line. The difference in the final yield distributions for γ = 15 MeV and γ = 25 MeV is very small. This difference is much pronounced in the new calculation. The final isotopic distributions in this case are wider and shifted towards neutron-rich side.

The lower value of the symmetry energy (γ = 15 MeV) required in this analysis was obtained by assuming a constant freeze-out density of 1/3 ρ_0 in the SMM calculation and is consistent with our Fe, Ni + Fe, Ni analysis, where the comparison between the experiment and the calculations was made for each excitation energy with evolving density.

The above results indicate that the properties of nuclei produced at high excitation energy, isospin and reduced density could be significantly different from those of the cold isolated nuclei.

[1] D.V. Shetty *et al.*, Phys. Rev. C **71**, 024602 (2005).
[2] A. LeFevre *et al.*, Phys. Rev. Lett **94**, 162701 (2005).
[3] D. Henzlova *et al.*, nucl-ex/0507003 (2005).
[4] J. Iglio *et al.*, Phys. Rev. C (Submitted).

Isospin Distillation and the Reduced Nucleon Densities in ^{40}Ar, ^{40}Ca + ^{58}Fe, ^{58}Ni Reactions at 25, 33, 45 and 53 MeV/nucleon

D.V. Shetty, J. Iglio, S.J. Yennello, G.A. Souliotis, M. Jandel, A.L. Keksis, S.N. Soisson, B.C. Stein, S. Wuenschel and A.S. Botvina[1]

[1]*Institute for Nuclear Research, Russian Academy of Science, Moscow, Russia*

The Liquid-Gas phase transition in isospin asymmetric nuclear matter may result in an inhomogeneous distribution of the neutrons and the protons within the system (isospin distillation), where a dilute neutron-rich (N/Z > 1) gas (light clusters) and a dense and symmetric (N/Z ~ 1) liquid (heavy fragments) is formed [1]. In this work, the composition of the gas phase in ^{40}Ar + ^{58}Fe and ^{40}Ar + ^{58}Ni reactions with respect to ^{40}Ca + ^{58}Ni reaction were studied at 25, 33, 45 and 53 MeV/nucleon. Figure 1 below shows the relative neutron and proton densities in the gas phase obtained from the measured isotope and isotone yield ratios as a function of the difference in N/Z of the composite systems. It is observed that the neutron content of the gas phase is sensitive to both the isospin (N/Z) of the initial colliding nuclei and the excitation energy. The asymmetry (difference in the neutron and the proton density) in the gas phase increases with increasing difference in N/Z of the composite systems, and decreases with increasing beam energy. The asymmetry is observed to decrease from ~ 1.0 at 25 MeV/nucleon to ~ 0.6 at 45 MeV/nucleon for the Ar + Fe and Ca + Ni pair of reaction. The observed decrease indicates a decrease in the sensitivity of the isospin effect with increasing temperature. The observed result is in good agreement with those determined in the past using the Ni, Fe + Ni, Fe reactions at 30, 40, and 47 MeV/nucleon.

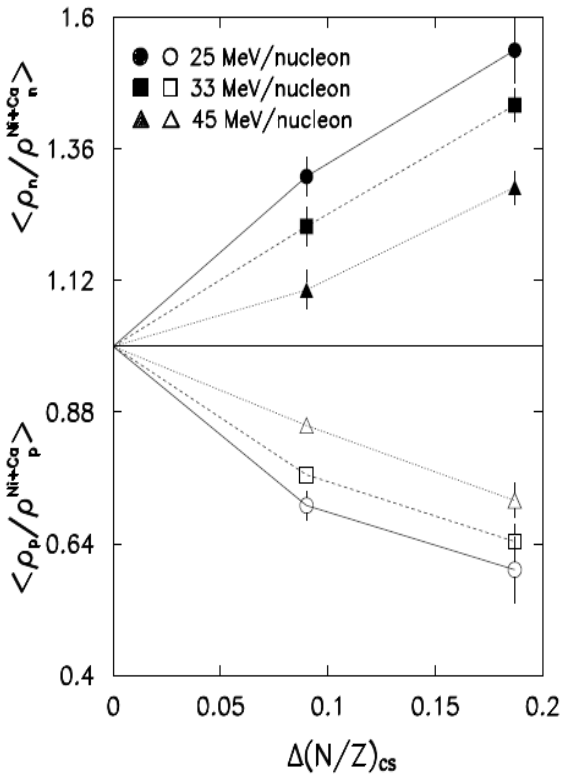

Figure 1. Relative neutron (top) and proton densities (bottom) as a function of the difference in N/Z of the composite systems for various beam energies.

[1] D.V. Shetty *et al.*, Phys. Rev. C **68**, 021602 (2003).

[2] J. Iglio *et al.*, Phys. Rev. C (Submitted).

Isoscaling Properties of the Fragments Pproduced in Multifragmentation of ^{40}Ar, ^{40}Ca + ^{58}Fe, ^{58}Ni Reactions at 25, 33, 45 and 53 MeV/nucleon

D.V. Shetty, J. Iglio, S.J. Yennello, G.A. Souliotis, M. Jandel, A.L. Keksis, S.N. Soisson, B.C. Stein, S. Wuenschel and A.S. Botvina[1]

[1]*Institute for Nuclear Research, Russian Academy of Science, Moscow, Russia*

In multifragmentation reactions, the ratio of fragment yields in two different systems, 1 and 2, $R_{21}(N,Z) = Y_2(N,Z)/Y_1(N,Z)$, are known to obey an exponential dependence on the neutron number (N) and the proton number (Z) of the fragments in an observation known as isoscaling. The dependence is given by a simple relation,

$$R_{21}(N,Z) = Y_2(N,Z)/Y_1(N,Z) = C \exp(\alpha N + \beta Z)$$

Where Y_2 and Y_1 are the yields from the neutron-rich and neutron-deficient systems, respectively. C is the overall normalization factor, and α and β are the parameters characterizing the isoscaling behavior.

The isoscaling parameters obtained in ^{40}Ar, ^{40}Ca + ^{58}Fe, ^{58}Ni reactions at 25, 33, 45 and 53 MeV/nucleon are presented in this report. Fig. 1 (left) shows the experimentally measured relative isotopic yield distributions for the Li, Be and C elements in ^{40}Ca + ^{58}Ni reactions (star symbols), ^{40}Ar + ^{58}Ni (circle symbols) and ^{40}Ar + ^{58}Fe (square symbols) for 25, 33 and 45 MeV/nucleon beam energies. The distributions for each element show higher fragment yield for the n-rich isotopes in ^{40}Ar + ^{58}Fe reaction (square), which has the largest neutron-proton ratio (N/Z), in comparison to the ^{40}Ca + ^{58}Ni

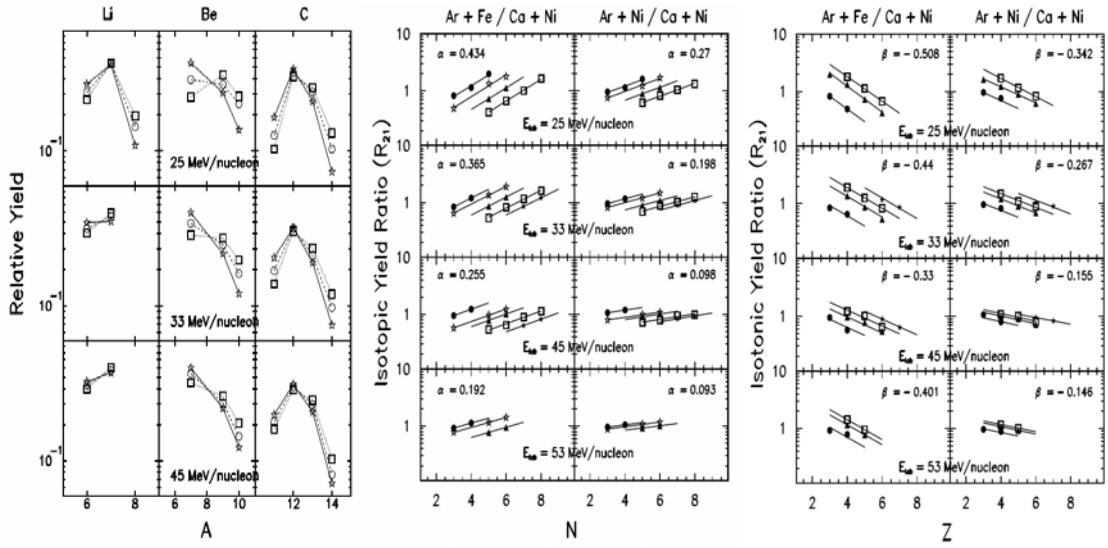

Figure 1. (Left) Relative isotopic yield distributions. (Center) Isotopic yield ratios as a function of neutron number N. (Right) Isotonic yield ratios as a function of proton number Z.

reaction (star), which has the smallest neutron-to-proton ratio. The yields for the reaction, ^{40}Ar + ^{58}Fe

(circles), which has an intermediate value of the neutron-to-proton ratio, are in between those of the other two reactions. It is observed from this figure that the isotopic composition of the fragments produced in multifragmentation reaction is sensitive to the isospin (N/Z) of the composite system. The relative difference in the yield distribution between the reactions is also observed to decrease with increasing beam energy.

The isotopic yield ratio as a function of neutron number N, is shown in Fig. 1 (center). The isoscaling parameter α for all the reactions were obtained by simultaneously fitting the ratio of the isotopic yields using the above equation. It is observed that α is larger for the ^{40}Ar + ^{58}Fe and ^{40}Ca + ^{58}Ni reactions, which has a larger difference in the N/Z of the systems in the pair, compared to the ^{40}Ar + ^{58}Ni and ^{40}Ca + ^{58}Ni reactions, which has a smaller difference in the corresponding N/Z. Fig. 1 (right) shows the isotonic yield ratio as a function of the proton number Z and parameter β obtained from them. Fig. 2 (left) shows the evolution of the isoscaling parameters α and β as a function of the beam energy and the isospin of the system. It is observed that α (β) decrease (increase) with increasing beam energy. The α (β) parameters are observed to be larger (smaller) for systems with higher isospin (N/Z).

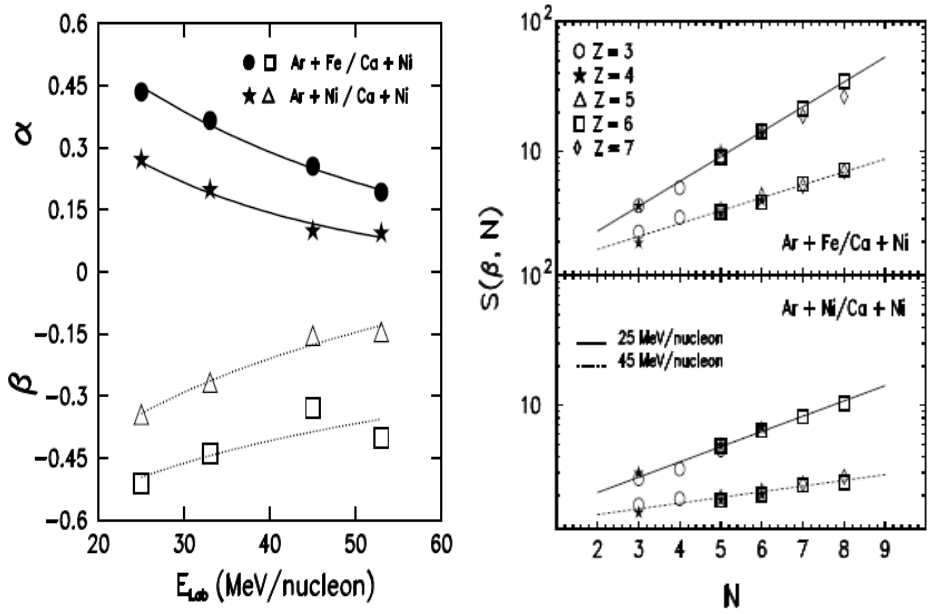

Figure 2. (Left) Isoscaling parameters α and β as a function of the beam energy. (Right) Scaled isotopic ratio S(β,N) as a function of neutron number N.

The isoscaling properties were also studied by constructing the scaling factor, $S(\beta,N) = R_{21}(N,Z)e^{-\beta Z}$. Fig. 2 (left) shows the S(β,N) from two different reaction pairs plotted as a function of neutron number N for beam energies of 25 and 45 MeV/nucleon. A significant difference in the scaling for the two beam energies are observed, indicating the influence of temperature on the isotopic yields of the light clusters. The present observation demonstrates the role played by the temperature in the distillation of nuclear matter into a neutron-rich gas and a symmetric liquid phase.

[1] J. Iglio *et al.*, Phys. Rev. C (Submitted).

Constraining the Density Dependence of the Symmetry energy in the Nuclear Equation of State

D.V. Shetty, S.J. Yennello, and G.A. Souliotis

The key element for constructing the nuclear Equation Of State (EOS) is the basic nucleon-nucleon interaction. Until now our understanding of the nucleon-nucleon interaction has always come from studying nuclear matter that is symmetric in isospin and close to normal nuclear matter density (ρ = 0.16 fm^{-3}). It is not known how far this understanding remains valid as one moves away from normal nuclear density and symmetric nuclear matter. Various interactions used in "ab initio" microscopic calculations predict different forms of the nuclear equation of state above and below the normal nuclear matter density, and away from the symmetric nuclear matter. As a result of which, the symmetry energy, which is the difference in energy between the pure neutron matter and the symmetric nuclear matter, show a very different behavior below and above normal nuclear density. Constraining the form of the density dependence of the symmetry energy is important for a better understanding of the nucleon-nucleon interaction, and hence the structure of atomic nuclei. It is also important for understanding the structure of compact stellar objects such as the neutron stars. The figure below shows the form of the density dependence of the symmetry energy obtained from the present isotopic yield distribution measurements in multifragmentation reactions of ^{40}Ar, ^{40}Ca, ^{58}Fe, ^{58}Ni + ^{58}Fe, ^{58}Ni at beam energies from 25 – 53 AMeV. A comparison with several other recent independent studies is also shown. The green curve corresponds

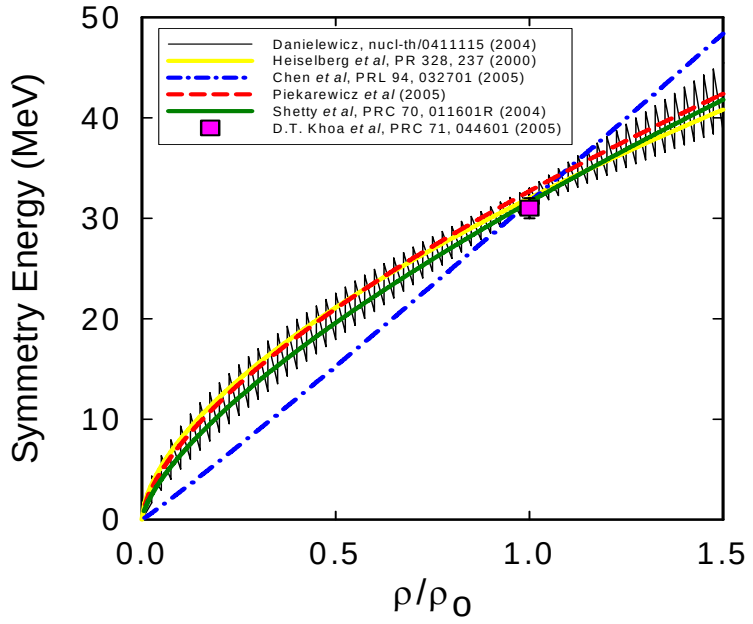

Figure 1. Comparison of the density dependence of the symmetry energy obtained from various different studies.

to the one obtained from Gogny-AS interaction that explains the present results from the fragment isotopic distribution, assuming a small sequential decay effect [1,2]. The red dashed curve correspond to

those obtained recently from an accurately calibrated relativistic mean field interaction, used for describing the Giant Monopole Resonance (GMR) in ^{90}Zr and ^{208}Pb, and the IVGDR in ^{208}Pb by Piekarewicz *et al.* [3]. The blue dot-dashed curve correspond to the one used for explaining the isospin diffusion data of NSCL-MSU by Chen *et al.* [4]. This dependence has now been modified to include the isospin dependence of the in-medium nucleon-nucleon cross-section, and is in good agreement with the present study. The shaded region in the figure corresponds to those obtained by constraining the binding energy, neutron skin thickness and isospin analogue state in finite nuclei using the mass formula of Danielewicz [5]. The yellow curve correspond to the parameterization adopted by Heiselberg *et al.* [6] in their studies on neutron stars, and obtained by fitting the predictions of the variational calculations of Akmal *et al.* [7]. Finally, the solid square point in the figure correspond to the value of symmetry energy obtained by fitting the experimental differential cross-section data in a charge exchange reaction using the isospin dependent optical potential by Khoa *et al.* [8]. The parameterized forms of the density dependence of the symmetry energy obtained from all these studies are as shown in table below. The close agreement between various studies leads to a constraint on the density dependence of the symmetry energy, which can be given as, $E_{sym}(\rho) = C(\rho/\rho_o)^{\gamma}$, where C = 31 – 33 MeV and γ = 0.6 – 1.0 . The present constrain leads to nuclear matter compressibility K ~ 230 MeV, neutron skin thickness, $R_n - R_p \sim 0.21$ fm for ^{208}Pb nuclei, radius of 11 – 13 km for the canonical neutron star and a direct URCA cooling for neutron stars above 1.4 times the solar mass.

Table I. Parameterized form of the density dependence of the symmetry energy obtained from various independent studies.

Reference	Parameterization	Studies
Heiselberg *et al.* [6]	$\mathbf{32.0(\rho/\rho_o)^{0.60}}$	**Variational calculation**
Danielewicz *et al.* [5]	$\mathbf{31(33)(\rho/\rho_o)^{0.55(0.79)}}$	**BE, Skin,Isospin analogue states**
Chen *et al.* [4]	$\mathbf{31.6(\rho/\rho_o)^{1.05}}$	**Isospin diffusion**
Piekarewicz *et al.* [3]	$\mathbf{32.7(\rho/\rho_o)^{0.64}}$	**GMR, IVGDR**
Shetty *et al.* [1,2]	$\mathbf{31.6(\rho/\rho_o)^{0.69}}$	**Isotopic distribution**

[1] D.V. Shetty *et al*., Phys. Rev. C **70**, 011601 (2004).
[2] D.V. Shetty *et al*., *nucl-ex/*0512011 (2005).
[3] J. Piekarewicz (Private Communication) (2005).
[4] L.W. Chen *et al*., Phys. Rev. Lett. **94**, 032701 (2005).
[5] P. Danielewicz, *nucl-th/*0411115 (2004).
[6] H. Heiselberg and M. Hjorth-Jensen, Phys. Rep. **328**, 237 (2000).
[7] A. Akmal *et al.*, Phys. Rev. C **58**, 1804 (1998).
[8] D.T. Khoa *et al*., Phys. Rev. C **71**, 044601 (2005).

Mapping the Symmetry Energy Using Reconstructed Quasiprojectile Sources

A.L. Keksis, M. Veselsky, G.A. Souliotis, D.V. Shetty, M. Jandel, E. Bell, A. Ruangma, E.M. Winchester, J. Garey, S. Parketon, C. Richers, and S.J. Yennello

To fully understand the symmetry energy term in the nuclear binding energy equation, a detailed mapping of the variation of the symmetry energy as a function of temperature and density is needed. The current study uses projectile-like sources, called quasiprojectiles, that were reconstructed from isotopically identified fragments formed from the reactions 32 and 45 MeV/nucleon ^{40}Ar, ^{40}Ca and ^{48}Ca on ^{112}Sn and ^{124}Sn. The technique of isoscaling was used on the isotopically resolved yields from these

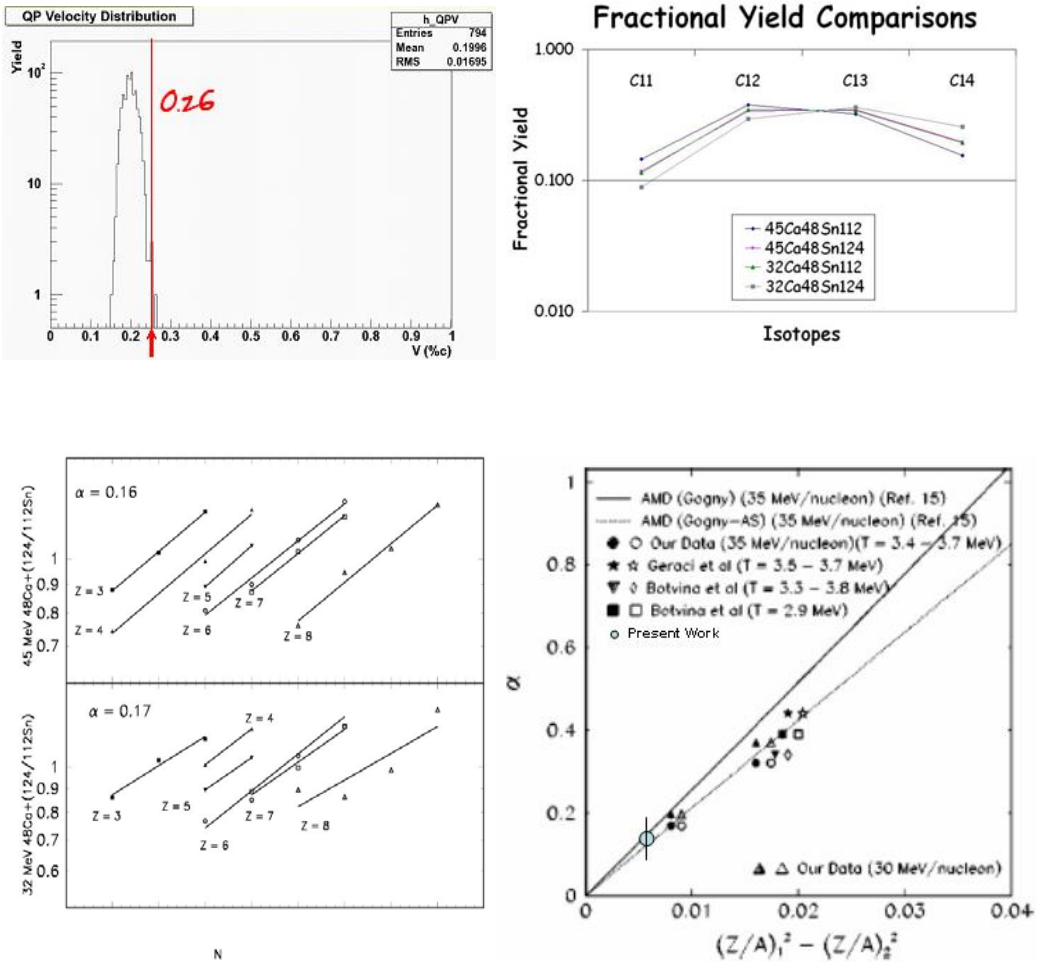

Figure 1. Top Left -Velocity spectrum of reconstructed sources from the reaction 32MeV/nucleon ^{48}Ca + ^{124}Sn. These sources have $Z_{source} = Z_{beam}$ and multiplicity greater than 3. The red arrow shows the beam velocity at 0.26c. Top Right -The fractional yields of Carbon, for four systems. Bottom Left - Isoscaling of the fragment yields from Lithium to Oxygen for two sets of systems. Bottom Right - Comparison of experimental a (32 MeV/nucleon) with literature values (35 MeV/nucleon) is consistent with the observed trend (Figure from Ref.[3]).

sources to determine the isoscaling parameter α. α will also be determined from the isotopic yields from a

hybrid model, using DIT, the Deep Inelastic Transfer code of Tassan-Got [1], to simulate the interaction stage and form the quasiprojectiles, and SMM, the Statistical Multifragmentation Model of Botvina [2], to simulate the breakup stage of the quasiprojectile sources.

Quasiprojectiles are forward focused, so a forward array with good forward angle coverage and granularity is needed, and is provided by, FAUST, the Forward Array Using Silicon Technology [2]. FAUST has 68 detector telescopes arranged in 5 rings covering 2° to 33° with 90% angular coverage. The experimental details and analysis can be found in [4-7]. To reconstruct an event the quasiprojectile charge, Z_{qp}, and apparent quasiprojectile mass number, A_{qp}, are calculated using $Z_{qp} = \sum Z_f$ and $A_{qp_{Apparent}} = \sum A_f$, where the summations are over the charge of the fragment, Z_f, and the mass number of the fragment, A_f. FAUST does not detect neutrons, so future analysis using the technique of Rowland will be used to correct for missing neutrons [8]. The apparent quasiprojectile excitation energy is calculated using the balance of energy: $E^*_{qp_{Apparent}} = \sum (m_f + E_{f_{cms}}) - m_{qp}$, where the masses can be calculated from the mass number and the mass excesses, which are know from the mass tables of Audi *et al*. [9], and the energy of the fragment in the center of mass frame is given by, $E_{f_{cms}} = \frac{1}{2} m_f v^2_{f_{cms}}$.

Since we want quasiprojectiles that have undergone multifragmentation a multiplicity requirement of greater than 3 is used, which discards lower multiplicity events that can be from other sources, such as scattered beam and other sources. An additional cut of $Z = Z_{beam}$, which is opened to $Z = Z_{beam} \pm 5$ to increase statistics, also helps select quasiprojectile sources. To verify that the reconstructed sources are projectile-like, the velocity spectrum should be sharply peaked near beam velocity. As shown in top left of the figure the peak is sharply peaked near the beam velocity at 0.26c.

The isotopic yields from the quasiprojectiles formed from the reactions ^{48}Ca on ^{112,124}Sn at 32 and 45MeV/nucleon were calculated. The isotopic yields were then used to find the fractional yields using, $FY = \frac{Y(^A X_Z)}{\sum Y(^A X_Z)}$, where the yield of a given isotope is divided by the yields of all the isotopes of that element, which is independent of the number of events and the systems can be compared to one another. The fractional yields of Carbon for these four systems are shown in the top right of the figure. The more neutron-rich system at each energy has larger fractional yields for the neutron rich isotopes than the proton-rich system. Comparing the energy effect the higher energy pair of systems have a reduced difference between the neutron-rich and proton-rich systems. The other elements, H, He, Li, Be, B, N and O exhibit the same trends.

The technique of isoscaling was then used on the isotopically resolved yields from these sources [10]. The reactions ^{48}Ca on ^{112,124}Sn at 32 and 45MeV/nucleon are shown at the bottom left of the figure. The 45 MeV/nucleon systems have a mean excitation energy around 146 MeV and an a of 0.16, while the 32 MeV/nucleon systems have a mean excitation energy around 108 MeV and an a of 0.17. The 32 MeV/nucleon α is compared to literature values (35MeV/nucleon data) in the bottom right of the figure and follows the trend.

[1] L. Tassan-Got *et al.*, Nucl. Phys. **A524**, 121 (1991).

[2] A.S. Botvina *et al.,* Phys. Rev. C **63**, 061601 (2001).
[3] Gimeno-Nogues *et al*., Nucl. Instrum. Methods Phys. Res. **A399**, 94 (1997).
[4] A.L. Keksis *et al*., *Progress in Research*, Cyclotron Institute, Texas A&M University (2001-2002), p. II-38.
[5] A.L. Keksis *et al*., *Progress in Research*, Cyclotron Institute, Texas A&M University (2002-2003), p. II-11.
[6] A.L. Keksis *et al*., *Progress in Research*, Cyclotron Institute, Texas A&M University (2003-2004), p. II-23.
[7] A.L. Keksis *et al*., *Progress in Research*, Cyclotron Institute, Texas A&M University (2004-2005), p. II-25.
[8] D. Rowland, Ph.D. Thesis, Texas A&M University (2000).
[9] G. Audi *et al*., Nucl. Phys. **A729**, 337 (2003).
[10] M.B. Tsang *et al*., Phys. Rev. C **64**, 041603R (2001).

SECTION III

NUCLEAR THEORY

Astrophysical Factor for the Neutron Generator $^{13}C(\alpha,n)^{16}O$ Reaction in the AGB Stars

A. M. Mukhamedzhanov , V. Z. Goldberg, G. Rogachev,[1] E. Johnson,[1]
S. Brown,[1] K. Kemper,[1] A. Momotyuk,[1] and B. Roeder[1]
[1]*Department of Physics, Florida State University, Tallahassee, FL 32306*

About half of all elements heavier than Iron are produced in Stellar environment through the s process. Reaction $^{13}C(\alpha,n)^{16}O$ is considered to be the main source of neutrons for the s processes at low temperatures in low mass stars at the asymptotic giant branch [1]. Accurate knowledge of the $^{13}C(\alpha,n)^{16}O$ reaction rates at relevant temperatures $(0.8-1.0)\times10^8$ K would eliminate an essential uncertainty regarding the overall neutron balance and will allow for better tests of modern Stellar models with respect to ^{13}C production in AGB stars (see [2] and references therein). The rate of the $^{13}C(\alpha,n)^{16}O$ reaction at temperatures $\sim10^8$ K is uncertain by $\sim500\%$ [3] due to prohibitively small reaction cross section at energies below 300 keV. Directly measured $^{13}C(\alpha,n)^{16}O$ cross section is only available at energies above 279 keV (see [3] and references therein). Below this energy the astrophysical S factor is dominated by the contribution from the $1/2^+$ sub-threshold resonance in ^{17}O at 6.356 MeV excitation energy, which is just 3 keV below α threshold. It was assumed in recent NACRE compilation [3] that this resonance has a well developed α cluster structure. This assumption leads to a strong enhancement of the cross section at low energies [3]. Recently an attempt has been made by Kubono et al. [4] to determine the contribution of the subthreshold 6.356 MeV in ^{17}O to the astrophysical factor for $^{13}C(\alpha,n)^{16}O$ at low energies by measuring the α-particle spectroscopic factor of this state. However, analysis of the data brings large uncertainty to the extracted spectroscopic factor [4,5]. It is the main goal of this work to resolve this controversy and to develop a technique which allows determining the contribution of sub-threshold resonances to the $^{13}C(\alpha,n)^{16}O$ reaction cross sections using a model-independent approach. Until now the ANC method has been applied to determine the astrophysical factors for radiative capture processes [6]. Here we present the first case of application of the ANC method to determine the astrophysical factor for the $^{13}C(\alpha,n)^{16}O$ reaction at astrophysically relevant energies by measuring the ANC for the virtual synthesis $\alpha+{}^{13}C\rightarrow{}^{17}O(6.356\ \text{MeV},1/2^+)$ using the sub-Coulomb α-transfer reaction $^{13}C(^6Li,d)^{17}O(6.356\ \text{MeV},1/2^+)$. The ANC of the 6.356 MeV state in ^{17}O was measured in the α-transfer reaction $^{13}C(^6Li,d)^{17}O$ performed at two sub-Coulomb energies 8.0 and 8.5 MeV of ^{13}C at Florida State University Tandem-LINAC facility. Choice of inverse kinematics, ^{13}C beam and ^6Li target, allowed to make measurements at very low energies in c.m. system and to avoid background associated with admixture of ^{12}C isotope in ^{13}C. Normalizing the DWBA cross section of the peripheral reaction to the experimental one and knowing the ANC for $\alpha+d\rightarrow{}^6Li$ we can determine the ANC for $\alpha+{}^{13}C\rightarrow{}^{17}O(6.356\ \text{MeV},1/2^+)$. The extracted ANC, unlike the spectroscopic

factor, does not depend on the number of the nodes of the α-particle bound state wave function and geometrical parameters of the Woods-Saxon potential. The total uncertainty in determination of the square of the ANC is determined by 7% statistical uncertainty, 7% systematic uncertainty, and 20% of the uncertainty due to the ambiguity of the optical potential parameters. Using the determined ANC we calculated the astrophysical factor $S(0) = [2.5 \pm 0.2(\text{stat}) \pm 0.2(\text{syst}) \pm 0.5(\text{theor})] \times 10^6$ MeVb. The calculated astrophysical factor is dominated by the contribution of the subthreshold state $^{17}\text{O}(6.356\ \text{MeV}, 1/2^+)$. Besides we took into account the contribution of the low energy tail of the higher lying resonances and the background. This value is ten times smaller than adopted in NACRE compilation [3] and a factor of 5 higher than in [4].

[1] I. Iben, Jr., Astrophys. J. **395**, 202 (1976).
[2] S. Goriely and L. Siess, Astron. Astrophys. **378**, L25 (2001).
[3] C. Angulo *et al.*, Nucl. Phys. **A656**, 3 (1999).
[4] S. Kubono *et al.*, Phys. Rev. Lett., **90**, 062501 (2003).
[5] N. Keeley, K. W. Kemper, and Dao T. Khoa, Nucl. Phys. **A726**, 159 (2003).
[6] A. M. Mukhamedzhanov *et al.*, Phys. Rev. C **56**, 1302 (1997).

The Trojan Horse Method: an Indirect Technique in Nuclear Astrophysics

A.M. Mukhamedzhanov, R. E. Tribble, and C. Spitaleri [1]

[1] *DMFCI, Università di Catania and INFN - Laboratori Nazionali del Sud,, Catania, Italy*

To obtain the astrophysical factor at astrophysical energies different indirect techniques are being used to overcome the presence of the Coulomb barrier. The Trojan Horse (TH) method is a powerful indirect technique which allows one to determine the astrophysical factor for rearrangement reactions. The TH method, first suggested by Baur [1], involves obtaining the cross section of the binary $x + A \to b + B$ process at astrophysical energies by measuring the two-body to three-body $(2 \to 3)$ process $a + A \to y + b + B$, in the quasi-free (QF) kinematics regime, where particle $a = (xy)$ is accelerated at energies above the Coulomb barrier. After penetrating through the Coulomb barrier, nucleus a undergoes breakup leaving particle x to interact with target A while projectile y flies away. From the measured $a + A \to y + b + B$ cross section, the energy dependence of the binary sub-process, $x + A \to b + B$, is determined. The main advantage of the TH method is that the extracted cross section of the binary sub-process does not contain the Coulomb barrier factor. Consequently the TH cross section can be used to determine the energy dependence of the astrophysical factor, $S(E)$, of the binary process, $x + A \to b + B$, down to zero relative kinetic energy of the particles x and A without distortion due to electron screening. The absolute value of $S(E)$ must be found by normalization to direct measurements at higher energies. At low energies where electron screening becomes important, comparison of the astrophysical factor determined from the TH method to the direct result provides a determination of the screening potential. Even though the TH method has been applied successfully to many direct and resonant processes [2], there are still reservations about the reliability of the method due to two potential modifications of the yield from off-shell effects and initial and final state interactions in the TH $a + A \to y + b + B$ reaction. In the TH reaction, particle x in the binary sub-process $x + A \to b + B$ is virtual (off-energy-shell). In the standard analysis, the virtual nature of x is neglected and the plane wave approximation is used. We addressed, for the first time, the reliability of these assumptions. It has been explained why the reaction cross sections with virtual particles are not affected by the barrier factor. We have also explained why the energy dependence of the cross section of the direct binary reaction $x + A \to b + B$ with the virtual particle x and plane wave approximation in the initial state is similar to the energy dependence of the astrophysical factor for this reaction. We demonstrated how to take into account the Coulomb interaction in the initial state of the TH reaction $a + A \to y + b + B$ when extracting the astrophysical factor for the binary reaction $x + A \to b + B$. Our results justify the application of the TH as indirect technique in nuclear astrophysics.

[1] G. Baur, Phys. Lett. **178B**, 135 (1986).
[2] C. Spitaleri *et al.*, Phys. Rev. C **69**, 055806 (2004).

The Lowest Excited States of ^{13}O and Astrophysical Implications

V.Z. Goldberg and A. Mukhamedzhanov, B.B. Skorodumov,[1] P. Boutachkov,[1]
A. Aprahamian,[1] S. Almaraz,[1] J.J. Kolata,[1] L.O. Lamm,[1] M. Quinn,[1] A. Woehr,[1]
G.V. Rogachev,[2] H. Amro,[3] F. D. Becchetti,[3] Y. Chen,[3] H. Jiang,[3] and S. Brown[4]
[1]*Institute of Structure and Nuclear Astrophysics, University of Notre Dame, Notre Dame, IN 46556*
[2] *Physics Department, Florida State University, Tallahassee, FL 32306*
[3] *Physics Department, University of Michigan, Ann Arbor, Michigan 48109*
[4]*Physics Department, Florida State University, Tallahassee, FL 32306 and Department of Physics, University of Surrey, GU2 7XH, United Kingdom*

Quantum characteristics of excited states in A=13 T=3/2 nuclei were unknown before this work. Hence there was no knowledge about their nuclear structure.

The nuclear structure of ^{13}O is important for evolution of very low-metallicity massive stars [1]. It has been shown that ^{12}N can be depleted into ^{12}C through β^+ decay or by photodisintegration ^{12}N(γ,p)^{11}C. However, ^{12}N may capture a proton to form ^{13}O through the process ^{12}N(p,γ)^{13}O. This process can compete with β^+ decay and photodisintegration of ^{12}N at some temperatures and densities. It is important

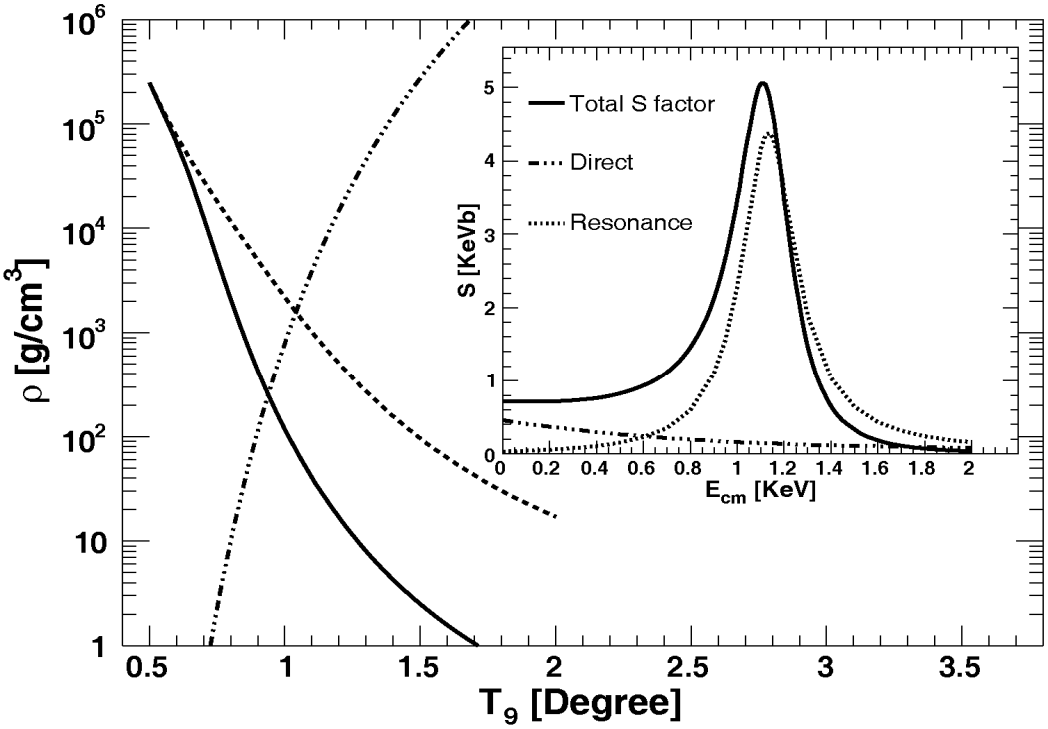

Figure 1. The temperature and density conditions where the ^{12}N(p,γ) reaction is important. The solid line (new results) and dashed line Ref. [1] show where the rates for ^{12}N proton capture and beta decay of ^{12}N will be equal. In addition, the density should be above the dashed-dotted line to produce ^{13}O faster than it can be photo-dissociated. The inserted figure shows astrophysical S factor calculations: the solid line is total S factor; the dashed line shows only resonance capture; the dashed-dotted line shows only direct capture

to evaluate the density and temperature regime where that occurs.

In this work, we present results for ^{12}N+p scattering at several angles using thick target inverse kinematics method [2]. We obtained definite information on the spin-parity ($½^+$), width (Γ=0.45±0.1 MeV), and nuclear structure ($S_{s.p.}$~0.7) of the first excited state of ^{13}O. We also identify for the first time a second excited state at excitation energy of 3.29 MeV with quantum characteristics J^π=$½^-$ or $3/2^-$ and with Γ=0.075±0.03 MeV. These results were obtained by using the ***R*** matrix analysis of the experimental data, and were supported by application of a potential well approach to the isobaric level shifts.

We examined the impact of new experimental information of the first excited state $½^+$ on ^{12}N(p,γ)^{13}O reaction which might play important role in nucleosynthesis reactions of low-metallicity stars. Fig.1 presents the temperature and density conditions, where the ^{12}N(p,γ) reaction is important, together with the astrophysical S factor calculated for both direct capture and capture through the resonance in question.

[1] M. Wiescher *et al.*, Astrophys. J. **343**, 352 (1989).
[2] K.P. Artemov *et al.*, Sov. J. Nucl. Phys. **52**, 406 (1990).

Can We Measure the Spectroscopic Factors from Nuclear Reactions?

A.M. Mukhamedzhanov and F. M. Nunes[1]

[1]*NSCL and Department of Physics and Astronomy, Michigan State University, East Lansing, MI 48864*

The spectroscopic factor (SF) is the square of the norm of the overlap function. Hence it is mainly determined by the behavior of the overlap function in the nuclear interior. Experimentally the SFs are determined from transfer, breakup and knockout reactions. Electron induced knockout reaction $(e,e'p)$ is considered to be one of the most accurate tool to extract the phenomenological spectroscopic factor (SF) because, by increasing the electron transfer momentum, one can probe the nucleon overlap function down to very small distances. Recently we have proposed a new method to determine the spectroscopic factor from transfer reactions [1]. This method is based on the introduction into analysis the information about the asymptotic normalization coefficient (ANC). Introduction of the ANC fixes the external contribution and makes the determined SF sensitive to the coupled channels and optical potential in the internal region. Application of this combined method demonstrated the failure of the standard technique of determination of the SF. Meantime recently it has been shown in the effective field theory that it is impossible to determine the SF from the $(e,e'p)$ processes due to the existence of the infinite number of Lagrangians corresponding to different field redefinitions [2] . These Lagrangians generate different reaction amplitudes where the final state proton-residual nucleus interaction is traded in with the short-range nucleon-nucleon correlations. It is important to demonstrate a connection between our phenomenological approach and effective filed theory result. To do it we start from the nonrelativistic Schrödinger equation. We introduce a unitary transformation of the wave functions using the short-range nucleon correlation operator which is equivalent to the field redefinition. We demonstrate that such a unitary transformation does not affect the ANC but changes the overlap function and, correspondingly, the SF. As the next step we derived an explicit equation for the $(e,e'p)$ amplitude. Application of the unitary transformation generates the short-range correlations similar to those which appear in the effective filed theory. We have estimated the range of the effective potential corresponding to the short-range correlation. This correlation is described by the triangular diagram corresponding to the two-nucleon contact interaction with the external photon leading to one-nucleon knockout. A typical radius of the short-range correlation is ≤ 1.5 fm. It is important to estimate the impact of the short range correlations on the SF and $(e,e'p)$ amplitude and we are working on that.

[1] A. M. Mukhamedzhanov and F. M. Nunes, Phys. Rev. C **72**. 017602 (2005).

[2] R. J. Furnstahl and H.W. Hammer, arXiv: nucl-th/0108069 (2001).

Wide Resonant States in ^{15}F

B.F. Irgaziev,[1] V.Z. Goldberg, and A.M. Mukhamedzhanov
[1]*GIK Institute of Engineering Sciences and Technology, Topi, District Swabi, N.W.F.P.,Pakistan*

Many important for nuclear astrophysics radiative capture reactions proceed through resonance states. The Breit-Wigner formula for analysis of resonant reactions is conventionally used. But it is correct for a narrow resonance. There are many important wide resonant states. This is a common situation for the resonances in nuclei on the drip lines, where the mistakes in the analysis of the resonances can result in the wrong conclusions on the nuclear structure.

In ^{15}F nucleus, the ground state ($1/2^+$) and the fist exited state ($5/2^+$) are wide resonances and poorly known. The $5/2^+$ state is narrower than state $1/2^+$, the earliest estimation was performed many years ago [1], the latest results are represented in [2,3].

In this report, we used three different methods: the scattering phase shift, scattering wave function and the pole of the S matrix in the complex energy plane to make calculations for ^{15}F. The scattering phase shift method is a standard one. In this method the resonance energy is determined by the point where the scattering phase shift is 90°. The resonance width is equal to $\Gamma=2/(d\delta/dE)$ calculated at $\delta = 90^\circ$. In the scattering wave function method, the scattering wave function is calculated at real energies and the resonance energy corresponds to the peak of the scattering wave function in the nuclear interior. In the third method, we calculated the Gamov wave functions for both resonance states ($1/2^+$, $5/2^+$) in the neighborhood of the complex energies $W=E-i\Gamma/2$ obtained by the phase shift method. For each resonance we found the complex energy at which the coefficient of the incoming wave is equal to zero. It corresponds to the pole of the S-matrix on the second sheet of the Reeman surface. Results for the energies and widths are shown in Table I. The calculations are made using the Wood-Saxon potential with the set of parameters from [2]. The potential generates the $s_{1/2}$ and $d_{5/2}$ states in ^{15}F.

Table I. The energies and widths of ^{15}F calculated by three different methods.

	E (MeV)	Γ (MeV)	Methods
	$\mathbf{1.290^{0.08}_{0.06}}$	**0.7**	Ψ_{max}
Ground state $1/2^+$	**1.463**	**1.326**	$\delta=\pi/2$
	1.203	**0.538**	Pole of the S-matrix
	$\mathbf{2.795 \pm 0.045}$	$\mathbf{0.325 \pm 0.06}$	Ψ_{max}
First exited state $5/2^+$	**2.697**	**0.266**	$\delta=\pi/2$
	2.677	**0.257**	Pole of the S-matrix

One can conclude that the position and the width of the broad resonance, in contrast to the narrow resonance, is sensitive to the method of calculation.

In Ref. [3] the lowest states of isospin T=3/2 in A=15 were treated as a combination of one-particle, two-hole and three-particle, four-hole states with various percentage according to the shell model and the authors predicted the following energies : 1.19-1.29 MeV for $1/2^+$, and 2.75-2.78 MeV for $5/2^+$. The Gamov wave function of the resonance state is complex. Fig. 1 shows the real and imaginary parts of the Gamow wave function describing the $5/2^+$ state. We can see that the probability to find the proton inside the potential well is high and the solution of Schrödinger equation coincides with the outgoing wave in the nuclear exterior.

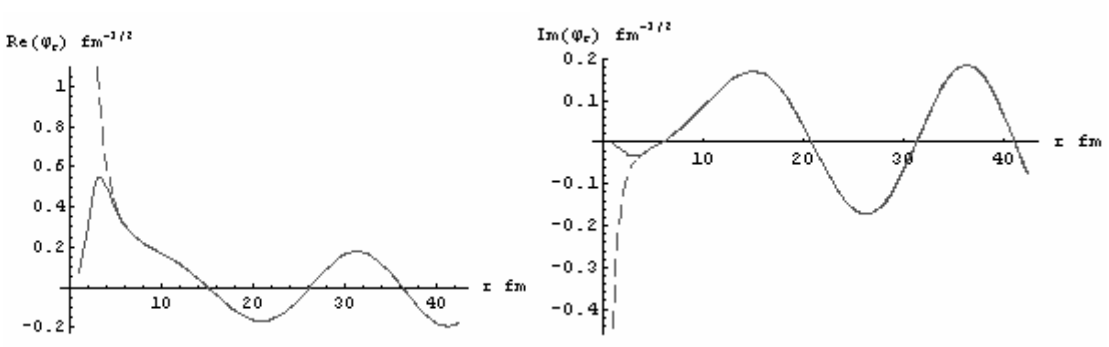

Figure 1. Real and imaginary parts of the wave function of the $5/2^+$ resonant state of ^{15}F. Solid line is the solution of the Schrödinger equation, dashed line is the outgoing Coulomb function (Whittaker function).

[1] G.J. KeKelis *et al.*, Phys. Rev. C **17**, 1929 (1978).

[2] V.Z. Goldberg *et al.*, Phys. Rev. C **69**, 031302(R) (2004).

[3] H.T. Fortune and R. Sherr, Phys. Rev. C **72**, 024319 (2005).

Self-Consistency in Hartree-Fock RPA and Low-Lying States in Nuclei

Tapas Sil and S. Shlomo

Low-lying collective states are the key features of nuclear excitations and provide important clue on nuclear shell structure [1]. Hartree-Fock (HF) based RPA describes the whole excitation spectrum along with the low-lying states with the small amplitude approximation. For accurate implementation of HF-RPA method, the calculation should be fully self-consistent. One of the essential conditions for self-consistency is to use exactly the same interaction in the HF as well as in the RPA calculations. But, in most of the available HF-RPA calculations are contaminated with the self-consistency violation (SCV) because often for the numerical difficulties, some part of interaction used in HF, such as spin-orbit and Coulomb, are dropped out in the RPA [2]. In Fig. 1, we plot the strength function S(E) versus energy E for ^{208}Pb for fully self-consistent calculation (SC), missing ph spin-orbit interaction(LS) and missing ph Coulomb interaction (CO) for L=2 and 3. It is seen from the figure that for both of the modes, the energy of the low-lying state increases for the LS cases (0.58 MeV and 0.26 MeV for L=2,3 respectively) where it decreases for the CO cases (0.10 MeV and 0.20 MeV respectively). Unlike low-lying states, for the giant resonances the centroid energies are reduced for both the of modes for LS (0.11 MeV and 0.24 MeV) and for CO (0.19 MeV and 0.04 MeV for L=2,3 respectively). It is to be noted that the effects of SCV on low-lying states are of similar order of those for giant resonances but for low-lying states, the shift (~0.5 MeV) is large in comparison to the excitation energy. Therefore, for the study of low-lying states, a fully self-consistent calculation is necessary.

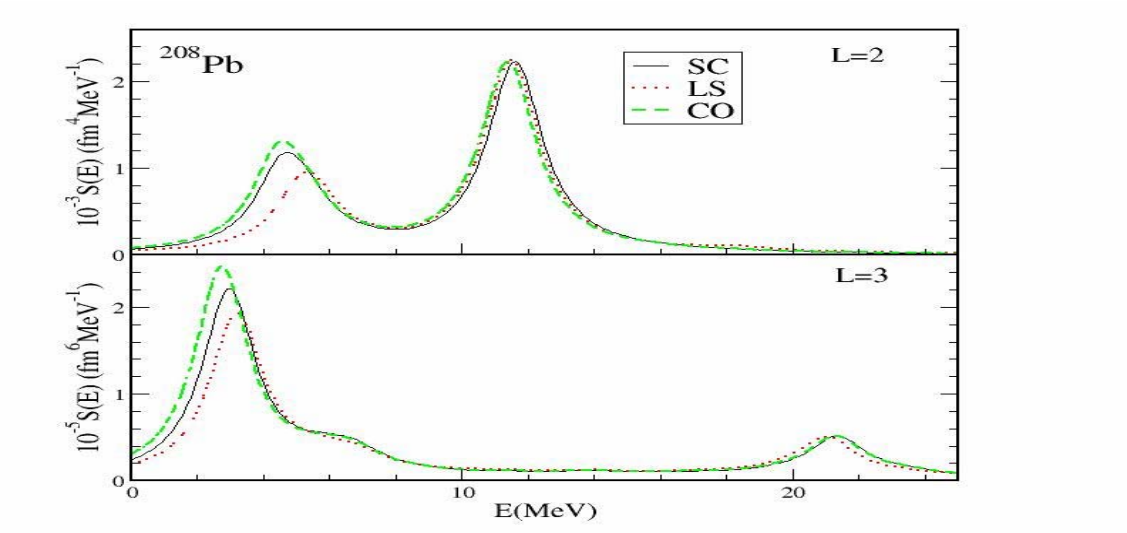

Figure 1. Strength function of isoscalar giant resonances calculated with SGII interaction.

[1] A. Bohr and B. R Mottelson, Nuclear Structure (Benjamin, London, 1975) Vol. II.

[2] T. Sil, S. Shlomo, B. K. Agrawal and P.-G. Reinhard, Phys. Rev. C **73**, 034316 (2006).

Self-Consistent Hartree-Fock RPA and Energy Weighted Sum Rule

Tapas Sil, S. Shlomo, and P.-G. Reinhard[1]
[1]*Institute fur Theoretische Physik, Universitat Erlangen, D-91058 Erlangen, Germany*

Giant resonances of nuclei give important information about the structure of nuclei as well as bulk properties of nuclear systems. The basic theory for the microscopic description of nuclear giant resonances is the Hartree-Fock (HF) based random phase approximation (RPA). Nowadays, very accurate experimental measurement of centroid energy demands that the theoretical calculations should be highly accurate and self-consistent. Unfortunately, most of the available HF-RPA calculations are not fully self-consistent. We have shown in Ref. [1] that self-consistency violation in HF-RPA calculations may cause an error of around 1 MeV in the centroid energy for isoscalar giant monopole mode (ISGMR) which will lead to an error of 30 MeV in the estimate of nuclear matter incompressibility K. A very important and necessary condition for the self-consistency and high accuracy of HF-RPA calculation is to recover the energy weighted sum rule (EWSR) from the calculated RPA strength function S(E) by,

$$m_1 = \int_0^\infty ES(E)dE\,, \tag{1}$$

where, $S(E) = \sum_j |<0 \mid F_L \mid j>|^2 \ \delta(E_j - E_0)$ and the scattering operator is given by,

$$F_L = \sum_i f(r_i)Y_{L0}(i) \qquad \text{for isoscalar} \tag{2}$$

$$F_L = \frac{Z}{A}\sum_n f(r_n)Y_{L0}(n) - \frac{N}{A}\sum_p f(r_p)Y_{L0}(p) \qquad \text{for isovector} \tag{3}$$

with $f(r) = r^2, r^2$ and r^3 for L=0,2 and 3 respectively. We take for the dipole mode $f(r) = r$ for (T=1) and $f(r) = r^3 - \frac{5}{3} < r^2 > r$ for (T=0).

The energy weighted sum rule which is obtained from the double commutator [2], can be calculated using the ground state HF density ρ(r) by,

$$EWSR(L, T=0) = \frac{1}{4\pi}\frac{\hbar^2}{2m}A\frac{1}{A}\int g_L(r)\rho(r)4\pi r^2 dr \tag{4}$$

where,

$$g_L(r) = \left(\tfrac{df}{dr}\right)^2 + L(L+1)\left(\tfrac{f}{r}\right)^2. \tag{5}$$

For isovector mode

$$EWSR(L, T=1) = EWSR(L, T=0)\left[1 + \kappa - \kappa_{np}\right]\left(\frac{NZ}{A}\right) \tag{6}$$

where κ is the enhancement factor because of the momentum dependence of the effective nucleon-nucleon interaction and is given by,

$$\kappa = \frac{(1/2)[t_1(1+x_1/2)+t_2(1+x_2/2)]}{(\hbar^2/2m)(4NZ/A^2)} \cdot \frac{2\int g_L(r)\rho_p(r)\rho_n(r)4\pi r^2 dr}{\int g_L(r)\rho(r)4\pi r^2 dr} \qquad (7)$$

where t_i and x_i are the parameters of the Skyrme interaction and the correction κ_{np} which arises because $\left(\rho_n(r)-\rho_p(r)\right) \neq \frac{(N-Z)}{A}\rho(r)$, is given by

$$\kappa_{np} = \frac{(N-Z)}{A}\frac{A}{NZ}\frac{\int g_L(r)[Z\rho_n(r)-N\rho_p(r)]4\pi r^2 dr}{\int g_L(r)\rho(r)4\pi r^2 dr}. \qquad (8)$$

To see how the necessary condition of self-consistency and high accuracy is fulfilled in our calculation, we compare in Table I, the values of m_1 calculated using the RPA strength functions in Eq. (1) with the corresponding EWSR obtained from Eqs. (4) and (6) for three sample nuclei (^{40}Ca, ^{90}Zr and ^{208}Pb) from different mass regions. We have presented results for these nuclei for both isoscalar and isovector modes of various multipolarities (L=0-3). It is seen that for these nuclei and for all the modes, the deviation of m_1 from the corresponding EWSR are very small (less than 0.3%). This demonstrates the high accuracy of our HF-RPA calculations.

Table I. Comparison of m_1 calculated from RPA strength function [Eq. (1)] with those (EWSR) obtained from the double commutator, Eqs. (4) and (6). The ratio R=m_1/EWSR demonstrates the high accuracy of our calculations.

Mode		^{40}Ca		^{90}Zr		^{208}Pb	
L	T	EWSR	R	EWSR	R	EWSR	R
0	0	2889	0.9983	10505	0.9994	41872	0.9971
	1	896.3	0.9992	3330	0.9994	13041	0.9998
1	0	57253	0.9990	289907	0.9995	1823110	0.9999
	1	64.62	0.9999	148.9	1.0001	337.8	0.9999
2	0	7222	1.0001	26262	1.0007	104681	1.0015
	1	2241	1.0000	8326	0.9998	32604	1.0002
3	0	238240	0.9996	1300645	0.9999	8584813	1.0003
	1	69328	0.9994	389266	0.9996	2519881	1.0001

We note that for the SGII interaction used in this calculation, the enhancement factor κ=0.314, 0.381, 0.314 and 0.253 and the factor κ_{np}=0.010, 0.000, 0.010 and 0.024 for the isovector L=0, 1, 2 and 3 in ^{208}Pb, respectively. We point out that the correction term κ_{np} in Eq.(8) for isovector modes, usually missing in the literature, is not negligible for asymmetric nuclei. As for example , for ^{208}Pb, L=3, κ_{np} has an effect of 2% in the calculation of EWSR. The effect of κ_{np} will be more significant for nuclei near the drip lines because of the large difference between the neutron and proton density distributions and also for the large asymmetry (N-Z)/A.

[1] T. Sil, S. Shlomo, B. K. Agrawal and P.-G. Reinhard, Phys. Rev C **73**, 034316 (2006).
[2] A. Bohr and B. R. Mottelson, Nuclear Structure (Benjamin London 1975), Vol. II

Continuous Phase Transition and Negative Specific Heat in Finite Nuclei

J.N. De,[1] S.K. Samaddar,[1] S. Shlomo, and J.B. Natowitz
[1] *Saha Institute of Nuclear physics, 1/AF Bidhannagar, Kolkata 700064, India*

Mean-field models have often been employed to explore liquid-gas phase transition in infinite and finite nuclear systems. In this model, the phase transition is found to be continuous, both for asymmetric nuclear matter and also for finite nuclei. Though approximate, the model serves the purpose of giving an orientation for understanding some important features of the liquid-gas phase transition. Moreover, the vapor phase may not consist of only monomers, but may contain various clusters along with the nucleons; the influence of clusters on the caloric curve should also be explored.

The model we employ in our calculation is in the framework of mean-field theory. The excited nucleus is viewed as a charged liquid drop composed of N_0 neutrons and Z_0 protons with mass number $A_0 = N_0 + Z_0$. In its journey from the liquid to the gas phase, the depleted nucleus is taken to be in complete thermodynamic equilibrium with its own emanated vapor so that the total number of neutrons and protons are conserved. Besides nucleons, the vapor contains clusters that alter the equilibrium conditions, which will be reflected in the caloric curve and the resulting heat capacity.

It is found that in the liquid-vapor coexistence region the pressure is not a constant on an isotherm, indicating that the transition is continuous. At constant pressure, the caloric curve shows some anomalies; namely, the systems studied exhibit negative heat capacity in a small temperature domain. The dependence of this specific feature on the mass and isospin of the nucleus, Coulomb interaction, and the chosen pressure was studied. The effects of the presence of clusters in the vapor phase on specific heat have also been explored [1].

[1] J. N. De, S. K. Samaddar, S. Shlomo, and J. B. Natowitz, Phys. Rev. C **73**, 034602 (2006).

Fully Self-Consistent HF-RPA Calculations with Modern Skyrme Interaction

V. Kim Au, David Carson Fuls,[1] and S. Shlomo
[1]REU student: *Stephen F. Austin State University, Nacogdoches, TX 75961, USA*

Recently we have determined a new set of parameters for the Skyrme interaction, namely KDE0 [1]. This Skyrme interaction was obtained by the fitting of the Hartree-Fock (HF) results to an extensive set of experimental data: binding energies for 14 nuclei ranging from the normal to exotic ones, charge rms radii for 7 nuclei, spin-orbit splittings for the 2*p* proton and neutron orbits of the ^{56}Ni nucleus and rms radii for the $1d_{5/2}$ and $1f_{7/2}$ valence neutron orbits in the ^{17}O and ^{41}Ca nuclei, respectively. Some constraints on the Skyrme parameters were also included: the critical density ρ_{cr} determined from the stability conditions for the Landau parameters, the quantity $P = 3\rho\, dS/d\rho$, directly related to the slope of the symmetry energy *S*, the enhancement factor κ, associated with the Thomas-Reiche-Kuhn sum rule for the isovector giant dipole resonance, and the Landau parameter G_0'.

We have carried out fully self-consistent HF based Random-Phase-Approximation (RPA) calculations for the strength function $S(E)$, centroid energies E_0 of the isoscalar giant monopole resonance (ISGMR) in ^{90}Zr, ^{116}Sn, ^{144}Sm, and ^{208}Pb following Ref. [2, 5]. A comparison with available experimental data is given in Table I, where *J* is the symmetry energy at the saturation density. We find a close agreement between our results for KDE0 interaction and experimental data. We have deduced the value of the nuclear matter incompressibility K = 230±20 MeV. Figure 1 shows $S(E)$ for the ISGMR obtained using the KDE0 and SG2 interactions.

Table I. Fully self-consistent HF based RPA results for breathing mode energy (in MeV)

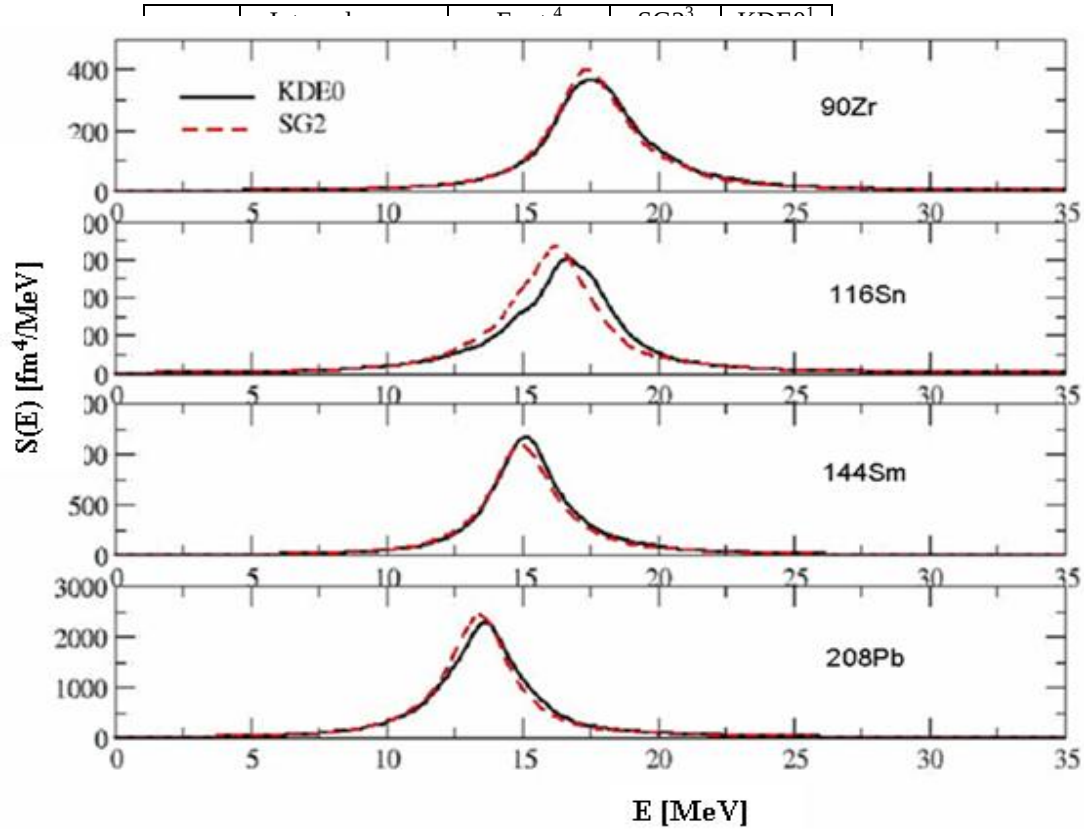

Figure 1. Isoscalar monopole strength functions.

[1] B. K. Agrawal, S. Shlomo, and V. Kim Au, Phys. Rev. C **72**, 014310 (2005).
[2] Tapas Sil, S. Shlomo, B. K. Agrawal, and P.-G. Reinhard, Phys. Rev. C **73**, 034316 (2006).
[3] Nguyen Van Giai and H. Sagawa, Phys. Lett. **B106**, 379 (1981).
[4] D. H. Youngblood *et al.*, Phys. Rev. C **69**, 034315 (2004); C **69**, 054312(2004).
[5] P.-G. Reinhard, Ann Phys. (leipzig) **1**, 632 (1992); Nucl. Phys. **A649**, 305c (1999).

Nuclear Incompressibility Coefficient within Fermi Liquid Drop Model

O. Pochivalov, S. Shlomo, and V. M. Kolomietz[1]
[1] *Institute for Nuclear Research, Kiev 03680, Ukraine*

New experimental data for the isoscalar giant monopole (ISGMR) and dipole (ISGDR) resonances and inability of the self-consistent Hartree-Fock (HF) random phase approximation (RPA) calculations to simultaneously reproduce the experimental values of the centroid energies E0, and E1 and widths $\Gamma 0$, and $\Gamma 1$, of the ISGMR and ISGDR, respectively, and the experimental value E1/E0, have renewed interest in research of theoretical description of multiple particle-hole excitation. We have previously shown that experimental value of ratio E1/E0 can be reproduced by the introduction of collisional damping into the Fermi Liquid Drop Model (FLDM). However, the absolute values of the centroid energies E0, and E1, and the widths $\Gamma 0$, and $\Gamma 1$, obtained from FLDM with collisional FSD, are overestimated with respect to experimental data.

To address this issue we study the dependence of the energies for ISGMR and ISGDR in ^{208}Pb as functions of the nucleus incompressibility coefficient K_A. We start from the fluid dynamic equations of motion for the viscous Fermi liquid [1]. Within the FLDM, the eigenfrequency ω of the compression modes satisfies the dispersion equation

$$\omega^2 - c_0^2 q^2 + i\omega\gamma q^2 = 0, \qquad c_0^2 = \left(K_A + 12\mu/\rho_0\right)/9m, \qquad \gamma = 4\nu/3\rho_0 m, \tag{1}$$

where ρ_0 = 0.17 fm^{-3} is the bulk particle density corresponding to the sharp radius $R_S = 1.12A^{1/3}$ fm, and m is the nucleon mass. The transport coefficients μ and viscosity ν in Eq. (1) are due to the Fermi surface distortion (see Ref. [1]) and are given by

$$\mu = \mathrm{Im}\left(\omega\tau/\left(1 - i\omega\tau\right)\right)\ P_{eq}, \qquad \nu = \mathrm{Re}\left(\tau/\left(1 - i\omega\tau\right)\right)\ P_{eq}, \tag{2}$$

where P_{eq} is the equilibrium pressure in the nuclear interior. The memory effect is introduced into the model by the dependence of transport coefficients on the excitation eigenfrequency through the relaxation time τ

$$\tau = 4\pi^2\beta\ \hbar/\left(\hbar\,\mathrm{Re}(\omega)\right)^2\ . \tag{3}$$

The wave number q in Eq. (1) is derived by the boundary conditions on the free surface of the nucleus. Solving appropriate secular equations for boundary conditions of isoscalar monopole and dipole excitations we obtain centroid energies and widths of compression excitations. We have found that the damping coefficient β = 0.65 provides a good fit of calculated value of the ratio E1/E0 to the experimental value. Then, by varying the nucleus incompressibility K_A in Eq. (1) as a parameter we studied behavior of E1, and E0, appropriate widths $\Gamma 0$, and $\Gamma 1$, and compared the nucleus

incompressibility coefficient K_A with the scaling approximation value K_S, obtained with ISGMR energy taken as described in [2]:

$$K_S = \frac{m\langle r^2 \rangle}{\hbar^2}\left(\mathrm{E0}^2 + 3(\Gamma 0/2.35)^2\right). \qquad (4)$$

Assuming a Fermi density distribution, the rms-radius was calculated using

$$\langle r^2 \rangle = \tfrac{3}{5}R^2\left[1 + \tfrac{10}{3}(\pi a/R)^2 + \tfrac{7}{3}(\pi a/R)^4\right] \Big/ \left[1 + (\pi a/R)^2\right], \qquad (5)$$

where a = 0.53 fm and R are the diffuseness and half radius of the charge distribution, corresponding to R_S. Results of the calculation for ^{208}Pb with $\beta = 0.65$ are presented in Table I. Results of our calculations show that within the current model, the experimental values of E0, and E1, and E1/E0 for ^{208}Pb are very well reproduced.

Table I. Centroid energies and widths of ISGMR and ISGDR, and the nucleus incompressibility K_S for ^{208}Pb as a function of input coefficient K_A, in MeV

K_A	E0	E1	Γ0	Γ1	K_S
130.0	12.61	20.52	2.76	7.06	120.78
135.0	12.83	20.76	2.81	7.09	125.00
140.0	13.04	20.98	2.86	7.10	129.30
145.0	13.26	21.19	2.91	7.10	133.67
150.0	13.46	21.43	2.96	7.12	137.67
155.0	13.67	21.65	3.01	7.12	142.17
Exp.*	13.97 ± 0.20	22.20 ± 0.30	2.88 ± 0.20	9.39 ± 0.35	145.96

* Ref. [4].

[1] V.M. Kolomietz and S. Shlomo, Phys. Rev. C **61**, 064302 (2000).

[2] S. Shlomo and D. H. Youngblood, Phys. Rev. C **47,** 529 (1993).

[3] D. H. Youngblood, *et al.*, Phys. Rev. C **69**, 034315 (2004).

Charm Elliptic Flow at RHIC

B. Zhang,[1] L.W. Chen,[2] and C.M. Ko
[1]*Department of Chemistry and Physics, Arkansas State University, Jonesboro, AR 72467*
[2] *Institute of Theoretical Physics, Shanghai Jiao Tong University, Shanghai 200030, China*

Using a multiphase transport (AMPT) model, we have studied charm elliptic flow in heavy ion collisions at the Relativistic Heavy Ion Collider [1]. Assuming that the cross section for charm quark scattering with light quarks is the same as that between light quarks, we find that both charm and light quark elliptic flows are sensitive to the value of the cross section. As shown in left window of Fig.1, the elliptic flow of charm quarks is smaller than that of light quarks at low transverse momentum but approaches the latter at high transverse momentum as a result of their large masses. Similar features are seen in the elliptic flow of charmed mesons as well as that of the electrons from their semileptonic decays when charmed mesons are produced from quark coalescence during hadronization of the partonic matter. To describe the large electron elliptic flow observed in experimental data requires a charm quark scattering cross section that is much larger than that given by the perturbative QCD as shown in right window of Fig.1.

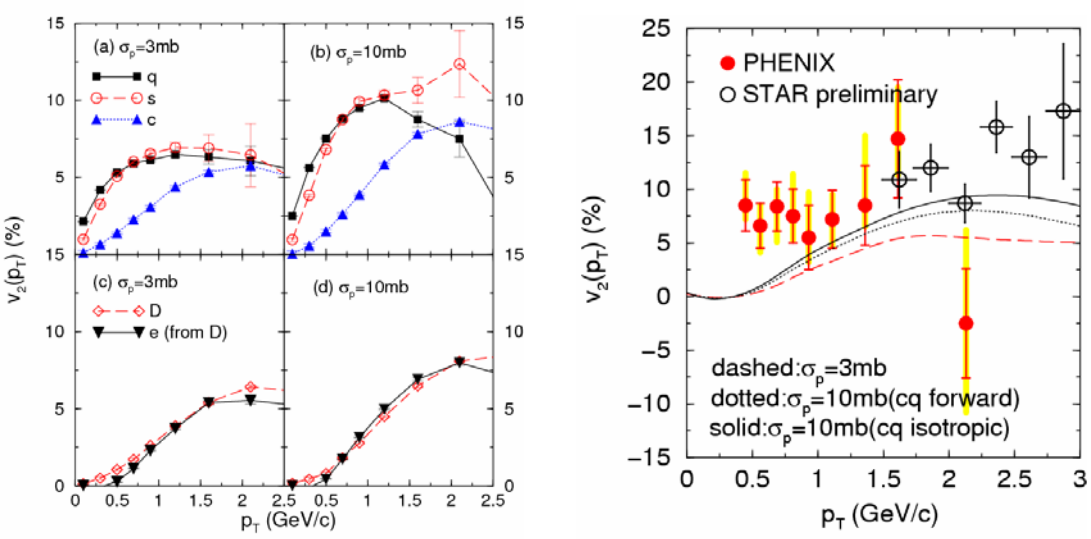

Figure 1. Left: Elliptic flows of light, strange, and charm quarks, D mesons, and their decay electrons in minimum-bias Au + Au collisions at $s^{½}_{NN}$ = 200 GeV for parton cross sections of 3 and 10 mb. Right: Elliptic flow of electrons from charmed meson decays for different parton scattering cross sections of 3 (dashed curve) and 10 (dotted curve) mb with forward peaking angular distribution as well as 10 mb with isotropic angular distribution (solid curve).

[1] B. Zhang, L.W. Chen, and C.M. Ko, Phys. Rev. C **72**, 024906 (2005).

Anisotropic Flows in Cu+Au Collisions at $\sqrt{s_{NN}} = 200$ GeV

L.W. Chen[1] and C.M. Ko

[1]*Institute of Theoretical Physics, Shanghai Jiao-Tong University, Shanghai 200240, China*

Using a multi-phase transport (AMPT) model, we have studied the anisotropic flow of charged hadrons in asymmetric Cu+Au collisions at the Relativistic Heavy Ion Collider [1]. Compared with results for symmetric Au+Au collisions, charged hadrons produced around midrapidity in asymmetric collisions are found to have a stronger directed flow v_1 and their elliptic flow v_2 is also more sensitive to parton scattering cross section. While higher-order flows v_3 and v_4 are small at all rapidities, both v_1 and v_2 in these collisions are appreciable and show an asymmetry in forward and backward rapidities as shown in Fig.1.

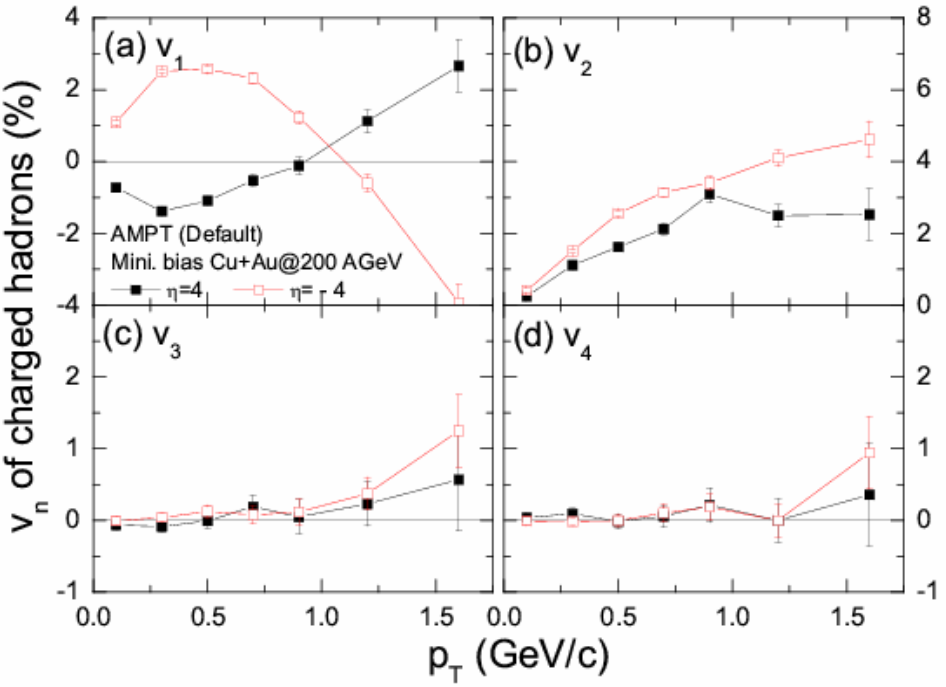

Figure 1. Transverse momentum dependence of v_1 (a), v_2 (b), v_3 (c) and v_4 (d) for charged hadrons at large forward (η=4, solid squares) and backward pseudorapidities (η=-4, open squares) from minimum bias events of Cu+Au collisions at $\sqrt{s_{NN}} = 200$ AGeV.

[1] L.W. Chen and C.M. Ko, Phys. Rev. C **73**, 014906 (2006).

System Size Dependence of Elliptic Flows in Relativistic Heavy-Ion Collisions

L.W. Chen[1] and C.M. Ko

[1]*Institute of Theoretical Physics, Shanghai Jiao-Tong University, Shanghai 200240, China*

We have studied in the framework of a multi-phase transport (AMPT) model the elliptic flows in both Cu+Cu and Au+Au collisions at the Relativistic Heavy Ion Collider [1]. For both collisions at same reduced impact parameter and minimum bias collisions, the elliptic flow of charged hadrons in Cu+Cu collisions is about a factor of three smaller than that in Au+Au collisions at same energy as shown in Fig.1. The reduction factor is similar to the ratio of the sizes of the two colliding systems and is also related to the combined effects of initial energy density and spatial elliptic deformation in the two reactions. Similar system size dependence is also seen in the elliptic flow of partons from minimum bias collisions.

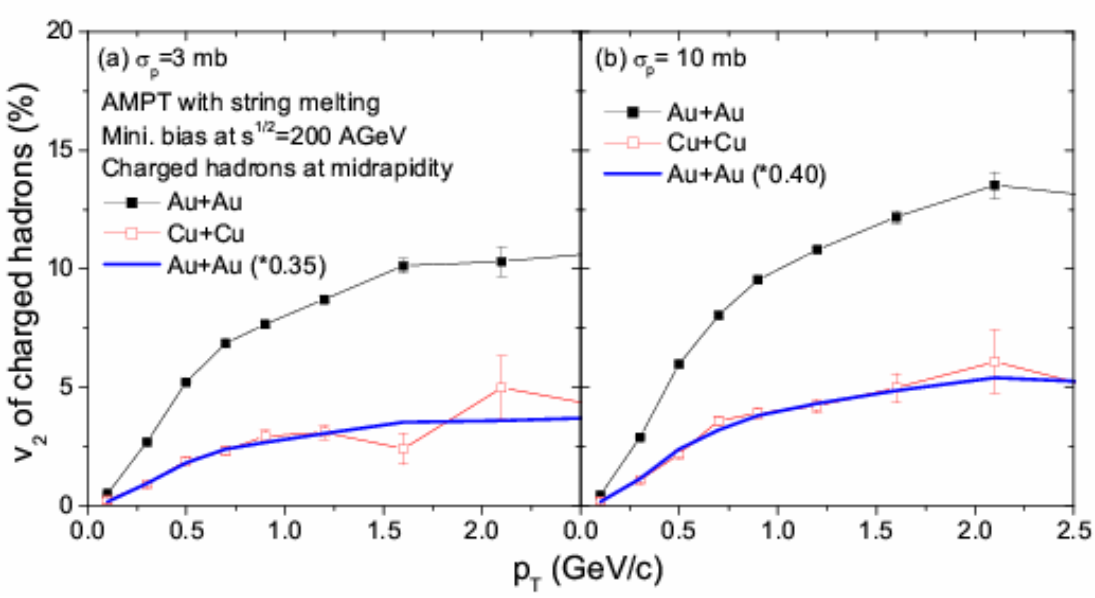

Figure 1. Transverse momentum dependence of v_2 of midrapidity charged hadrons from minimum bias events in Au+Au (solid squares) and Cu+Cu (open squares) collisions at $s^{1/2}$ = 200 A GeV for parton scattering cross sections of 3 mb (left panel) and 10 mb (right panel). The solid line is 0.35 (0.4) times of v_2 of Au+Au for parton cross section of 3 (10) mb.

[1] L.W. Chen and C.M. Ko, Phys. Lett. B **634**, 205 (2006).

Diomega Production in Relativistic Heavy Ion Collisions

S. Pal,[1] C.M. Ko, and Z.Y. Zhang[2]
[1] *National Superconducting Cyclotron Laboratory and Department of Physics and Astronomy, Michigan State University, East Lansing, MI 444824*
[2] *Institute of High Energy Physics, Beijing 10039, China*

Using a multiphase transport (AMPT) model, we have studied the production of a new strange dibaryon $(\Omega\Omega)_{0+}$ in dense hadronic matter formed in relativistic heavy ion collisions [1]. The (multi-)strange baryons (Ξ and Ω) are produced by strangeness-exchange reactions between antikaons and hyperons in the pure hadronic phase. The rescattering involving Ω(s) at midrapidity leads to a production probability of ~ $2.8X10^{-6}$ $(\Omega\Omega)_{0+}$ per event for central Au+Au collisions at the RHIC energy of $s_{NN}^{1/2}$ = 130 A GeV. The production probability would be enhanced by about one order of magnitude if $(\Omega\Omega)_{0+}$ and Ω reach chemical equilibrium during heavy ion collisions. We further find that the yield of $(\Omega\Omega)_{0+}$ increases continuously from SPS to the highest RHIC energy as shown in Fig.1.

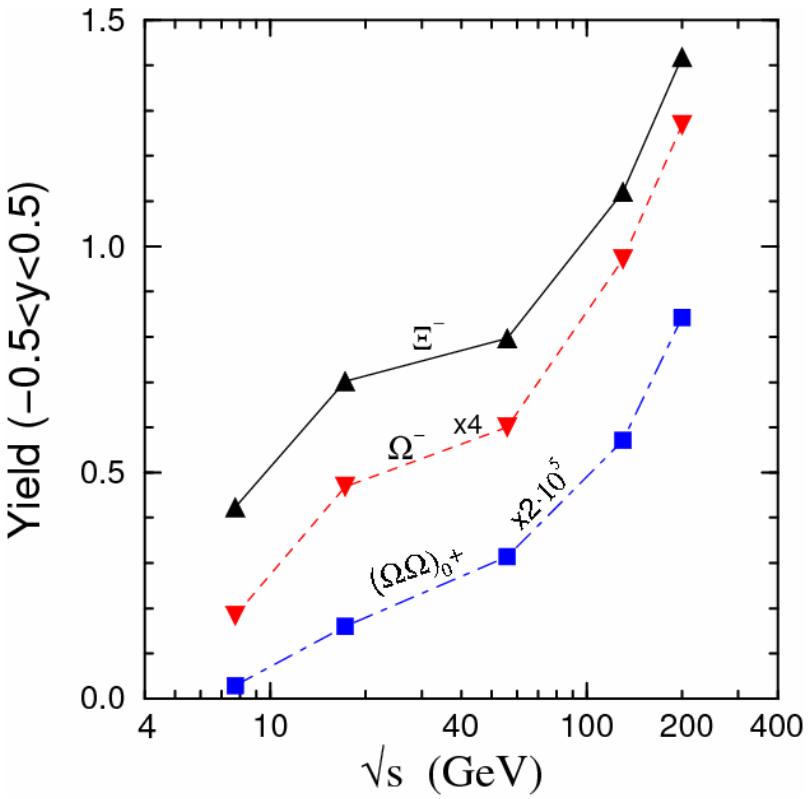

Figure 1. Energy dependence of Ξ^-, Ω^-, and $(\Omega\Omega)_{0+}$ at midrapidity $|y|<0.5$ for heavy ion collisions at impact parameters of b<3 fm in the AMPT model.

[1] S. Pal and C.M. Ko, Phys. Lett. B **624**, 210 (2005).

Eta Absorption by Mesons

W. Liu, C.M. Ko, and L.W. Chen[1]
[1]*Institute of Theoretical Physics, Shanghai Jiao-Tong University, Shanghai 200240, China*

Using the $[SU(3)_L x SU(3)_R]_{global} x [SU(3)_V]_{local}$ chiral Lagrangian with hidden local symmetry, we have evaluated the cross sections for the absorption of eta meson (η) by pion (π), rho (η), omega (ω), kaon (K), and kaon star (K^*) in the tree-level approximation [1]. With empirical masses and coupling constants as well as reasonable values for the cutoff parameter Λ in the form factors at interaction vertices, we find that most cross sections are less than 1 mb, except the reactions $\rho\eta \to KK^*(KK^*)$, $\omega\eta \to KK^*(KK^*)$, $K^*\eta \to \rho K$, and $K^*\eta \to \omega K$, which are a few mb, and the reactions $\pi\eta \to KK$ and $K\eta \to \pi K$, which are more than 10 mb. Including these reactions in a kinetic model based on a schematic hydrodynamic description of relativistic heavy ion collisions, we find that the abundance of eta mesons likely reaches chemical equilibrium with other hadrons in nuclear collisions at the Relativistic Heavy Ion Collider as shown in Fig.1.

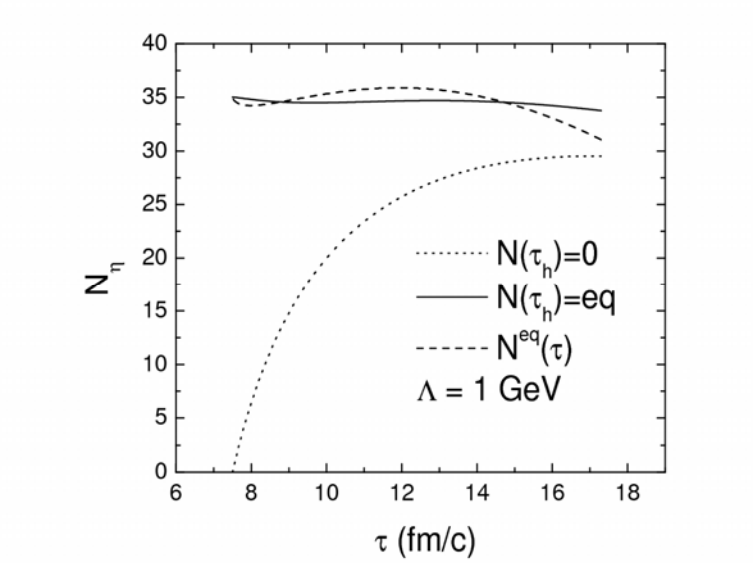

Figure 1. Time dependence of the abundance of midrapidity eta mesons in the hot hadronic gas formed from central Au+Au collisions at $s^{1/2}_{NN}$=200 GeV at RHIC for cutoff parameter Λ=1 GeV. Solid and dotted lines correspond, respectively, to eta mesons that are chemically equilibrated or absent at beginning of the hadronic phase, while the dashed line corresponds to eta mesons that are always in chemical equilibrium.

[1] W. Liu and C.M. Ko, Nucl. Phys. A **765**, 401 (2006).

Nuclear Symmetry Energy and the Neutron Skin Thickness of Heavy Nuclei

L.W. Chen,[1] C.M. Ko, and Bao-An Li[2]

[1]*Institute of Theoretical Physics, Shanghai Jiao Tong University, Shanghai 200030, China*

[2]*Department of Chemistry and Physics, Arkansas State University, Jonesboro, AR 72467*

We have studied in the Skyrme Hartree-Fock model the correlations between the thickness of the neutron skin in finite nuclei and the nuclear matter symmetry energy [1]. From the most recent analysis of the isospin diffusion data in heavy-ion collisions based on an isospin- and momentum-dependent transport model with in-medium nucleon-nucleon cross sections, a value of L=88±25 MeV for the slope of the nuclear symmetry energy at saturation has been extracted, and this imposes stringent constraints on both the parameters in the Skyrme effective interactions and the neutron skin thickness of heavy nuclei. Predicted thickness of the neutron skin is S = 0.22±0.04 fm for ^{208}Pb as shown in Fig.1, where S is shown as a function of L as well as the nuclear symmetry energy $E_{sym}(\rho_0)$ and its curvature K_{sym} at saturation density ρ_0 for 21 sets of Skyrme interaction parameters. For ^{132}Sn and ^{124}Sn, their neutron skins are predicted to have thickness of 0.29±0.04 fm and 0.22±0.04 fm, respectively.

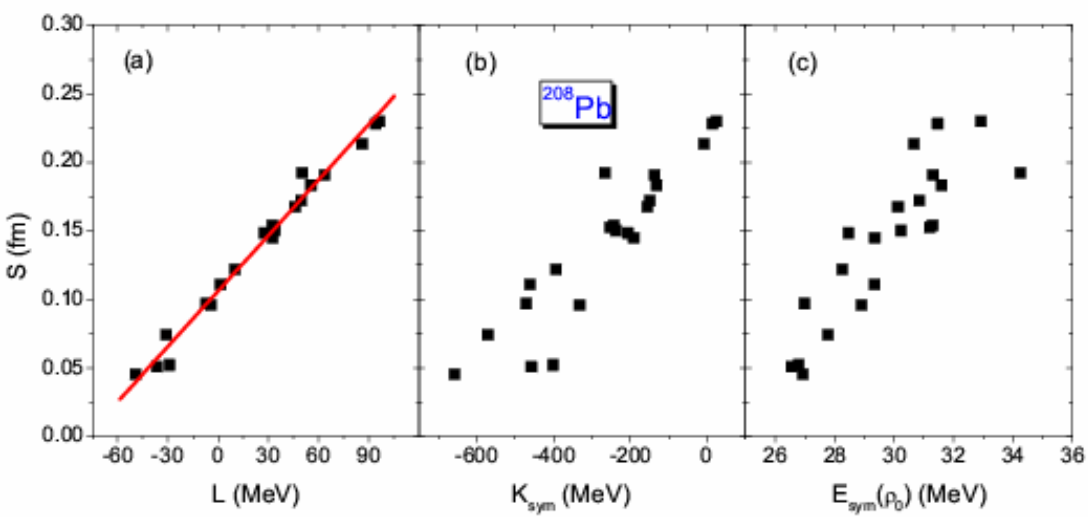

Figure 1. Neutron skin thickness S of ^{208}Pb as a function of (a) L, (b) K_{sym}, and (c) $E_{sym}(\rho_0)$ for 21 sets of Skyrme interaction parameters. The line in panel (a) represents a linear fit.

[1] L.W. Chen, C.M. Ko, and Bao-An Li, Phys. Rev. C **72**, 064309 (2005).

φ and Ω Production in Relativistic Heavy-Ion Collision in a Dynamical Coalescence Model

L.W. Chen[1] and C.M. Ko

[1]*Institute of Theoretical Physics, Shanghai Jiao-Tong University, Shanghai 200240, China*

Based on the phase-space information obtained from a multi-phase transport (AMPT) model within the string melting scenario for strange and antistrange quarks, we have studied the yields and transverse momentum spectra of φ mesons and Ω baryons as well as their anisotropic flows in Au+Au collisions at RHIC using a dynamical quark coalescence model that includes the effect due to quark phase-space distributions inside hadrons [1]. With current quark masses and fixing the φ and Ω radii from fitting measured yields, we first studied the ratio of the yield of Ω baryons to that of φ mesons as well as their elliptic and fourth-order flows as functions of their transverse momentum (Fig.1). How the elliptic and fourth-order flows of φ mesons and Ω baryons are related to those of strange and antistrange quarks was then examined. The dependence of above results on φ and Ω radii as well as on the strange quark mass has also been studied.

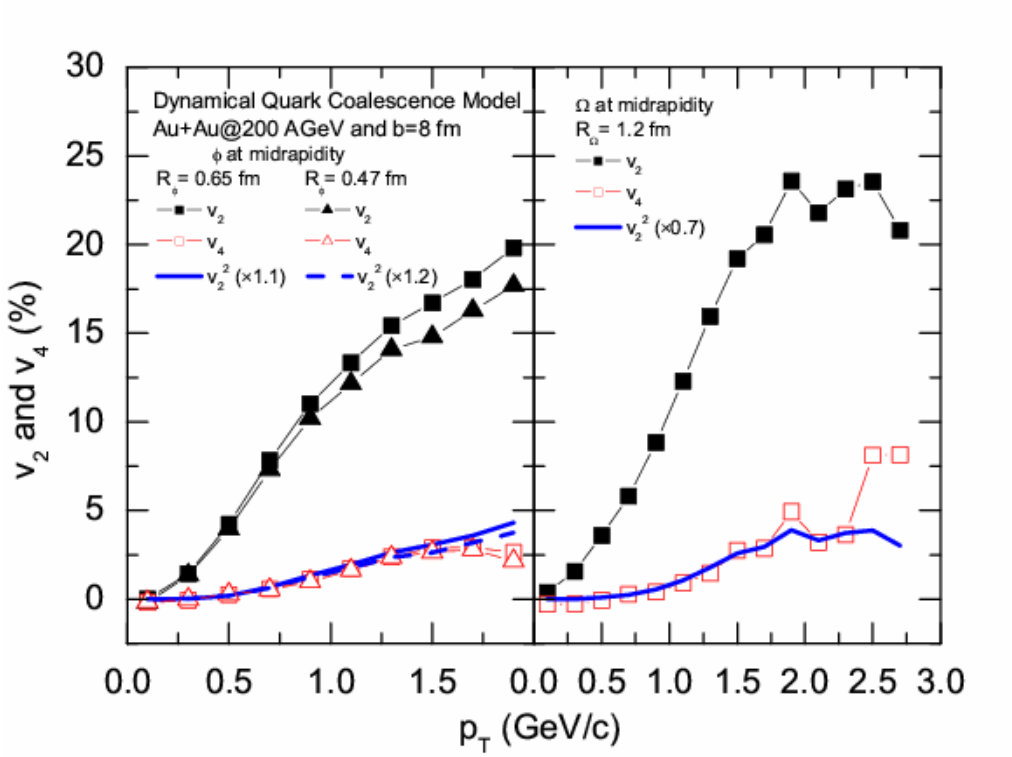

Figure 1. Transverse momentum dependence of anisotropic flows v_2 and v_4 of mid-rapidity φ mesons (left panel) and Ω baryons (right panel) produced in Au+Au collisions at $s^{1/2}$ = 200 A GeV and impact parameter b=8 fm. Solid and dashed lines in left panel are, respectively, $1.1v_2^2$ and $1.2v_2^2$ for φ mesons, while solid line in right panel is $0.7v_2^2$ for Ω baryons.

[1] L.W. Chen and C.M. Ko, Phys. Rev. C **73**, 044903 (2006).

Hadron Production from Quark Coalescence and Jet Fragmentation

V. Greco, C.M. Ko, and I. Vitev[1]
[1]*Theory Division and Physics Division, Los Alamos National Laboratory, Mail Stop H846, Los Alamos, New Mexico 87545*

Based on a model that includes both quark coalescence from the dense partonic matter and fragmentation of the quenched perturbative minijet partons, we have studied the transverse momentum spectra of pions, protons and antiprotons in Au+Au collisions at intermediate RHIC energy of $s^{1/2}_{NN}$ = 62 GeV [1]. The resulting baryon to meson ratio at intermediate transverse momenta is predicted to be larger than that seen in experiments at higher center of mass energies as shown in Fig.1.

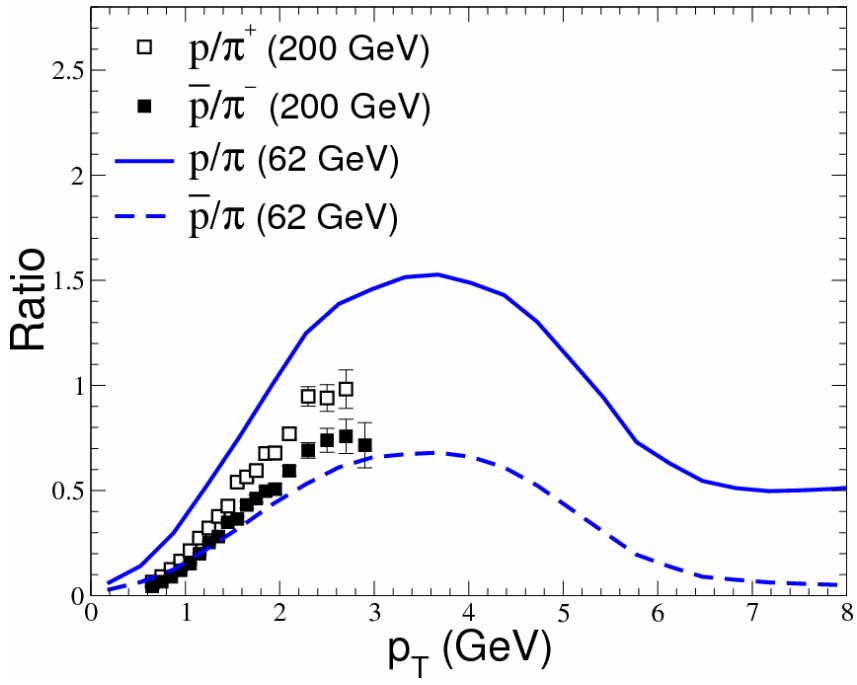

Figure 1. Ratios of proton (solid line) and antiproton (dashed line) to pion spectra from central Au+Au collisions at $s^{1/2}_{NN}$ = 62 GeV. Experimental data given by open and filled squares at $s^{1/2}_{NN}$ = 200 GeV are shown for reference.

[1] V. Greco, C.M. Ko, and I. Vitev, Phys. Rev. C **71**, 041901(R) (2005).

High-Energy Behavior of the Nuclear Symmetry Potential in Asymmetric Nuclear Matter

L.W. Chen,[1] C.M. Ko, and Bao-An Li[2]

[1]*Institute of Theoretical Physics, Shanghai Jiao Tong University, Shanghai 200030, China*

[2]*Department of Chemistry and Physics, Arkansas State University, Jonesboro, AR 72467*

Using the relativistic impulse approximation with empirical NN scattering amplitude and the nuclear scalar and vector densities from the relativistic mean-field theory, we have evaluated the Dirac optical potential for neutrons and protons in asymmetric nuclear matter for different parameter sets NL3, Z27v, and HA [1]. From the resulting Schrodinger-equivalent potential, the high energy behavior of the nuclear symmetry potential has been studied. We find that the symmetry potential at fixed baryon density is essentially constant once the nucleon kinetic energy is greater than about 500 MeV. Moreover, for such high energy nucleon, the symmetry potential is slightly negative below a baryon density of about ρ=0.22 fm^{-3} and then increases almost linearly to positive values at high densities as shown in Fig.1, where results from the non-relativistic momentum-dependenct (MDI) interaction are also given. Our results provide an important constraint on the energy and density dependence of nuclear symmetry potential in asymmetric nuclear matter.

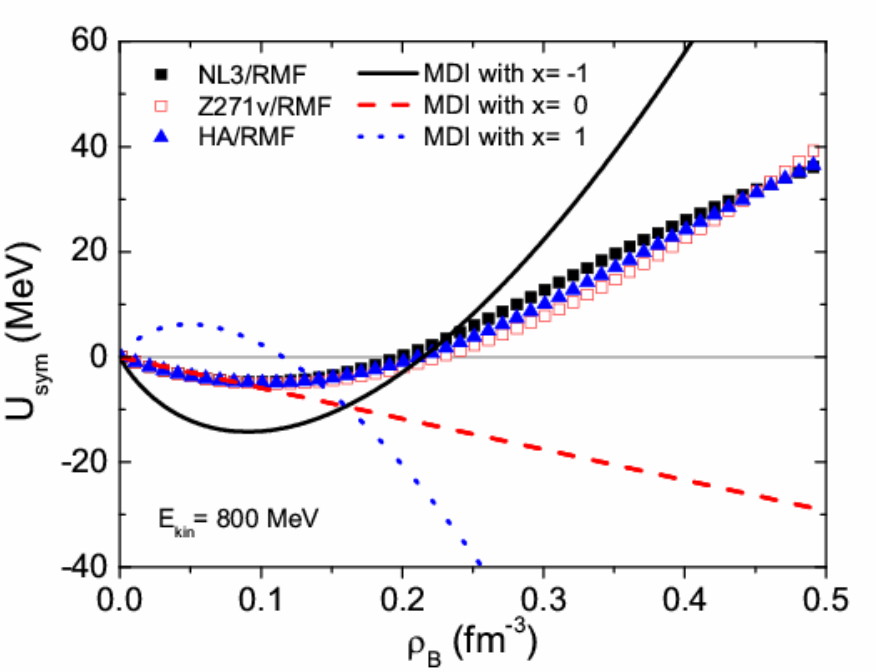

Figure 1. Density dependence of the nuclear symmetry potential using the parameter sets NL3, Z271v, and HA as well as from the MDI interaction with x=1, 0, and 1 at a fixed nucleon kinetic energy of 800 MeV.

[1] L.W. Chen, C.M. Ko, and B.A. Li, Phys. Rev. C **72**, 064606 (2005).

Comprehensive Interpretation of Thermal Dileptons at the SPS

Hendrik van Hees and Ralf Rapp

Electromagnetic (e.m.) probes, i.e., leptons and photons, are especially valuable for the investigation of strongly interacting matter as created in ultrarelativistic heavy-ion collisions (URHICs) since they are emitted at all stages of the collision and penetrate the medium with negligible final-state interactions [1]. Here we investigate medium modifications of the hadronic e.m. current correlator in the context of dimuon spectra as recently measured in 158 *A*GeV In-In collisions by the NA60 collaboration at the CERN Super Proton Synchrotron (SPS) [2].

At low invariant mass (M≤1 GeV), the e.m. current correlator is saturated by the light vector mesons ρ, ω, and φ. Since the dominant contribution is from the ρ-meson, its medium modifications have been studied in great detail [1]. Here, we employ hadronic many-body theory (HMBT) to evaluate the spectral properties of the ρ-meson, including modifications of its pion cloud by baryon-hole excitations and thermal Bose factors, as well as direct interactions with thermal mesons (π, *K*, ρ) and baryons (nucleons, Δ's, hyperons etc.) [3]. The coupling constants and form factors have been fixed by hadronic and radiative decay branchings, photoabsorption data on nucleons and nuclei, and $\pi N \to \rho N$ scattering. When averaged over a typical space-time evolution of URHICs at SPS, its spectral width amounts to ~350 MeV (compared to about 150 MeV in vacuum). The ω-meson is evaluated in the same HMBT framework as the ρ, leading to an average width of about 100 MeV [4]. For the φ meson-gas effects are expected to generate a broadening of ~20 MeV at T=150 MeV [5], while the dressing of the kaon cloud in nuclear matter induces an increase of the width by ~25 MeV at saturation density [6] (recent nuclear photoproduction data suggest an even larger value [7]). Since there is no comprehensive study of medium effects on the φ-meson in hot and dense matter currently available, we here assume an average width of 80 MeV.

In the intermediate-mass region (1 GeV≤M≤1.5 GeV) we use model-independent predictions based on chiral symmetry in connection with a (leading order) virial expansion. One finds that thermal pions induce a mixing of the vacuum isovector-vector (V) and –axialvector (A) current correlators [8],

$$\Pi_{V,A}(s) = (1-\varepsilon)\,\Pi^{vac}_{V,A}(s) + \varepsilon\,\Pi^{vac}_{A,V}(s)\,.$$

The mixing parameter ε, following from thermal tadpole diagrams, is evaluated for finite pion mass and pion-chemical potential as $\varepsilon = 1/2 \;\; I(T,\mu_\pi)/I(T_c,0)$ with

$$I(T,\mu_\pi) = \int \frac{d^3k}{(2\pi)^3}\,\frac{f^\pi(\omega_\pi)}{\omega_k}$$

(f^π: Bose distribution, ω_π: pion energy) [9], where, as an upper estimate, we enforced V-A degeneracy at $T=T_c$, a direct signature of chiral-symmetry restoration. The vacuum V and A correlators are fitted to τ-decays into even and odd numbers of pions, respectively, as measured by the ALEPH collaboration [10].

Dilepton emission from the Quark-Gluon Plasma (QGP) is calculated using the leading-order hard-thermal-loop improved perturbative QCD expression for quark-antiquark annihilation [11]. The corresponding dilepton rate resembles the HMBT results around the critical temperature, being suggestive for chiral restoration via a "quark-hadron duality".

Dilepton spectra are calculated by convoluting the thermal rates over an expanding thermal fireball assuming isentropic expansion and utilizing ideal QGP and hadronic resonance-gas equations of state to infer the temperature and baryon-density evolution. Initial and final temperatures for central In(158*A*GeV)-In are 197 MeV and 120 MeV, respectively.

The comparison with NA60 data [2] (Fig.1) confirms the prevalence of the ρ-meson at low-mass in connection with its substantial broadening as predicted by HMBT. At intermediate masses 4-pion contributions in the e.m. correlator take over, resulting in good agreement with experiment, especially if chiral mixing effects are included [2]. Current experimental uncertainties in the cocktail subtraction (late hadron decays) do not yet allow to draw any conclusions about possible medium effects on ω- and φ-mesons. While the fireball model implies theoretical uncertainties in the overall (absolute) normalization of 20-30% (without impact on the spectral shape), we emphasize that the relative strength of all thermal sources as calculated here is essentially fixed. The overall agreement of our approach with the data thus suggests that the medium produced in URHICs at the SPS is in indeed close to chiral-symmetry restoration. To further corroborate this finding, a detailed study of a manifestly chirally symmetric model, including baryons, is mandatory.

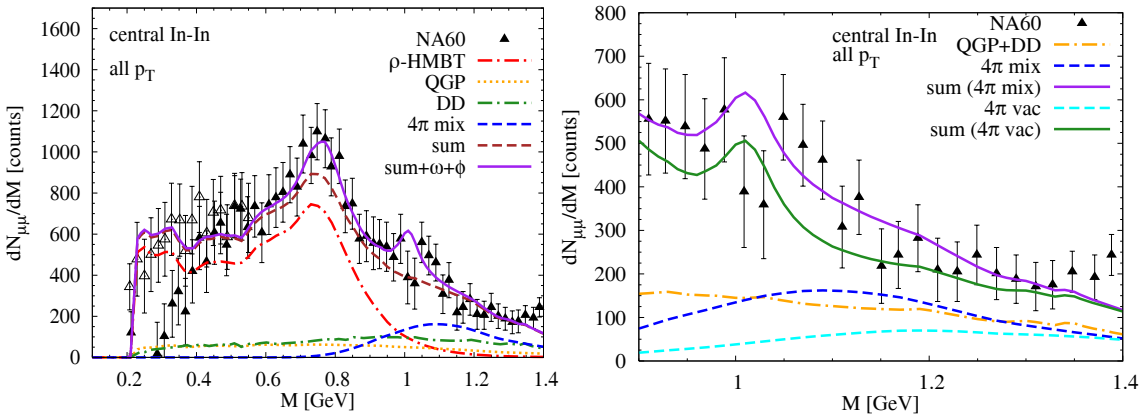

Figure 1. (Left panel) NA60 excess dimuon spectrum [2] in central In(158*A*GeV)-In collisions compared to thermal dimuon radiation using an in-medium e.m. current correlator evaluated using HMBT for the ρ-meson (dash-dotted red line), 4-pion contributions with chiral V-A mixing (dashed blue line), QGP (dotted orange line) and correlated open charm (dash-dotted green line); the upper dashed line is the sum of these contributions, and the solid purple line additionally includes in-medium ω– and ϕ–meson decays. (Right panel) NA60 data at intermediate mass compared to thermal dimuon spectra with different implementations of the 4-pion contribution, using either its vacuum form (lower dashed line) or with chiral mixing (upper dashed line). The corresponding total spectra are given by the lower and upper solid line, respectively.

[1] R. Rapp and J. Wambach, Adv. Nucl. Phys. **25**, 1 (2000).

[2] S. Damjanovic *et al.* (NA60 Collaboration), nucl-ex/0510044.

[3] R. Rapp and J. Wambach, Eur. Phys. J. A **6**, 415 (1999).
[4] R. Rapp, nucl-th/0204003.
[5] L. Alvarez-Ruso and V. Koch, Phys. Rev. C **65**, 054901 (2002).
[6] D. Cabrera *et al.*, Nucl. Phys. **A733**, 130 (2004).
[7] J. K. Ahn *et al.*, Phys. Lett. B **608**, 215 (2005).
[8] M. Dey, V.L. Eletsky, and B.L. Ioffe, Phys. Lett. **252**, 620 (1990).
[9] H. van Hees and R. Rapp, hep-ph/0603084.
[10] R. Barate et al. (ALEPH Collaboration), Eur. Phys. J. **C4**, 409 (1998).
[11] E. Braaten, R.D. Pisarski, T.-C. Yuan, Phys. Rev. Lett. B **64**, 2242 (1990).

Bottomonium Production at RHIC and LHC

L. Grandchamp, S. Lumpkins, D. Sun, H. van Hees, and R. Rapp

A prime goal of ultrarelativistic heavy-ion collisions (URHICs) is the production and investigation of the quark-gluon plasma (QGP), a state of matter with quarks and gluons as the relevant degrees of freedom. The suppression of heavy-quarkonium production in URHICs, relative to proton-proton (p-p) reactions, has long been considered as a signature of QGP formation [1]. However, more recent observations at the Relativistic Heavy-Ion Collider (RHIC) suggest that the created matter is a strongly interacting QGP (sQGP), which allows for the existence of heavy-quark bound states as suggested by lattice QCD [2]. Thus, with copious production of charmquarks at RHIC, secondary formation of charmonia via *c-cbar* coalescence might dominate their yield in central Au-Au collisions [3,4], contrary to the situation in Pb-Pb collisions at the CERN Super Proton Synchrotron (SPS), where *J/ψ* suppression is the main effect.

In the present work [5], we study consequences of this picture for bottomonium (*Y*) production at RHIC and the Large Hadron Collider (LHC). We assess the time evolution of *Y* states in A-A collisions via a kinetic rate equation,

$$\frac{dN_Y}{dt} = -\Gamma_Y (N_Y - N_Y^{eq})$$

(N_Y: number of Y, Γ_Y: *Y*-dissociation rate, N_Y^{eq}: *Y*-equilibrium number), which is valid if *b*-quarks (open-bottom states) are in thermal equilibrium with the surrounding QGP [6].

The dissociation rates for the various *Y* states are evaluated using dissociation cross sections with thermal quarks and gluons. Since the commonly employed gluo-dissociation process [7], *g+Y→b+bbar*, becomes inefficient for small *Y* binding energies, we use the quasi-free breakup mechanism, *g(q)+Y-> b+bbar+g(q)*, as suggested for charmonia [4]. The in-medium *Y* binding energies are taken from solutions of a Schrödinger equation with a color-screened Cornell potential [8]. We furthermore assume that the quarkonium masses are temperature independent, which implies that the *b*-quark mass also decreases with temperature (as indicated by lattice QCD as well).

Due to their large mass, *b*-quarks are not expected to kinetically equilibrate in A-A collisions. We account for this by multiplying the gain term of the rate equation with a schematic correction factor, $R = 1 - \exp(-\int d\tau / \tau_{eq})$, with τ_{eq} denoting the thermal relaxation time for *b*-quarks which we take from a recent resonance-scattering model [9].

The total number of *b-bbar* pairs in the system (which determines the *Y*-equilibrium number) is obtained from binary collision scaling (secondary production is expected to be negligible [10]) according to

$$N_{b\bar{b}} = \frac{\sigma_{pp\to b\bar{b}}}{\sigma_{pp}^{inelastic}} N_{coll}(b) R_y ,$$

with $\sigma_{pp}^{inelastic}$=42(78) mb: total inelastic p-p cross section at RHIC (LHC) [11], $N_{coll}(b)$: number of primordial N-N collisions at impact parameter *b*, $\sigma_{pp\to b\bar{b}}$=2(160)μb at RHIC (LHC) [12]. R_y=0.52(0.29) for RHIC (LHC) denotes the fraction of *b-bbar* pairs in the considered rapidity range [13]. The primordial numbers of bottomonia are taken to be proportional to the *b-bbar* number with a p-p production cross section of 3.5(152)nb at RHIC (LHC, including shadowing corrections) [14]. The initial bottomonium number in the rate equation, $N_\Upsilon(0)$, also incorporates (pre-equilibrium) nuclear absorption effects with a dissociation cross section of 3.1(4.6)mb at RHIC (LHC).

With the above ingredients we solve the rate equation for different impact parameters for A-A collisions at RHIC and LHC energies; the pertinent centrality dependencies for *Y(1S)* production are summarized in Fig. 1, including feeddown from excited bottomonia. A rather strong suppression turns out to be the main effect at both RHIC and LHC, mostly driven by the reduction in binding energies due to color-screening. This is in contrast with the findings of similar studies for charmonia [14], where *J/ψ* suppression is the prevalent effect at SPS, while regeneration takes over and becomes the dominant source at RHIC energies and above. Thus, the simultaneous observation of appreciable *Y(1S)* suppression and the absence of *J/ψ* suppression emerges as a promising signature of the sQGP at collider energies.

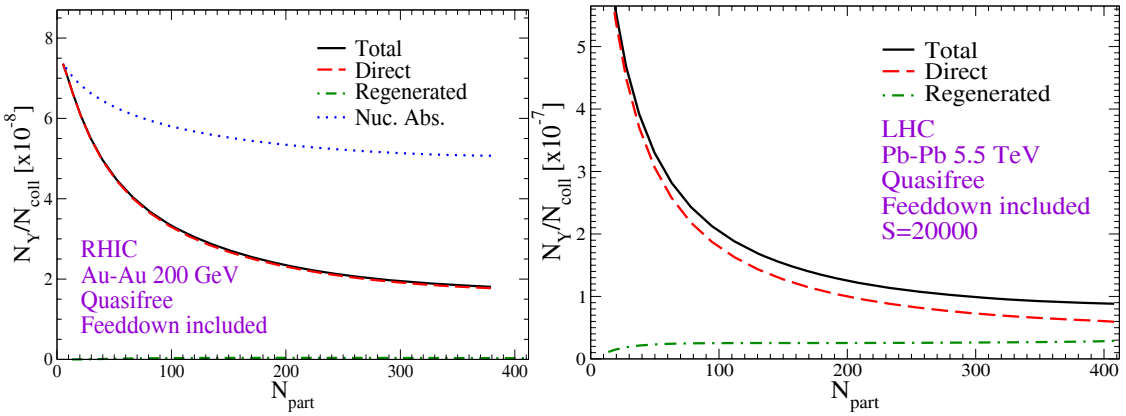

Figure 1. Centrality dependence of N_Υ / N_{coll} at RHIC (200 *A*GeV Au-Au collisions, left panel) and LHC (5.5 *A*TeV Pb-Pb collisions, right panel) using the quasi-free *Y*-dissociation cross sections with color Debye-screening.

[1] T. Matsui, H. Satz, Phys. Lett. B **178**, 416 (1986).

[2] Y. Asakawa and T. Hatsuda, Phys. Rev. Lett. **92**, 012001 (2004); S. Datta et al., Phys. Rev. D **69**, 094507 (2004).

[3] P. Braun-Munzinger and J. Stachel, Nucl. Phys. **A690**, 119 (2001); R. L. Thews, M. Schroedter and J. Rafelski, Phys. Rev. C **63**, 054905 (2001).

[4] L. Grandchamp and R. Rapp, Phys. Lett. B **523**, 60 (2001); Nucl. Phys. **A709**, 415 (2002).

[5] L. Grandchamp, S. Lumpkins, D. Sun, H. van Hees, R. Rapp, hep-ph/0507314.

[6] R. Rapp and L. Grandchamp, J. Phys. G **30**, S305 (2004).

[7] M. E. Peskin, Nucl. Phys. **B156**, 365 (1979); G. Bhanot and M. E. Peskin, Nucl. Phys. **B156**, 391 (1979).

[8] F. Karsch, M. T. Mehr and H. Satz, Z. Phys. C **37**, 617 (1988).
[9] H. van Hees and R. Rapp, Phys. Rev. C **71**, 034907 (2005).
[10] P. Levai, B. Müller and X. N. Wang, Phys. Rev. C **51**, 3326 (1995).
[11] S. Eidelmann *et al.* ([Particle Data Group), Phys. Lett. B **592**, 1 (2004).
[12] M. Bedjidian *et al.*, hep-ph/0311048; R. Vogt, Heavy Ion Phys. **18**, 11 (2003).
[13] R. Vogt (Hard Probe Collaboration), Int. J. Mod. Phys. E **12**, 211 (2003).
[14] L. Grandchamp, R. Rapp, and G. E. Brown, Phys. Rev. Lett. **92**, 212301 (2004).

Heavy-Quark Interactions in the Quark-Gluon Plasma and Single-Electron Spectra at RHIC

Hendrik van Hees and Ralf Rapp

Heavy quarks and quarkonia are believed to be valuable probes of the medium produced in ultrarelativistic heavy-ion collisions (URHICs). Recent spectra of semileptonic decay electrons associated with charm and bottom hadrons in Au-Au collisions at the Relativistic Heavy-Ion Collider (RHIC) have shown a surprisingly large suppression (small nuclear modification factor, R_{AA}) [1-3] and elliptic flow (v_2) [4-6], indicating significantly stronger interactions of heavy quarks in the quark-gluon plasma (QGP) than expected within perturbative QCD (pQCD).

To study microscopic reaction mechanisms underlying the behavior of heavy quarks in a strongly interacting QGP (sQGP), we have introduced *D*- and *B*-meson like resonance states [7] mediating elastic rescattering of *c*- and *b*-quarks. Here, we study the consequences of this conjecture for the thermalization and flow of the heavy quarks in the sQGP formed in Au-Au collisions at RHIC, employing a Fokker-Planck approach, followed by a combined quark-coalescence/fragmentation model for the hadronization of the heavy quarks. The resulting transverse-momentum (p_T) spectra and v_2 of the single decay-electrons are confronted with RHIC data [8].

The drag and diffusion coefficients for heavy-quarks, entering the Fokker-Planck equation, are calculated from elastic rescattering off light antiquarks in the sQGP via *D*- and *B*-meson resonances assumed to survive above the critical temperature. This is motivated by recent lattice QCD (lQCD) computations of hadronic correlators and lQCD-based potential models which indicate colorless resonances in both the light- and heavy-quark sector [9]. The resonant $Q\text{-}\bar{q}$ cross sections are supplemented with leading-order pQCD elastic scattering [10]. We find that the resulting drag coefficients imply thermalization times which are lower by a factor ~3 compared to pQCD scattering alone [7].

The coefficients are used in a relativistic Langevin simulation for heavy-quark interactions in an isentropically expanding, elliptic QGP fireball corresponding to impact parameter b=7fm 200 *A*GeV Au-Au collisions at RHIC. The expansion parameters are adjusted to resemble the time evolution of radial and elliptic flow of the bulk matter in hydrodynamic simulations [11]. The proper thermal equilibrium limit in the Langevin process is implemented via the Hänggi-Klimontovich realization [12], cf. also Ref. [13].

The initial heavy-quark p_T-distributions and the relative magnitude of *c*- and *b*-quark spectra are determined by fitting experimental *D*- and *D**- spectra in d-Au collisions [14] and attributing the missing yield of the corresponding semileptonic electrons [15] at higher p_T to *B*-meson decays. This leads to a cross-section ratio for *b*- and *c*-quark pair production of $4.9\cdot10^{-3}$ and a crossing of *D*- and *B*-decay electrons at p_T~5 GeV, in line with expectations from pQCD.

The *c*- and *b*-quark output spectra from the Langevin simulation are subjected to coalescence with light antiquarks following the model of Ref. [16]. Conservation of *c*- and *b*-quark number is ensured by hadronizing unpaired heavy quarks via δ-function fragmentation. Finally, the single-electron spectra are

obtained from *D*- and *B*-meson three-body decays. Fig. 1 shows that resonance scattering leads to a substantial decrease in R_{AA} and increase in v_2 compared to elastic pQCD rescattering. While coalescence with light antiquarks amplifies v_2, it also leads to *harder D*- and *B*-meson momentum spectra, which increases the electron R_{AA}. The approach to thermalization of *c*-quarks leads to a strong quenching of their electron-decay spectra, entailing that *B*-meson decay contributions become prevalent for electron momenta of p_T >2.5 GeV. This substantially reduces the effects in the single-electron spectra, since *b*-quarks (due to their large mass) are much less affected in the sQGP than *c*-quarks.

In conclusion, resonance formation in the sQGP could play an essential role in understanding current observations on semileptonic single-electron spectra at RHIC. Future calculations should aim at a consistent inclusion of radiative energy-loss which is expected to become the dominant effect at (very) high p_T.

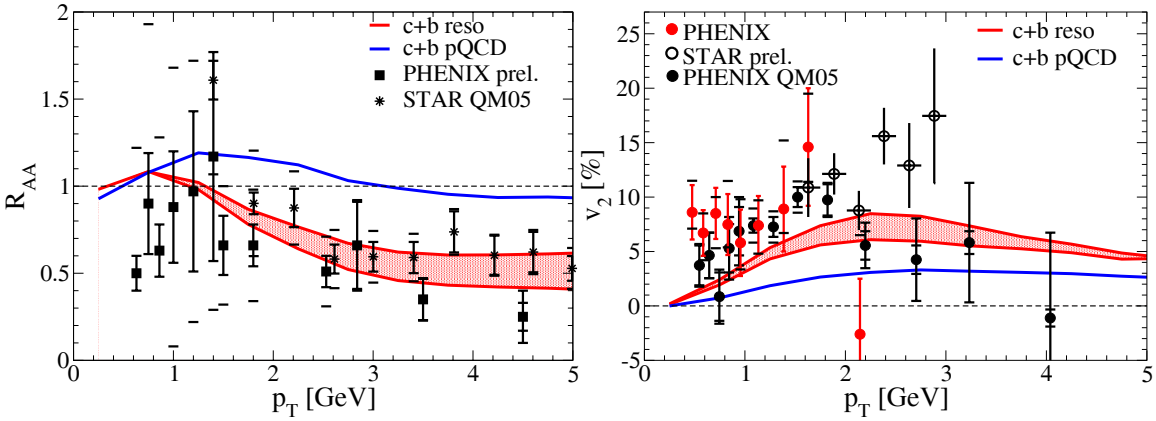

Figure 1. Nuclear Modification factor, R_{AA} (left panel)**,** and elliptic flow, v_2 (right panel)**,** of semileptonic *D*- and *B*-meson decay electrons in *b*=7 fm 200 *A*GeV Au-Au collisions assuming different elastic heavy-quark interactions in the QGP with subsequent hadronization via coalescence and fragmentation, compared to PHENIX and STAR data [1,2,5,6].

[1] S. S. Adler *et al.* (PHENIX Collaboration), Phys. Rev. Lett. **94**, 082301 (2005).

[2] B. Jacak *et al.* (PHENIX Collaboration), nucl-ex/0508036.

[3] J. Bielcik *et al.* (STAR Collaboration), nucl-ex/0511005.

[4] S. S. Adler *et al.* (PHENIX Collaboration), Phys. Rev. C **72**, 024901 (2005).

[5] F. Laue *et al.* (STAR Collaboration), J. Phys. G **31**, S27 (2005).

[6] Y. Akiba *et al.* (PHENIX Collaboration), nucl-ex/0510008.

[7] H. van Hees and R. Rapp, Phys. Rev. C **71**, 034907 (2005).

[8] H. van Hees, V. Greco and R. Rapp, Phys. Rev. C. **73**, 034913 (2006).

[9] M. Asakawa and T. Hatsuda, Phys. Rev. Lett. **92**, 012001 (2004); F. Karsch and E. Laermann, hep-lat/0305025; R. Morrin *et al.*, PoS LAT2005 (2005) 176; E.V. Shuryak and I. Zahed, Phys. Rev. C **70**, 021901(R) (2004); C. Y.Wong, Phys. Rev. C **72**, 034906 (2005); M. Mannarelli and R. Rapp, Phys. Rev. C **72**, 064905 (2005); Á. Mócsy and P. Petretczky, Phys. Rev. D **73**, 074007 (2006).

[10] B.L. Combridge, Nucl. Phys. **B151**, 429 (1979).
[11] P.F. Kolb, J. Sollfrank, and U. Heinz, Phys. Rev. C **62**, 054909 (2000).
[12] J. Dunkel and P. Hänggi, Phys. Rev. E **71**, 016124 (2005).
[13] G.D. Moore and D. Teaney, Phys. Rev. C **71**, 064904 (2005).
[14] J. Adams *et al.* (STAR Collaboration), Phys. Rev. Lett. **94**, 062301 (2005); A. Tai *et al.* (STAR Collaboration), J. Phys. G **30**, S809 (2004).
[15] A.A. P. Suaide *et al.* (STAR Collaboration), J. Phys. G **30**, S1179 (2004).
[16] V. Greco, C. M. Ko, and R. Rapp, Phys. Lett. **B595**, 202 (2004).

Low-Energy Thermal Photons from Hadronic Matter

Wei Liu and Ralf Rapp

Within a hadronic model including electromagnetism via a U(1) gauge, we reinvestigate photon Bremsstrahlung from a hot hadron gas as expected to be formed in relativistic heavy-ion collisions at SPS energies [1]. We calculate photon emission from the reactions $\pi\pi\rightarrow\pi\pi\gamma$ and $\pi K\rightarrow\pi K\gamma$ by explicit (numerical) evaluation of the multi-dimensional phase space integral (Fig. 1). This, in particular, allows to overcome the commonly employed soft photon approximation (SPA), as well as to incorporate final-state Bose enhancement factors. Both improvements are shown to result in an appreciable increase of the pertinent photon production over previous calculations [2] by up to a factor of 2 at low photon energies (q_0=0.1~0.5 GeV).

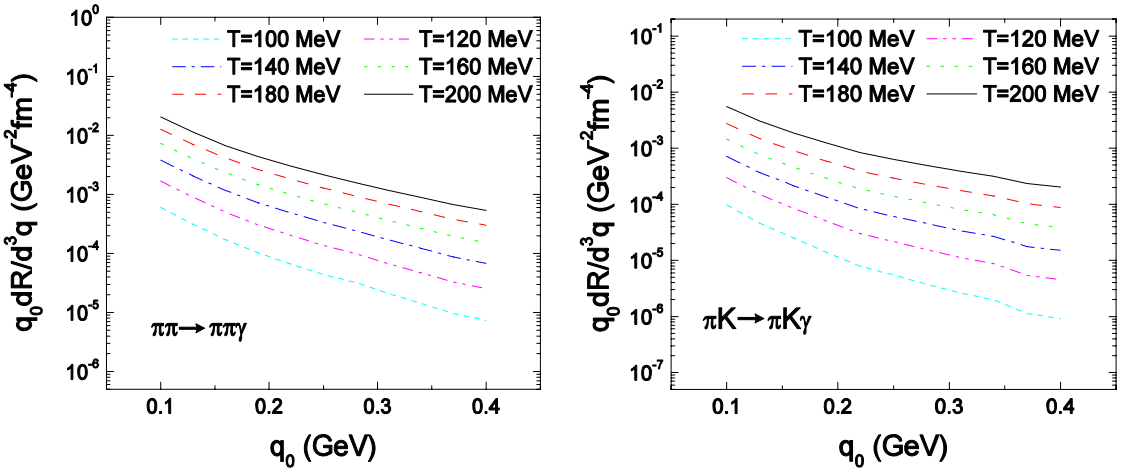

Figure 1. Thermal photon emission rate from Bremsstrahlung via $\pi\pi\rightarrow\pi\pi\gamma$ (left) and $\pi K\rightarrow\pi K\gamma$ (right) reactions as a function of photon energy at different temperatures.

We apply the thermal emission rates to the calculation of photon spectra at low transverse momentum (q_t) in central Pb(158 AGeV)-Pb collisions at SPS via a convolution over a thermal fireball. When comparing the total yield to recent WA98 data [3], we find that Bremsstrahlung leads to a significant improvement in the description of the low-q_t part of the spectrum (Fig. 2).

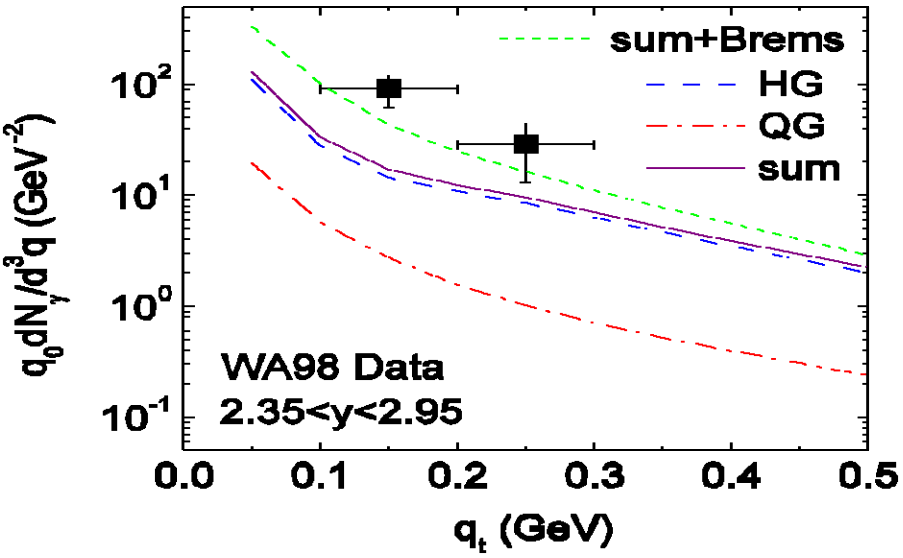

Figure 2. Direct low-q_t photon spectra as measured in central Pb-Pb collisions at SPS [3] compared to the thermal emission spectra from an expanding fireball with QGP phases.

[1] W. Liu and R. Rapp, submitted to Nucl. Phys. **A**; arXiv:nucl-th/0604031.

[2] S. Turbide, R. Rapp, and C. Gale, Phys. Rev. C **69,** 014903 (2004).

[3] M.M. Aggarwal *et al.* (WA98 Collaboration), Phys. Rev. Lett. **93**, 022301 (2004).

Self-Consistent Approximations to a Model with Spontaneously Broken O(N) Symmetry

Yu.B. Ivanov, F. Riek, H. van Hees, and J. Knoll

Self-consistent Φ-derivable Schwinger-Dyson resummation schemes for quantum field theories (QFT's) are preferable to other schemes since only they obey the conservation laws for the expectation values of energy, momentum and charge and at the same time guarantee the thermodynamic consistency for thermal-equilibrium systems [1]. However, these kind of approximations violate the Ward-Takahashi identities of symmetries underlying the QFT's for two-point and higher vertex functions, leading especially to the violation of the Nambu-Goldstone (NG) theorem in the phase of spontaneously broken symmetry (NG phase) [2].

Earlier we have shown that Φ-derivable approximations to renormalizable QFT's can be renormalized with temperature-independent counter terms [3]. Recently a "gapless Φ-derivable" approximation scheme to a linear O(N)-σ model has been proposed which obeys the NG theorem in the NG phase [4]. Here we apply the previously developed renormalization procedure [3] to this model and discuss remaining problems in the NG phase at finite temperature [5].

As has been demonstrated in [4], for the linear O(N)-σ model a modification to the two-loop approximation of the Φ functional can be uniquely defined by the assumption that (i) it restores the NG theorem in the NG phase, (ii) it leaves the approximation in the phase with restored symmetry (Wigner-Weyl phase) unchanged to the two-loop approximation (i.e., the Hartree-Fock (HF) approximation), (iii) it does not change the HF equation of motion for the mean field. Thus, according to [3], this model can be renormalized with temperature-independent counter terms. In contrast to the usual HF equation, the renormalized gapless HF (gHF) approximation for T=0 resulting from the modified Φ functional is O(N) symmetric in the mass-independent renormalization scheme, and thus the physical mass and coupling can be chosen independently from the renormalization-scale, μ.

As shown in the figure, at finite temperature the gHF equations lead to a rather complex phase structure: There exist two critical temperatures, T_1 and T_2. For $T>T_1$ the equations have a metastable solution in addition to the stable one which shows a phase transition at the temperature $T_2>T_1$. While the latter critical temperature is approximately renormalization-scale independent, the former depends logarithmically on the renormalization scale, μ. For $T>T_2$, in the stable branch the mean field vanishes, but the pion and the σ masses are different up to a temperature $T_{\rm cross,}$ where chiral symmetry is finally completely restored. Above a certain temperature, no physically meaningful solutions of the renormalized gHF equations exist. This can be traced back to large renormalization-scale dependent logarithms which become the driving terms of the equations for higher temperatures. For the same reason, another metastable symmetric solution with much higher meson masses exists. This solution corresponds to the usual HF approximation in the Wigner Weyl phase of the model and ceases to exist at the same limiting temperature as the other branches, described above. The existence of this artificial limiting temperature has been already found in the paper by Baym and Grinstein [2].

This renormalization-scale dependence of Φ-derivable approximations has also been analyzed from the point of view of the renormalization-group equation [6]: The β function, evaluated from a Φ-

derivable approximation, deviates from its perturbative expansion, beginning at orders in the expansion parameter (like the coupling or number of loops in the diagrams taken into account) higher than that explicitly used to define the approximate Φ functional. The reason is the violation of "crossing symmetry" in the sense of [3]: Solving the self-consistent equations of motion leads to a partial resummation of perturbative diagrams to any order in the expansion parameter which is necessarily incomplete for any truncation of the Φ functional.

Within the here applied renormalization scheme for the gHF approximation, the renormalization-scale dependence at finite temperature originates from the subtraction of the "hidden subdivergence" of the four-point function inside the self-consistent tadpole loop. As shown in [3], the corresponding four-point function consists in the resummation of diagrams of arbitrarily high orders in the coupling, λ, but only in one of three channels, and thus the β function of this resummed four-point function deviates from the correct one at orders $O(\lambda^2)$.

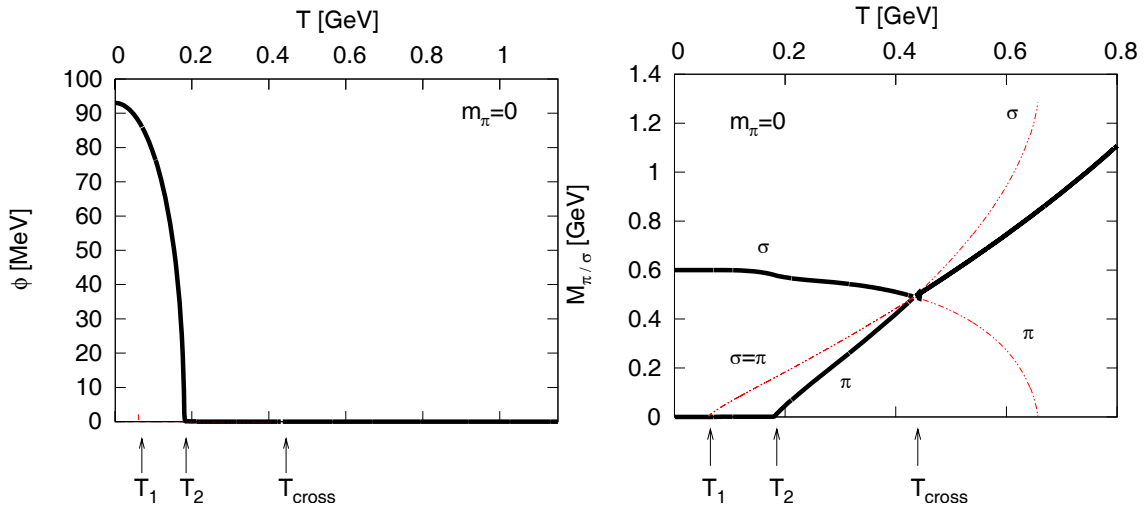

Figure 1. The solution of the gHF equation for the mean field, ϕ (left panel), and the meson masses (right panel) in the chiral limit. The solid (dashed) lines represent the stable (metastable) solutions. The renormalization scale has been chosen to μ=0.6 GeV.

[1] J. M. Luttinger and J. C. Ward, Phys. Rev. **118**, 1417 (1960); G. Baym, Phys. Rev. **127**, 1391 (1962); J. M. Cornwall, R. Jackiw and E. Tomboulis, Phys. Rev. D **10**, 2428 (1974).

[2] P. C. Hohenberg and P. C. Martin, Ann. Phys. (N.Y.) **34**, 291 (1965); G. Baym and G. Grinstein, Phys. Rev. D **15**, 2897 (1977); Z. Aouissat, G. Chanfray, P. Schuck and J. Wambach, Nucl. Phys. **A603**, 458 (1996); H. van Hees and J. Knoll, Phys. Rev. D **66**, 025028 (2002).

[3] H. van Hees and J. Knoll, Phys. Rev. D **65**, 025010 (2002); **65**, 105005 (2002).

[4] Yu. B. Ivanov, F. Riek and J. Knoll, Phys. Rev. D **71**, 105016 (2005).

[5] Yu. B. Ivanov, F. Riek, H. van Hees, J. Knoll, Phys. Rev. D **72**, 036008 (2005).

[6] E. Braaten and E. Petitgirard, Phys. Rev. D **65**, 085039 (2002); C. Destri and A Sartirana, Phys. Rev. D **72**, 065093 (2005).

A New Analysis of ^{14}O Beta Decay: Branching Ratios and CVC Consistency

I.S. Towner and J.C. Hardy

The nucleus ^{14}O decays predominantly by a Fermi transition to the 2.313 MeV 0^+ state in ^{14}N. Weak Gamow-Teller (GT) branches are evident to the 1^+ state at 3.95 MeV in ^{14}N (branching ratio, R_{GT} = 0.055 %) and to the 1^+ ground state, with R_{GT} ~0.6 %. This ground-state GT transition is strongly inhibited: its *ft*-value is roughly 10^4 times larger than is typical for favored $0^+ \longrightarrow 1^+$ transitions. (Even more inhibition is evident in the analog ^{14}C —> ^{14}N transition.) The inhibition is attributed to accidental cancellation in the allowed GT matrix element for this transition. Because the allowed matrix elements are so small, the induced terms – particularly "weak magnetism" – as well as the relativistic and the second-forbidden terms, are expected to contribute appreciably to the decay probability. As a consequence, many of the usual assumptions in the allowed approximation may not be valid. For example, the spectrum shape may deviate markedly from the allowed (or statistical) spectrum shape.

To date there has only been one measurement, by Sidhu and Gerhart [1, 2], of the detailed shape of the beta spectrum from ^{14}O decay. It was performed with an iron-free, beta-ray spectrometer, and was published 40 years ago! More recently, calculations by Garcia and Brown [3] could not satisfactorily fit the observed beta spectrum, which led the authors to suggest that there might be some systematic problem with Sidhu and Gerhart's measurement. This conclusion would have a serious impact on the branching ratio for the Fermi transition. For this reason, we have reanalyzed [4] the data of Sidhu and Gerhart, which we obtained from a copy of Sidhu's Ph.D. thesis [2]. Our conclusion is that the ^{14}O spectrum shape can be understood, but only if renormalized operators are used in the shell-model calculations of the nuclear matrix elements. Our re-analysis [4] yields a ground-state branching ratio of 0.54(2) %, compared with the originally published result [1] of 0.61(1) % – a large shift in terms of the uncertainties quoted.

Our re-analysis used shell-model calculations for the relevant nuclear matrix elements in model spaces that included both $|2h\rangle$ and $|4h\text{-}2p\rangle$ configurations relative to a closed-shell ^{16}O core. As was noted by Garcia and Brown [3] the GT transition strength to the lowest 1^+ state is very small compared to the strength of the transition to the second 1^+ state at 3.95 MeV excitation energy. Thus, any small mixing between these two 1^+ states in the model will have a large effect on the weak transition rate. To make use of this fact, we write the wave function for the lowest 1^+ state in ^{14}N as

$$|1^+ \text{ low}\rangle = \alpha\, |1^+(1)\rangle + \beta\, |1^+(2)\rangle \,,$$

with $\alpha^2 + \beta^2 = 1$. Here (1) and (2) refer to the first and second model states obtained in the shell-model calculation. Our strategy is then to adjust α to minimize the χ^2 between the calculated and experimental shape-correction function. The magnitude of this function yields the GT matrix element while the slope depends on the interference between the weak magnetism and the GT matrix elements. The difficulty encountered by Garcia and Brown [3] was that the weak magnetism matrix element determined from the slope did not agree with the M1 matrix element determined from the electromagnetic transition between isobaric analog states and the ground state of ^{14}N – a requirement of the conserved vector current (CVC)

hypothesis. We resolved this dilemma by recognizing that renormalized rather than free-nucleon operators should be used in the shell-model calculations of these matrix elements.

In the mirror decay of ^{14}C a similar situation occurs. Consistency between the ^{14}C lifetime, the slope of the shape-correction function and the M1 matrix element from gamma decay can only be achieved with renormalized operators in the shell-model calculation.

[1] G.S. Sidhu and J.B. Gerhart, Phys. Rev. **148**, 1024 (1966).

[2] G.S. Sidhu, *An experimental study of the spectrum shape for the Gamow-Teller transition ^{14}O —> ^{14}N*, Ph.D. thesis, University of Washington (1966).

[3] A. Garcia and B.A. Brown, Phys. Rev. C **52,** 3416 (1995).

[4] I.S. Towner and J.C. Hardy, Phys. Rev. C **72**, 055501 (2005).

SECTION IV

ATOMIC, MOLECULAR AND MATERIALS SCIENCE

A Pyroelectric Crystal Particle Accelerator

J. Kalodimos and R.L. Watson

Recent demonstrations of D-D fusion induced by a pyroelectric crystal accelerator [1,2] have stimulated interest in the possibility of utilizing this novel technique for the development of a portable neutron generator. Such a device could employ the high electric field produced by heating or cooling a pyroelectric crystal under vacuum to dissociate and field ionize deuterium molecules, producing deuterons that are then accelerated by the electric field into a deuterated target at energies ~ 100 to 200 keV. At 100 keV, the D-D fusion cross section (16 mb) is sufficiently high that useful fluxes of 2.5 MeV neutrons conceivably could be produced via the $d(d,n)^3He$ reaction.

We have designed and constructed a pyroelectric crystal accelerator for the purpose of assessing the parameters that determine the energy and intensity of the particle beam. A photograph of the apparatus is shown in Fig. 1. The system consists of an inner chamber, containing the pyroelectric crystal and a remotely controlled target wheel, and an outer chamber containing a liquid nitrogen cooled "cold finger". The vacuum in the outer chamber is maintained by two 1000 L/s diffusion pumps and an automated gas control system enables delivery of gas to the inner chamber and regulation of its pressure via differential pumping. The pyroelectric crystal, a 10 mm x 20 mm-dia. cylinder of $LiTaO_3$, is attached to a copper block with epoxy. The copper block is connected to the cold finger by means of a ground strap. Two resistors, mounted on the copper block provide the ability to heat the crystal. A Li(Si) x-ray detector, inserted into a port in the side of the outer chamber, views the crystal and target through a 0.25 mm thick beryllium window in the inner chamber wall. Monitoring of the crystal temperature is accomplished by means of a thermocouple attached to the copper block.

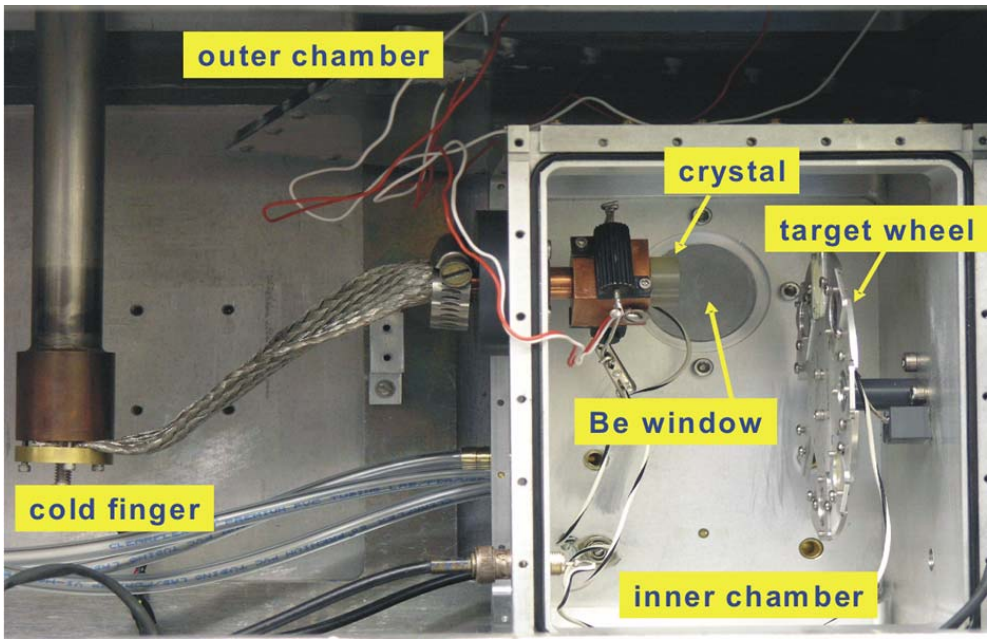

Figure 1. A photograph of the pyroelectric crystal accelerator system.

The crystal was mounted with its z − surface (which is positive during heating and negative during cooling) facing the target. The distance between the target and the crystal face was 4.0 cm. During the heating cycle, electrons from gas molecules in the inner chamber are field ionized by the strong electric field and accelerated toward the surface of the crystal. As a result, bremsstrahlung and x rays are emitted as the electrons impact the crystal surface. During the cooling cycle, the electrons are accelerated toward the target, causing bremsstrahung and x rays to be emitted from the target surface. Spectra of the radiation observed in the Si(Li) detector during a typical heating and cooling cycle are shown in Fig. 2.

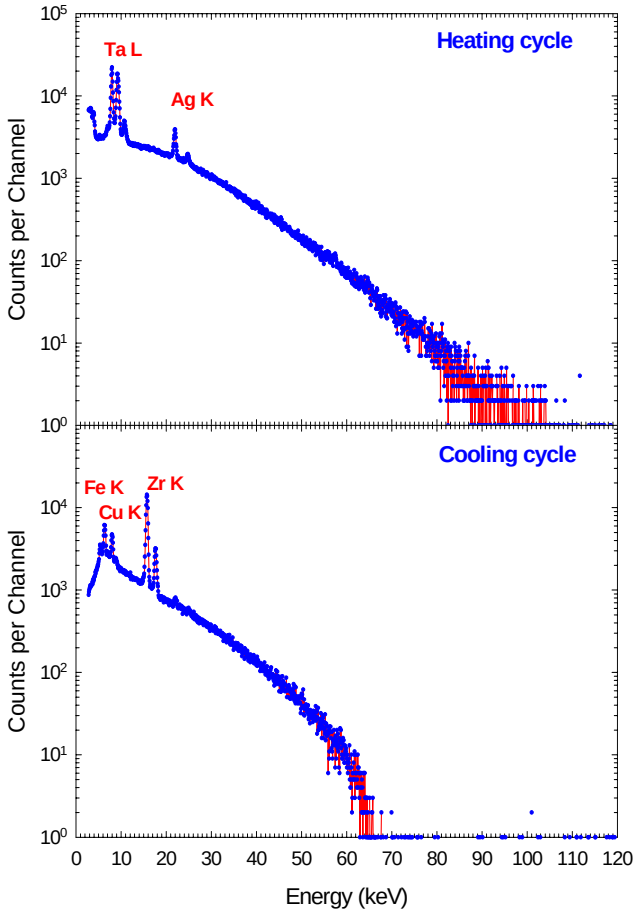

Figure 2. Spectra of radiation observed in the Si(Li) detector during a heating and cooling cycle.

The Ta L x-ray lines appearing in the heating cycle spectrum originate from tantalum atoms in the crystal, while the Ag K x rays are from a thin coating of silver on the crystal surface. The target used during this run was a zirconium foil, and hence Zr K x rays were observed during the cooling cycle. The Fe and Cu K x rays in the cooling cycle spectrum originate from the screws that held the target to the target wheel. The most prominent feature in each spectrum is the large bremsstrahlung continuum. The endpoint of a bremsstrahlung spectrum provides a measure of the electron acceleration potential created between the point of origin and the crystal surface. The above spectra indicate that the acceleration

potential during the heating cycle is approximately 100 kV, while during the cooling cycle, it is about 65 kV. The lower potential achieved in the cooling cycle may be due to the fact that the cooling rate was much slower than the heating rate.

The counting rate in the Si(Li) detector and the temperature of the Cu block are shown as a function of time in Fig. 3 for one of the runs. Typically, the count rate in the Si(Li) detector rises rapidly as the crystal is heated and soon reaches a maximum. Thereafter, it slowly decreases until the power to the resistive heaters is turned off. After the crystal begins to cool, the count rate again rises, but at a much slower rate of ascent, reaches a maximum, and then decreases very slowly. The maximum count rate obtained in any of the runs was 2.2×10^4 s^{-1} during the heating cycle. Taking into account the detector solid angle fraction and efficiency curve, the total photon emission rate (above 3.5 keV) was approximately 3.6×10^9 s^{-1}. Finally, in a run in which 5 mTorr of nitrogen was injected into the inner chamber, a current integrator connected to the target registered a positive particle current of 1 na.

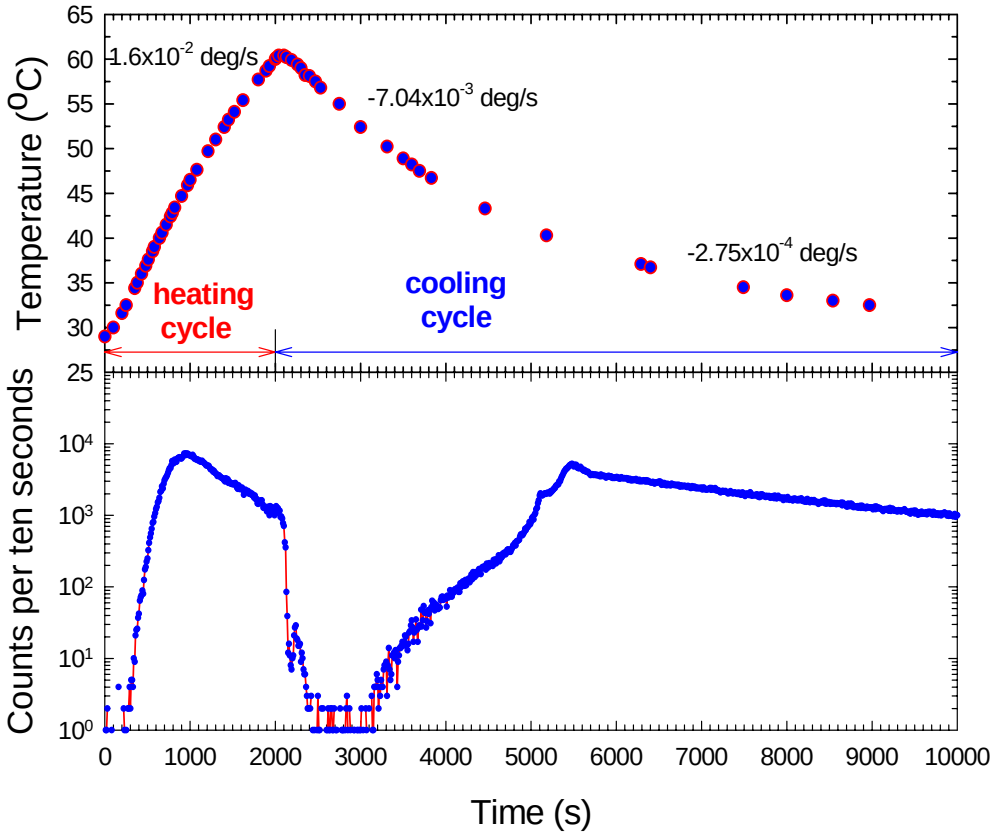

Figure 3. Counting rate in the Si(Li) detector and temperature of the Cu block as a function of time for one of the runs.

[1] B. Naranjo, J. K. Gimzewski, and S. Putterman, Nature **434**, 1115 (2005).

[2] J Geuther, Y. Danon, and F. Saglime, Phys. Rev. Lett. **96**, 054803 (2006).

Polarization of *Kα* Satellite Transitions in Potassium

K.S. Fruchey, R.L. Watson, V. Horvat, and Yong Peng

Spectra of potassium K x rays, produced by bombardment of a thick KCl target with 4.0 MeV/amu Xe ions, were measured using a high resolution curved crystal spectrometer employing a LiF crystal. The object of the experiment was to examine the polarizations of the Kα satellite transitions by utilizing a specially designed spectrometer system configuration [1] to measure spectra at angles (δ) between the beam axis and the plane of the focal circle ranging from 90° to 180°. Of particular interest were the $1s2p \rightarrow 1s^2$ He-like transitions $^3P \rightarrow {}^1S$ and $^1P \rightarrow {}^1S$. The measurements were performed in first order diffraction at δ-angle increments of 15°.

A potassium K x-ray spectrum obtained at δ = 90° is shown in Figure 1. It contains an intense doublet of diagram lines ($K\alpha_1$and $K\alpha_2$) that are produced mainly by ionizing collisions of secondary electrons and L x rays from the Xe projectiles, along with the a prominent series of satellite peaks ($K\alpha L^1$ to $K\alpha L^7$). The Kβ diagram line (which is also enhanced by the same secondary ionization processes) is visible at the high energy end of the spectrum, positioned among the low intensity Kα hypersatellites. The diagram lines provided internal energy calibration points for each spectrum. All of the spectra obtained at the various δ angles were analyzed with a peak-fitting program employing both Gaussian and Voigt functions. While both peak shape functions provided equally good representations of the spectra, it

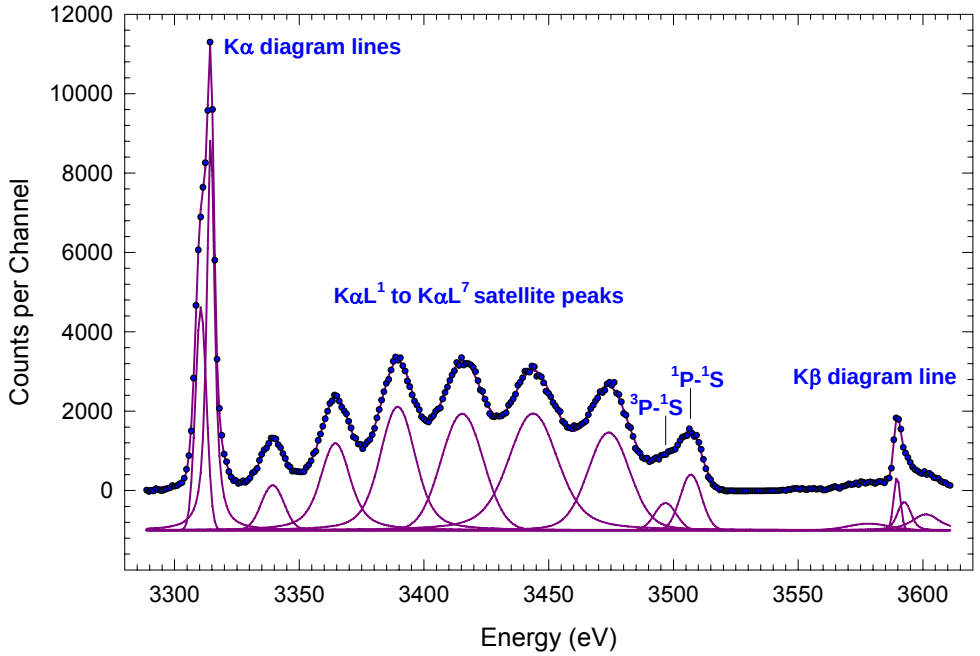

Figure 1. Spectrum showing potassium Kα and Kβ diagram lines and Kα satellite peaks excited in collisions of 4.0 MeV/amu Xe ions.

was found that the fits with Gaussians gave more consistent intensities in comparisons of multiple spectra taken at the same angle.

The polarization fraction of an x-ray line is defined as

$$P = \frac{I_{\perp} - I_{\parallel}}{I_{\perp} + I_{\parallel}}, \tag{1}$$

where $I_{\parallel}$ and $I_{\perp}$ are the x-ray intensities at 90° to the beam direction with electric vector parallel and perpendicular to the beam direction, respectively. Because the reflectivity of the LiF crystal depends on the polarization fraction of the incident x rays, it is possible to determine the polarization fraction by measuring the relative intensity of an x-ray line as a function of the angle δ between the plane of the focal circle and the beam axis. The relationship between the relative intensity at angle δ and the polarization fraction is [1]

$$\frac{I(\delta)}{I_0} = \left(1 - \frac{2P}{3-P}\right) + \left(\frac{2P}{1-P/3}\right)\cos^2(\delta). \tag{2}$$

The intensities of the satellite peaks were measured relative to the intensity of the K_α diagram peak at each angle since the latter transition is expected to be unpolarized. Linear regression analysis of the relative intensity as a function of $\cos^2\delta$ yields

$$P = \frac{m}{2 + m/3}, \tag{3}$$

where m is the slope of the regression line. The data and regression lines for the ^{3}P and ^{1}P peaks are shown in Fig. 2. The experimental polarization fractions were corrected for crystal polarization sensitivity by assuming the crystal behaved as an ideal mosaic crystal, as described in Ref. [1].

The polarization fractions obtained in this work are listed in Table I. It is evident that none of the satellite peaks displayed a significant polarization. This result is not surprising for the KαL^1 through KαL^6 peaks because the individual polarization fractions of the numerous unresolved multiplet lines contributing to each of these peaks would tend to average to zero. However, the ^{3}P and ^{1}P KαL^7 peaks are presumed to contain single lines and it is surprising that they also do not exhibit significant polarization fractions. In previous measurements of the Kα x rays emitted by 2 MeV/amu He-like sulfur projectiles, substantial polarization fractions were observed (28% for the ^{1}P–^{1}S transition and −16% for the ^{3}P–^{1}S transition) [2]. In this latter case, the ^{1}P and ^{3}P states were populated by electron capture as the projectiles emerged from the back surface of a carbon foil, whereas in the present experiments, they are populated primarily by direct Coulomb excitation of target atoms. It is possible that direct ionization of target atoms in collisions ejecting many inner shell electrons does not give rise to unequal substate

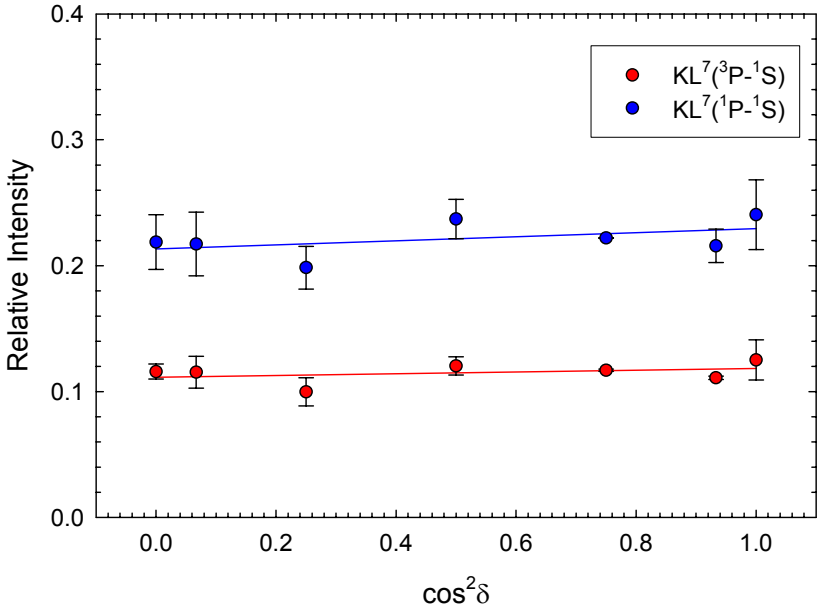

Figure 2. Angular distribution of the He-like $1s2p - 1s^2$ ($^1P - {}^1S$ and $^3P - {}^1S$) transition relative intensities.

populations. Another possibility is that the presence of outer-shell electrons causes the excited state population to be spread over a number of multiplets, thereby diluting the alignment. Furthermore, all of the observed x rays in this experiment originate from inside the target and under such conditions fast electron rearrangement transitions can modify the initial distribution of excited states before x-ray emission occurs, thereby destroying any alignment produced in the collision.

Table I. Measured polarization fractions of the Kα satellites.

Transition	Polarization fraction
$K\alpha L^1$	-1.09 ± 1.34%
$K\alpha L^2$	0.97 ± 3.17%
$K\alpha L^3$	-0.31 ± 4.28%
$K\alpha L^4$	1.72 ± 7.47%
$K\alpha L^5$	2.09 ± 6.01%
$K\alpha L^6$	3.12 ± 6.01%
$K\alpha L^7$ ($^3P-{}^1S$)	0.53 ± 0.76%
$K\alpha L^7$ ($^1P-{}^1S$)	1.35 ± 1.44%

[1]G.J. Pedrazzini, J. Palinkas, R.L. Watson, D.A. Church, and R.A. Kenefick, Nucl. Instrum. Methods **B10/11**, 904 (1985).

[2] D.A. Church, R.A. Kenefick, D.W. Wang, and R.L. Watson, Phys. Rev. A **26**, 3093 (1985).

Systematics of *Kα* X-ray Satellite Peak Widths

V. Horvat, R.L. Watson, and Y. Peng

Spectra of $K\alpha$ x rays emitted from a variety of solid targets (atomic number Z_2 = 17-32) under bombardment by fast heavy ions (atomic number Z_1 = 6-93) at 2.5-25 MeV/amu were measured in high resolution using a curved crystal spectrometer. The spectra were analyzed in order to examine the systematics of $K\alpha$ x-ray satellite structure [1]. In this report the focus is on the Gaussian widths of the satellite peaks.

Structure of the measured spectra was described in terms of a background function (a constant in most cases) and 18 peaks having Voigt profiles. The peaks represented the contributions from $K\alpha_1$ and $K\alpha_2$ diagram transitions as well as those from $K\alpha_1 L^i$ and $K\alpha_2 L^i$ satellite transitions (i = 0, 1, 2, 3, 4, 5, 6, 7). Here index i represents the number of spectator L vacancies at the time of the $K\alpha$ x-ray transition, while the number of spectator outer-shell vacancies (in the M shell or above) is unspecified.

A Voigt function is a convolution of a Gaussian function and a Lorentzian function. For the most part, the width of the Lorentzian component represents the natural transition width, which was fixed based on the literature values of level widths [2]. For a single diagram peak, the Gaussian component width of the Voigt function represents the resolution of the spectrometer. This parameter was varied in order to obtain the best fit to the diagram peaks in each measured spectrum.

Gaussian component widths of the peaks representing $K\alpha_1 L^i$ or $K\alpha_2 L^i$ satellite transitions were in most cases fitted independently from each other and from all other parameters of the fit, because each one of them is determined primarily by the distribution of a large number of unresolved transitions having a range of transition energies that contribute to the given satellite peak. The spread of transition energies is due to the coupling of electronic angular momenta before and after the x-ray emission, as well as due to the probability distribution of outer-shell vacancy configurations. For the satellite peaks that were not resolved from other peaks and represented a relatively small fraction of the satellite peak distribution, Gaussian widths could not be fitted independently. Instead, their values were estimated and held constant. However, those values were *not* included in the analysis described below.

Independently determined Gaussian component widths of the satellite peaks were grouped according to their associated numbers of spectator L vacancies (i) and the target atomic number (Z_2), regardless of the projectile atomic number and projectile energy. The data in each group were then replaced by their average value $\sigma_s(i, Z_2)$. A similar procedure was applied to the Gaussian widths of the diagram peaks. They were sorted in groups based on Z_2 and then the data in each group were replaced by their average value $\sigma_d(Z_2)$. The differences $\Delta\sigma(i, Z_2) = \sigma_s(i, Z_2) - \sigma_d(Z_2)$ are shown in Fig. 1 on the top left and top right, as a function of i and Z_2, respectively. The curves in the graphs represent the results of unconstrained linear regression applied to each individual set of data with the given values of i or Z_2. Based on the trends observed in the two graphs, it was found that $\Delta\sigma(i, Z_2)$ can be approximated by

$$\Delta\sigma(i, Z_2) = a_1\, i\, (a_2 - i)\, (Z_2 - a_3)\ , \qquad (1)$$

where a_1, a_2, and a_3, are constants. Their best-fit values were found to be

$$a_1 = 0.0246 \pm 0.0018 \qquad a_2 = 9.86 \pm 0.23 \qquad a_3 = 10.40 \pm 0.74\ . \qquad (2)$$

Figure 1 on the bottom left and bottom right illustrates how well the data points are represented by eq.(1). On the bottom left $\Delta\sigma(i, Z_2) / (Z_2 - a_3)$ is plotted as a function of i, while on the bottom right $\Delta\sigma(i, Z_2) / [i\,(a_2 - i)]$ is plotted as a function of Z_2. The data points in these graphs represent the average values of all the derived data points at the given value of the abscissa, while the error bars represent sample standard deviations.

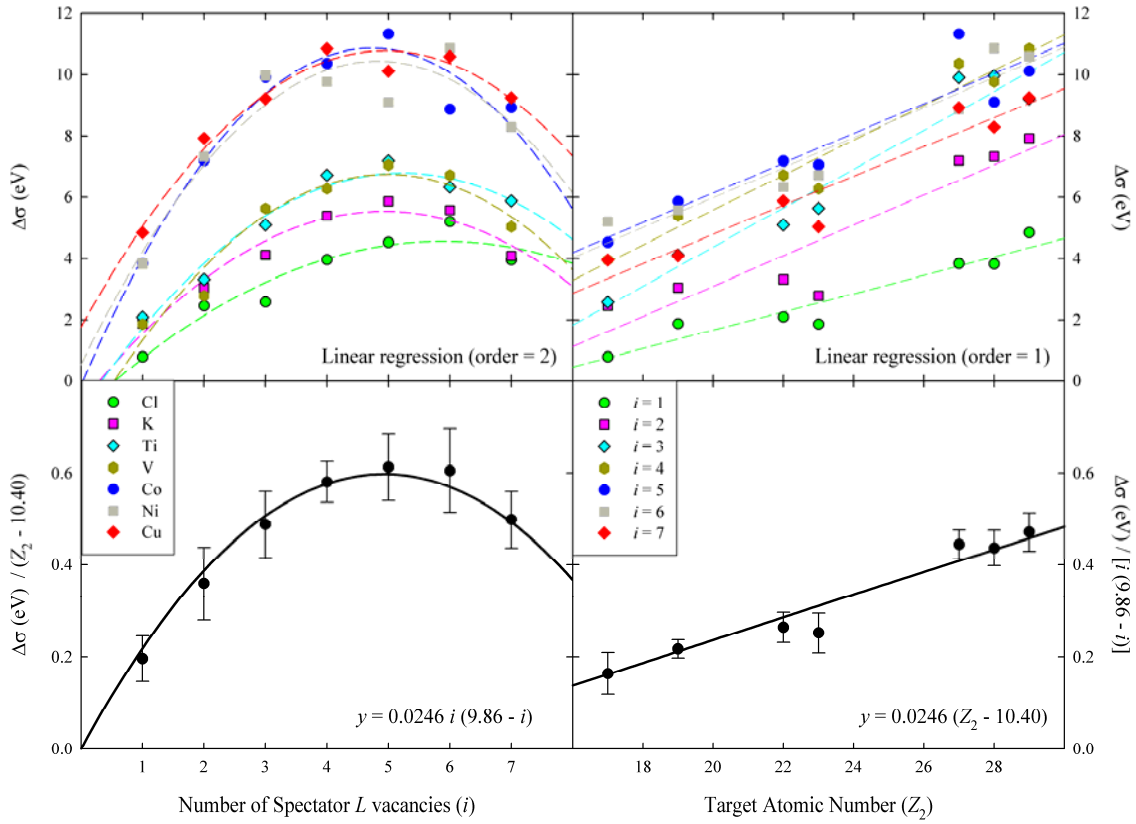

Figure 1. Systematics of the satellite peak widths.

[1] V. Horvat *et al.*, *Progress in Research*, Cyclotron Institute, Texas A&M University (2004-2005), p. IV-9.

[2] J. L. Campbell and T. Papp, At. Data Nucl. Data Tables **77**, 1 (2001).

Systematics of *Kα* X-Ray Satellite Peak Centroids

V. Horvat, R.L. Watson, and Y. Peng

Gaussian widths of the satellite peaks were the subject of a systematic analysis of the spectra of *K*α x rays, as described in the preceding report [1]. Presented here is an extension of this analysis that focuses on the systematics of the satellite peak centroids. The study was restricted to satellite peaks whose centroids were determined in a least squares fitting procedure without any constraints.

For each target, independently determined centroids of the satellite peaks were plotted as a function of their associated numbers of spectator *L* vacancies (*i*) and the apparent average number of *L* vacancies (n_L) present in the target atom at the time of *K* x-ray emission [2]. In order to reduce the error due to uncertainties in the energy calibrations, the satellite peak centroids were determined relative to the centroid of the corresponding *K*α diagram peak. In Fig. 1, the satellite shifts as a function of n_L are shown for a Cu target. The data indicate that, for a given value of *i*, the satellite shifts are linear functions of n_L.

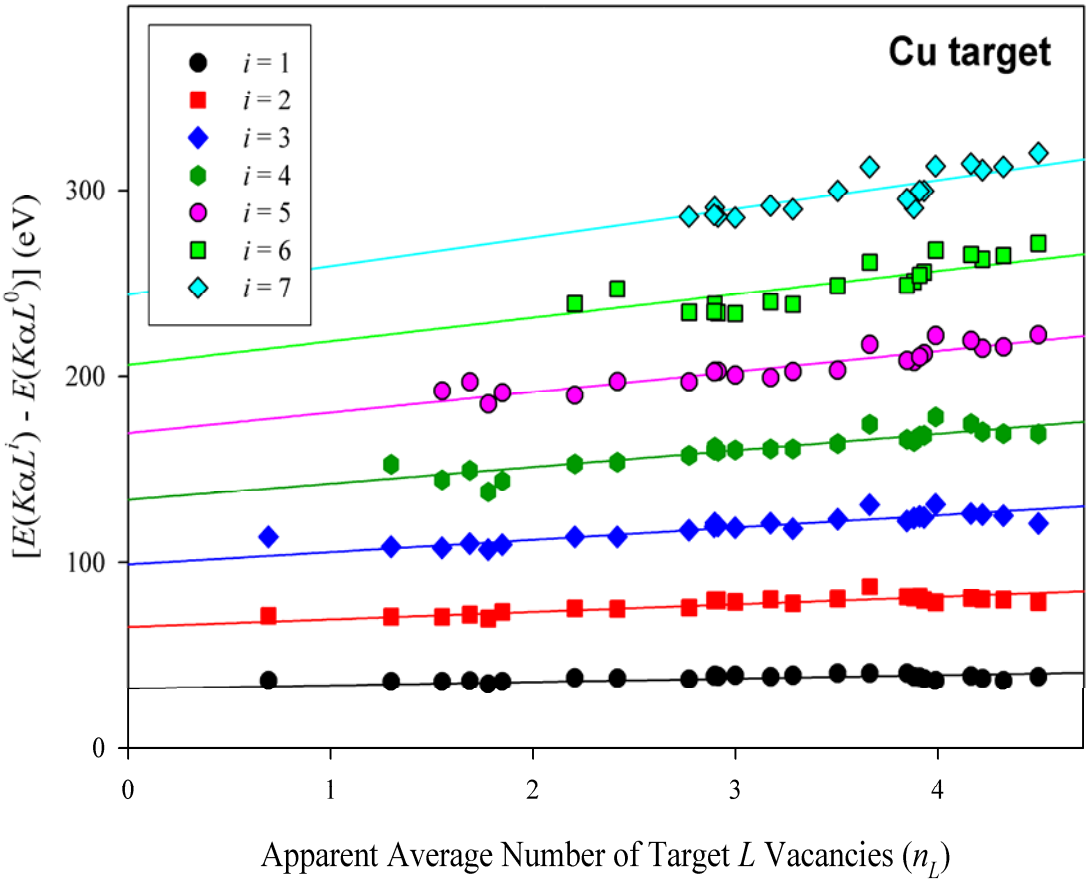

Figure 1. Cu *K*α satellite peak centroid shifts as a function of the associated number of *L* vacancies (*i*) and the apparent average number of target *L* vacancies (n_L).

As n_L approaches zero, it seems reasonable to expect that the degree of outer-shell ionization approaches to zero as well. Consequently, the satellite shifts for $n_L = 0$ can be predicted by atomic structure calculations. This was accomplished using the multiconfigurational Dirac-Fock code of Desclaux [3]. The results were then used as the ordinate intercepts of the straight lines shown in Fig. 1, while their slopes were determined from the available data using linear regression. The slope of each one of the seven straight lines in Fig. 1 can be interpreted as the excess shift ΔE^i divided by n_L, where ΔE^i is the difference between the actual shift of a $K\alpha$ satellite peak corresponding to i spectator L vacancies and its corresponding value at $n_L = 0$.

A similar analysis was also applied to the data obtained for six other targets. This resulted in a set of 49 values of $\Delta E^i / n_L$, each corresponding to a different target and a different value of i. They are plotted in Fig. 2 as a function of i and as a function of the target atomic number (Z_2).

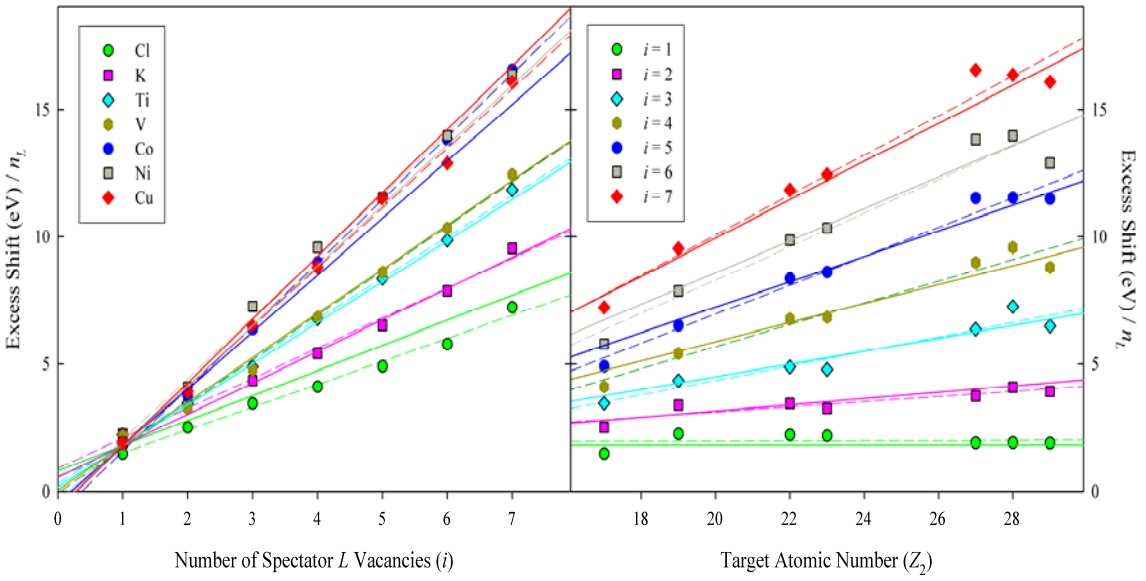

Figure 2. Excess shift of $K\alpha$ satellite peaks divided by the apparent average number of L vacancies (n_L) as a function of the associated number of spectator L vacancies (i) and the target atomic number (Z_2).

Based on the trends observed in the two graphs of Fig. 2, it was found that with reasonable accuracy $\Delta E^i / n_L$ can be parameterized as

$$\Delta E^i (Z_2) / n_L = (i - 1)\,(Z_2 - b_1) / 8 + b_2\,, \qquad (1)$$

where a_1, and b_2 are constants. Their best-fit values were found to be

$$b_1 = 9.11 \pm 0.28 \qquad b_2 = 1.79 \pm 0.12\,. \qquad (2)$$

The dashed lines in Fig. 2 represent the results of linear regression applied to each individual set of data points with the given value of i or Z_2, while the solid lines represent the predictions based on eq.(1) and eq.(2).

In summary, based on a large number of measurements and a large variety of projectile, target, and collision energy combinations, a comprehensive analysis was undertaken in order to study the systematics of the spectra of *K*α x rays. The main result is a set of semi-empirical formulas that can be used to predict the shape of the spectrum with reasonable accuracy. The apparent average number of *L* vacancies present at the time of *K* x-ray emission (n_L) can be estimated using the formula given in ref.[2]. Then, eq.(1) and eq.(2) can be used to estimate the satellite peak centroids. Finally, eq.(1) and eq.(2) of ref.[1] can be used to estimate the Gaussian widths of the satellite peaks. The remaining parameter that needs to be estimated is the instrumental resolution. Additionally, for a complete description of the structure of Kα x-ray spectra, the contributions to the diagram peaks due to secondary ionization need to be calculated. Examples of calculations were presented in ref.[4] and ref.[5]. These results are expected to apply to any collision system involving a solid target with atomic number Z_2 = 17-29, a projectile with atomic number Z_1 = 6-83, and energy between 2.5 and 25 MeV/amu.

[1] V. Horvat *et al.*, *Progress in Research*, Cyclotron Institute, Texas A&M University (2005-2006), p. IV-7.

[2] V. Horvat *et al.*, *Progress in Research*, Cyclotron Institute, Texas A&M University (2004-2005), p. IV-9.

[3] J. P. Desclaux, Comp. Phys. Commun. **9**, 31 (1975).

[4] R. L. Watson, J. M. Blackadar and V. Horvat, Phys. Rev. A **60**, 2959 (1999).

[5] V. Horvat and R. L. Watson, J. Phys. B **34**, 777 (2001).

SECTION V

SUPERCONDUCTING CYCLOTRON AND INSTRUMENTATION

K500 Operations and Development

D.P. May, G.J. Kim, H.L. Clark, F.P. Abegglen, G.J. Derrig,
R.S. Olsen and W.H. Peeler

Introduction

During the 2005-2006 reporting period a total of 50 different beams, including 19 newly developed beams, were used for experiments. There were a total of 69 beam tunings not counting multiple tunes of beams for the SEE program. The SEE program will be treated separately.

Ion Sources

The plasma chamber of ECR2 was replaced in the fall with a new chamber in the fall of 2005. The 14-year-old 14.5 GHz transmitter began to fail almost immediately as recommissioning of the source began, and the klystron was finally replaced in February. During the January shut-down period the first focusing solenoid for ECR2 was replaced with one of the two Glaser lenses that had been constructed years earlier. The Glaser resulted in a significantly more sharply focused beam at the image point and higher transmission of beam through the defining slits. Progress on the ECR2 ion source will be described in a separate contribution.

Cyclotron Beams

Of the newly developed beams, a potassium beam is of note. This element was introduced into the ECR1 ion source via the low-temperature oven using a mixture of potassium chloride and calcium. A powder of calcium was produced by filing a rod of calcium metal. The calcium was immediately mixed with the potassium chloride using a mortar and pestle, the mixture was then placed in the oven, and the oven was placed in the source. The weight ratio of calcium to potassium chloride was approximately 1/1.

Operations

For the period April 1, 2005 through March 31, 2006, the operational time is summarized in Table I, while Table II lists how the scheduled time was divided. The only major repair that caused a significant loss of time was the replacement of an rf coupler. At the same time that the rf coupler failed a small water leak developed in the water jacket of an upper dee stem. Together the repairs cost three days of beam time.

Table I. 2005-2006 Operational Time.

Time	Hrs.	%Time
Beam on target	5264.50	**69.2**
Tuning, optics, set-up	719.25	**9.5**
Beam development	538.50	**7.1**
Scheduled maint.	426.75	**5.6**
Unscheduled maint.	198.75	**2.6**
Idle time	460.25	**6.0**
Cool down	0.00	**0.0**
Total	**7608.00**	**100.0**

Table II. Scheduled Beam Time.

Time	Hrs.	%Time
Nuclear physics	1216.00	**17.9**
Nuclear chemistry	1784.50	**26.2**
Atomic physics	201.25	**3.0**
Outside collaboration	164.00	**2.4**
Outside users	2902.25	**42.6**
Beam development	538.50	**7.9**
Total	**6806.50**	**100.0**

Progress on ECR2

D.P. May, F.P. Abegglen, G.J. Derrig, and R.S. Olsen

A new aluminum plasma chamber has been designed, machined and installed in the ECR2 ion source. This replacement plasma chamber (Fig. 1) has no water-to-vacuum seals and has a different

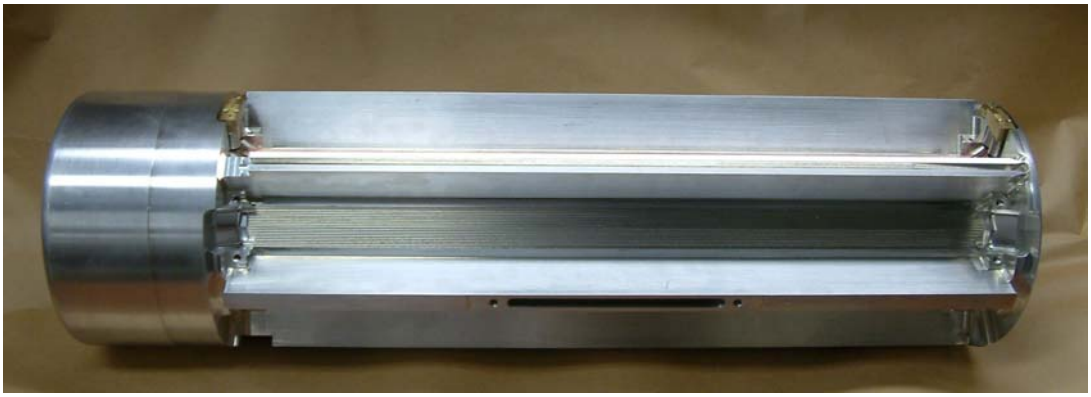

Figure 1. The newly machined plasma chamber. Grooves are machined into the bottom of the magnet channels. Three ports are machined radially between the channels.

concept for water-cooling. Figure 2 shows a cross-section through the chamber and one magnet pole. Eighteen copper tubes, each with an inner diameter of 0.7 mm and an outer diameter of 1.8 mm, lie between the aluminum of the plasma chamber wall and each of the six magnet bars. All eighteen tubes

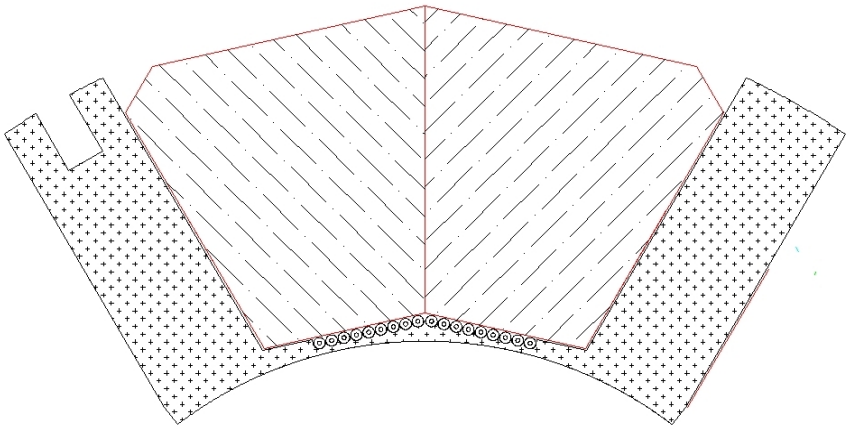

Figure 2. Cross-section through magnet channel showing the eighteen copper tubes interposed between the aluminum plasma chamber and the Nd-Fe-B bar. Each tube has an outer diameter of 1.8 mm and an inner diameter of 0.7 mm.

were soldered into a copper fitting for connection to a water fitting. The tubes were positioned into parallel grooves in the aluminum along the face of the bars (Fig. 3). They were flow tested and then potted in place using a thermal epoxy. A sheet of 0.25 mm stainless steel was positioned over the tubes and then the Nd-B-Fe bars were inserted into their channels.

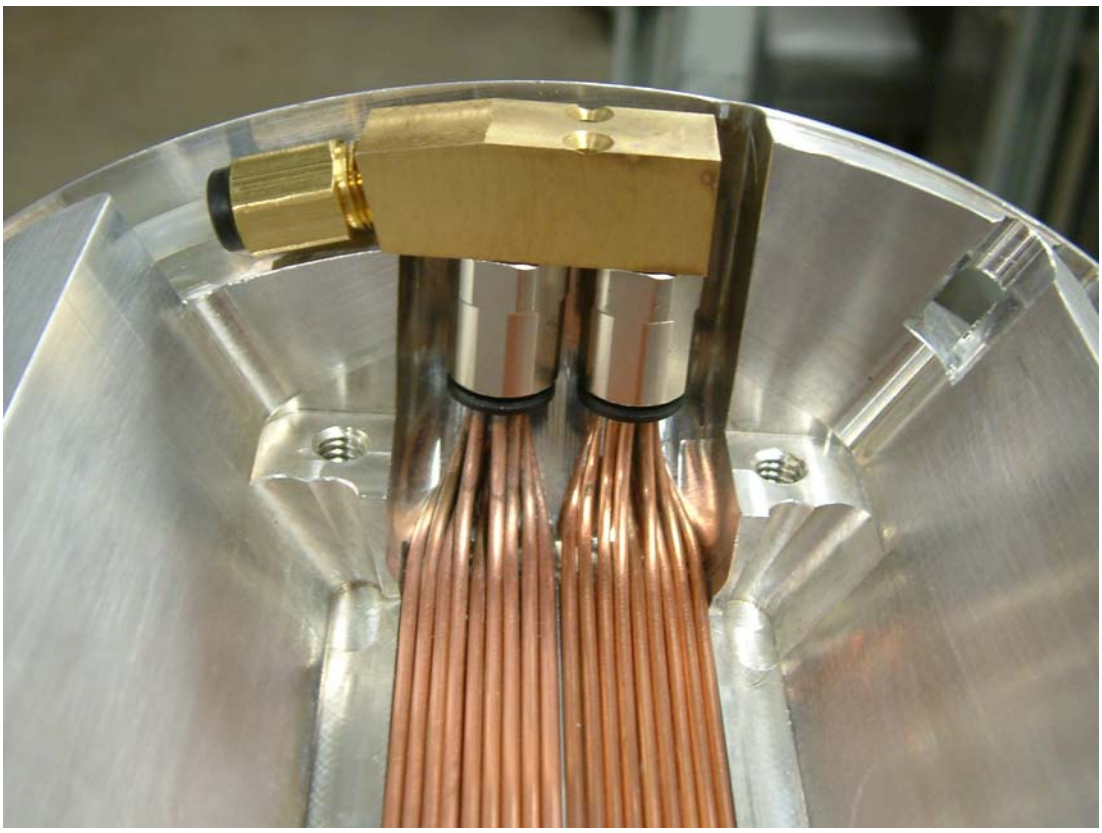

Figure 1. The copper water tubes positioned in the magnet channel with water fitting.

Before the design was finalized the concept was tested using a flat array of 18 tubes sandwiched between a thin aluminum plate and a 0.25 mm thick, stainless-steel plate. First, flow tests determined that 36 cc/sec of water would flow through the bundled tubes with a water pressure of 90 psi. Then with this flow, a 300 watt electrical strip heater was attached to the center of the aluminum plate on the side opposite to the tubes. The contact area for the heater was rectangular measuring 2.2 cm wide by 14.6 cm long. The temperature of the stainless steel directly opposite the heater was measured with water flowing as the heater power was increased. At 300 watts the temperature rise at this point was measured to be 13º C. This corresponds to small area heating of the plasma chamber using well over 1.8 kW of microwave power dissipation.

The water flow through the new plasma chamber is approximately three times the flow through the old chamber. So far the power from the 14.5 GHz microwave transmitter into the source has reached 1.5 kW on a continuous basis with no sign of excess heating to the chamber. After the installation of the new plasma chamber and Glaser lens, ECR2 has produced 239 eμA of 6+ oxygen and 131 eμA of 7+ at

10 kV extraction voltage through a 13 mm collimator onto a biased faraday cup. The microwave power level was 1.4 kW. Also at this power level the source has produced 111 eμA of $^{40}Ar^{11+}$, 50 eμA of $^{40}Ar^{12+}$ and 33 eμA of $^{84}Kr^{17+}$ (from non-isotopic gas).

Plans for the ECR2 ion source include two-frequency heating with the addition of a 11 GHz TWT transmitter capable of greater than 400 watts, the construction of a gas system making the switching between gases easier, further development of the sputtering system, and in an effort to decrease the high x-ray flux the addition of much more surrounding lead shielding.

Radiation Effects Facility

H.L. Clark, G. Chubarian, V. Horvat, B. Hyman, G. Souliotis, and G. Tabacaru

The activity of the Radiation Effects Facility (REF) increased over the previous reporting year. In this reporting period, the facility was used for 2,314 hours, which is a ~15% increase over the 2,012 hours used in the 2004-2005 reporting period. Users of the facility (and hours used) over the past year were: NASA GSFC (332.75), Boeing Satellite Systems (317.25), NAVSEA (299.5), NASA JPL (240.75), Aeroflex (167.75), Xilinx (156.25), International Rectifier (143.75), Lockheed Martin (130), BAE Systems (75), Prairie View A&M University (59), ATK-Mission Research Corp. (45), General Dynamics (44.75), Sandia National Lab (44), Raytheon (43.5), Maxwell Technologies (37.5), Peregrine Semiconductor (30), TRAD (28.25), Northrop Grumman (26), NASA JSC (24), Harris (20), Honeywell (18.25), Sun Tronics (15.75) and Boeing Seattle (15). Peregrine Semiconductor, TRAD and Sun Tronics were new customers of the facility.

Table I compares the facility usage by commercial and government customers. The ratio from this reporting year (57% to 43%) is similar to the trend seen in previous reporting periods and commercial hours still dominate. However while the number of commercial hours remained about the same, the number of government hours increased by ~400 hours or 69% over 2004-2005. Much of the testing conducted at the facility has been for defense systems by both government and commercial agencies. It is expected that the facility will continue to be as active in future years.

Table I. Radiation Effects Facility usage by commercial and government customers for this and previous reporting years.

Reporting Year	Total Hours	Commercial Hours (%)	Government Hours (%)
2005-2006	2,314	1,314 (57%)	1000 (43%)
2004-2005	2,012	1,421 (71%)	591 (29%)
2003-2004	1,474	785 (53%)	689 (47%)
2002-2003	1,851	1,242 (67%)	609 (33%)
2001-2002	1,327	757 (57%)	570 (43%)
2000-2001	1,500	941 (63%)	559 (37%)
1999-2000	548	418 (76%)	131 (24%)
1998-1999	389	171 (44%)	218 (56%)
1997-1998	434	210 (48%)	224 (52%)
1996-1997	560	276 (49%)	284 (51%)
1995-1996	141	58 (41%)	83 (59%)

Table II lists the beams used this year and the number of times each was requested. In total, 511 beams were run this year which is 28% more than the previous year. 15 and 25 MeV/u Kr and Xe were most utilized as well as 15 MeV/u Au. No new beams were added to SEELine users list.

Table II. Beams used and the number of times requested for this reporting year and previous years. 511 beams were run this year.

Particle Type	A MeV	Requests 2000-01	Requests 2001-02	Requests 2002-03	Requests 2003-04	Requests 2004-05	Requests 2005-06
^{20}Ne	15	1	13	19	15	23	36
^{40}Ar	“	4	24	43	46	51	56
^{63}Cu	“	N/A	N/A	5	14	22	23
^{84}Kr	“	6	26	55	47	49	75
^{109}Ag	“	N/A	N/A	6	18	15	26
^{129}Xe	“	5	18	43	51	50	78
^{141}Pr	“	N/A	N/A	2	2	1	4
^{165}Ho	“	3	11	17	7	8	22
^{181}Ta	“	4	5	4	3	5	3
^{197}Au	“	12	9	23	34	34	46
^{22}Ne	25	27	13	19	6	15	21
^{40}Ar	“	31	20	32	16	25	31
^{84}Kr	“	32	20	35	26	33	40
^{129}Xe	“	25	18	24	15	25	34
H-D	40	1	8	10	4	7	4
^{20}Ne	“	5	3	5	6	11	2
^{40}Ar	“	12	8	10	7	13	7
^{78}Kr	“	13	9	6	5	10	3
Total		192	207	360	324	399	511

Radiation Effects Facility Beam Line Relocation

B. Hyman, G. Chubarian, H. L. Clark, V. Horvat, G. Souliotis, and G. Tabacaru

As necessitated by the Cyclotron Institute Upgrade Project, the Radiation Effects Facility beam line has been moved from its original location in the 88”-cyclotron vault to its new location in cave 1. This move was conducted over a period of five weeks beginning the first week of January 2006. After a brief beam development period, the relocated facility served its first outside users on February 8, 2006.

Several task where completed prior to the beam line relocation and the actual move was carried out during the Cyclotron Institute’s annual maintenance period in order to minimize the down time of the Radiation Effects Facility. Two equipment lifts were installed in December of 2004; one located at the southwest end of the high bay and another in cave 1. A staircase for user access to cave 1 was also fabricated. New roof planks and walls for a radiation shielding maze were also installed. A pre-fabricated office was ordered and assembled to serve as a data room for users. This data room allows for a climate and noise controlled environment. Two cable conduits, 4” in diameter, were drilled through the roof planks up to the newly constructed data room to provide the shortest distance possible for user cabling needs. A setup area was created just outside of the data room by constructing a plywood floor on top of the existing roof planks. A three dimensional rendering of the data room and setup area is shown in figure 1. Cabling for items such as detector signals, detector high voltage, video cameras and a new intercom system were also put in place prior to the beam line relocation.

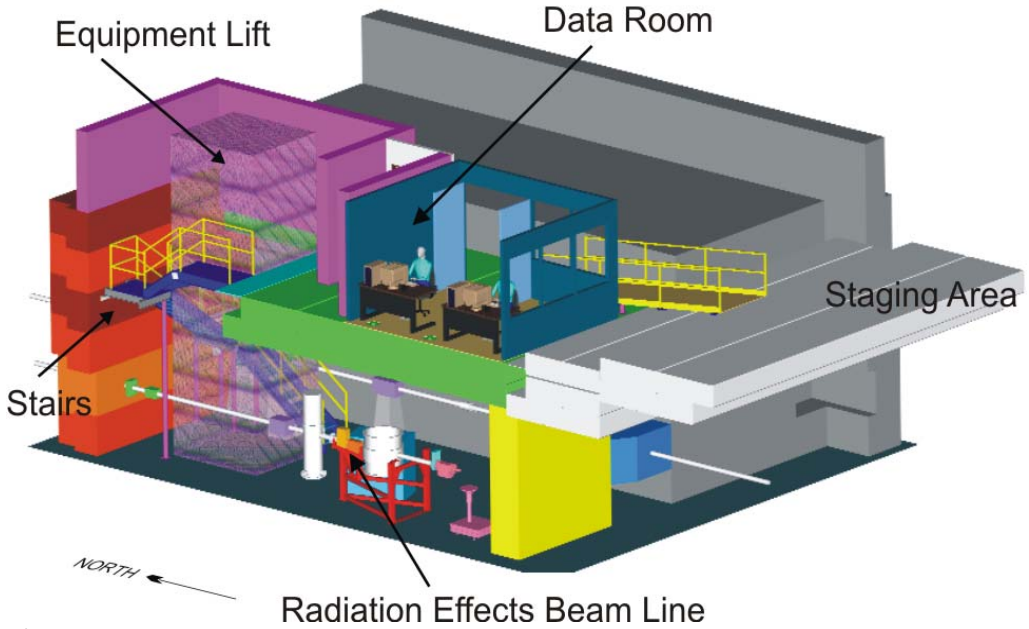

Figure 1. Three dimensional rendering of the Radiation Effects Facility relocation.

All beam line components including the Ortec chamber, degrader chamber, and the in-air station were first disassembled in the original 88”-vault location. This allowed for several vacuum system components to be replaced and some much needed general cleaning. Next, the beam line components were moved to cave 1 where they were aligned and reinstalled with minimal problems (figure 2). All beam line electronics, including CAMAC and NIM modules, the positioning system control unit, and the user interface computer were relocated to the PSP counting room.

Operations have run smoothly during the first two months of use. User feedback has been overall positive. Minor suggestions for improvements have been made and have been implemented when feasible.

Figure 2. Radiation Effects Facility beam line relocated to cave 1.

Radiation Effects Testing Facility Control Software

V. Horvat

DOS-based version of the Radiation Effects Testing Facility control software (program Seuss) has been upgraded. The new version (program SeussW) is designed as a Microsoft Windows™ application. Although SeussW has the graphical users interface (GUI) typical of the Windows-based applications, it retains all the functionality of the previous version, so that the users familiar with Windows operating system and the old Seuss should have no trouble adjusting to the new software. The goal was to make SeussW as easy to use as possible. This was accomplished by putting all the controls on the screen, rather than having them "hidden" as menu items. Also, all the buttons and edit boxes are labeled in plain English and those that are not available in the given context are disabled or hidden. Furthermore, user controls are separated from the controls intended for use by the authorized Cyclotron Institute personnel. Guidance via pop-up message boxes and status bar messages is provided for the procedures that require more than a single step. The need to use the keyboard was minimized, so that most of the features can be activated using the mouse.

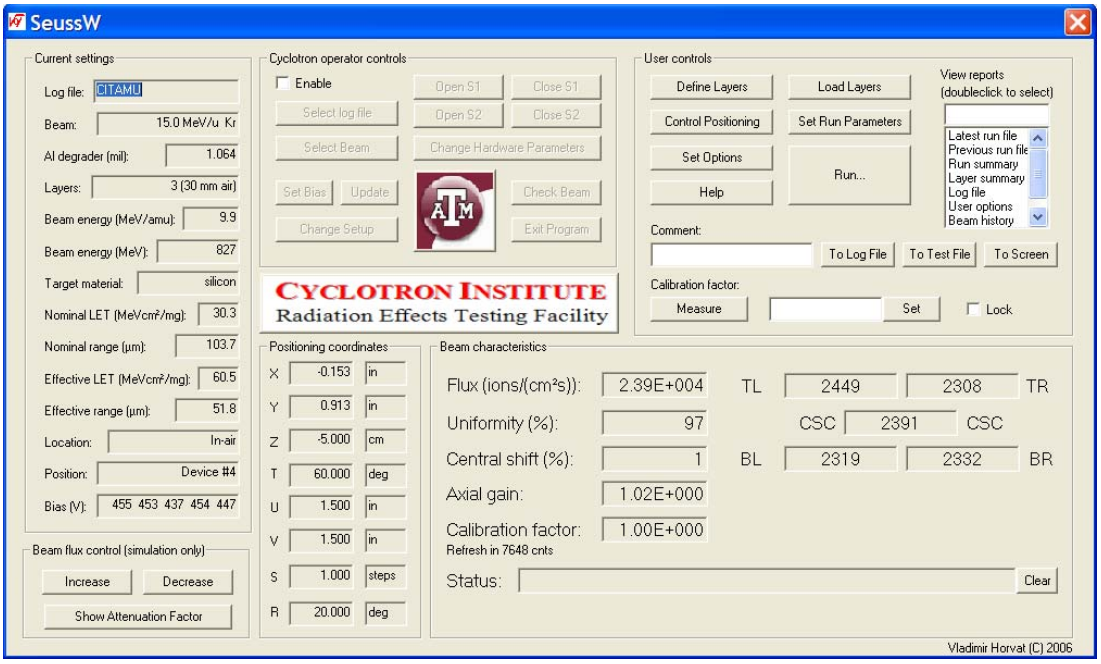

Figure 1. The screen snapshot of the new version of program SeussW

SeussW is designed to control the hardware present at the Radiation Effects Testing Facility. However, if a required hardware component is not detected, the program runs a simulation. This feature enables the users to become familiar with the software before arriving to the site. The files necessary to run the control software using simulated data are distributed in an archive that can be downloaded from

http://cyclotron.tamu.edu/vladimir/SeussW.zip

Under Windows XP™, the files can be extracted from the archive using Windows Explorer™. Generally, SeussW should run on any Windows operating system. However, the use of Windows XP™ is recommended.

The screen snapshot above in Figure 1 shows the main application window. Other windows pop up when certain features are selected. Currently, there are 14 separate program units performing various tasks ranging from file management and hardware control to data acquisition and ion energy loss calculations. As an example, the window containing positioning controls is shown below in Figure 2.

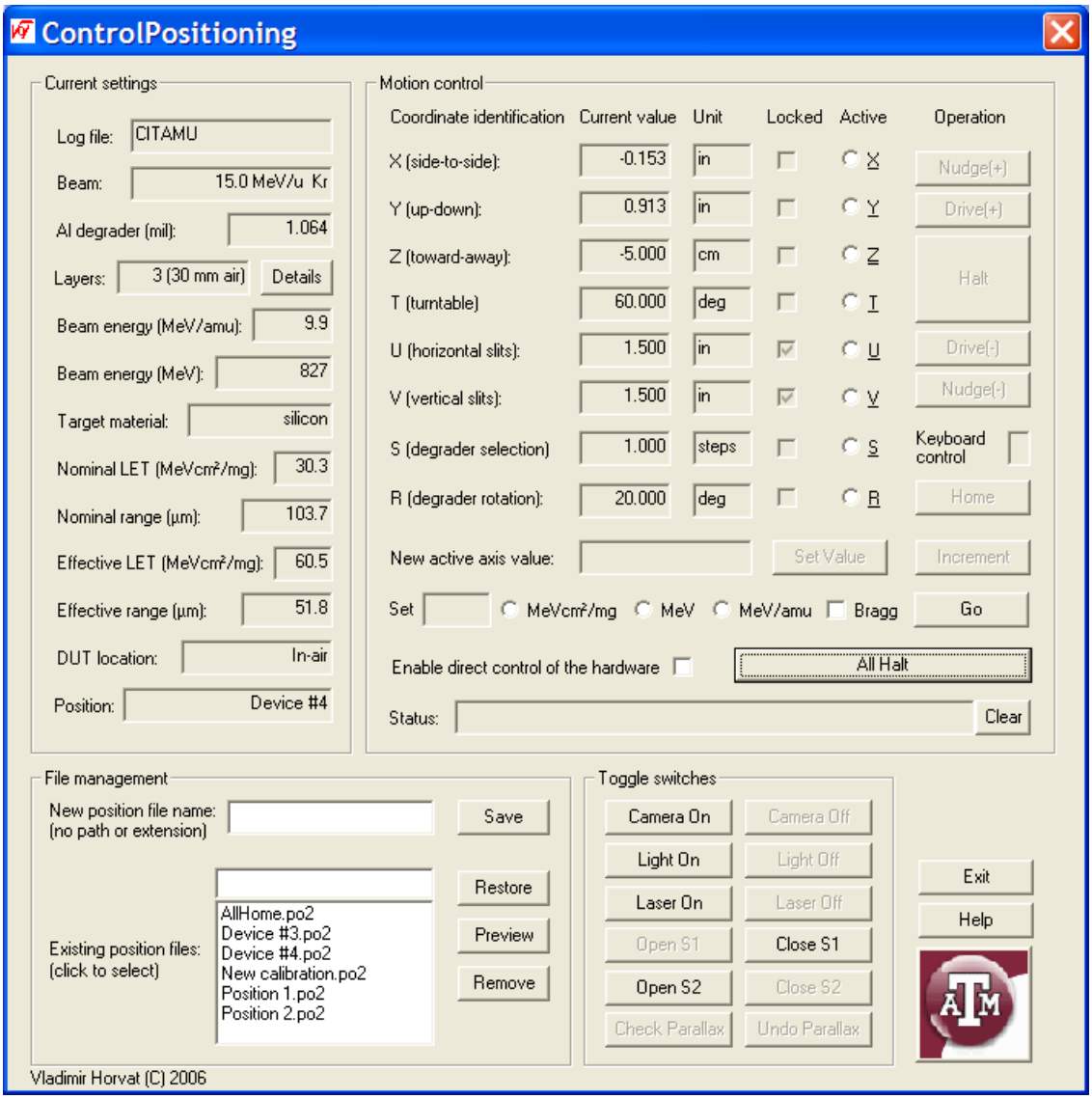

Figure 2. The window containing positioning controls in program SeussW

Cyclotron Computing

R. Burch, K. Hagel, and T. Materna

This past year, we finished the evaluation of SL (Scientific Linux) as our principle operating system for lab's analysis and administrative servers [1]. "SL is a Linux release put together by Fermilab, CERN, and various other labs and universities around the world. Its primary purpose is to reduce duplicated effort of the labs, and to have a common install base for the various experimenters. The base SL distribution is basically [Redhat] Enterprise Linux, recompiled from source [2]. SL uniquely fits our lab's mission as a nuclear research institute. It has proved to be robust and simple to install and maintain, and it contains the applications, preconfigured, that enable and enhance the lab's ability to execute its mission. Based on our evaluation, we chose the SL 4 distribution that utilizes the newer 2.6 kernel. We have since upgraded all the general lab analysis servers to SL 4, upgraded sjygroup's analysis servers to SL 4 and intergrated retgroup's analysis servers into the lab's analysis farm. Here SL 3.0.5 was chosen to maintain required compatibility with STAR system computers, as requested.

We have since rebuilt our fileserver, migrating it from Fermi Linux 3.0.1 [1] to SL 4. After the migration and nfs optimization, we find that data throughput is limited by network bandwidth: 100Mega Bit at each analysis server, 1 Giga Bit at the fileserver. In order to keep abreast of the lab's ever growing need for storage, we added a Dell PowerVault SCSI enclosure, added 750 Giga bytes of disk space for general lab data usage. We added 1 Tera byte (500 Giga bytes reserved) for sjygroup and 500 Giga bytes for snapshot backups of critical directories both using SATA drives and an external SATA enclosure. We are experimenting with SATA drives which are cheaper considerably than SCSI drives. Total disk storage mounted on the fileserver has reached 14 disks totaling 2.7 Tera bytes of capacity.

The new SL 4 based mail server [1] has been in production since November. It is very successful at its task, currently delivering between 2500-3500 email daily while it correctly tags and "defangs" between 5-20 viruses (Phishing attempts mostly) daily and tags between 100-150 messages as ***SPAM*** daily. The SL 4based WebMail application we integrated also allows user to change their password without administrator intervention, which they must now do every 90 days in accordance with university policy.

We added 8 new high performance analysis servers to the lab's analysis farm: totaling 10 for general lab use, 5 dedicated to sjygroup, and 3 dedicated to retgroup. Condor [3], a load balancing job submission system was integrated to the analysis farm. It enables the submission of a large number of jobs to a central server which then migrates the jobs to other analysis servers based on resource availability, priority, and ownership.

[1] R. Burch and K. Hagel, *Progress in Research*, Cyclotron Institute, Texas A&M University (2004-2005), p.V-5.

[2] https://www.scientificlinux.org/

[3] http://www.cs.wisc.edu/condor

Cyclotron Institute Upgrade Project

H.L. Clark

On January 3, 2005 the Cyclotron Institute Upgrade Project (CIUP) began with the approval of the CIUP management plan by the Department of Energy Nuclear Physics Office. The project will extend to the first quarter of calendar year 2011. When completed, the upgraded facility will provide high-quality re-accelerated secondary beams in a unique energy range in the world. Funding for the upgrade comes from several sources: the Department of Energy, matching support from TAMU, the Robert A. Welch Foundation and beam time sales for testing electronics components at the Cyclotron Institute.

The CIUP is divided into three major tasks: (1) Re-commission the existing K150 (88") cyclotron and refurbish beam lines; (2) Construct light-ion and heavy-ion guides and produce 1+ radioactive ions; (3) Transport and charge boost radioactive ions and accelerate in the K500 cyclotron.

Most of the effort during this reporting period focused on Task 1, restoring the K150 cyclotron major equipment. This included design, procurement and installation of the K150 high vacuum system and equipment, procurement and installation of K150 electrical and LCW utilities, assembly of K150 RF system, installation of K150 coil power supplies, design and procurement of K150 ECR & injection line materials, procurement and assembly of K150 beam line equipment. Progress was also made on Tasks 2 and 3. This included assembly and testing of the light ion guide chambers, flanges and support structures, procurement of the light ion guide vacuum equipment, development of the ion guide beam dump by utilizing complex radiation transmission computer codes, development of heavy ion guide gas cell system and compiling the list of major equipment that will be needed to complete the CB ECR ion source provided by a DOE Small Business Innovative Research (SBIR) project. Below is a description of the progress made. Figure 1 illustrates the project schedule and major milestones.

TASK 1:

1) **K150 Cyclotron Vacuum System:** The design calls for vacuum equipment to be installed on the two main sections of the vacuum space (resonator tank and dee tank) as follows: The resonator tank will be equipped with one new 35" diffusion pump with a modern cryogenic baffle system and one new roots blower package (initial system). The initial system will provide a vacuum pressure of $5x10^{-6}$ torr for testing the RF System, identifying any major leaks and producing first beams. The dee tank will be equipped with one internal liquid nitrogen cryogenic panel and four external cryopumps (high vacuum system). The high vacuum system will provide a vacuum pressure of low 10^{-7} torr for beams later in the project.

   All pieces of the initial system have been procured. The bid for the 35" diffusion pump was awarded to Varian in July and was delivered to the cyclotron in late September 2005. The bid for the roots blower package was awarded to Aerzen and the equipment was delivered in late November 2005. The bid for the 35" diffusion pump cryogenic baffle system was awarded to Connecticut Vacuum Products Inc and was delivered in late December 2005. Upon inspection it was found that the baffle piece was damaged during delivery from the factory to the cyclotron. In an agreement

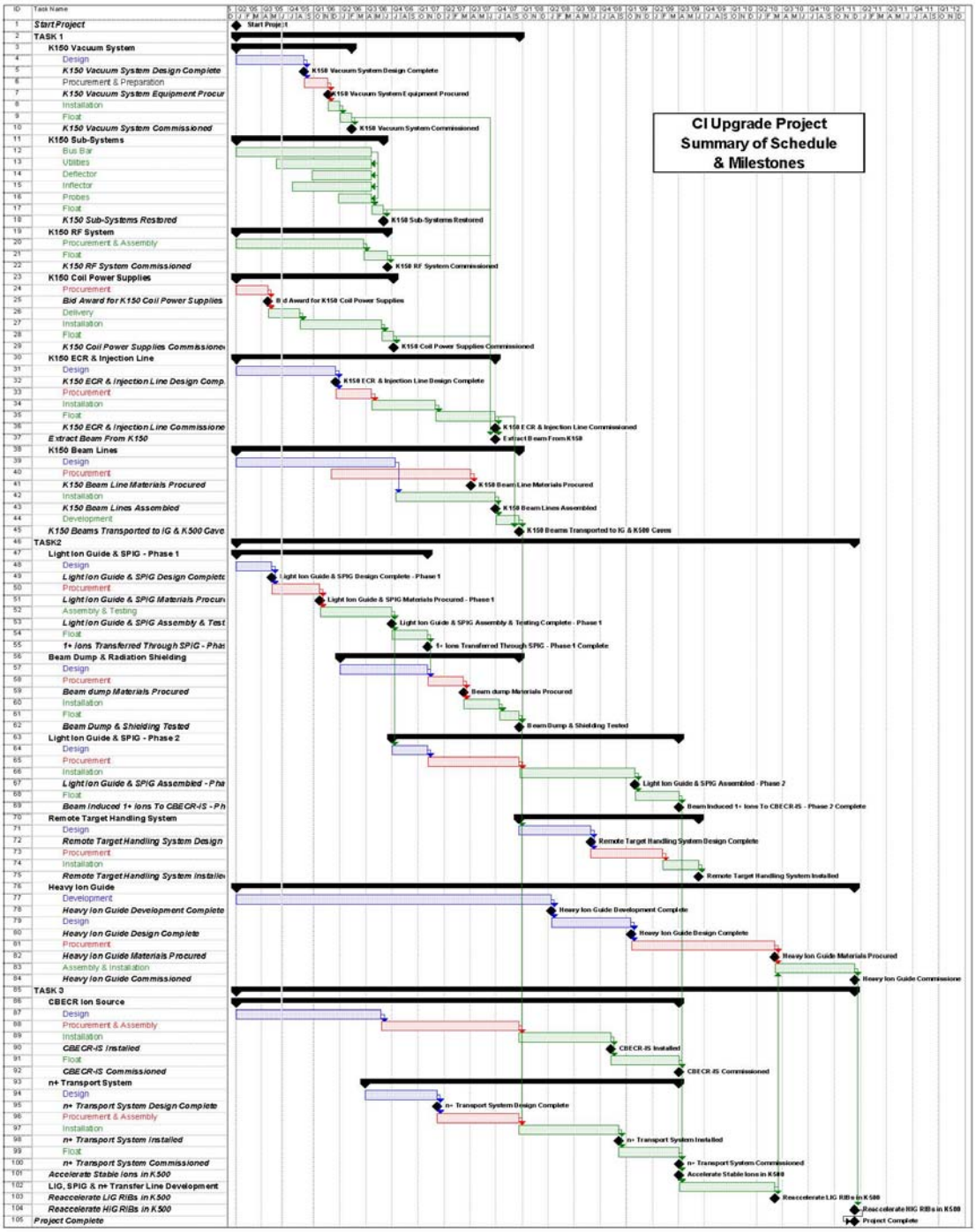

Figure 1. The project schedule and major milestones.

between the shipping company, Connecticut Vacuum and the Cyclotron Institute the baffle piece was sent back to the factory for repairs. The repaired baffle was returned to the Cyclotron Institute in early March 2006 which has subsequently delayed installation and commissioning of the initial vacuum system.

The roots blower system, the baffle system and the 35" diffusion pump are set in place on the cyclotron. Cyclotron engineering configured a lift system to safely remove the original baffle and install the new baffle and diffusion pump. Before the baffle and diffusion pump were installed, the large 35" gate valve was tested and found to operate properly and to be leak tight. Engineering also found that in the open position, the valve o-rings can be easily removed and replaced. The electrical and cooling water hook ups to these systems have been installed. The 12" diameter vacuum pipe/valve work between the roots blower system and cyclotron gate valve is nearly complete. It is anticipated that the initial vacuum system will be operational in late June 2006.

The pieces of the high vacuum system are currently being procured. The bid for the external cryopump system (four pumps, two compressors and helium transfer lines) was awarded to Austin Scientific in March 2006. The bid for the high vacuum isolation valves was awarded to VAT Inc. also in March 2006. The pumps and valves are scheduled to arrive in May 2006. The bid request for the liquid nitrogen transfer and dewar system is being prepared. This system will be used to feed liquid nitrogen to both the internal cryopanel of the cyclotron and the cryopanel system of the vertical injection line. A list of materials needed for the internal liquid nitrogen cryogenic panel is being compiled. Three sets of valves and external cryopumps will be installed along with the initial vacuum system; however the fourth set and the internal cryopanel will installed after the cyclotron is made operational.

2) **K150 Cyclotron Buss Bar Work:** Most of the original buss bar that connected the power supplies to the K150 cyclotron was salvaged for the K500 cyclotron project and needs to be replaced. As each coil power supply is set in place, final buss bar sections are cut, bent and insulated. After each supply passes inspection, the final buss bar sections are soldered into place. Final buss bar sections have been installed for twenty two of twenty three coil power supplies. It appears that buss bar installation will be complete in June 2006.

3) **Upgrade Project Utilities:** The bid for the building power improvement (to add electrical power capacity for the K150 cyclotron, K150 power supplies, K150 RF system, K150 beam lines, ion guides, etc.) was awarded to Britt Rice which is the same contractor that installed the electrical utility equipment for the K500 project. The transformer, motor controls, switch gear and building feed equipment were installed in November and December 2005. The "tie-in" of the transformer to the cyclotron building occurred in January 2006 during the K500 maintenance period. Currently, the K500 cyclotron, its equipment and beam lines and the Cyclotron Institute building are drawing electrical power from the new transformer. The original building transformer and its switch gear will power the K150 cyclotron and all of its associated equipment.

Construction of the new LCW loop (to add cooling water capacity for the K150 cyclotron, K150 power supplies, K150 RF system, K150 beam lines, ion guides, etc.) is in continuation. More than half of the system has been installed. All of the pipes, connectors, valves, pumps and control gear

have been procured. The bids for the large surge tank and demineralizer system have been awarded and these systems are currently being transported to the cyclotron. It is planned to "tie-in" the new LCW loop in fall of 2006.

A list of electrical and LCW utility items needed to restore the K150 cyclotron has been compiled and most of the electrical and LCW items have been procured. Items will continue to be procured over the next reporting period. Utility items include electrical wire, conduit, breaker boxes, cabinets, flow switches, flow indicators, strainers, valves and pipe. LCW plumbing and electrical restoration to cool the interior of the cyclotron (cooling lines to the rf panels, deflectors, etc…) is nearly complete.

4) **K150 Cyclotron Deflector:** The bid for two new deflector power supplies was awarded to Spellman in February 2006 and delivery is expected in May 2006. The trolley system used to remove the K150 deflector assembly has been restored. It is anticipated that the deflector assembly will be pulled from the cyclotron in April 2006 and the deflector and its controls can be cleaned and tested for proper operation.
5) **K150 Cyclotron Inflector:** The original K150 cyclotron "mirror" inflector was pulled from the machine, cleaned and tested. The mirror inflector will be used at initial start up of K150 cyclotron. A spiral inflector will be designed during the vertical injection design stage.
6) **K150 Cyclotron RF System:** All major components of the RF system have been procured including the filament power supply (plus a spare). Assembly is ongoing and it is anticipated that the RF system will be operational in early spring 2006 as planned.
7) **K150 Cyclotron Coil Power Supplies:** Twenty-two of twenty-three power supplies have arrived. Each supply has been tested for proper operation and control. All twenty-two supplies have been set in place in the K150 pit vault. Wiring, plumbing and buss bar hook ups are nearly complete. The last supply to arrive is the large main coil supply. The original "Ling" main coil supply is currently still in place and in addition is currently used to power the MDM spectrometer and the MARS velocity filter. This supply is very large and heavy and cannot be removed all in one piece, so it will be cut up and removed from the K150 cyclotron pit vault in several sections. Additionally, the MDM and MARS spectrometers will be powered by a new supply that was purchased in 2005. This supply is located in the sub-basement and is nearly ready for connection to the two spectrometers. It is anticipated that the remaining supply will be delivered and installed in June 2006.
8) **K150 ECR & Injection Line:** The design for the injection line was determined by closely following the design of the Berkeley AECRU – to – 88'' cyclotron injection line and incorporating the existing elements from our ECR2 injection line. To obtain the highest transmission efficiency possible, two additional focusing elements (Glaser lenses) and two additional sets of steering magnets will need to be procured. Power supplies and control equipment for these additional elements will be procured as well. Vacuum pressure in the low 10^{-7} torr will be obtained along the vertical injection line and into the inflector region with an internal liquid nitrogen cryopanel. A materials list for the additional magnets and the cryopanel system has been prepared and some items have already been procured. Materials for the vertical support structure and the new cyclotron center plug are being procured. Construction and installation of the injection line will begin in April 2006.

ECR2 was fit with a new plasma chamber and was put back online in November 2005. Beams created from ECR2 were accelerated in the K500 cyclotron in December 2005. As described in the CI Upgrade Management Plan, ECR2 will be the ion source for the K150 cyclotron.

9) **K150 Beam Line:** Plans for the vacuum chambers of the switching magnets are being drafted. A materials list for the entire beam line is being compiled and includes electrical utility, LCW utility, beam boxes, vacuum equipment, valves and shield wall plugs. A list of magnet power supplies and switch gear is also being compiled. Most materials needed to fabricate the quadrupole magnets, x-y magnets and their support structures have been procured, including insulated copper wire for the magnet coils. The insulated copper wire was delivered in March 2006. All magnets, support structures and beam boxes will be built by cyclotron personnel. All pole and yoke pieces have been machined and winding of eight complete quadrupole magnet coils has been completed using surplus copper wire. Two quadrupole magnets made entirely from surplus materials have been completed. Ten existing quadrupole magnets have been completely refurbished and are ready for installation. All pieces for x-y magnets have been machined and are ready for assembly. Stands for x-y magnets, quadrupole magnets and beam boxes have been constructed.
10) **K150 Control System:** A new *standard* for the K150 cyclotron project has been developed. The new system was developed since the equipment of the current K500 control system is being phased out by industry. A prototype unit using a "Rabbit" brand control card was developed and thoroughly tested by incorporating it into the existing K500 control system and was found to operate the K500 equipment properly. The prototype was also configured to control the new coil power supplies of the K150 cyclotron and was found to operate this equipment properly as well. Mass production of the new control equipment is currently under way. This new system is both simpler in design and much less expensive compared to the existing K500 control system.

TASK 2:

1) **Light Ion Guide:** Materials for the ion guide chambers, support structure, chamber flanges and gas control system equipment have been procured. The bid for the oil-free Roots1 and Roots2 systems was awarded to Pfieffer Vacuum Inc. in January 2006. The systems have been fabricated and are currently being tested for proper performance and operation at the Pfieffer factory. It is anticipated that the systems will arrive in April 2006.

   Both large ion guide chambers have been constructed, cleaned and vacuum tested. All flanges and connection pieces have been machined and tested. The support structures for the ion guide chambers have been constructed and are ready for installation in the ion guide cave. The internal spark discharge chamber has been fabricated. The electrical switch gear needed to power the roots systems and ion guide equipment has been installed. The ion guide cave is currently being cleaned and prepared for the roots systems and installation of the Phase 1 system. It is anticipated that the phase 1 system will be operational by June 2006.
2) **Beam Dump and Radiation Shielding:** Computer codes that model radiation transmission through various materials and system configurations have been procured. These codes (PHITS, MORITZ and MCNPX) have been installed on our computers and are being used to design the beam dump in the ion guide cave. Dr. Reg Ronningen (Senior Physicist & Radiation Safety Officer) from the NSCL

has agreed to help us with our design and has provided us additional software for studying the system. Dr. Ronningen will visit the Cyclotron Institute in May 2006. Before proceeding with construction, the CI will set up a review panel made from outside experts to study the design.

3) **Heavy Ion Guide:** The collaboration with the ANL gas cell group is in continuation. It is anticipated that the Cyclotron Institute will participate with future testing at ANL and GSI. The front-end separator design work is in progress with the Big-Sol spectrometer at the Cyclotron Institute.

TASK 3:

1) **CBECR Ion Source:** SBIR Phase 2 funding was awarded to Wayne Cornelius to build a CBECR-IS. The SBIR project schedule has been determined to be 18 months, starting in October 2005 with a delivery in March 2007. It has been estimated that ~half of major equipment will need to be supplied by the CI to complete the CBECR IS. This will include turbo pump systems, coil power supplies, microwave transmitters and control equipment. A memorandum of understanding is being drafted by the DOE SBIR Office and will state that the CBECR-IS will be delivered and tested at the Texas A&M Cyclotron Institute. Winding of the CBECR-IS magnetic coils will be underway soon and is reported to be on schedule for completion.

Shielding Evaluation for the Beam Dump Design for the Light Ion Guide Facility

G. Tabacaru and H.L. Clark

In the Cyclotron Institute Upgrade Project [1], one of the key devices in the production of the Radioactive Ion Beams (RIB) will be the Light Ion Guide (LIG). This device produces and extracts radioactive ions using the helium gas technique. The technique is based on slowing down ions in helium gas which leaves them as 1^+ ions and on the differential pressure between the reaction place and the extraction chamber. The radioactive ions are guided through a long sextupole into a second chamber where low vacuum should be achieved.

In order to obtain a substantial amount of radioactive ions from the LIG, the primary beam delivered by the upgraded K150 Cyclotron should be very intense, tens of μA's. The first test/commissioning reaction will be $^{27}Al(p,n)^{27}Si$ at 30 MeV proton energy. The proton beam will be stopped in a beam dump located at around 1.70 m from the aluminum target. Our goal is to perform Monte Carlo transport radiation calculations using the specialized codes MCNPX [2] and PHITS [3] and evaluate the amount of secondary radiation coming from the interaction of the proton beam with the beam dump material. We will design appropriate shielding needed to protect human personnel and the sensitive radiation hardware located near the beam dump and the production target.

The transport radiation codes need a special geometry input file. The geometry of the cave is built with the geometry tool MORITZ from the White Rock Science Company. The software is currently installed on our computers and is up and running. Building the geometry of the LIG cave is not an easy task and should be completely error free for realistic calculations for the MCNPX and PHITS codes. The initial conditions of the problem are the following: 30 MeV proton beam with an intensity of 20 – 30 μA bombarding a beam dump. The beam dump is covered by additional borated polyethylene and lead (Pb). Our first code used in the evaluation of radiation fields was MCNPX and we compared the neutron fluxes in the beam dump for three different materials: carbon, aluminum and copper. Mainly we are concerned about the neutron fluxes because of the sensitivity of the Charge Breeding Electron-Cyclotron Resonance Ion Source permanent magnets and other hardware (pumping stations, helium gas flow system electronics) sitting in the proximity of the production target. We found out that carbon has the lowest neutron production, but high-energy gammas are present, thus requiring additional Pb shielding. A carbon beam dump needs good cooling also. A second radiation code PHITS showed us that aluminum could be a good candidate in our choice of beam dump material in terms of neutron and gamma production, except the fact that ^{22}Na is formed and it has a half-life of 2.6 years. At this stage we found out that a third code is necessary in our evaluation: DCHAIN-SP2001 [4] provided by Radiation Safety Information Computational Center in Oak Ridge National Laboratory. This code analyzes the decay and build-up characteristics of spallation products. Using this we determined that a copper beam dump is also a very good candidate because it has no dangerous activation and spallation products. The neutron flux is higher relative to a carbon beam dump, but systematic work and comparisons are needed. Appropriate shielding, geometry and material, could eliminate the problem of prompt radiation (neutron and gamma). Figure 1 shows the evolution of the activity in a beam dump of Copper. Only three isotopes are major contributors to the total activity: ^{64}Cu, ^{60}Co and ^{65}Ni.

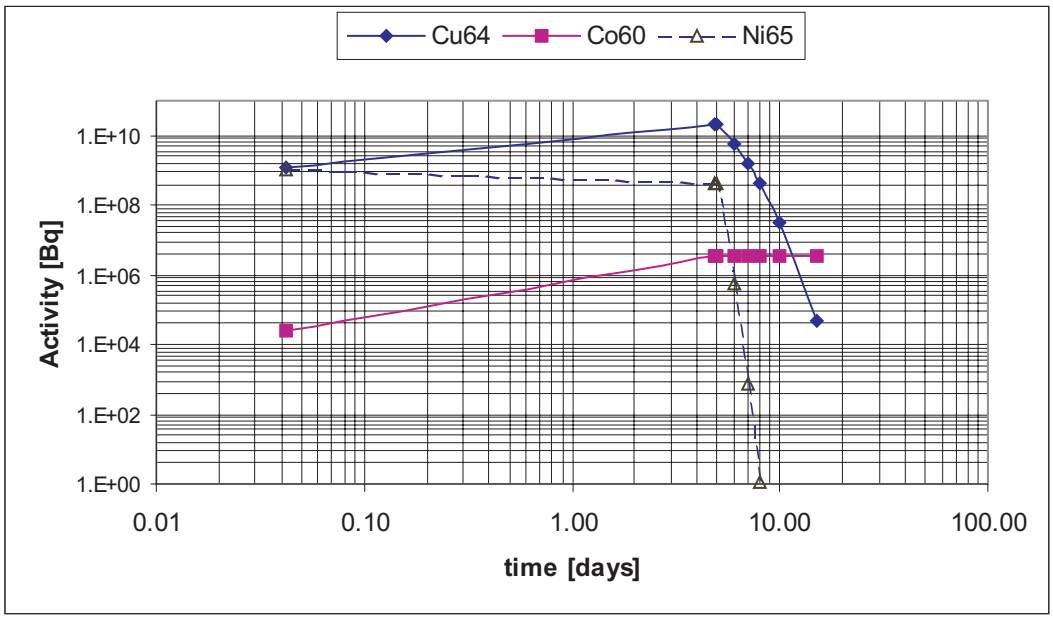

Figure 1. Evolution of the activity in the beam dump. The material (Copper) is irradiated 5 days and cooled for 10 days.

[1] H.L. Clark and R.E. Tribble, Project Management Plane for the Cyclotron Institute Upgrade at Texas A&M University, (December 2004).

[2] Denise B. Pelowitz, editor, MCNPX – LA – CP – 0369, Los Alamos National Laboratory.

[3] H. Iwase, K. Niita, and T. Makamura, J. Nucl. Sci. Tech., **39**, 1142 (2002).

[4] H. Takada and K. Kosako, DCHAIN-SP2001: Code System for Analyzing Decay and Build-up Characteristics of Spallation Products, JAERI, Tokai-mura, Ibaraki-ken, Japan.

Computer Control System for K150 Cyclotron

T. Cowden, F.P. Abegglen, R. Burch, and T. O'Berski

Since the most recent upgrade of the cyclotron computer control system, five years ago, the computer and semiconductor industry has rapidly changed. Almost all of the STD bus cards and the companies that made them have ceased to exist. Even the DIP chip is an endangered species. The extension of the computer control system to the twenty four power supplies of the K150 cyclotron would have to start from scratch.

The current system is based on using an STD bus crate to handle an average of eight power supplies a piece. Each crate has a processor card, a network card and various analog and digital I/O cards. The initial effort was to build on the existing STD bus interface, but simplify the I/O by shifting the burden to the power supply. With only a simple parallel TTL level or relay interface, no complex and unavailable analog STD cards would be needed. There was an added benefit of simpler digital electrical isolation, rather than the more complex analog isolation used previously. The standard interface for each new power supply was set at sixteen (16) bits read for the current, sixteen (16) bits written for the current control, six (6) relays to control the power supply and five (5) relay closures read as status bits.

Many systems were considered as replacements, but most fell short in the number of I/O points they could handle. It was stated that the ideal solution would be an inexpensive processor with Ethernet and enough I/O embedded in each power supply. It was speculated that such a product was still a few years down the road. In fact, subsequent searches found that such products already existed, and two different samples were purchased for test and evaluation. Both work with the existing control system on the communications level and have controlled a power supply under test. Both have C language development systems with multitasking extensions and example libraries. One system, the Rabbit 3200, is more suited than the other for the task at hand, but the second embedded processor is retained as a back up in an uncertain world.

Some of the advantages of the distributed embedded system were realized after the fact. The real time multitasking requirements of the system are reduced to one task per processor. The external wiring for the system is reduced to power and Cat5 Ethernet cable, all other wiring is short and inside the power supply. Each bank of supplies has an Ethernet hub/switch to further consolidate the wiring. Most of the adaptation of the hardware was to match the pinout of the processor to the wiring of the power supply. Only three semiconductors were added, a voltage regulator, a relay driver, and an LED indicator. The board the processor card attaches to is three inches by five inches (3"x5").

Nothing is without cost, however, as the total number of system messages goes up an order of magnitude. This can be countered with a differential message sending scheme, doing less frequent updates when the power supply values are static, more frequent while they change. The load handling ability of the higher levels of the control system do not seem to be taxed. The remaining unknown is long term reliability in a working cyclotron environment. The embedded systems seem robust, surviving the abuses of test and development well enough.

Repair of the Oxford Detector

J. Brinkley, M. McCleskey, T. Al-Abdullah, C.A. Gagliardi,
M. Farooqi,[1] L. Trache, and R.E. Tribble
[1]*2005 REU studen, University of Texas – Pan American, Edinburg, TX 78541*

The Oxford detector [1,2] is an ionization chamber that consists of two electrodes to measure ions energy loss and four sensitive avalanche counters (ACs) to determine the position. It has been used frequently for low energy beams and experiments with heavy ions at the MDM spectrometer [3,4]. The detector has a multi-wire Frisch grid that is located 10.5 cm above the cathode. Unfortunately, at the end of an experiment in May 2005 and while the detector was under a low pressure, the 50 μm Mylar exit window imploded. As a consequence, many wires of the grid were broken and could not be repaired.

A new rectangular frame of G10 glass fiber was designed to support the wires. The thickness of the frame was increased to 1.5 cm for the purpose of including the four smaller (screening) grids that shield the lower (Frisch) grid from positive ions generated in the ACs. Grooves were added to the frame as shown in Fig. 1 to space the wires uniformly and make future repairs easier. Each 80 μm Be-Cu wire was straightened and tensioned by hanging weights on both ends, then epoxy glue was applied to keep it taut, and it was soldered to the attached circuit boards along the edges for electrical contact. In addition to the damage in the Frisch grid, the horizontal field shaping wires near the front and exit windows were also broken and required fixing. The 80 μm Be-Cu wires are double banks with 7 mm separation between each two banks and 7 mm vertical spacing. They are built to correct the electric field between the electrodes. The entrance and exit windows were replaced with new 25 μm and 50 μm Mylar foils, respectively.

Recently, in a short test experiment with a ^{22}Ne beam at 12 MeV/A, the detector was tested under vacuum. High voltages, 600-1000 V, were applied on the cathode and the ACs to check that they produce the right signals. The few remaining glitches revealed by the test were fixed, and now the Oxford detector is in full working condition.

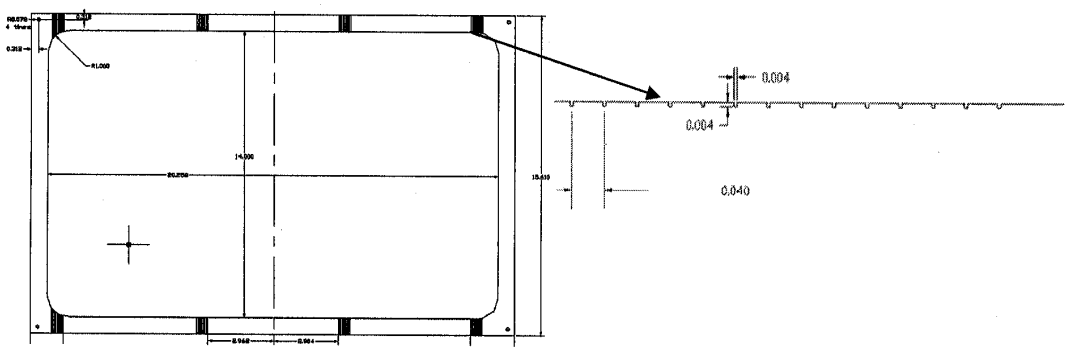

Figure 1. Blue prints that show the design of the frame, the spacing between the screening grids, and the grooves.

[1] J.S. Winfield, *et al*, Nucl. Instrum. Methods. **A251**, 297 (1986).

[2] D.H. Youngblood, *et al*, Nucl. Instrum. Methods. Phys. Res. **A361**, 539 (1995).
[3] L. Trache, *et al*, Phys. Rev. C **61**, 024612 (2000).
[4] T. Al-Abdullah, *et al*, *Progress in Research*, Cyclotron Institute, Texas A&M University (2005-2006), p. I-11.

SECTION VI

PUBLICATIONS

PAPERS PUBLISHED
April 1, 2005 – March 31, 2006

Isoscalar Giant Resonance for Nuclei with Mass between 56 and 60, Y.-W. Lui, D.H. Youngblood, H.L. Clark, Y. Tokimoto, and B. John, Phys. Rev. C **73**, 014314 (2006).

Indirect Techniques in Nuclear Astrophysics: the ANC Method, R.E. Tribble, Nucl. Instrum. Methods Phys. Res. **B241**, 204 (2005).

Indirect Techniques in Nuclear Astrophysics: Asymptotic Normalization Coefficient and Trojan Horse, A. Mukhamedzhanov, L.D. Blokhintsev, B.A. Brown, V. Burjan, C. Cherubini, C.A. Gagliardi, B.F. Irgaziev, V. Kroha, F.M. Nunes, F. Pirlepesov, G.L. Pizzone, S. Romano, C. Spitaleri, X.D. Tang, L. Trache, R.E. Tribble, A. Tumino, Eur. Phys. J. A **27,** Suppl. 1, 205 (2006); DOI: 10.1140/epja/i2006-08-032-7 (2006).

Scattering of ^{7}Be and ^{8}B and the Astrophysical S_{17} Factor, G. Tabacaru, A. Azhari, J. Brinkley, V. Burjan, F. Carstoiu, C. Fu, C.A. Gagliardi, V. Kroha, A.M. Mukhamedzhanov, X. Tang, L. Trache, R.E. Tribble, and S. Zhou, Phys. Rev. C **73**, 025808 (2006).

Asymptotic Normalization Coefficients from the ^{20}Ne(^{3}He,*d*)^{21}Na Reaction and Astrophysical Factor for ^{20}Ne(*p*,γ)^{21}Na, A.M. Mukhamedzhanov, P. Bem, V. Burjan, C.A. Gagliardi, B.F. Irgaziev, V. Kroha, J. Novak, S. Piskor, E. Simeckova, R.E. Tribble, F. Vesely, and J. Vincour, Phys. Rev. C **73**, 035806 (2006).

Global Analysis of Muon Decay Measurements, C.A. Gagliardi, R.E. Tribble, and N.J. Williams, Phys. Rev. D **72**, 073002 (2005).

Elastic Scattering of the Proton Drip-Line Nucleus ^{17}F, J.C. Blackmon, F. Carstoiu, L. Trache, D.W. Bardayan, C.R. Brune, C.A. Gagliardi, U. Greife, C.J. Gross, C.C. Jewett, R.L. Kozub, T.A. Lewis, J.F. Liang, B.H. Moazen, A.M. Mukhamedzhanov, C.D. Nesaraja, F.M. Nunes, P.D. Parker, L. Sahin, J.P. Scott, D. Shapira, M.S. Smith, J.S. Thomas, and R.E. Tribble, Phys. Rev. C **72**, 034606 (2005).

Few-Body Problems in Nuclear Astrophysics, A.M. Mukhamedzhanov, E.O. Alt, L.D. Blokhintsev, S. Cherubini, B.F. Irgaziev, A.S. Kadyrov, D. Miljanic, A. Musumarra, M.G. Pellegriti, F. Pirlepesov, C. Rolfs, S. Romano, C. Spitaleri, N.K. Timofeyuk, R.E. Tribble, and A. Tumino, J. Phys. G: Nucl. Part. Phys. **31**, S1413 (2005).

Indirect Measurement of the ^{15}N(p,α)^{12}C Reaction Cross Section through the Trojan-Horse Method, M. La Cognata, S. Romano, C. Spitaleri, R. Tribble, L. Trache, S. Cherubini, Changbo Fu, L.

Lamia, A. Mukhamedzhanov, R.G. Pizzone, C. Rolfs, G. Tabacaru, and A. Tumino, Eur. Phys. J. A **27**, Suppl. 1, 249 (2006); DOI: 10.1140/epja/i2006-08-039-0.

Breakup of Loosely Bound Nuclei as Indirect Method in Nuclear Astrophysics: ^{8}B, ^{9}C, ^{23}Al, L. Trache, F. Carstoiu, C.A. Gagliardi, and R.E. Tribble**,** Eur. Phys. J.ournal A, 27, Suppl. 1, 237 (2006); DOI: 10.1140/epja/i2006-08-037-2

Standard-Model Tests with Superallowed β-Decay: Nuclear Data Applied to Fundamental Physics, J.C. Hardy, *International Conference on Nuclear Data for Science and Technology*, AIP Conference Proceedings **769**, 678 (2005).

Understanding the rp-Process with the Canadian Penning Trap Mass Spectrometer, J. Clark, R.C. Barber, B. Blank, C. Boudreau, F. Buchinger, J.E. Crawford, J.P. Greene, S. Gulick, J.C. Hardy, A.A. Hecht, A. Heinz, J.K.P. Lee, A.F. Levand, B.F. Lundgren, R.B. Moore, G. Savard, N.D. Scielzo, D. Seweryniak, K.S. Sharma, G.D. Sprouse, W. Trimble, J. Vaz, J.C. Wang, Y. Wang, B.J. Zabransky, and Z. Zhou, Eur. Phys. J. A **25**, Suppl. 1, 629 (2005).

Superallowed $0^{+} \rightarrow 0^{+}$ β Decay and CKM Unitarity: A New Overview Including More Exotic Nuclei, J.C. Hardy and I.S. Towner**,** Eur. Phys. J. A **25**, 695 (2005).

Precise Measurement of *K*-Shell Fluorescence Yield in Iridium: An Improved Test of Internal-Conversion Theory, N. Nica, J.C. Hardy, V.E. Iacob, J.R. Montague, and M.B. Trzhaskovskaya**,** Phys. Rev. C **71**, 054320 (2005).

High Precision Measurements of ^{26}Na β^{-} Decay, G.F. Grinyer, C.E. Svensson, C. Andreoiu, A.N. Andreyev, R.A.E. Austin, G.C. Ball, R.S. Chakrawarthy, P. Finlay, P.E. Garrett, G. Hackman, J.C. Hardy, B. Hyland, V.E. Iacob, K.A. Koopmans, W.D. Kulp, J.R. Leslie, J.A. Macdonald, A.C. Morton, W.E. Ormand, C.J. Osborne, C.J. Pearson, A.A. Phillips, F. Sarazin, M.A. Schumaker, H.C. Scraggs, J. Schwarzenberg, M.B. Smith, J.J. Valiente-Dobin, J.C. Waddington, J.L. Wood, and E.F. Zganjar, Phys. Rev. C **71**, 044309 (2005).

Q Value of the Superallowed Decay of ^{46}V and its Influence on V_{ud} and the CKM Matrix, G. Savard, F. Buchinger, J.A. Clark, J.E. Crawford, S. Gulick, J.C. Hardy, A.A. Hecht, J.K.P. Lee, A.F. Levand, N.D. Scielzo, H. Sharma, I Tanihata, A.C.C. Villari, and Y. Wang**,** Phys. Rev. Lett. **95**, 102501 (2005).

A New Analysis of ^{14}O β Decay: Branching Ratios and Conserved Vector Current Consistency, I.S. Towner and J.C. Hardy**,** Phys. Rev. C. **72**, 055501 (2005).

CVC Tests and CKM Unitarity, J.C. Hardy**,** Acta Phys. Polonica B **37**, 77 (2006).

Mass Measurements and Superallowed β Decay, J.C. Hardy, I.S. Towner, and G. Savard, Int. J. Mass Spectrometry **251**, 95 (2006).

Continuous Phase Transition and Negative Specific Heat in Finite Nuclei, J.N. De, S.K. Samaddar, S. Shlomo, and J.B. Natowitz, Phys. Rev. C **73**, 034602 (2006).

Tracing the Evolution of Temperature in Near Fermi Energy Heavy Ion Collisions, J. Wang, R. Wada, T. Keutgen, K. Hagel, Y.G. Ma, M. Murray, L. Qin, A. Botvina, S. Kowalski, T. Materna, J.B. Natowitz, R. Alfarro, J. Cibor, M. Cinausero, Y. El Masri, D. Fabris, E. Fioretto, A. Keksis, M. Lunardon, A. Makeev, N. Marie, E. Martin, Z. Majka, A. Martinez-Davalos, A. Menchaca-Rocha, G. Nebbia, G. Prete, V. Rizzi, A. Ruangma, D.V. Shetty, G. Souliotis, P. Staszel, M. Veselsky, G. Viesti, E.M. Winchester, S.J. Yennello, and W. Zipper, Phys. Rev. C **72**, 024603 (2005).

Critical Behavior in Light Nuclear Systems: Experimental Aspects,Y.G. Ma, J.B. Natowitz, R. Wada, K. Hagel, J. Wang, T. Keutgen, Z. Majka, M. Murray, L. Qin, P. Smith, R. Alfaro, J. Cibor, M. Cinausero, Y. El Masri, D. Fabris, E. Fioretto, A. Keksis, M. Lunardon, A. Makeev, N. Marie, E. Martin, A. Martinez-Davalos, A. Menchaca-Rocha, G. Nebbia, G. Prete, V. Rizzi, A. Ruangma, D.V. Shetty, G. Souliotis, P. Staszel, M. Veselsky, G. Viesti, E.M. Winchester, and S.J. Yennello, Phys. Rev. C **71**, 054606 (2005).

Ghoshal-Like Test of Equilibration in Near-Fermi-Energy Heavy-Ion Collisions, J. Wang, T. Keutgen, R. Wada, K. Hagel, Y.G. Ma, M. Murray, L. Qin, P. Smith, J.B. Natowitz, R. Alfaro, J. Cibor, A. Botvina, M. Cinausero, Y. El Masri, D. Fabris, A. Keksis, S. Kowalski, M. Lunardon, A. Makeev, N. Marie, E. Martin, Z. Majka, A. Martinez-Davalos, A. Menchaca-Rocha, G. Nebbia, S. Moretto, G. Prete, V. Rizzi, A. Ruangma, D. V. Shetty, G. Souliotis, P. Staszel, M. Veselsky, G. Viesti, E.M. Winchester, S.J. Yennello, and W. Zipper, Phys. Rev. C **71**, 054608 (2005).

THOMATE: A New Protocol to Compare Simulated Data and Experiment by Minimizing a χ^2, T. Materna, Nucl. Instrum. Methods Phys. Res. **A544**, 679 (2005).

Heavy-Residue Isoscaling as a Probe of the Symmetry Energy of Hot Fragments, G.A. Souliotis, D.V. Shetty, A. Keksis, E. Bell, M. Jandel, M. Veselsky, and S.J. Yennello, Phys. Rev. C **73**, 024606 (2006).

Effect of Nuclear Periphery on Nucleon Transfer in Peripheral Collisions, M.Veselsky and G.A. Souliotis, Nucl. Phys. **A765**, 252 (2006).

Forward Indiana Ring Silicon Telescope (FIRST) : A Tool for Studying Projectile-Like Decay, T. Paduszynski, P. Sprunger, R.T. de Souza, S. Hudan, A. Alexander, B. Davin, G. Fleener, A. Mcintosh, C. Metelko, R. Moore, N. Peters, J. Poehlman, J. Gauthier, F. Greiner, R. Roy, D. Theriault, E. Bell, J.

Garey, J. Iglio, A.L. Keksis, S. Parketon, C. Richers, D.V. Shetty, S.N. Soisson, G.A. Souliotis, B. Stein, and S.J. Yennello , Nucl. Instrum. Methods, Phys. Res. **A547**, 464 (2005).

Doppler Shift as a Tool for Studies of Isobaric Analog States of Neutron-Rich Nuclei: Application to ^{7}He , P.Boutachkov, G.V. Rogachev, V.Z. Goldberg, A.Aprahamian, F.D. Becchetti, J.P. Bychowski, Y.Chen, G.Chubarian, P.A. DeYoung, J.J. Kolata, L.O. Lamm, G.F. Peaslee, M.Quinn, and B.B. Skorodumov, Phys. Rev. Lett. **95**, 132502 (2005).

Isobaric Analog States of Neutron-Rich Nuclei. Doppler Shift as a Measurement Tool for Resonance Excitation Functions, P. Boutachkov, G.V. Rogachev, V.Z. Goldberg, A. Aprahamian, F.D. Becchetti, J.P. Bychowski, Y. Chen, G. Chubarian, P.A. DeYoung, J.J. Kolata, L.O. Lamm, G.F. Peaslee, M.Quinn, B.B. Skorodumov, and A. Wohr , Eur. Phys. J. A **25**, Suppl. 1, 259 (2005).

Alpha-Cluster States in ^{18}O, V.Z. Goldberg, K.-M. Kallman, T. Lonnroth, P. Manngard, and B.B. Skorodumov, Phys.Atomic Nuclei **68**, 1079 (2005).

Isobaric Analog States as a tool for Spectroscopy of Exotic Nuclei, G.V. Rogachev, A. Aprahamian, F.D. Becchetti, P. Boutachkov, Y. Chen, G. Chubarian, P.A. DeYoung, A. Fomichev, V.Z. Goldberg, M.S. Golovkov, J.J. Kolata, Yu.Ts. Oganessian, G.F. Peaslee, M. Quinn, A. Rodin, B.B. Skorodumov, R.S. Slepnev, G.Ter-Akopian, W.H. Trzaska, A. Wohr, and R. Wolski , Nucl. Instrum. Methods Phys. Res. **B241**, 977 (2005).

Ionization Cross-sections for Ion-atom Collisions in High-energy Ion Beams, D. Kagonovich, E.A. Startsev, R.C. Davidson, S.R. Kecskemeti, A. Bin-Nun, D. Mueller, L. Grisham, R.L. Watson, V. Horvat, K.E. Zaharakis, and Y. Peng, Nucl. Instrum. Methods Phys. Res. **A544**, 91 (2005).

Electron Stripping Cross Sections for Fast, Low Charge State Uranium Ions, R.E. Olson, R.L. Watson, V. Horvat, K.E. Zaharakis, R.D. DuBois, and Th. Stöhlker, Nucl. Instrum. Methods Phys. Res. **A544**, 333 (2005).

L X Rays Emitted by Multiply Ionized Holmium Atoms, V. Horvat, R.L. Watson, J.M. Blackadar, A.N. Perumal and Y. Peng, Phys. Rev. A **71**, 062709 (2005).

Leading Asymptotic Terms of the Three-Body Coulomb Scattering Wave Function, A.M. Mukhamedzhanov, A. S. Kadyrov, and F. Pirlepesov, Phys. Rev. A **73**, 012713 (2006).

Photodisintegration Cross Section Measurements on ^{186}W, ^{187}Re, and ^{188}Os: Implications for the Re-Os Cosmochronology, T. Shizuma, H. Utsunomiya, P. Mohr, T. Hayakawa, S. Goko, A. Makinaga, H. Akimune, T. Yamagata, M. Ohta, H. Ohgaki, Y.-W. Lui, H. Toyokawa, A. Uritani, and S. Goriely, Phys. Rev. C **72**, 025808 (2005).

Analysis of Fusion-Fission Dynamics by Pre-scission Neutron Emission in ^{58}Ni + ^{208}Pb System, Y. Aritomo, M. Ohta, T. Materna, F. Hanappe, O. Dorvaux, and L. Stuttge, Nucl. Phys. **A759**, 309 (2005).

High-Energy Two-Neutron Removal from ^{10}Be, N.I. Ashwood, M. Freer, D.J. Millener, N.A. Orr, F. Carstoiu, S. Ahmed, J. C. Angélique, V. Bouchat, W.N. Catford, N.M. Clarke, N. Curtis, F. Hanappe, M. Horoi, Y. Kerckx, J. L. Lecouey, F. M. Marqués, T. Materna, G. Normand, S. Pain, N. Soic, C. Timis, A. Unshakova, and V. A. Ziman,, Phys. Rev. C **72**, 024314 (2005).

Progress on Reactions with Exotic Nuclei, F. M. Nunes, A.M. Moro, and A.M. Mukhamedzhanov , N.C. Summers, Eur. Phys. J. A **25**, Suppl. 1, 295 (2005).

Scattering Theory for Arbitrary Potentials, A.S. Kadyrov, I. Bray, A.M. Mukhamedzhanov, and A.T. Stelbovics, Phys. Rev. A **72**, 032712 (2005).

Combined Method to Extract Spectroscopic Factors from Transfer Reactions, A.M. Mukhamedzhanov and F. M. Nunes, Proceedings of 2nd Argonne/MSU/JINA/INT RIA Workshop on Reaction Mechanisms for Rare Isotope Beams (2005) pg 40.

Combined Method to Extract Spectroscopic Information, A.M. Mukhamedzhanov and F.M. Nunes, Phys. Rev. C **72**, 017602 (2005).

Three-Body Coulomb Final-State Interaction Effects in the Coulomb Breakup of Light Nuclei, E. O. Alt, B.F. Irgaziev, and A.M. Mukhamedzhanov, Mod. Phys. Lett. A **20**, 947 (2005).

Quark Coalescence and Charm(onium) in QGP, R. Rapp, Eur. Phys. J. C **43**, 91 (2005).

Fireballs from Quark Stars in the CFL Phase: Application to Gamma Ray Bursters, R. Ouyed, R. Rapp, and C. Vogt, Astrophys. J. **632**, 1001 (2005).

Reply to "Comment on' Hadronic Production of Thermal Photons'", S. Turbide, R. Rapp, and C. Gale, Phys. Rev. C **71**, 059803 (2005).

Hadronic Modes and Quark Properties in the Quark-Gluon Plasma, M. Mannarelli and R. Rapp, Phys. Rev. C **72**, 064905 (2005).

Heavy-Quark Probes of the Quark-Gluon Plasma at RHIC, H. van Hees, V. Greco, and R. Rapp, Phys. Rev. C **73**, 034913 (2006).

Renormalized Φ-Derivable Approximations to Theory with Spontaneously Broken O(N) Symmetry, Yu.B. Ivanov, F. Riek, H. van Hees, and J. Knoll, Phys. Rev. D **72**, 036008 (2005).

Hadron Production from Quark Coalescence and Jet Fragmentation, V. Greco, C.M. Ko, and I. Vitev, Phys. Rev. C **71**, 041901(R) (2005).

Transport Theories for Heavy-Ion Collisions in the 1 A GeV Regime, E.E. Kolomeitsev, C. Hartnack, H.W. Barz, M. Bleicher, E. Bratkovskaya, W. Cassing, L.W. Chen, P. Danielewicz, C. Fuchs, T. Gaitanos, C.M. Ko, A. Larionov, M. Reiter, Gy. Wolf, and J. Aichelin, J. Phys. G **31**, S741 (2005).

Charm Elliptic Flow in Relativistic Heavy-Ion Collisions, B. Zhang, L.W. Chen, and C.M. Ko, Phys. Rev. C **72**, 024906 (2005).

Diomega Production in Relativistic Heavy Ion Collisions, S. Pal, C.M. Ko, and Z.Y. Zhang, Phys. Lett. B **624**, 210 (2005).

Multiphase Transport Model for Relativistic Heavy Ion Collisions, Z.W. Lin, C.M. Ko, B.A. Li, B. Zhang, and S. Pal, Phys. Rev. C **72**, 064901 (2005).

Nuclear Matter symmetry Energy and the Neutron Skin Thickness of Heavy Nuclei, L.W. Chen, C.M. Ko, and B.A. Li, Phys. Rev. C **72**, 064309 (2005).

High-Energy Behavior of the Nuclear Symmetry Potential in Asymmetric Nuclear Matter, L.W. Chen, C.M. Ko, and B.A. Li, Phys. Rev. C **72**, 064606 (2005).

Eta Absorption by Mesons, W. Liu, C.M. Ko, and L.W. Chen, Nucl. Phys. **A765**, (2006).

Anisotropic Flow in Cu + Au Collisions at $\sqrt{s_{NN}}$ =200 GeV, L.W. Chen and C.M. Ko, Phys. Rev. C **73**, 014906 (2006).

Effect of Isovector-Scalar Meson on Neutron-Star Matter in Strong Magnetic Fields, F.X. Wei, G.J. Mao, C.M. Ko, L.S. Kisslinger, H. Stoecker, and W. Greiner, J. Phys. G **32** (2006).

System Size Dependence of Elliptic Flows in Relativistic Heavy-Ion Collisions, L.W. Chen and C.M. Ko, Phys. Lett. B **634**, 205 (2006).

φ and Ω Production in Realtivistic Heavy Ion Collisions in a Dyanmical Quark Coalescence Model, L.W. Chen and C.M. Ko, Phys. Rev. C, 73, 044903 (2006).

Determination of a Skyrme Type Effective Interaction Using the Simulated Annealing Approach, B.K. Agrawal, S. Shlomo and V. Kim Au, Phys. Rev. C **72**, 014310 (2005).

Breathing Mode Energy and Nuclear Matter Incompressibility Coefficient within Relativistic and Non-Relativistic Models, B. K. Agrawal, S. Shlomo, and V. Kim Au, Eur. Phys. J. A **25**, 525 (2005).

Splitting of Isovector Giant Dipole Resonance in Spherical Nuclei, V.M. Kolomietz, A.G. Magner and S. Shlomo, Phys. Rev. C **73**, 024312 (2006).

Effects of Self-Consistency Violations in HF-RPA Calculations of The Energies of Isoscalar and Isovector Giant Multipole Resonances, T. Sil, S. Shlomo, B.K. Agrawal, and P.G. Reinhard, Phys. Rev. C **73**, 034316 (2006).

Multiplicity and Pseudorapidity Distributions of Charged Particles and Photons at Forward Pseudorapidity in Au+Au Collisions at $\sqrt{s_{NN}}$ = 62.4 GeV, J. Adams *et al*. (STAR Collaboration), Phys. Rev. C **73**, 034906 (2006).

Hadronization Geometry from Net-Charge Angular Correlations on Momentum Subspace (η,φ) in Au-Au Collisions at $\sqrt{s_{NN}}$ = 130 GeV, J. Adams *et al*. (STAR Collaboration), Phys. Lett. B **634**, 347 (2006).

Directed Flow in Au+Au Collisions at $\sqrt{s_{NN}}$ = 62 GeV, J. Adams *et al*. (STAR Collaboration), Phys. Rev. C **73**, 034903 (2006).

Incident Energy Dependence of p_t Correlations at Relativistic Eenergies, J. Adams *et al*. (STAR Collaboration), Phys. Rev. C **72**, 044902 (2005).

Event-Wise $\langle p_t \rangle$, Fluctuations in Au-Au Collisions at $\sqrt{s_{NN}}$ = 130 GeV, J. Adams *et al*. (STAR Collaboration), Phys. Rev. C **71**, 064906 (2005).

Multi-strange Baryon Elliptic Flow in Au+Au Collisions at $\sqrt{s_{NN}}$ = 200 GeV, J. Adams *et al*. (STAR Collaboration), Phys. Rev. Lett. **95**, 122301 (2005).

Recent High-p_T Results from STAR, C.A. Gagliardi, on behalf of the STAR Collaboration, Eur. Phys. J. C **43**, 263 (2005).

Future of Low-x Forward Physics at RHIC, L.C. Bland, F. Bieser, R.L. Brown, H.J. Crawford, A.A. Derevshchikov, J.L. Drachenberg, J. Engelage, L. Eun, C.A. Gagliardi, S. Heppelmann, E.G. Judd, V.I. Kravtsov, Yu.A. Matulenko, A.P. Meschanin, D.A. Morozov, L.V. Nogach, S.B. Nurushev, A. Ogawa, C. Perkins, G. Rakness, K.E. Shestermanov, and A.N. Vasiliev, Eur. Phys. J. C **43**, 427 (2005).

Multiplicity and Pseudorapidity Distributions of Photons in Au+Au Collisions at $\sqrt{s_{NN}}$ = 62.4 GeV, J. Adams *et al*. (STAR Collaboration), Phys. Rev. Lett. **95**, 062301 (2005).

Distributions of Charged Hadrons Associated with High Transverse Momentum Particles in p+p and Au+Au Collisions at $\sqrt{s_{NN}}$ = 200 GeV, J. Adams *et al*. (STAR Collaboration), Phys. Rev. Lett. **95**, 152301 (2005).

Experimental and Theoretical Challenges in the Search for the Quark Gluon Plasma: The STAR Collaboration's Critical Assessment of the Evidence from RHIC Collisions, J. Adams *et al*. (STAR Collaboration), Nucl. Phys. **A757**, 102 (2005).

***K*(892)* Resonance Production in Au+Au and *p+p* Collisions at $\sqrt{s_{NN}}$ = 200 GeV at RHIC**, J. Adams *et al*. (STAR Collaboration), Phys. Rev. C **71**, 064902 (2005).

Pion Interferometry in Au+Au Collisions at $\sqrt{s_{NN}}$ = 200 GeV, J. Adams *et al*. (STAR Collaboration), Phys. Rev. C **71**, 044906 (2005).

Azimuthal Anisotropy in Au+Au Ccollisions at $\sqrt{s_{NN}}$ = 200 GeV, J. Adams *et al*. (STAR Collaboration), Phys. Rev. C **72**, 014904 (2005).

Pion, Kaon, Proton and Anti-proton Transverse Momentum Distributions from p+p and d+Au Collsions at $\sqrt{s_{NN}}$ = 200 GeV, J. Adams *et al*. (STAR Collaboration), Phys. Lett. B **616**, 8 (2005).

ϕ Meson Production in Au+Au and *p+p* Collisions at $\sqrt{s_{NN}}$ = 200 GeV, J. Adams *et al*. (STAR Collaboration), Phys. Lett. B **612**, 181 (2005).

High-p_T Results from STAR, C.A. Gagliardi, for the STAR Collaboration, Proc. Workshop Jet Corr. RHIC, Brookhaven, NY, 2005, ed. by M. Gyulassy, M. Tannenbaum, and F. Wang (RIKEN BNL Research Center 73, 2005) 3.

Recent Results from the BRAHMS Experiment at RHIC, I Aesene *et al.* (BRAHMS Collaboration), Int J. Mod. Phys. A 20, 4369 (2005).

The Forward High p_T Puzzle, J.J. Gaardhoje *et al.* (BRAHMS Collaboration), Eur. Phys. J. C 43 , 287 (2005).

Centrality Dependent Particle Production at y = 0 and y ~ 1 in Au+Au Collisions at $\sqrt{s_{NN}}$ = 200 GeV, I. Aesene *et al.* (BRAHMS Collaboration), Phys. Rev. C **72**, 014908 (2005).

Quark-Gluon Plasma and Color Glass Condensate at RHIC? The Perspective from the BRAHMS Experiment, I. Arsene *et al.* (BRAHMS Collaboration), Nuclear Physics **A757**, 1 (2005).

Charged Meson Rapidity Distributions in Central Au+Au Collisions at $\sqrt{s_{NN}}$ = 200 GeV, I.G. Bearden *et al.* (BRAHMS Collaboration), Phys. Rev. Lett. **94**, 162301 (2005).

Measurement of Identified π^0 and Inclusive Photon Second-Harmonic Parameter v_2 and Implications for Direct Photon Production in $\sqrt{s_{NN}}$ =200 GeV Au+Au, S.S. Adler *et al.* (PHENIX Collaboration), Phys. Rev. Lett. **96**, 032302 (2006).

Nuclear Modification of Electron Spectra and Implications for Heavy Quark Energy Loss in Au+Au Collisions at $\sqrt{s_{NN}}$ =200 GeV, S.S. Adler *et al.* (PHENIX Collaboration), Phys. Rev. Lett. **96**, 032301 (2006).

Nuclear Modification of Single Electron Spectra and Implications for Heavy Quark Energy Loss in Au+Au Collisions at $\sqrt{s_{NN}}$ =200 GeV, S.S. Adler *et al*. (PHENIX Collaboration), Phys. Rev. Lett. **96**, 032301 (2006).

Single Electrons from Heavy-Flavor Decays in p+p Collisions at $\sqrt{s_{NN}}$ =200 GeV, S.S. Adler *et al.* (PHENIX Collaboration), Phys. Rev. Lett. **96**, 032001 (2006).

Measurement of Transverse Single-Spin Asymmetries for Mid-Rapidity Production of Neutral Pions and Charged Hadrons in Polarized p+p Collisions at $\sqrt{s_{NN}}$ =200 GeV, S.S. Adler *et al.* (PHENIX Collaboration), Phys. Rev. Lett. **95**, 202001 (2005).

Deuteron and Antideuteron Production in Au+Au Collisions at $\sqrt{s_{NN}}$ =200 GeV, S.S. Adler *et al.* (PHENIX Collaboration), Phys. Rev. Lett. **94**, 122302 (2005).

Centrality Dependence of Direct Photon Production in $\sqrt{s_{NN}}$ =200 GEV Au+Au Collisions, S.S. Adler *et al.* (PHENIX Collaboration), Phys. Rev. Lett. **94**, 232301 (2005).

Measurement of Single Electron Event Anisotropy in Au+Au Collisions $\sqrt{s_{NN}}$ =200 GeV, S.S. Adler *et al.* (PHENIX Collaboration), Phys. Rev. C **72**, 024901 (2005).

Mid-Rapidity Direct-Photon Production in p+p Collisions at $\sqrt{s_{NN}}$ =200 GeV, S.S. Adler *et al.* (PHENIX Collaboration), Phys. Rev. D **71**, 071102 (2005).

Nuclear Modification Factors for Hadrons at Forward and Backward Rapidities in Deuteron-Gold Collisions at $\sqrt{s_{NN}}$ =200 GeV, S.S. Adler *et al.* (PHENIX Collaboration), Phys. Rev. Lett. **94**, 082302 (2005).

Saturation of Azimuthal Anisotropy in Au + Au Collisions at $\sqrt{s_{NN}}$ =62-200 GeV, S.S. Adler *et al.* (PHENIX Collaboration), Phys. Rev. Lett. **94**, 232302 (2005).

Production of φ Mesons at Mid-Rapidity in $\sqrt{s_{NN}}$ =200 GeV Au+Au Collisions at RHIC, S.S. Adler *et al.* (PHENIX Collaboration), Phys. Rev. C **72**, 014903 (2005).

Systematic Studies of the Centrality and $\sqrt{s_{NN}}$ Dependence of the $dE_T/d\eta$ and $dN_{Ch}/d\eta$ in Heavy Ion Collisions at Mid-Rapidity, S.S. Adler *et al.* (PHENIX Collaboration), Phys. Rev. C **71**, 034908 (2005).

Jet Structure of Baryon Excess in Au+Au Collisions at $\sqrt{s_{NN}}$ =200 GeV S.S. Adler *et al.* (PHENIX Collaboration), Phys. Rev. C **71**, 051902 (2005).

Formation of Dense Partonic Matter in Relativistic Nucleus-Nucleus Collisions at RHIC: Experimental Evaluation by the PHENIX Collaboration, S.S. Adler *et al.* (PHENIX Collaboration), Nucl. Phys. **A757**, 184 (2005); DOI: 10.1016/j.nuclphysa.2005.03.086.

Centrality Dependence of Charm Production from a Measurement of Single Electrons in Au+Au Collisions at $\sqrt{s_{NN}}$ =200 GeV, S.S. Adler *et al.* (PHENIX Collaboration), Phys. Rev. Lett. **94**, 082301 (2005).

Texas A&M 14.5 and 6.4 GHz Electron Cyclotron Resonance Ion Source, D.P. May, F.P. Abegglen, G.J. Derrig, and R.S. Olsen , Rev. Sci. Instrum. **77**, 03A328 (2006).

SECTION VII

APPENDIX

TALKS PRESENTED
April 1, 2005 – March 31, 2006

Systematic of Giant Monopole Energy and the Isotopic Dependence, **Y.-W. Lui**, D.H. Youngblood, H.L. Clark, Y. Tokimoto and B. John, **Invited Talk**, Workshop on Nuclear Imcompressibility, University of Notre Dame, South Bend, Indiana, (July 2005).

Giant Resonance Study by ^{6}Li Scattering, **X. Chen**, Y.-W. Lui, H.L. Clark, Y. Tokimoto, and D.H. Youngblood, 2005 2nd Joint Meeting of the Nuclear Physics Divisions of the APS and the Physical Society of Japan, Maui, Hawaii, (September 2005).

Indirect Methods in Nuclear Astrophysics, **R.E. Tribble**, **Invited Talk**, Carpathian Summer School of Physics 2005, Mamaia-Constanta, Romaina, (June 2005).

Radioactive Ion Beams: Applications in Nuclear Astrophysics, **R.E. Tribble**, **Invited Talk**, Workshop on The Future of Nuclear Physics at LANSCE, Los Alamos, New Mexico, (July 2005).

Indirect Methods in Nuclear Astrophysics: ANCs, **R.E. Tribble**, **Invited Talk**, Third European Summer School on Nuclear Astrophysics, Catania, Sicily, Italy, (October 2005).

Asymptotic Normalization Coefficients Measured with Stable and Radioactive Ion Beams for Nuclear Astrophysics, **R.E. Tribble**, **Invited Talk**, 50th Symposium on Nuclear Physics, Mumbai, India, (December 2005).

The Texas A&M Upgrade: Accelerated Beams at Intermediate Energies, **R.E. Tribble**, NSCL at Michigan State University, East Lansing, Michigan, (February 2006).

Report to RISAC on NSAC Report: Guidance to Implementing the 2002 Long Range Plan, **R.E. Tribble**, Irvine, California, (February 2006).

d+Au and p+Au Collisions at RHIC, **C.A. Gagliardi, Invited Talk**, PANIC'05 Satellite Meeting: New Frontiers at RHIC, Santa Fe, New Mexico, (October 2005).

Some Striking New STAR Results, **C.A. Gagliardi (for the STAR Collaboration)**, **Invited Talk**, 18th Int. Conf. on Ultra-Relativistic Nucl.-Nucl. Coll. (Quark Matter 2005), Budapest, Hungary, (August 2005).

d+Au and p+Au at RHIC, **C.A. Gagliardi**, **Invited Talk**, Worhshop on Prot.-Nucl. Coll. LHC, CERN, Geneva, Switzerland, (May 2005).

d+Au at RHIC: Past and Future, **C.A. Gagliardi**, **Invited Talk**, Workshop on pA and eA Physics at RHIC, Brookhaven, Upton, New York, (May 2005).

Extracting the ANCs in Neutron Transfer Reactions to Determine Proton Capture Reaction Rates, **T. Al-Abdullah**, X. Chen, C.A. Gagliardi, Y.-W. Lui, G. Tabacaru, Y. Tokimoto, L. Trache, and R.E. Tribble, 2005 2nd Joint Meeting of the Nuclear Physics Divisions of the APS and the Physical Society of Japan, Maui, Hawaii, (September 2005).

TWIST Measurement of the Decay Parameters ρ and δ of Normal Muon Decay, **J.R. Musser (for the TWIST Collaboration)**, 2005 April Meeting of the APS, Tempa, Florida, (April 2005).

Extracting the ANCs for $^{23}Al \rightarrow {}^{22}Mg+p$ from the Mirror System $^{23}Ne \rightarrow {}^{22}Ne+n$, **T. Al-Abdullah**, X. Chen, H.L. Clark, C. Fu, C.A. Gagliardi, Y.-W. Lui, G. Tabacaru, Y. Tokimoto, L. Trache, R.E. Tribble, F. Carstoiu, and S. Piskor, 2005 April Meeting of the APS, Tempa, Florida, (April 2005).

Breakup of Loosely Bound Nuclei as Indirect Method in Nuclear Astrophysics: ^{8}B, ^{9}C, ^{23}Al, **L. Trache**, International Conference on Nuclear Physics for Astrophysics II, Debrecen, Hungary, (May 2005).

Breakup of Loosely Bound Nuclei as Indirect Method in Nuclear Astrophysics: ^{8}B, ^{9}C, ^{23}Al, **L. Trache**, , C.A. Gagliardi, R.E. Tribble, A.M. Mukhamedzhanov, and F. Carstoiu, 2005 2nd Joint Meeting of the Nuclear Physics Divisions of the APS and the Physical Society of Japan, Maui, Hawaii, (September 2005).

Nuclear Physics for Astrophysics with Radioactive Beams, **L. Trache**, **Invited Talk**, EURISOL Workshop, Trento, Italy, (January 2006).

The Structure of ^{23}Al and the Consequences on the $^{22}Mg(p,\gamma)^{23}Al$ Stellar Reaction Rates, **Yongjun Zhai , Invited Talk**, School of Physics, Peking University, Beijing, China, (December 2005).

Experimental Status of V_{ud}, **J.C. Hardy, Invited Talk**, KAON2005, Northwestern University, Evanston, Illinois, (June 2005).

Probing the Weak Interaction in Nuclei: Nuclear Structure as Background, **J.C. Hardy, Invited Talk**, Nuclear Chemistry Gordon Conference, New London, New Hampshire, (June 2005).

CVC Tests and CKM Unitarity, **J.C. Hardy**, **Invited talk**, XXIX Mazurian Lakes Conference on Physics: Nuclear Physics and the Fundamental Processes, Piaski, Poland, (August 2005).

Test of Internal-Conversion Theory with Precise γ- and X-Ray Spectroscopy, **J.C. Hardy**, **Invited talk**, 15th International Conference on Radionuclide Metrology and its Application, Oxford, England, (September 2005).

Weak Interaction Parameters from Superallowed β Decay, **J.C. Hardy**, **Invited talk**, 2005 2nd Joint Meeting of the Nuclear Physics Divisions of the APS and the Physical Society of Japan, Maui, Hawaii, (September 2005).

Precision and Pandemonium, **J.C. Hardy**, **Invited talk**, Symposium on Advances in Rare Isotope Research (in Memory of Peder Gregers Hansen), Michigan State University, East Lansing, Michigan, (November 2005).

How Idiosyncratic is the Weak Force? **J.C. Hardy**, Colloquium at Abilene Christian University, Abilene, Texas, (November 2005).

Weak Interaction Parameters from Superallowed β Decay, **J.C. Hardy**, Colloquium at Thomas Jefferson National Accelerator Facility, Newport News, Virginia, (November 2005).

Weak Interaction Parameters from Superallowed β Decay, **J.C. Hardy**, Seminar at University of Jyvaskyla, Jyvaskyla, Finland, (January 2006).

The Weak Force: Dancing to Its Own Tune, **J.C. Hardy**, Saturday Morning Physics at Texas A&M, College Station, Texas, (February 2006).

Precise Half-Life Measurement of ^{34}Ar, a Superallowed β Emitter, **V.E. Iacob**, J.C. Hardy, C.A. Gagliardi, V.E. Mayes, N. Nica, G. Tabacaru, L. Trache, and R.E. Tribble, Carpathian Summer School of Physics 2005, Mamaia-Constanta, Romaina, (June 2005).

Precise Half-Life Measurement for the Superallowed β^+ emitter ^{34}Ar Emitter, **V.E. Iacob**, J.C. Hardy, C.A. Gagliardi, V.E. Mayes, N. Nica, G. Tabacaru, L. Trache, and R.E. Tribble, 2005 2nd Joint Meeting of the Nuclear Physics Divisions of the APS and the Physical Society of Japan, Maui, Hawaii, (September 2005).

Nuclear Structure from a Completeness Perspective, **N. Nica**, Seminar at National Nuclear Data Center (NNDC), Brookhaven National Laboratory, Upton, New York, (March 2005).

Precision Spectroscopy, **N. Nica**, Workshop on Nuclear Structure and Decay Data: Theory and Evaluation, Abdus Salam International Center for Theorectical Physics, Triestle, Italy, (April 2005).

Precision Spectroscopy, **N. Nica**, Seminar at National Institute of Physics and Nuclear Engineering, Bucharest, Romania, (April 2005).

Nuclear Structure from a Completeness Perspective, **N. Nica**, Seminar at National Superconducting Cyclotron Laboratory, Michigan State University, East Lansing, Michigan, (September 2005).

Future Plans at RHIC, **S. Mioduszewski**, **Invited Talk**, CNS-RIKEN Workshop on Physics of Quark Gluon Plasma, Tokyo, Japan, (February 2006).

Do We Really Understand Energy Loss at RHIC? **S. Mioduszewski**, Seminar at Purdue University, West Lafayette, Indiana, (November 2005).

Tools to Characterize the Matter Created at RHIC, **S. Mioduszewski**, **Invited Talk**, Sambamurti Memorial Lectureship, Brookhaven National Laboratory, Upton, New York, (July 2005).

Where Are We in the Search for the QGP? **S. Mioduszewski**, **Invited Talk**, RHIC Retreat 2005, Montauk, New York, (June 2005).

Direct Photons at RHIC, **S. Mioduszewski**, Workshop on Electromagnetic Probes, ECT*, Trento, Italy, (June 2005).

Probing the Matter Created at RHIC, **S. Mioduszewski**, BNL Lecture, Brookhaven National Laboratory, Upton, New York, (April 2005).

Recent Experiments on Resonance Scattering with Rare Beams and R matrix Analysis, **V.Z. Goldberg**, **Invited Talk**, Internaltional Conference on Direct Reactions with Exotic Beams 2005, NSCL, Michigan State University, East Lansing, Michigan, (June 2005).

Former Aims and New Horizons in Studies of Reverse Kinematics Resonance Scattering, **V.Z. Goldberg**, **Invited Talk**, LV Internaltional Nuclear Physics Conference on Frontiers in the Physics of Nuclei, St. Petersburg, Russia, (July 2005).

Resonance Scattering Induced by Radioactive Beams, **V.Z. Goldberg**, **Invited Talk**, Internaltional Workshop on Nuclear Physics, San Paulo, Brazil, (September 2005).

History of the Russian Nuclear Bomb Program, **V.Z. Goldberg**, Lecture Series on Thoughts on the Unthinkable, University of Notre Dame, South Bend, Indiana, (September 2005).

$^{11}C+p$ Resonance Interaction and Nuclear Structure ^{12}N, **V.Z. Goldberg**, Seminar on LBNL, University of California, Berkley, California, (June 2005).

Super Heavy Hydrogen, ^{7}H, Will be Discovered Soon, **V.Z. Goldberg**, Seminar on St. Petersburg State University, St. Petersburg, Russia, (June 2005).

α Cluster Structure in N≠Z Light Nuclei, **V.Z. Goldberg**, Seminar on Moscow State University, Moscow, Russia, (July 2005).

Resonance Scattering Induced by Radioactive Beams (from α to ω), **V.Z. Goldberg**, Seminar on Institute of Nuclear Physics, Kiev, Russia, (July 2005).

Heavy-Ion Collision Studies of the Symmetry Energy at High Temperature and Very Low Density, **J.B. Natowitz**, **Invited Talk**, CCAST Workshop on Isospin Physics and Nuclear Liquid Gaas Phase Transition, Beijing, China, (August 2005).

The Symmetry Energy at high Temperature and Very Low Density, **J.B. Natowitz**, **Invited Talk**, Shanghai Institute Of Applied Physics, Shanghai, China, (August 2005).

From Nuclear Collisions to the Equation of State of Nuclear Matter, **J.B. Natowitz**, **Invited Talk**, Washington University, St. Louis, Missouri, (August 2005).

Symmetry Energy in Low Density Nuclear Gases, **J.B. Natowitz**, **Invited Talk**, University of Padova, Padova, Italy, (March 2006).

Symmetry Energy in Low Density Nuclear Gases, **J.B. Natowitz**, **Invited Talk**, Labioratoi Nazionali di sud Catania, Catania, Italy, (March 2006).

Heavy Ion Reaction Dynamics and the Properties of Highly Excited Nuclei, **J.B. Natowitz**, **Invited Talk**, Workshop on Heavy Ions & Isotopes, Chandigarh, India, (October 2005).

Isoscaling and Primary Fragment Distribution in Nucleus-Nucleus Collisions at Intermediate Energies, **S. Kowalski,** IWM2005, Catania, Italy, (December 2005).

Broad Range Relativistic Heavy Ion Measurements Overview, **K. Hagel, (**for the BRAHMS Collaboration), **Invited Talk**, VI Latin American Symposium on Nuclear Physics and Applications, Iguazu, Argentina, (October 2005).

The Future of Nuclear Science Education : The Need for Increased Participation, **S.J. Yennello, Invited Talk**, 231st ACS meeting, Atlanta, Georgia, (March 2006).

*Rare Isotope Beam (RIB) Capabilities Expected from the Upgrade Project of the Texas A&M Cyclotron Institute***, G.A. Souliotis, Invited Talk**, HRIBF Fusion-Fission Workshop, Oak Ridge National Laboratory, Oak Ridge, Tennessee, (December 2005).

Symmetry Energy in the Equation of State of Asymmetric Nuclear Matter from Heavy Ion Collisions, **S.J. Yennello, Invited Talk**, PACIFICHEM, Honolulu, Hawaii, (December 2005).

The Heart of Matter: The World of Nucleus, **S.J. Yennello, Invited Talk**, Women in Science, Queens College, New York, (November 2005).

Symmetry Energy in the Equation of State of Asymmetric Nuclear Matter, **S.J. Yennello, Invited Talk**, VI Latin American Symposium on Nuclear Physics and Applications, Iguazu, Argentina, (October 2005).

Studying the Nuclear Equation of State (EOS) Using Heavy Ions, **S.J. Yennello, Invited Talk**, Institute of Modern Physics, Lanzhou, China (August 2005).

Using Isoscaling to Understand the Symmetry Energy of the Nuclear Equation of State, **S.J. Yennello, Invited Talk**, CCAST Workshop on Isospin Physics and Liquid Gas Phase Transition, Beijing, China (August 2005).

Nuclear Reactions, **S.J. Yennello, Invited Talk**, RIA Summer School, Berkeley, California (August 2005).

Connections between Nuclear Reactions and Astrophysics, **S.J. Yennello, Invited Talk**, RIA Summer School, Berkeley, California (August 2005).

Nuclear Equation of State : What Can We Learn about Neutron Stars from Atomic Nuclei ? **D.V. Shetty**, Texas Section of the APS Meeting, University of Houston, Houston, Texas, (October 2005).

Density Dependence of the Symmetry Energy in the Equation of State of Asymmetric Nuclear Matter, **S.J. Yennello, Invited Talk**, VI Latin American Symposium on Nuclear Physics and Applications, Iguazu, Argentina, (October 2005).

Scaling of Projectile Residue Yields from Peripheral Heavy-Ion Collisions Below the Fermi Energy, **G.A. Souliotis**, DNP Meeting, Maui, Hawaii, (September 2005).

Projectile Residue Studies Around and Below the Fermi Energy, **G.A. Souliotis, Invited Talk**, GSI, Darmstadt, Germany, (September 2005).

Survival of Very Neutron Rich Fragments in Multifragmentation, **G.A. Souliotis**, APS Meeting, Tampa, Florida, (April 2005).

Critical Analysis of Data from Peripheral Si + Sn Reaction at 50 MeV/nucleon – Probing N/Z Degree of Freedom, **M. Jandel,** APS Meeting, Tampa, Florida, (April 2005).

Using Light Cluster Production to Explore the Density Dependence of the Nuclear Symmetry Energy, **S. Soisson,** APS Meeting, Tampa, Florida, (April 2005).

Determining the Density Dependence of the Symmetry Energy: Theoretical Perspectives, **C. M. Ko**, Workshop on Nuclear Equation of State for Nuclei, Neutron Stars and Supernovae, Jonesboro, Arkansas (April 2005).

Heavy Flavor Flow, **C. M. Ko**, RHIC II Heavy Flavor Meeting, Brookhaven National Laboratory, Upton, New York (April 2005).

Hadronization via Coalescence, **C. M. Ko,** Chinese STAR Collaboration Summer School, Wuhan, China (June 2005).

Quark Coalescence and the Scaling of Hadron Elliptic Flow, **C. M. Ko**, Chinese STAR Collaboration Workshop, Wuhan, China (June 2005).

Anisotropic Flow in Relativistic Heavy Ion Collisions, **C. M. Ko**, Eastern Forum on International Collaboration for High Energy Nuclear Physics and China's Opportunity, Shanghai, China (June 2005).

Transport Model Study of HBT at RHIC, **C. M.** Ko, Proceedings of International Workshop on Particle Correlations and Femtoscopy, Kromeriz, Czech Republic (August 2005).

Parton Hadronization in Medium, **C. M. Ko**, International Workshop on Parton Propagation Through Strongly Interacting Matter, Trento, Italy (September 2005).

Paronic Degree of Freedom and Hadronization Dyanmics at RHIC, **C. M. Ko,** International Conference on Strgangeness in Quark Matter, Los Angeles (March 2006).

Can the Spectroscopic Factors be Extracted fromTransfer Reactions?, **A.M. Mukhamedzhanov**, **Invited Talk**, RIKEN, Tokyo, Japan, (April 2005).

Three-Body Coulomb Effects in the Coulomb Breakup Reactions, **A.M. Mukhamedzhanov**, **Invited Talk**, Workshop on Coulomb Breakup Reactions, RIKEN, Tokyo, Japan, (April 2005).

Three-body Integral Equations with Coulomb Interactions, **A.M. Mukhamedzhanov**, **Invited Talk**, Tokyo University of Science, Tokyo, Japan, (April 2005).

Indirect Techniques in Nuclear Astrophysics, **A.M. Mukhamedzhanov**, **Invited Talk**, International Conference on Nuclear Physics in Astrophysics II, Debrecen, Hungary, (May 2005).

Trojan Horse as Indirect Technique in Nuclear Astrophysics, **A.M. Mukhamedzhanov**, **Invited Talk**, Physics Department, University of Surrey, Guilford, England, (October 2005).

Trojan Horse as Indirect Technique in Nuclear Astrophysics, **A.M. Mukhamedzhanov**, **Invited Talk**, 3rd European School on Experimental methods in nuclear astrophysics, Santa Tecla, Sicily, Italy, (October 2005).

Indirect Techniques in Nuclear Astrophysics, **A.M. Mukhamedzhanov**, **Invited Talk**, International Symposium on Origin of Matter and Evolution of Galaxies (OMEG05)-New Horizon of Nuclear Astrophysics and Cosmology, University of Tokyo, Tokyo, Japan, (November 2005).

Asymptotic Normalization Coefficients in Nuclear Reactions and Nuclear Astrophysics, **A.M. Mukhamedzhanov**, **Invited Talk**, TRIUMF, Vancouver, Canada, (January 2006).

Indirect Techniques in Nuclear Astrophysics: Asymptoitic Normalization Coefficients and Trojan Horse, **A.M. Mukhamedzhanov**, **Invited Talk**, ORSAY, France, (March 2006).

Hadrons in Medium - Theory, **R. Rapp**, **Invited Talk**, 2005 April Meeting of the APS, Tempa, Florida, (April 2005).

Dileptons in Heavy-Ion Reactions and (Light) Vector Mesons in Medium, **R. Rapp**, **Invited Talk**, International School on Quark-Gluon Plasma and Heavy-Ion Collisions: Past, Present and Future, Torino Italy, (May 2005).

Electromagnetic Probes in Heavy-Ion Reactions, **R. Rapp**, **Invited Talk**, European Graduate School Day Basel-Tübingen, Tübingen University, Tübingen, Germany, (May 2005).

Introduction to Dileptons and in-Medium Vector Mesons, **R. Rapp**, **Invited Talk**, International Workshop on Electromagnetic Probes of Hot and Dense Matter, ECT*, Trento, Italy, (June 2005).

Quarkonia in Medium and in Heavy-Ion Collisions, **R. Rapp**, **Invited Talk**, Heavy-Flavor Workshop of RHIC & AGS Users Meeting, Brookhaven National Laboratory, Upton, New York, (June 2005).

Theoretical Perspectives on RHIC: Heavy Flavor and Thermal Radiation, **R. Rapp**, **Invited Talk**, STAR Collaboration Meeting, Warsaw, Poland, (August 2005).

Heavy-Quark Thermalization and Resonances in the QGP, **R. Rapp**, 18th International Conference on Ultrarelativistic Nucleus-Nucleus Collisions (Quark Matter 2005), Budapest, Hungary, (August 2005).

What is the Origin of Mass? ... and the Quest for the Quark-Gluopn Plasma, **R. Rapp**, Physics Department Graduate Orientation, Texas A&M University, College Station, Texas, (August 2005).

Diagnosis of the Quark-Gluon Plasma: Thermal Radiation and Heavy-Quark Probes, **R. Rapp**, Colloquium at Texas A&M University, College Station, Texas, (September 2005).

Heavy-Quark Spectra at RHIC and Resonances in the QGP, **R. Rapp**, **Invited Talk**, Heavy-Flavor Tracker Workshop, Lawrence Berkeley National Laboratory, Berkeley, California, (October 2005).

Electromagnetic Probes at the LHC (in Real + Virtual Light of SPS and RHIC Results), **R. Rapp**, **Invited Talk**, Satellite Meeting on Heavy-Ion Physics at the LHC at the Particle and Nuclear Interactions Conference (PANIC '05), Santa Fe, New Mexico, (October 2005).

The Case for Future RHIC (in Real+Virtual Light of Electromagnetic Probes), **R. Rapp**, **Invited Talk**, BNL Physics Advisory Committee Meeting, Brookhaven National Laboratory, Upton, New York, (November 2005).

Quark-Gluon Plasma: Thermal Radiation + Heavy-Quark Probes, **R. Rapp**, **Invited Talk**, Triangular Nuclear Theory Colloquium, Duke University, Durham, North Carolina, (November 2005).

Dilepton Spectroscopy in (Ultra-) Relativistic Heavy-Ion Collisions, **R. Rapp**, **Invited Talk**, International Workshop on The Physics of Compressed Baryonic Matter, GSI, Darmstadt, Germany, (December 2005).

Heavy-Quark Diffusion, Flow and Recombination at RHIC, **R. Rapp**, **Invited Talk**, International Conference on Strangeness in Quark Matter (SQM06), University of California, Los Angeles, California, (March 2006).

Medium Modifications of Hadrons and Electromagnetic Probes, **H. van Hees**, **Invited Talk**, 22nd Winter Workshop on Nuclear Dynamics, La Jolla, California, (March 2006).

Medium Modifications and Chiral Symmetry, **H. van Hees, Invited Talk**, STAR Collaboration Meeting, BNL, Brookhaven National Laboratory, Upton, New York, (March 2006).

Collective Flow, RAA and Heavy Flavor Rescattering, **H. van Hees, Invited Talk**, Heavy Flavor Productions & Hot/Dense Quark Matter, Riken BNL Research Center, Upton, New York, (December 2005).

Schwerionenstöße und das stark wechselwirkende Quark-Gluon Plasma, **H. van Hees,** Colloquium at Fakultät für Physik der Universität Bielefeld, Bielefeld, Germany, (November 2005).

Thermalization and Flow of Heavy Quarks in the QGP, **H. van Hees,** Particles and Nuclei International Conference (PANIC 05), Santa Fe, New Mexico, (October 2005).

Thermalization of Heavy Quarks in the QGP, **H. van Hees,** 2nd RHIC II Science Workshop, BNL, Brookhaven National Laboratory, Upton, New York, (April 2005).

Chiral Symmetry and Electromagnetic Probes, **H. van Hees,** 2nd RHIC II Science Workshop, BNL, Brookhaven National Laboratory, Upton, New York, (April 2005).

Current Status of The Nuclear Matter Equation of State, **S. Shlomo**, **Invited Talk**, The LV National Conference on Nuclear Physics on Frontiers in the Physics of Nucleus, St. Petersburg, Russia, (July 2005).

Microscopic Analysis of Excitation of Giant Resonances by α Scattering and Nuclear Compressibility, **S. Shlomo**, **Invited Talk**, INST School on Nuclear Physics and Astrophysics, Hanoi, Veitnam, (August 2005).

Fully self-consistent HF-based RPA calculations for giant resonances, **S. Shlomo**, **Invited Talk**, 2005 2nd Joint Meeting of the Nuclear Physics Divisions of the APS and the Physical Society of Japan, Maui, Hawaii, (September 2005).

The Equation of State of Symmetric and Asymmetric Nuclear Matte, **S. Shlomo**, **Invited Talk**, VI Latin American Symposium on Nuclear Physics and Application, Iguazu, Argentina, (October 2005).

Determining the Parameters of a New Skyrme Effective Interaction Using the Simulated Annealing Method, **S. Shlomo**, **Invited Talk**, International Symposium on Structure of Exotic Nuclei and Nuclear Forces (SENUF06), Tokyo University, Tokyo, Japan, (March 2006).

Nuclear Matter Equation of State and Giant Resonances in Nuclei, **S. Shlomo**, **Invited Talk**, International Workshop on Nuclear Physics With RIBF (RIBF2006), RIKEN, Wako, Japan, (March 2006).

Effects of Self-Consistency Violations in Hatree-Fock Based RPA Calculations for Giant Resonances, **S. Shlomo**, **Invited Talk**, RIKEN Symposium 2006 on Methods of Many-Body Systems: Mean Field Theories and Beyond, RIKEN, Wako, Japan, (March 2006).

RESEARCH PERSONNEL AND ENGINEERING STAFF

April 1, 2005 - March 31, 2006

Faculty and Research Group Leaders

Carl A. Gagliardi, Professor of Physics
John C. Hardy, Professor of Physics
Che Ming Ko, Professor of Physics
Saskia Mioduszewski, Assist. Prof. of Physics – From 8/22/05
J. B. Natowitz, Professor of Chemistry, Bright Chair
Ralf Rapp Assist. Prof. of Physics
Shalom Shlomo, Senior Scientist
Robert E. Tribble, Professor of Physics, Director
Rand L. Watson, Professor of Chemistry
Sherry J. Yennello, Professor of Chemistry
Dave H. Youngblood, Professor of Physics
Akram M. Zhanov, Senior Scientist

Research Staff

Henry Clark, Accelerator Physicist (50%)
Grigor Chubaryan, Research Scientist
John C. Hagel, Research Scientist (50%)
Vladimir Horvat, Research Scientist (50%)
Victor Iacob, Associate Research Scientist
Yiu-Wing Lui, Research Scientist
Ninel Nica, Assist. Research Scientist – From 9/1/05
George Souliotis, Assistant Research Scientist
Livius Trache, Research Scientist
Maxim Vasilyev, Assistant Research Scientist (80%) – To 8/31/05
Ryoichi Wada, Research Scientist

Visiting Scientists

Daniel Cabrera-Urban – From 8/1/05
Florin Carstoiu – To 4/5/05
Vladilen Goldberg
V. Kolomietz – To 7/10/05
Ian Towner – From 6/30/05 To 8/31/05

Accelerator Physics And Radiation Line Staff

Henry Clark, Accelerator Physicist (50%)
Vladimir Horvat, Research Scientist (50%)
Bruce Hyman, Research Associate
George Kim, Accelerator Physicist
Don May, Accelerator Physicist
Gabriel Tabacaru, Accelerator Physicist – From 6/1/05
Dennis Utley, Research Associate (25%) – To 7/28/05

Computer Systems Staff

Robert Burch, Jr., Systems Analyst/Sr. Microcomputer/LAN Administrator
John C. Hagel, Assoc. Research Scientist (50%)
Maxim Vasilyev, Asst. Research Scientist (20%) – To 8/31/05

Engineering Staff

Greg Derrig, Senior Mechanical Engineer
Robert Olsen, Senior Mechanical Engineer – From 1/1/06

Postdoctoral Research Associates

Adriana Banu – From 10/1/05
Elizabeth Bell – From 11/14/05 To 1/19/06
Zhiqiang Chen – From 7/1/05
Vicenzo Greco – To 5/31/05
Victor Golovko – From 9/16/05
Marian Jandel – To 11/30/05
Seweryn Kowalski – To 9/5/05
Wei Liu – From 2/1/05
Thomas Materna
Ninel Nica – To 8/31/05
Fakhriddin Pirlepesov – From 5/16/05 To 8/31/05
Prakash Sahu – From 2/2/06
Murad G. Sarsour – From 8/1/05
Dinesh Shetty
Tapas Sils
Gabriel Tabacaru – To 5/31/05
Yoshiaki Tokimoto
Hendrik van Hees

STUDENTS

April 1, 2005 - March 31, 2006

Graduate Students

Tariq Al-Abdullah
Joseph Brinkley – To 12/31/05
Xinfeng Chen
Martin Codrington – From 6/1/05
James Drachenberg
Changbo Fu
John Goodwin
Thomas Henry
Jennifer Iglio – To 5/31/05
August Keksis
Yun Li – From 6/1/05
Ranjini Murthy – To 7/11/05
James Musser – To 8/15/05
Hyo-In Park
Yong Peng
Fakhriddin Pirlepesov – To 5/15/05
Oleksiy Pochivalov
Nathaniel J. Pogue – To 5/31/05
Li Jun Qin
Sarah Soisson
Brian Stein
Deqiang Sun
Au Kim Vuong
Sara Wuenschel
Yongjun Zhai
Xingbo Zhao – From 11/22/05

Undergraduates and Student Technicians

Michael G. Arvizu – To 8/25/05
Alfredo J. Echeverria – From 9/1/05
Joshua Garey
Stephen Hanssen
Jonathan Hunt – From 9/14/05
Jennifer Jeffress – From 1/18/06
Meagan Makarenko – From 1/6/05
Toby Martin – From 5/25/05 to 8/3/05
Larry May – From 1/16/06
Matthew McCleskey
Emily Melton – To 12/16/05
Barrett C. Parker
Casseday Richers
Michael Sarahan – To 5/31/05
William D. Wright – To 5/15/05
Shauna Yow – From 1/18/06
Peter J. Yunker – To 5/10/05
Kylee Ziegler – To 1/3/06

ORGANIZATIONAL CHART - CYCLOTRON INSTITUTE

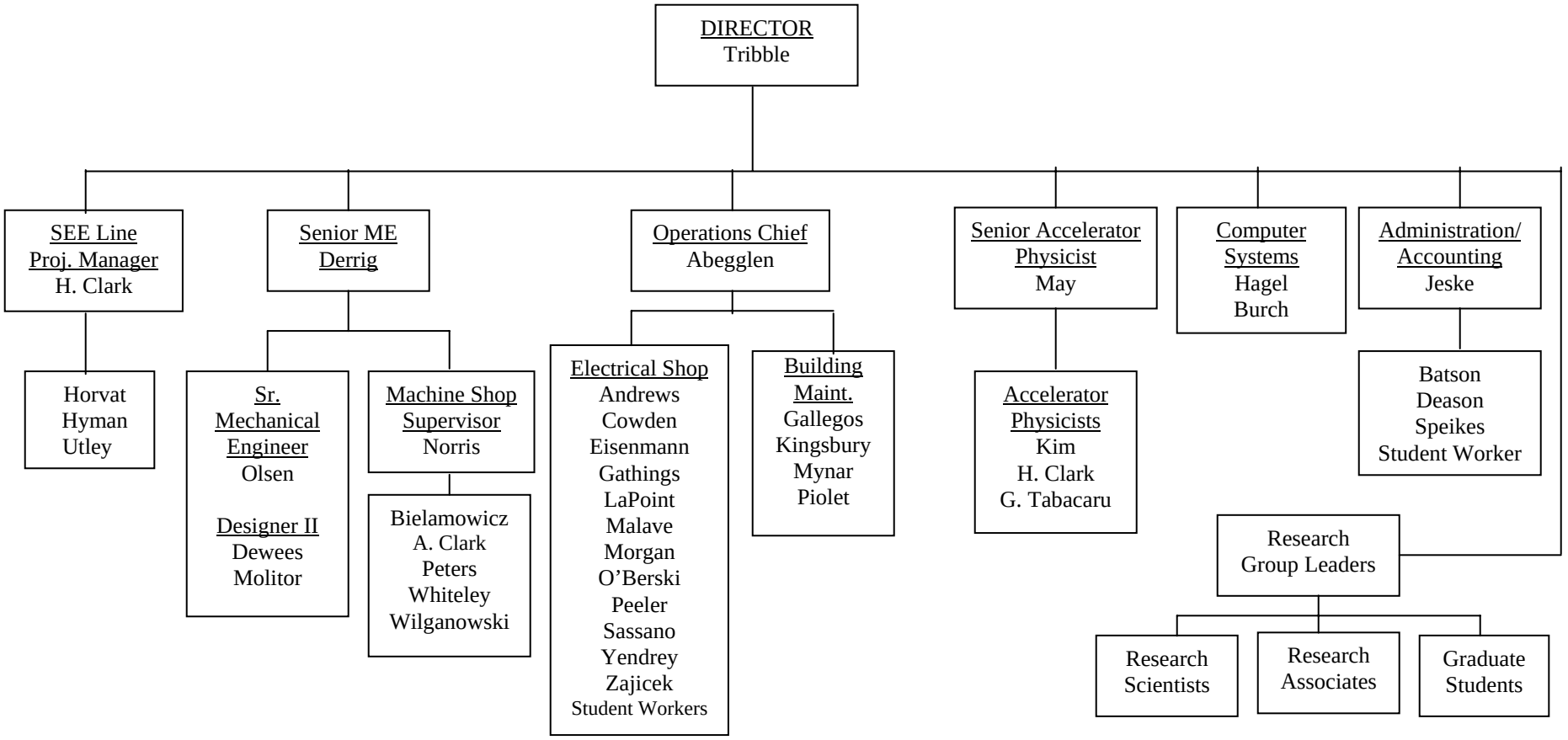

STUDENTS WHO RECEIVED GRADUATE DEGREES
FROM THESIS WORK CONDUCTED
AT
THE CYCLOTRON INSTITUTE

April 1, 2005 – March 31, 2006

Name	Year	Thesis Title	Advisor	First Position	Present Position
Elizabeth Bell	2005	*N /Z Equilibration*	S.J. Yennello	Graduate Research Assistant	Chemistry Instructor st Blinn College, Texas
Fakhriddin Pirlepesov	2005	*Asymptotic scattering wave function for three charged particles and astrophysical capture processes*	R.E. Tribble/ A.M. Mukhamedzhanov	Graduate Teaching Assistant	Pursuing degree at Department of Statistics, Texas A&M University
Jim Musser	2005	*Measurement of the Michel Parameter ρ in Muon Decay*	C.A. Gagliardi	Graduate Research Assistant	Assist. Professor, Arkansas Tech. University, Rusellvilla, AR

INSTITUTE COLLOQUIA AND SEMINARS
April 1, 2005-March 31, 2006

2005

April 1	Dr. Ralf Rapp, Cyclotron Institute, Texas A&M University, College Station, Texas	*Thermal Field Theory and Instantons II*
April 8	Mr. Deqiang Sun, Cyclotron Institute, Texas A&M University, College Station, Texas	*Bottomonium in QGP and Heavy-Ion Collisions*
April 22	Dr. Ralf Rapp, Cyclotron Institute, Texas A&M University, College Station, Texas	*Thermal Field Theory and Instantons III*
May 6	Dr. Massimo Mannarelli, Massachusetts Institute of Technology, Cambridge, Massachusetts	*Hadronic Modes in the QGP*
May 10	Dr. Murad Sarsour, IUCF, Indiana University, Bloomington, Indiana	*Measurement of the Absolute Differential Cross Section for np Elastics Scattering near 200 MeV*
June 21	Professor Khoa Tien Dao, Institute for Nuclear Science & Technique, Vietnam Atomic Energy Comission, Nghai Do, Hanoi, Vietnam	*Microscopic Study of the Quasi-Elastic Nuclear Scattering*
July 5	Dr. John Hardy, Cyclotron Institute, Texas A&M University, College Station, Texas	*How Idiosyncratic is the Weak Force?*
July 11	Mr. James R. Musser, Cyclotron Institute, Texas A&M University, College Station, Texas	*Measurement of the Michel Parameter ρ in Muon Decay*
July 12	Dr. Plamen Boutachkov, Department of Physics, University of Notre Dame, South Bend, Indiana	*Development of New Techniques for Studies of Neutron Rich Exotic Nuclei: Spectroscopy of ^{7}He*
July 20	Professor Akira Ono, Department of Physics, Tohoku University, Sendi, Japan	*Density Dependence of the Symmetry Energy in Multifragmentation*
July 26	Dr. Cristina Bordeanu, NPL-CENPA, University of Washington, Seattle, Washington	*$^{3}He+^{4}He$ Cross Section Measurement-Project Overview*

August 9	Dr. I. S. Towner, Queen's University, Kingston, Ontario, Canada	*The Current Status of V_{ud}, V_{us} and the Unitarity Test*
September 2	Dr. Daniel Cabrera, Cyclotron Institute, Texas A&M University, College Station, Texas	*Interaction of the θ^+ with the Nuclear Medium and its Effect on the Kaon Optical Potential*
September 9	Dr. Daniel Cabrera, Cyclotron Institute, Texas A&M University, College Station, Texas	*Φ and Ω Mesons in a Nuclear Medium and the Nuclear Photoproduction Reaction*
September 13	Professor Raymond Moreh, Physics Department, Ben-Gurion University of the Negev, Beer-Sheva, Israel and Rensselaer Polytechnic Institute, Troy, New York	*Neutron Scattering of keV Neutrons from H-containing Samples and the Role of Quantum Entanglement*
September 16	Dr. Daniel Cabrera, Cyclotron Institute, Texas A&M University, College Station, Texas	*Φ and Ω Mesons in a Nuclear Medium and the Nuclear Photoproduction Reaction II*
September 27	Dr. John C. Hagel, Cyclotron Institute, Texas A&M University, College Station, Texas	*An Overview of Relativistic Heavy-Ion Measurements over a Large Region of Phase Space*
October 7	Dr. Elena Gubankova, Massachusetts Institute of Technology, Cambridge, Massachusetts	*Superfluidity in Cold Atoms and in Dense Quark matter*
October 21	Mr. Nathan Grau, Iowa State University, Ames, Iowa	*Jet Correlations at RHIC*
October 21	Dr. Stefan Leupold, University of Giessen, Giessen, Germany	*Weinberg Sum Rules, Four-Quark Condensates and Chiral Restoration*
November 1	Dr. Adriana Banu, Cyclotron Institute, Texas A&M University, College Station, Texas	*^{108}Sn Studied with Intermediate-Energy Coulomb Excitation*
November 8	Professor Charles J. Horowitz, IUCF Indiana University, Bloomington, Indiana	*Neutron Rich Matter in Heaven and Earth*
November 15	Mr. Au Kim Vuong, Cyclotron Institute, Texas A&M University, College Station, Texas	*New Effective Nucleon-Nucleon Interaction*
November 15	Mr. Lijun Qin, Cyclotron Institute, Texas A&M University, College Station, Texas	*p-A, A-A Collisions with NIMROD*

November 15	Mr. Yong Peng, Cyclotron Institute, Texas A&M University, College Station, Texas	*Systematics of Cross Sections for Target K - Vacancy Production in Heavy Ion Collisions*
November 29	Mr. Oleksiy Pochivalov, Cyclotron Institute, Texas A&M University, College Station, Texas	*Properties of Isoscalar Giant Dipole Resonance in Nuclei*
November 29	Mr. Tariq Ai-Abdullah, Cyclotron Institute, Texas A&M University, College Station, Texas	*Extracting the ANCs in Neutron Transfer Reactions to Determine the Reaction Rate for $^{22}Mg(p,\gamma)^{23}Al$ and $^{17}F(p,\gamma)^{18}Ne$*
November 29	Mr. Yongjun Zhai, Cyclotron Institute, Texas A&M University, College Station, Texas	*The Structure of ^{23}Al and the Consequences on the $^{22}Mg(p,\gamma)^{23}Al$ Stellar Reaction Rate*
December 6	Mr. Xinfeng Chen, Cyclotron Institute, Texas A&M University, College Station, Texas	*Giant Resonance Study by ^{6}Li scattering*
December 6	Mr. August L. Keksis, Cyclotron Institute, Texas A&M University, College Station, Texas	*Quasiprojectile Fragmentation with 32 and 45 MeV/u ^{40}Ar, ^{40}Ca and ^{48}Ca on ^{112}Sn and ^{124}Sn*
December 6	Mr. Thomas Henry, Cyclotron Institute, Texas A&M University, College Station, Texas	*Nuclear k_T in d+Au Collisions from Multiparticle Jet Reconstruction at STAR*
December 13	Dr. M. Mukherjee, GSI/University of Innsbruck, Innsbruck, Austria	*Mass that Matters-Penning Trap Mass Spectroscopy on Rare Isotopes*
December 16	Dr. Bao-An Li, Department of Chemistry and Physics, Arkansas State University, Jonesboro, Arkansas	*Constraining the Radii of Neutron Stars with Terrestrial Nuclear Laboratory Data*

2006

January 24	Mr. Changbo Fu, Cyclotron Institute, Texas A&M University, College Station, Texas	*Study of the Cluster Structures and Decay Properties of Drip Line Nuclei*
January 31	Professor H.M.M. Mansour, Physics Department, Faculty of Science, Cairo University, Giza, Egypt	*Asymmetric Nuclear Matter using Effective Potentials*
February 7	Dr. Xiaodong Tang, Physics Division, Argonne National Laboratory, Argonne, Illinois	*A New Measurement of the E1 Component of the $^{12}C(\alpha,\gamma)^{16}O$ Reaction*

February 14	Dr. Charles M. Folden III, Department of Chemistry, University of California, Berkeley and Nuclear Science Division, Lawrence Berkeley National Laboratory, Berkeley, California	*Production of Transactinide Elements in Cold Fusion Reactions at LBNL*
February 20	Mr. Thomas Henry, Cyclotron Institute, Texas A&M University, College Station, Texas	*Jet and Di-Jet Reconstruction in p+p and d+Au Collisions at RHIC*
February 24	Dr. Jorge Casalderrey, State University of New York, Stony Brook, New York	*Hydrodynamic Flow from Jets*
February 24	Dr. Sevil Salur, Yale University, New Haven, Connecticut	*Investigation of Hadronic Resonances with STAR*
March 7	Dr. Aurora Tumino, INFN, laboratori Nazionali del Sud, and University of Catania, Catania, Italy	*Measurement of the Bare Nucleus Cross Section via the Trojan Horse Method*
March 10	Dr. Michael Ramsey-Musolf, California Institute of Technology, Pasadena, California	*Electric Dipole Moments and the Origin of Baryonic Matter*
March 10	Dr. Gang Wang, Kent State University, Kent, Ohio	*Anisotropic Flow at RHIC Based on Transverse Deflection of Spectator Neutrons*
March 21	Dr. Rainer Fries, University of Minnesota, Minneapolis, Minnesota	*From Color Fields to Quark Gluon Plasma*
March 24	Dr. Lorenzo Ravagli, State University of New York, Stony Brook, New York	*A Study of the QCD Phase Diagram Based on Microscopic Models*